UNIVERSITAT DE BARCELONA

Development of GasChromatographic/Mass Spectrometric procedures and Synchroton Radiation based techniques for the study of painting materials in works of art

Anna Lluveras Tenorio

Development of GasChromatographic/Mass Spectrometric procedures and Synchroton Radiation based techniques for the study of painting materials in works of art

PhD thesis

Barcelona, June 2009

Director of the thesis:
Prof. Marius Vendrell Saz

Candidate doctor:
Anna Lluveras Tenorio

Co-directors of the thesis:
Prof. Maria Perla Colombini
Dr. Ilaria Bonaduce

Index

Introduction and scope of the thesis

A work-of-art is not only an artistic expression but also a material object. From ancient times to modern ones the materials and the techniques used by the painter have been of great importance to achieve the wanted aesthetical effect and to assure them durability. Cennino Cennini in the 15th century wrote about what a painting is: "(…) The foundation of art are design and coloring. Both things require this: grinding, sizing, plastering, gilding, burnishing, dusting, scratching, coloring, ornamenting, and varnishing a table (…)[i]" while Joan Miro adviced Enric C. Ricart the following " I have changed the way of preparing canvas (…) I prepare them with the egg yolk, following a recipe from Sunyer, who learned it from Matisse. If you want I will send you the formula. If you continue to prepare your canvases with such a thick plaster layer, next winter, if there is the exhibition in Madrid, you shoud transport you canvases by WAGO-lit and with a nurse that ensures canvases do not crumble[ii]" [1, 2].

During the Middle Ages different manuscripts described the painting techniques [3,4, 5, 6], and listed the materials and qualities to use. From the *Codex Lucensis* or *De coloribus et artibus Romanorum* by Heraclius (8th century) to the medieval artistic recipe books such as *De Diversis artibus* from Teophilus (12th century), the *Trattato della Pittura* of Leonardo da Vinci, *Il libro dell'Arte* by Cennino Cennini, the *Mappae Clavicula* or *Bolognese manuscript* (15th century), these treaties illustrated the know-how of the epoch. Also during the Renaissance this interest persisted with books such as *A los Profesores del Arte de la Pintura(1649) from Francisco Pacheco*.

When restoration of works-of-art started claiming for technical information, several books on painting techniques were published. Mary P. Merrifield presented in 1846 'The Art of Fresco Painting in the Middle Ages and the Renaissance' where

[i] "El fondamento dell'arte, e di tutti questi lavorii di mano principio, è il disegno e 'l colorire. Queste due parti vogliono questo, cioè: sapere tritare, o ver macinare, incollare, impannare, ingessare, e radere i gessi, e pulirli, rilevare di gesso, mettere di bolo, mettere d'oro, brunire, temperare, campeggiare, spolverare, grattare, granare, o vero camusciare, ritagliare, colorire, adornare, e invernicare in tavola o vero in cona. Lavorare in muro, bisogna bagnare, smaltare, fregiare, pulire, disegnare, colorire in fresco, trarre a fine in secco, temperare, adornare, finire in muro."

[ii] "He canviat la manera de preparar tela (...)la preparo amb rovell d'ou, segons recepta d'en Sunyer, a qui li ensenyà en Matisse. Si t'interessa ja t'enviaré la formula. Si tu continues preparant les teves teles amb aquell gruix de guix ja cal que l'hivern vinent, si exposem a Madrid, transportis les teves pintures amb un wago-lit i amb una enfermera que que vigili que pel viatge no se t'acrivellin (...)"

descriptions of painting methods used by masters such as Alberti, Cennini, Vasari, and Borghini were translated. Moreover, the author also discussed the causes of fresco degradation and how to retouch, repair, and clean these works of art [5,6,7, 8,9].

Nowadays, the study of painting samples pursues different goals. On the one hand, to identify the materials and painting technique of an epoch and thus the know-how of an historical period. On the other hand, to study the degradation, ageing and decay processes undergone by paintings in order to prevent its disappearance and apply the most suitable restoration and conservation processes, together with the choice of the proper conservation and exhibition conditions.

From a physico-chemical point of view, paintings are composite arrays of several layers made of an heterogeneous mixture of organic and inorganic materials. Moreover, these materials experiment interactions among them and an heterogeneous ageing with time and exposure to pollutants, light and conservation conditions such as humidity and temperature. In paintings both inorganic (pigment, thickeners, polishers, stabilizers, dryers and extenders) and organic materials (binding media, varnishes, colorants) are present, mixed together in unknown proportions, and arranged in micrometric layers. Moreover, organic materials used as binding media (milk, casein, animal glue, linseed oil, blood, beeswax, plant gums, honey, plant resins, etc) are complex natural mixtures in different proportions consisting of proteins, triglycerides, terpenic compounds, sterols, hydrocarbons, esters, aliphatic alcohols, free fatty acids, polysaccharides, etc. [10,11, 12]. As a result, paintings are not static objects but complex systems that constitute a difficult issue for the analytical chemist.

Different strategies have been used from the beginning of the 20th century in order to investigate the materials constituents of works-of-art. An overview of the literature on the study and characterization of painting samples highlight the wide range of techniques applied on works-of-art in general and painting samples in particular. Spectroscopic techniques such as FTIR (Fourier Transform Infrared Spectroscopy) and Raman, S-Ray Diffraction (XRD) , X-Ray Fluorescence (XRF) or Magnetic Nuclear Ressonance (RMN) and electrochemical techniques have been applied to the characterisation of painting materials [13,14, 15, 16, 17]. To characterise the organic species in paint samples and to study their behaviour with aging, to

chromatographic/mass spectrometric techniques (HPLC, GC/MS, DE/MS, Py/GC/MS) are the methods of choice [18, 19,20,21,22, 23,24,25,26,27].

The nature of paintings as multi-layered arrays and the heterogeneous ageing of the materials requires a 2D mapping approach in order to be able, not only to characterize and identify the materials present but also to obtain their distribution in the sample build-up. Thus, Imaging techniques are required as they allow resolving the elemental and molecular heterogeneities both within and between layers. The micrometric of the sample indicates that micro imaging techniques are required to establish a reliable distribution Traditionally light microscopy (LM) and scanning electron coupled with energy dispersive x-ray analysis (SEM-EDS) have been extensively applied to painting samples cross-sections. Imaging Secondary Ion Mass Spectrometry (SIMS), FTIR and also Synchrotron radiation advantages have been exploited in order to obtain distributional information on paintings [28, 29 , 30, 31, 32, 33, 34,35, 36].

However, as imaging techniques presents some difficulties in the unequivocal characterisation of the painting materials and the decay-by-products, a multy-analytical approach has been proposed to completely characterise the materials, degradation products, painting technique and ageing mechanisms in painting samples [37, 38].

In this frame, the goal of this thesis is filling some gaps in the analysis and characterization of painting systems. Thus, though each chapter presents a different issue the aim of completing the partial knowledge obtained previously is the guiding thread.

This thesis represents a contribution to Conservation Science due to the fact that its main goal is the improvement of analytical techniques for the study of historical and archaeological paintings.

With this aim two different paths were contemporary followed. First of all, the development of preparation methods and analytical procedures to study of painting samples and secondly, the characterisation of the composition of materials and of their degradation processes applying the analytical methodologies developed.

The main objectives of this thesis can be summarized as follows:

1) To test preparation methods to obtain thin sections for FTIR imaging in transmission mode. The capabilities of the preparation methods were evaluated on highly inorganic paint samples to ascertain the possibilities to perform synchrotron radiation FTIR imaging on them.

2) To study the formation of oxalates in paintings by using, among others, imaging techniques, both SR micro FTIR and SR micro XRD, to gain information on oxalate distribution, nature and relate them to other materials present in the sample.

3) To exploit a multy-analytical approach to elucidate the materials present in particularly complex samples (both organic and inorganic) and their distribution, with the aim to establish the painting technique.

4) To settle-up a reliable GC/MS procedure for polysaccharide material characterisation.

5) To shed new light on the nature of polysaccharide materials as binding media and adhesives establishing compositional changes due to ageing, pigment presence, inorganic materials and biological attack.

6) To establish a combined GC/MS procedure for the characterisation of proteinaceous, lipid, resinous and polysaccharide materials from a unique and micrometric sample collected from works of art.

References

[1] Cennino Cennini, in F. Frezzato (Editor), Il libro dell'Arte, Neri Pozza Editore, Vicenza, 1st ed., 2003.

[2] Mirò a Enric C. Ricart (Mont-Roig 16 de juliol de 1918) published by Diari Avui, desembre 2008

[3] Das Straβburg Manuskript, translated by Viola Rosamund Borradile, London, 1966

[4] G. Badger, ' A classical Technology Edited from Codex Lucensis', Ed. J.M. Burnam, The Gorham Press, Boston, 1920

[5] Mary P. Merrifield, The Art of Fresco Painting in the Middle Ages and the Renaissance, Courier Dover Publications, 2004, ISBN 0486432939

[6] Doerner, Los materiales de pintura y su empleo en el arte (18ª edición Editorial Reverté Barcelona 1998).

[7] R.Mayer, 'The Artist's Handbook of Materials and Techniques', Editor Steven Sheehan 5th Revised Edition 1991

[8] M. Matteini, A. Moles, 'La chimica nel restauro. I materiali dell'arte pittorica', NEREA,1984

[9] M.Luisa Gómez, , La Restauración Examen científico aplicado a la conservación de obras de arte,Cuadernos Arte Cátedra,2000

[10] J. S. Mills, R. White, 'The Organic Chemistry of Museum Objects', 2nd ed.; Butterworth Heinemann Ltd: Oxford, 1994.

[11] M.P. Colombini, G.Gautier, F.Modugno, E. Ribechini 'Combined GC/MS Analytical Procedure for the Characterization of Glycerolipid, Waxy, Resinous, and Proteinaceous Materials in a Unique Paint Microsample', Analytical Chemistry. 2006, vol. 78, pp. 4490-4500, ISSN: 0003-2700.

[12] MR. Derrick, DC. Stulik, JM. Landry, 'Infrared Spectroscopy in Conservation Science, Scientific Tools for Conservation', The Getty Conservation Institute, Los Angeles, 1999.

[13]F. Casadio, F. Toniolo, ' The analysis of polychrome works of art: 40 years of infrared spectrocopic investigations', Journal of Cultural Heritage2 (2001) 71-78

[14] M.T. Doménech-Carbó, 'Novel analytical methods for characterising binding media and protective coatings in artworks', Analytical Chimica Acta 621 (2008)109

[15] G. Bitossi, R. Giorgi, M. Mauro, B. Salvadori, L. Dei, 'Spectroscopic Techniques in Cultural Heritage Conservation: A Survey', Applied Spectroscopy Reviews, 40, 3 (2005) 187 - 228

[16] A. Spyros, D. Anglos, 'Studies of organic paint binders by NMR spectroscopy', Applied Physics A 26 (2006) 705-708

[17] A. Adriaens, M.G. Dowsett, 'Applications of SIMS to cultural heritage studies', Applied Surface Science 252, 19, 30 (2006) 7096-7101

[18] Bonaduce, I.; Colombini, M. P. , 'Gas chromatography/mass spectrometry for the characterization of organic materials in frescoes of the Momumental Cemetery of Pisa (Italy)', *Rapid Commun. Mass Spectrom*. 2003, *17*,2523-2527.

[19] Colombini, M. P.; Modugno, F.; Giacomelli A., 'Two procedures for suppressing interference from inorganic pigments in the analysis by gas chromatography-mass spectrometry of proteinaceous binders in painting' *J. Chromatogr. A* 1999, *846*,101-111.

[20] J. de la Cruz-Canizares, M. T. Domenech-Carbo, J.V. Gimeno-Adelantado, R. Mateo-Castro, F. Bosch-Reig, , *J. Chromatogr. A* 2004, *1025*, 277-285.

[21] J. D. J van den Berg,.; van den Berg, K. J.; Boon, J. J. 'Identification of non-cross-linked compounds in methanolic extracts of cured and aged linseed oil-based paint films using gas chromatography – mass spectrometry', *J. Chromatogr. A*2002, *950*, 195-211.

[22] G. Chiavari, N. Gandini, P. Russo, D. Fabbri, 'Characterisation of standard tempera painting layers containing proteinaceous binders by pyrolysis (/methylation)-gas chromatography/mass spectrometry' *Chromatographia* 1998, *47*,420-426.

[23] J. V. Gimeno-Adelantado,.; R. Mateo-Castro, M. T. Domenech-Carbo, F. Bosch-Reig, F.; A. Domenech-Carbo,.; M. J.Casas-Catalan, L. Osete-Cortina, *J.Chromatogr. A* 2001, *922*, 385-90.

[24] M. P. Colombini, I. Bonaduce; G. Gautier, 'A diagnosis of the yellowing of the marble high reliefs and the black decorations in the chapel of the tomb of Saint Anthony (Padua, Italy)', *Chromatographia* 2003, *58*,357-364.

[25] I. Bonaduce, M.P. Colombini, 'The Characterization of Beeswax in works of Art by Gas Chromatography-Mass Spectrometry and Pyrolysis-Gas Chromatography-Mass Spectrometry Procedures', *J. Chromatogr. A* 2004, *1028*, 297-306.

[26] M. Regert, S. Colinart, L. Degrand; O. Decavallas, 'Chemical Alteration and use of beeswax through time: accelated ageing tests and analysis of archaeological samples from various environmental contexts', *Archaeometry* 2001,*43*, 549-569.

[27] A. Andreotti, I. Bonaduce, M.P. Colombini, G. Gautier, F. Modugno , E. Ribechini., 'Combined GC/MS Analytical Procedure for the Characterization of Glycerolipid, Waxy, Resinous, and Proteinaceous Materials in a Unique Paint Microsample', Anal. Chem. 2006, 78, 4490-4500

[28] J. van der Weerd, M.K. van Veen, R.M.Q. Heeren, J.Boon, 'Identification of pigments in paint cross-sections by reflection visible light imaging microspectroscopy, Journal of Analytical Chemistry, 75 (2003) 716-722

[29] I. Bonaduce, J. J. Boon, M. P. Colombini and G. Lanterna, "Chemical imaging techniques for the characterisation of materials and techniques in the art of gilding: a case study from a mural by F. Lippi", Proceedings of Conservation Science 2007, Milan , 10-11 May 2007.

[30] RMA Heeren, JJ Boon, P Noble, J Wadum, 'Integrating Imaging FTIR and Secondary Ion Mass Spectrometery for the Analysis of Embedded Paint Cross-Sections', ICOM, 12th Triennial Meeting Lyon, Lyon, 1999,

[31] MR Derrick, DC Stulik, JM Landry, SP Bouffard, Furniture Finish Layer Identification by Infrared Linear Mapping Microspectroscopy, Journal of the American Institute of Conservation 31: 1992, p. 225-236.

[32] JJ. Boon, K. Keune, J. van der Weerd, M. Geldof , JRJ. Van Asperen de Boer, 'Imaging Microspectroscopic, Secondary Ion Mass Spectrometric and Electron Microscopic Studies on Discoloured and Partially Discoloured Smalt in Cross-Sections of 16th Century Paintings', Chimia 55(11): 2001, p. 952-960.

[33] M. Cotte, J. Susini, V. A. Solé, Y. Taniguchi, J. Chillida, E. Checroun, P. Walter, 'Applications of synchrotron-based micro-imaging techniques to the chemical analysis of ancient paintings', Journal of Analytical Atomic Spectrometry, 23, 2008, 820-828

[34] D. Creagh In: D. Bradley and D. Creagh, Editors, Physical Techniques in the Study of Art,. 'Synchrotron Radiation and its Use in Art, Archaeometry, and Cultural Heritage Studies' Archaeology and Cultural Heritage vol. 2, Elsevier (2007), p. 1

[35] N. Salvadó, S. Butí, J. Nicholson, H. Emerich, A. Labrador, T. Pradell, 'Identification of reaction compounds in micrometric layers from gothic paintings using combined SR-XRD and SR-FTIR', Talanta, Article in Press

[36] E. Dooryhee, M. Anne, I. Bardies, J.L. Hodeau, P. Martinetto, S. Rondot, J. Salomon, G.B.M. Vaughan and Ph. Walter, Non-destructive synchrotron X-ray diffraction mapping of a Roman painting, Appl. Phys., A 81 (2005) (4), pp. 663–667

[37] I. Bonaduce, J.J. Boon, 'An integrated mass spectrometric and molecular imaging analytical approach to identify and localise constituents in paintings applied to gilded multilayer structures from the 14th to 16th C works of art', in New trends in analytical, environmental and cultural heritage chemistry, M.P. Colombini, L. Tassi editors, Transworld research Network (2008) 345-388

[38] JJ .Boon, K. Keune, T. Learner, 'Identification of Pigments and Media from a Paint Cross-Section by Direct Mass Spectrometry and High-Resolution Imaging Mass Spectrometric and Spectroscopic Techniques', ICOMCC Science symposium, Rio de Janeiro, 2002

Summary

A summary of the contents of the chapters is reported below :

Chapter 1. Synchrotron radiation based micro imaging FTIR to the study of painting cross-sections

This chapter will present the application of SR micro FTIR technique in transmission mode to decorative painting samples. The aim of the chapter is to show the results of the preparation methods tested on samples with a high inorganic content and provide discussion on the problematics arisen. The characteristic brightness of synchrotron radiation allows to work with micro- metric spot size without significant loss of energy flux. That means that micro-imaging techniques such as micro-XRF. Micro-FTIR, micro-XRD, micro-XANES can be applied to painting cross-sections providing chemical and elemental mappings and images of the cross-sections. FTIR is a technique that enables identifying both organic and inorganic materials and it is thus particularly interesting in painting samples were different kind of materials (organic/inorganic, crystalline/amorphous, natural/synthetic) are mixed in each layer.

Chapter 2. Characterisation and distribution of oxalates in mural painting samples

This chapter illustrates the analysis by synchrotron micro-analytical techniques of mural paintings presenting degradation. The challenge of the experiments was to identify and to obtain the spatial distribution of the decay by- products formed. The aim of this studies was to gain information on the formation of oxalates in painting samples to be able to add information on their formation mechanisms in mural painting samples. Determining the in depth distribution of oxalates respect to the organic material distribution and the nature of this oxalates would help attributing calcium oxalates to a bio-construction or to a chemical product of degradation of binding media. Synchrotron powder XRD, Synchrotron imaging μXRD and μFTIR experiments have been carried out to obtain material distribution. To complement the information SEM-EDS, FTIR, PyGCMS and GCMS techniques were applied in order to characterize the binding media and organic materials present as well as their degradation products.

Chapter 3. Mass Spectrometric and SR based techniques for the identification and distribution of painting materials in samples from works of art.

This chapter will present the combined use chromatographic-mass spectrometric techniques, such as GC/MS or Py/GC/MS, and the chemical mapping of functional groups by imaging SR FTIR in transmission mode on microtomed cross sections as a suitable approach to have a detailed characterisation of the organic materials in a paint sample, assuring their localisation in the sample build-up. In order to complement the information on them, SR XRD line scans have been used as the perfect tool for the inorganic materials unequivocal identification. This analytical approach has been used to study samples from the Catalan mural paintings by Josep Maria Sert y Badía (20^{th} century).

Chapter 4. GC/MS characterisation of saccharide materials in samples from works-of-art

In this chapter a GC/MS analytical procedure for the identification of polysaccharide materials present in painting samples has been optimized. Since the 3^{rd} millennium B.C., polysaccharides have been widely used as binding media and sizing agents. Polysaccharide materials, such as plant gums, sugar, flour or honey are considered in ancient recipes and they have also been widely employed for restoration and consolidation processes. The procedure is based on the silylation of aldoses and uronic acids, released from the sample by microwave assisted hydrolysis, and previously converted into the corresponding diethyl-dithioacetals and diethyl-dithioacetal lactones. Using this method only one chromatographic peak for each compound is obtained, providing simple and highly reproducible chromatograms. Purification from inorganic pigments, which can strongly interfere in the derivatisation step, is performed by using ion exchange resins. The polysaccharide material is then identified from the profile of aldoses and uronic acids through a decisional scheme. Paint samples from mural paintings of the Mediterranean area dating back from the 4^{th} century B.C. to the 19^{th} century A.D. will be discussed. Possible contamination of biological origin and polysaccharide degradation in painting samples will be also debated.

Chapter 5. GC/MS analytical procedure for the characterization of lipids, terpenoid resins, polysaccharide and proteinaceous materials in the presence of interfering inorganic pigments the same micro sample

This chapter a procedure for the analysis of the whole content of organic materials present in painting sample has been settled. The GC/MS procedure allows the identification of lipids, waxes, proteins, resinous and polysaccharide materials in the same microsample from painted works of art. It is based on a sample multistep chemical pretreatment consisting in the ammonia extraction of proteins and polysaccharide materials separated this way from lipid and resinous materials followed by the separation and purification of proteinaceous and polysaccharide materials before the hydrolysis, based on the use of the monolithic sorbent tip technology with a C4 stationary phase. Three fractions are generated and derivatised separately allowing the quantitative analysis of monosaccharides and uronic acids, aminoacids and lipid material and the identification of resins and waxes. The procedure was applied to ancient painting samples from a Greek icon of the 15^{th} century. Proteinaceous, lipid and polysaccharide materials were characterized in the samples. Results obtained will be discussed in details.

Chapter 1

Synchrotron radiation based micro imaging FTIR to study of painting cross-sections

The nature of paintings as multi-layered arrays and the heterogeneous ageing of the materials requires a 2D mapping approach in order to be able, not only to characterize and identify the materials present but also to obtain their distribution in the sample build-up.

The characteristic brightness of synchrotron radiation allows to work with micro- metric spot size without significant loss of energy flux. This means that micro-imaging techniques such as micro-XRF, micro-FTIR, micro-XRD, and micro-XANES can be applied to painting cross-sections providing chemical and elemental mappings and images of the cross-sections. FTIR is a technique that enables identifying both organic and inorganic materials and it is thus particularly interesting in painting samples were different kind of materials (organic/inorganic, crystalline/amorphous, natural/synthetic) are mixed in each layer.

This chapter will present the application of SR micro FTIR technique in transmission mode to decorative painting samples. The aim of the chapter is to show the results of the preparation methods tested on this kind of samples with a high inorganic content, providing discussion on the issues arisen.

1.1. Introduction

Considering paint samples, the chemical properties of the materials of adjacent areas can be completely different from one another due to the heterogeneity of the painting and its multilayered structure. Moreover, the degradation and ageing can also be considered as three-dimensional processes. Therefore the identification of painting materials can not be the only point of interest but a complete understanding of the painting requires both in plane and in depth information.

Imaging of organic and inorganic materials of the paint cross sections is required for the characterisation of painting systems as they allow resolving the elemental and molecular heterogeneities both within and between layers [1, 2, 3, 4, 5, 6, 7, 8, 9, 10, 11, 12, 13]. Until now, the study of the build-up of multi-layer systems, such as paintings, has been performed by Visible and UV- fluorescence microscopy, specular reflection imaging Fourier Transform Infrared Spectroscopy (FTIR), Scanning Electron Microscopy with Energy Dispersive X-Ray analysis (SEM-EDX) and Secondary Ion Mass Spectrometry (SIMS). The use of these techniques in a complementary way allows a detailed study of the distribution of materials and decay-by-products [2, 6, 9, 11]. Table 1.1. summarizes the main characteristics of these techniques.

Table 1.1. Conventional imaging methods and their minimum analysis area.

Technique	*Acronym*	*Description*	*Resolved area [12, 14]*
Optical microscopy	Vis	Morphological information	1 µm
Uv-fluorescence microscopy			
Energy Dispersive Spectroscopy	EDS	Elemental analysis	1-10 µm
X-Ray Fluorescence	XRF	Elemental analysis	3 mm
Secondary Ion Monitoring Spectroscopy	SIMS	Ions	1 µm
FTIR specular reflectance Fourier Transform Infrared Spectroscopy	FTIR	Functional groups (organic /inorganic)	20 µm
	ATR		100 µm

Synchrotron radiation (SR) techniques fulfil a wide range of the requirements needed to study painting samples, such as high spatial resolution, small spot size, high collimation of the beam, high detectivity, high signal-to-noise ratio, intensity and brilliance [15, 16 , 17, 18, 19, 20, 21, 22, 23, 24, 25, 26, 27, 28, 29].

1.1.1. Synchrotron radiation

Synchrotron radiation is based on the fact that high energy electrons traveling in a circular orbit close to the speed of light emit electromagnetic radiation tangential to their orbit. At this speed the electrons travel close to the velocity of light and the subsequent electromagnetic waves almost catch up providing continuous wide range energies of emitted radiation called synchrotron radiation. The synchrotrons accelerate the electrons and keep them in orbit producing the synchrotron radiation, and usually consist in doughnut shaped buildings containing a radiation shielded storage ring and several beamlines that are tangentially placed around it.

To generate the synchrotron light, “bunches” of electrons are injected in a circular accelerator called booster by means of a linear accelerator (LinAc). The accelerated electrons are transferred from the booster accelerator to the storage ring which keeps the electrons running and produces the synchrotron radiation. A single bunch of electrons can orbit around the storage ring and a numerous bunches of electrons can be grouped together into a "train" of bunches. The total length of each train and the spacing between consecutive trains can be varied giving a number of different modes of operation.

A typical storage ring comprises symmetric straight and bending sections of stainless steel tubes under ultra high vacuum with a set of complex magnetic devices to focus the electron bunches and bend their path but keeping them at the same time in a determined orbit. To produce the synchrotron radiation a normal (perpendicular) acceleration is applied to the electron bunches by means of bending magnets (BM) and insertion devices (IDs). BM are big dipole magnets installed in the curved sections of the ring. The IDs, known as wigglers and undulators, are inserted in the straight sections of the storage ring, and are mainly constituted by an array of oriented dipole

magnets. Magnets are arranged in a way that electron bunches oscillate sinusoidal in the horizontal plane as they pass through. The insertion device is called wiggler when the radiation resulting from each individual set of poles incoherently superimposes with the radiation from all the other poles, and it is called undulator when the radiation resulting from each dipole pair is coherently superimposed and the radiation constructively and destructively interferes with itself producing a narrower emission cone.

IDs could offer enhanced intensity over a narrow bandwidth for specific applications, but none exist on IR lines as yet. The IDs provide a continuous spectrum with a higher flux and extended to shorter wavelengths than the spectrum obtained by BM, however some differences can be appreciated between undulators and wigglers. Undulators, depending on their gap, provide a series of spikes corresponding to energies of different coherent interferences and their harmonics, and are very useful for microfocusing beamlines requiring high fluxes and lower energies. Wigglers provide a continous energy spectrum resulting from the incoherent interferences that provide higher flux at higher energies. This is specially useful in extreme conditions experiments where samples are inside an anvil or furnace and the beam is partially absorbed through the cells.

BM and ID are fitted to a beamline that collect and focus the photons emitted from these devices on the sample position. Beamlines are constituted by three parts, namely the front end, the beamline optics, the experimental station, and, optionally, a control panel. The front end usually houses a safety valve that separates the beamline from the ring. The beamline optics usually involve a set of optical elements such apertures, slits, mirrors and monochromators with the objective to deliver photons with the desired spatial resolution, energy resolution and spectral brightness.

The birth of the synchrotron radiation light is linked to the studies on the production of radiation as a result of energetic loss processes on accelerated electrons on 1920's, and especially from the studies that focused on the production of X-rays from magnetic induction of electrons acceleration on the 1940's. The first kind of synchrotrons consisted in a torus-shaped vacuum tube with and alternating current that accelerated

electrons around a circular path, and was first build in 1947 by General Electrics at the United States with the aim to built in a new generation of X-ray generation devices.

The improvement of circular-shaped electrons accelerators and the better understanding of the derived processes by particle physicists were followed by the development of the first synchrotron facilities.

There are some good reviews on synchrotron radiation history in different publications [30,31, 32, 33].

1.1.2. Synchrotron radiation characteristics

The main characteristics of synchrotron radiation are the energy spectral brightness or brilliance, and the wide range of wavelengths available [14,15,17,32].

Brightness (flux density in phase space) is an invariant quantity in statistical mechanics, so that no optical technique can improve it but it is depending on the source. Since SR is a polychromatic beam, incident radiation can be tuned in a continuous mode and thus, information of the sample using a continuous variation of the excitation can be obtained. This is particularly useful in some experiments using the X-ray range of energies, which penetration into the sample depends (among other factors) on its energy. X-Ray sources (X-ray tubes) wavelength depends on the anode material and the accelerating voltage [24, 28]. Tuning these features determines the kind of experiments that can be carried out in the experimental hutches (XRD, XRF, XANES, FTIR) [15,16,**Errore. Il segnalibro non è definito.**,21,26].

Initially, the characteristics of SR were used in the painting analysis as a source improvement that allow obtaining XRD patterns from small quantities of sample such as pigment layers [22] or the improvement of signal-to-noise ratio in FTIR experiments of a previously mechanically separated sample [34,35]. Some attempts have also been done on the use of SR as a non-destructive tool [35, 14,27].

However, the high SR brightness enables acquiring high resolution maps using a small spot and high signal-to-noise ratio.

1.1.3. Synchrotron radiation micro-focus techniques

The micro focusing beam lines optics providing a micrometric beam spot (from 10 μm down to 1 μm) are of special relevance when studying works of art such as paintings with a high degree of heterogeneity and enclosing relevant information within the micrometric layers. These techniques can resolve areas down to 1 μm due to the possibility of focusing the beam to a micrometric spot thanks to the high brilliance characteristic of SR, avoiding the complete lost of signal or the increase of the signal-to-noise ratio [17,19].

The variety of SR-based micro imaging techniques have been successfully applied to the study of cultural heritage objects [14,15,16,**Errore. Il segnalibro non è definito.**,21,22,23,24,25,26,27,28]. Mainly, micro FTIR, micro XRF, micro XRD and micro XANES have been applied to study the nanostructure of the decorations of lustre decorated ceramics [36,37], the chemical reasons for the blackening of the Pompeian cinnabar paintings [16] or mummies skin degradation [21]. Their combined use allowed gaining information on the elemental, chemical and crystalline distribution, giving information on the materials used in the work of art and the ageing mechanisms and degradation processes undergone by these materials [15].
Table 1.2 summarizes the Synchrotron Radiation based micro imaging techniques and their key characteristics.

Table 1.2. SR based micro imaging techniques

Table 1.2. SR based micro imaging techniqueTechnique	*Acronym*	*Description*	*Footprint/ beam size ([i])*
Micro X-ray Fluorescence	μXRF	Elemental mapping	1 μm
Micro X-ray Diffraction	μXRD	Crystalline phases	2 μm
Micro X-ray Absorption Near Edge Spectroscopy	μXANES	Single elemental analysis	5 μm
Micro Fourier Transform Infrared Spectroscopy	μFTIR	Functional group imaging	6 μm

1.1.4. Synchrotron Radiation based Fourier Transform Infrared Spectrosopy

Fourier Transform Infrared (FTIR) spectroscopy has been widely used to identify the different materials used in works-of-art. From 1950's it has been established as a basic analytical tool in laboratories. The introduction of the Fourier Transform Infrared (FTIR) spectrometers was a key factor for the use of this technique. The development of microspectrophotometers and accessories for IR spectrometers (1980's) has established FTIR as a powerful tool in the field of Archaeometry and Cultural Heritage science [5, 38,39,40,41,42,43,44]. FTIR mapping is an interesting tool for the study of the distribution of the materials in samples from works-of-art such as painting samples. As compared with other techniques, FTIR allows characterising inorganic and organic materials as well as their degradation products. Some interesting attempts have been already published on specular reflection experiments [1,2,3,6] and total attenuated reflection[4, 45] by using conventional sources on painting cross-sections. SR micro FTIR adds such a high brightness that transmission experiments are allowed with a reasonable signal-to-noise ratio.

Synchrotron radiation source advantages for infrared micro spectroscopy and its applications in the field of cultural heritage have been extensively and accurately described in the bibliography [34,17]. The first application of SR based FTIR were directed to obtain high signal-to-noise spectra of analysis areas lower than those permitted by conventional sources, taking profit of SR brightness [35,34]. Lately, imaging techniques such as micro FTIR have been used to produce high contrast chemical maps in order to establish the relations among materials and their

[i] ESRF charcteristics. Station ID 21 and ID 18F

arrangement in the painting build-up, the result of their interactions and the ageing mechanisms [15,16,**Errore. Il segnalibro non è definito.**,26]. This way, imaging of cross-sections has been obtained enabling to study the 2D distribution of functional groups in painting stratigraphies.

FTIR imaging allows molecular mapping of painting samples cross-sections. Thus, 2D false colour images corresponding to the imaging of functional groups are generated plotting intensity of a specific band versus position. To obtain FTIR measurements with a spatial resolution down to 6 μm (beam size at station ID 21 ESRF reported in Table 2) the IR beam is focused on the sample by means of a microscope coupled to a FTIR spectrophotometer and detector. The collimated synchrotron beam is introduced directly into the spectrophotometer toward the IR microscope. An sketch of the set-up for micro FTIR has been published [15, 29].

1.1.5. Sample preparation methods for micro FTIR experiments in transmission mode

The key issue in performing micro imaging experiments is the sample preparation methods. Different accessories and methods have been developed [1,5] and afterwards applied for the micro FTIR experiments at the SR beam lines [29].

The two main FTIR modes applied to Cultural Heritage materials, particularly in painting analysis, are transmission and specular reflection though recently ATR has been used on paintings cross-sections giving interesting results [4,45]. IR transmission mode, when possible, is preferred since transmission spectra libraries are larger than reflection ones, better signal-to-noise ratio than reflection analysis and no transformation of the data is necessary (the Kubelka-Munk transform must be applied when specular reflection experiments are performed) [1,5].

Traditionally, a dissection of the sample by using a knife, scalpel or tungsten needles [1,5,34,46] to separate sample layers or particles from the sample is attempted. By this way, particles or layers can be analysed separately in order to obtain some information on the distribution of the materials in the sample. However, the capacity to separate manually layers is generally not lower than 20 μm [5] while many painting layers are under this limit. Sub-sample can be analysed by making a KBr pellet or by using a

diamond cell. Diamond cells can be used as a window, where the squeezed sample is placed and through which the IR beam travels, or can be placed directly under the microscope [1,5].

Imaging analysis require the preparation of a cross-section of the sample without altering the sample build-up nor its composition. For reflection analysis, a very well polished section should be obtained [1,3]. Embedding in a synthetic resin and cutting with a diamond saw previously to the polishing process has been widely applied to morphological characterization of painting sample stratigraphies. However, reflection spectra present a high signal-to-noise ratio in the region with wavelengths > 2000 cm^{-1} that makes difficult the identification of organic compounds. Moreover, the high quantity of inorganic materials implies that spectra are dominated by inorganic characteristic peaks due to both the higher refraction index of inorganic compounds and the scattering phenomena that they produce [1,3]. Thus, generally variations in the composition can be detected but the identification of all components often requires the support of complementary analysis.

Transmission improves the quality of the data but requires samples thin enough to avoid the complete absorption of the beam. Therefore in performing SR micro FTIR mappings in transmission mode, the sample preparation method becomes a critical point. Typical thicknesses required for transmission measurements with conventional micro-FTIR are 4-20 μm [5]. Though SR characteristics allow the micro focusing and collimation of the beam with a good signal-to-noise ratio, absorbance of the beam is strongly dependant on the thickness of the sample. Thus, SR sample thickness for FTIR transmission experiments can not be more than for conventional sources ones but it is been reported that, in painting samples, it should not exceed 2-5 μm thickness depending on the sample mineral charge [29].

A summary of sample preparation strategies used on SR sources has been recently published [29]. Applying these procedures great results have been obtained with mummies skin, and oil and recent paintings [15,16,**Errore. Il segnalibro non è definito.**,17,19,21]. Table 1.3 summarizes the procedures for both transmission and reflection mode.

Table 1.3. Summary of sample preparation strategies for μFTIR experiments

FTIR mode	*Strategy*	*Procedure*	*Requirements*
Specular Reflection	Polished cross-section	Embedding in a synthetic resin and polishing	Shiny / flat surface
Transmission	Thin sections	Microtoming of samples embedded in paraffin, acrylic, polyester or epoxy resins	4-5 μm thickness
		Microtoming of embedded samples using barrier methods to prevent infiltration	
		Diamond cell squeezing of the sample	
		Polishing of KBr pellet system	

Several strategies for transmission experiments were tested and evaluated in order to study the painting technique of a group of samples. To this aim, SR μFTIR imaging was the chosen technique.

The mineral charge of the samples suggested the use of embedding strategies to increase the success of the operation. A system such as squeezing of the sample by using diamond micro-compression cells would avoid contamination of the sample but preventing the completely destruction of the sample is clearly a difficult matter [1, 29]. However, even if the positioning of the sample allows the maintenance of its layered structure, distributional information within the layer is lost due to the distortion on squeezing. That would not be a problem when the scope of the mapping is to study the use of materials in the different layers but would represent an important lost of information when trying to establish degradation mechanisms within and between layers.

1.2. Experimental Section

1.2.1. Embedding methods

Samples were embedded in a polyester resin polymerised by a peroxo organic hardener (Cronolite E.I., Spain). Cicular Sylicon moulds were filed with 2 ml of resin left to dry for 1 hour before putting the sample. This way the sample disposition could be controlled by working under the steromicroscope. Once added other 2 ml of the resin on the top of the samples, 48 hours in a desiccator are required for the complete hardening of the resin.

Epoxy (Spurr resin) embedding was performed in two separate stages: the first one to create polymerised layer of resin by introducing the mixture in half a BEEM mould and drying it at 60 ºC; the second one adding the sample on top of the already dried resin and new resin mixture to cover it. Drying again for 48 hours was necessary before cutting.

Paraffin embedding consisted in introducing hot paraffin in a metallic mould with a belly form. Once the belly was filled with paraffin, the sample was also situated inside it. After that, paraffin is added to cover everything. Before cutting the mould was left at least 30 minutes at 4ºC to harden it.

These procedures have been already described in the literature [47, 48, 49, 50, 51].

1.2.2. Samples

Decorative painting samples from significant Catalan buildings were selected. Samples are from different periods and locations, uses and support type. Table 1.4 presents a description of the samples and their provenance.

Sample SMM4 comes from a depicted beam. The design showed some faces and decorative motives in different colours mainly blue, red and black.

Sample AG2, from the Romanesque portico of Agramunt, exhibits several painting layers probably due to ancient restorations and re-paintings during its lifetime.

Sample PGe 2/4 comes from the ceiling of the called 'Gold Room' in the medieval palace of the Catalan Government (Saló Daurat, Palau de la Generalitat, Barcelona). Probably the decoration of the ceiling has been done in the 17th century and restored several times since then.

Sample B5 and P1 to P4 comes from the Royal Palace of the monastery of Santes Creus. B5 was sampled in a beam from the 15th century (probably restored later on) showing the design of the Catalan shield (red and yellow lines).

Samples P1 to P4 come from a wood door coated with silver and painted on top of the metallic leaf with the aim to resemble marble. Samples have been taken from the surface of the silver layer.

Some pictures of the works of art from which the samples have been collected are showed in Figure 1.4.

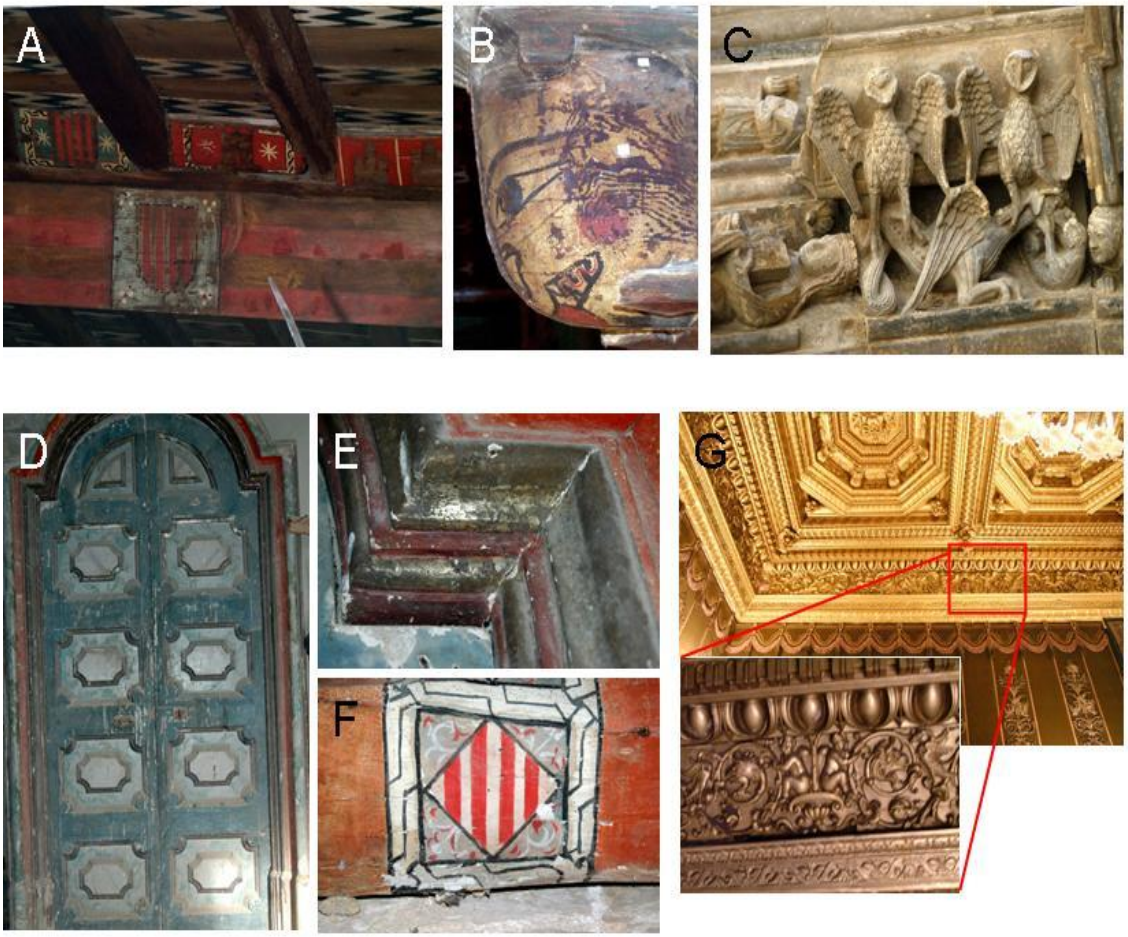

Figure 1.1. Sampled works-of-art (A) and (B) beams in Sant Miquel de Montblanc; (C) detail of the Romanesque portico of Agramunt; (D) and (E) silver door and a detail of it and (F) beam showing the Catalan shield, from the Royal Palace of Santes Creus; (G) ceiling of El Salo Daurat of the Generalitat Palace, and a detail of the sampled area.

Table 1.4. Samples prepared for SR micro FTIR experiments in transmission mode at station ID 21 (ESRF).

sample	*Procedence*	*Description*	*Sample build-up*	*Complementary results*[1]
SMM4	Sant Miquel de Montblanc (church, 13th century)	Decorative paintings on a beam (13th century)	Figure 1.8. B	indigo (layer 1) minium (layer 2) cinnabar (layer 3) polysaccharide material *Pinaceae* resin
AG	Romensche church of Agramunt (12th century)	Painting on the Romanesque door decoration (13th century)	Figure 1.20 B, C	aged siccative oil, pine resin, egg and a glycosidic material, lead white, cinnabar and indigo.
PGe 2/4	Generalitat Palace (15th century)	Gold ceiling decoration	Figure 1.13. A, B	
P1	Royal Palace of Santes Creus Monastery (14th century)	Silver door (17th century)	Figure 1.23. E, I	-
P2			Figure 1.23. F, J	-
P3			Figure 1.23. G, K	-
P4			Figure 1.23. H, L	-
B5	Royal Palace of Santes Creus Monastery (14th century)	Wood beam (16th century)	Figure 1.11	-

[1] Conventional FTIR, Py/GC/MS, GC/MS, SEM-EDS

1.2.3. Apparatus

- Microtome Ultracut E with a tungsten knife for slices of less than 12 μm was used at the ESRF laboraotries. Microtome Leica Ultracut UCT with a glass knife for slices of 10-15 μm was used at the PCB (University of Barcelona).
- Microtome Ultracut E (Reichert-Jung) with a diamond knife for slices of 6 to 14 μm was used at the PCB (University of Barcelona).
- Piramiton Leica EM Trim was used for the trimming process of the resin blocks before microtoming.
- Micromesh regular silicon carbide discs were used for polishing the surface of the cross-sections. Grits from 1500 to 12000 (BCP Instruments) were chosen.
- Bomem MB-120 Fourier Transform Infrared Spectrometer, equipped with a Spectra-Tech Analytical Plan microscope, was used with the diamond cell, as a sample holder. The spectrometer has a KBr beam splitter and a Globar source. The microscope has its own mercury cadmium telluride (MCT) detector refrigerated with liquid nitrogen. Spectra were recorded between 4000 and 720 cm^{-1} with a resolution of 4 cm^{-1} and an accumulation of 100 scans.
- Synchrotron radiation Fourier transform infrared microspectroscopy (SR FTIR) in transmision mode was performed at the station ID21 at the European Radiation Synchrotron Facility (ESRF, Grenoble). Experiments were performed with a Nicolet Continum microscope coupled to a Nexus spectrometer (www.esrf.fr/UsersAndScience/Experiments/Imaging/ID21). Resolution was fixed at 8 cm^{-1}. In all cases the aperture and the step size chosen generates overlapping areas in order to increase the resolution of the components. The step size and the number of accumulated scans were changed depending on the characteristics of the sample. Measuring conditions for the samples described above are reported in Table 1.5

Table 1.5. micro FTIR transmission experiments conditions summary.

Sample	*Slice thickness / µm*	*Beam size (Aperture) / µm²*	*scans*	*Step size / µm* [2] *(ii)*
SMM4	6	8x8	100	-
	12	8x8	50	6
AG	12	8x8	50	-
	12	10x10	50	8
PGe	12	6x6	50	6
	12	6x6	50	6
	10	8x8	128	6
	12	6x6	50	6
P1	6	8x8	50	4
P2	6	8x8	75	4
P3	4	8x8	40	4
P4	6	8x8	40	6
B5	12	8x8	50	6

- Imaging of functional groups was performed by using the OMNIC software (Thermo Nicolet Instruments).

1.2.4. Data interpretation

Table 1.6. shows the characteristic bands of the reference materials identified based on the data reported in the literature [5,40,52, 53, 54, 55, 56,57]

[ii] when mapping or linescan performed

Table 1.6. Summary of the materials identified in the samples, the FTIR bands observed in the spectra and the bands used for the mappings.

Material	*Formula*	*FTIR bands identified in the spectra*	*Vibration*	*Bands mapped*
Calcium sulphate	$CaSO_4.n\ H_2O$	3515, 3400, 3290 1680,1620, 1150	OH st OH bd SO42-	All
Calcium Oxalates	$CaC_2O_4.nH_2O$	1650 1315		(1[iii])
Indigo		1630,1480,1320, 1099,1073		-
Prussian Blue		2090	CN st	-
Azurite		3420 1516, 1464, 1416 1089 951, 831		3420 1400 ([iv])
Kaolinite		3715, 3650, 3626 1100-1000	OH st Si_O	3620
Clay		1050-900	SiO st	1010 990
Lead white	$PbCO_3$	3540 1400 1044	OH st CO32-	-
Calcite	CaCO3	1400 890	CO32-	1400 ([iv])
Proteinaceous material	-	3280 3080 shoulder 1640 1530 1415	 Amide II overtone Amide I Amide II C-C	3290 1650 ([i])
Polysaccharide material	-	2930 broad 1000-1150	CH st C-C	-
Lipid material	-	2930, 2850 1730-1715([v]) 1240,1156 1620,1530([vi])	CH st C=O st C-C MCOO	2929 1715 1620 1530

[iii] 1650 cm^{-1} broad band present in some spectra has been considered as the result of the sum of the OH bd bands of gypsum (1680 and 1620 cm^{-1}) with a band a around 1640 cm^{-1} from other materials in the layer such as calcium oxalates band in the presence of the other oxalates band at 1315 cm^{-1} or the Amide I band of a proteinaceous materials in the absence of oxalates.

[iv] Distribution of the broad band at 1400 cm^{-1} corresponds to the carbonate vibration. Identification of the kind of carbonate present (calcite, lead white or azurite) has been done by the study of individual spectra.

[v] C=O st band of esters (1730 cm^{-1}) is overlapped with the embedding resin band. Carboxylic acids formed by ageing present a C=O st band at 1715 cm^{-1}.

[vi] Metal Carboxylates have been also used as indicative of the presence of an oil and thus used to identify and map a lipidic material

1.3. Results and Discussion

1.3.1. Synthetic resin embedding and microtoming: issues for the preparation of multi-layer thin sections from painting samples

Embedding samples in a synthetic resin derives from the biomedical field [47,48,49,50,51]. Paraffin, polyester and epoxy resins were tested in order to compare their characteristics and advantages for embedding painting samples. Table 1.7. summarizes the characteristic transmission IR bands of the resins used for embedding samples (paraffin, epoxy and polyester) and Figure 1.2. shows the transmission FTIR spectra of the three resins used.

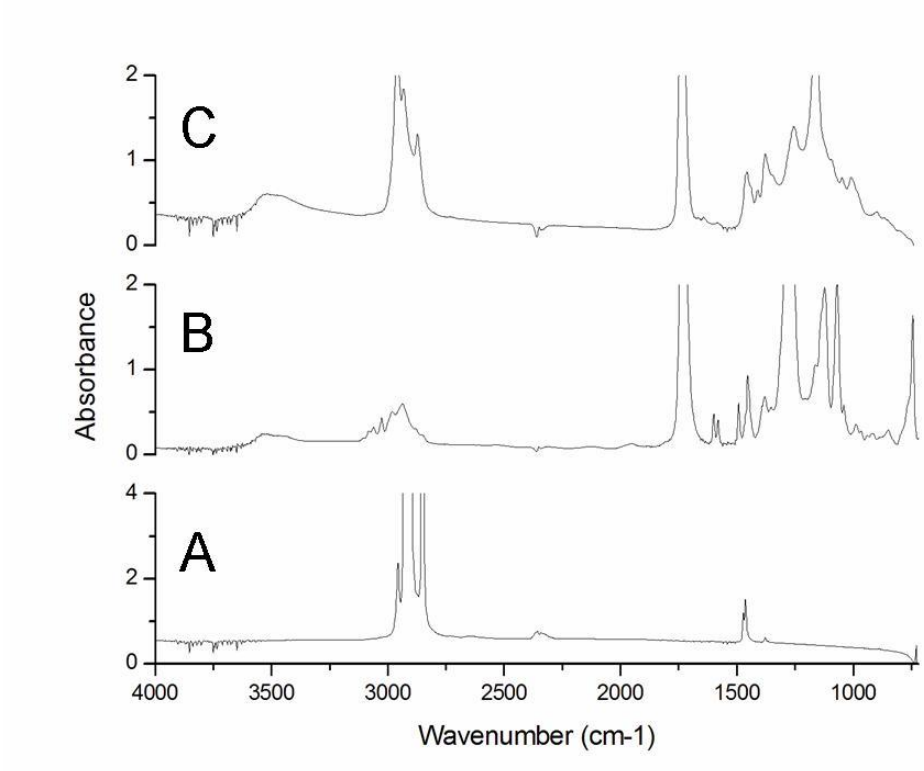

Figure 1.2. Conventional transmission FTIR spectra of the three resins. (A) paraffin, (B) polyester, (C) epoxy. Conditions were as follow: resolution 4 cm^{-1}, number of scans 100, wavelength range 4000-720 cm^{-1}.

Table 1.7. FTIR transmission bands of the resins tested for embedding the samples.

	Paraffin	*Epoxy*	*Polyester*
CH st	2917 2847	2961 2935 2871	3066 3029 2987 2940 2882 2852
Carbonyl bands	-	1736	1736
Vinyl st and bd			1601 1579
Characteristic fingerprint region bands	1472 1464	1457 1415 1377 1261 1161 1049 1005 901	1493 1453 1381 1282 1125 1067 984 847 743

1.3.1.1. Paraffin

Paraffin was evaluated as a possible embedding medium with a extremely moderate number of bands on the mid-IR (Table 1.7. and Figure 1.2.): its use would allow to obtain spectra with a minimum interference of the embedding medium.

Several issues should be considered when working with paraffin, mainly the lack of information on the sample disposition in the paraffin block, due to its opacity, and the difference in hardness between the sample and the paraffin.

The transparency of the paraffin block was increased by adding grinded KBr to the melted paraffin as suggested in the literature [5]. Different ratios KBr: paraffin (1:1, 2:1 and 4:1) were tested in order to establish the better conditions. While the ratio 1:1 do not present clear improvements respect to the use of paraffin alone, some improvement could be observed by using higher amounts of KBr. No difference could be determined between ratios 2:1 and 4:1.

However, it was impossible to obtain a section under 15 µm of thickness due to the big difference in hardness between the sample and the paraffin media: samples were completely lost leaving a hole in theri place when trying to obtain thinner slices. Moreover, using a refrigerating system while microtoming, changing both the knife orientation respect to the paraffin block and the knife angle demonstrated little improvement in the obtained results.

Different slices of a sample made by changing the orientation and the angle of the knife on microtoming are reported in Figure 1.3. and Figure 1.4., respectively.

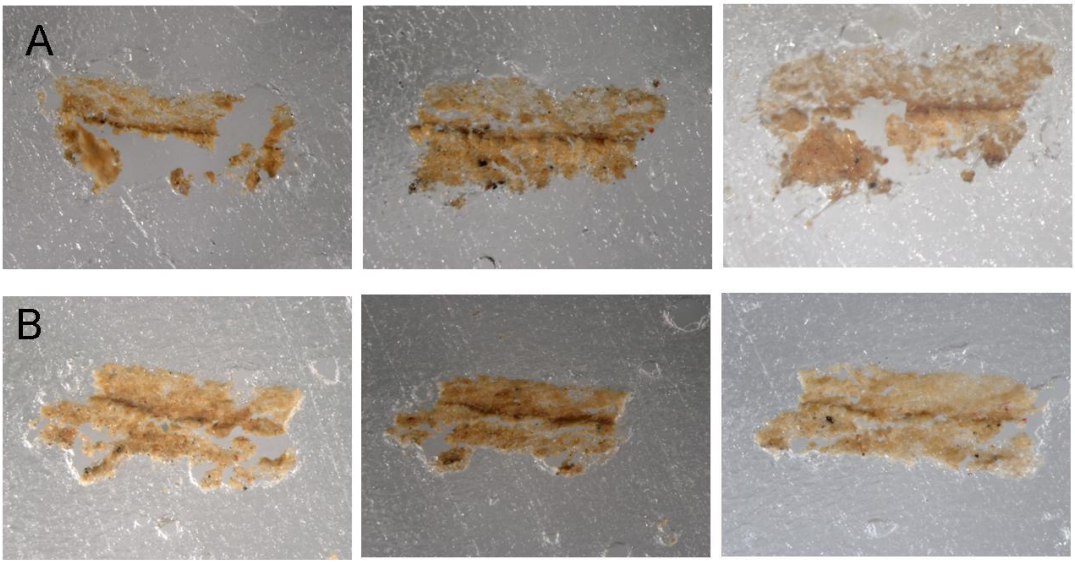

Figure 1.3. Different slices of a sample embedded in paraffin. All slices are 20 µm thick. (A) horizontal orientation of the knife respect to the paraffin block. (B) vertical orientation of the knife. The quality of the slices is not homogeneous though maintaining the conditions. Knife angle was 5 º in all the slices. All slices are obtained from the same block.

Figure 1.4. Different slices of 20 µm thick of a sample embedded in paraffin. Knife angle changes from 10 º(A) to 5º (B) and 0º(C).

1.3.1.2. Epoxy and Polyester resin

Epoxy and polyester embedding resins were evaluated as embedding media. We tried by mounting the cross section in the resin and then microtoming it. Trapezoidal silicon moulds (BEEM moulds) and a pre-microtoming step of trimming had been used to reduce the quantity of resin around the sample (with a different hardness) when cutting. Both resins are characterized by a low viscosity that facilitates their infiltration in porous samples and by being highly absorbent materials presenting a high number of bands in the mid IR region (Table 1.7.).

Epoxy resin (Spurr), though being a little bit yellow and curing at 60 ºC, was easier to cut than polyester blocks, and was thus adopted.

Some practical issues raise when embedding painting samples from works-of-art. In order to show how the sample processing allows to obtain reliable results, some of the samples studied (Table 1.1.) are presented here to illustrate the problems presented. They were selected as characteristic examples from several problems arisen. Samples have been all embedded in epoxy resin.

1.3.1.2.1. Infiltration of the embedding media

The relative content of inorganic materials present in decorative samples facilitates the infiltration of the embedding media into the painting layers. Infiltration clearly makes the interpretation of the spectra more difficult and can completely prevent the mapping of functional groups overlapped with resin bands when it occurs. As a result, when the penetration of the embedding medium occurs, sample binding media are difficult to identify due to the overlapping of the main peaks, such as the carbonyl stretching band (1650-1750 cm^{-1}) or the aliphatic CH stretching bands (2800-3000cm^{-1}), with the resin ones. However, the presence of the embedding resin, being a continuous medium in the slice, facilitates the preservation of the physical integrity of the sample [4,29]. In

the presence of infiltration, the material identification should be provided by other techniques such as conventional FTIR or mass spectrometric based techniques for a reliable interpretation of the functional group distribution. Once the composition of the sample is known, in fact, the distribution of materials can be reliable, though based on few bands.

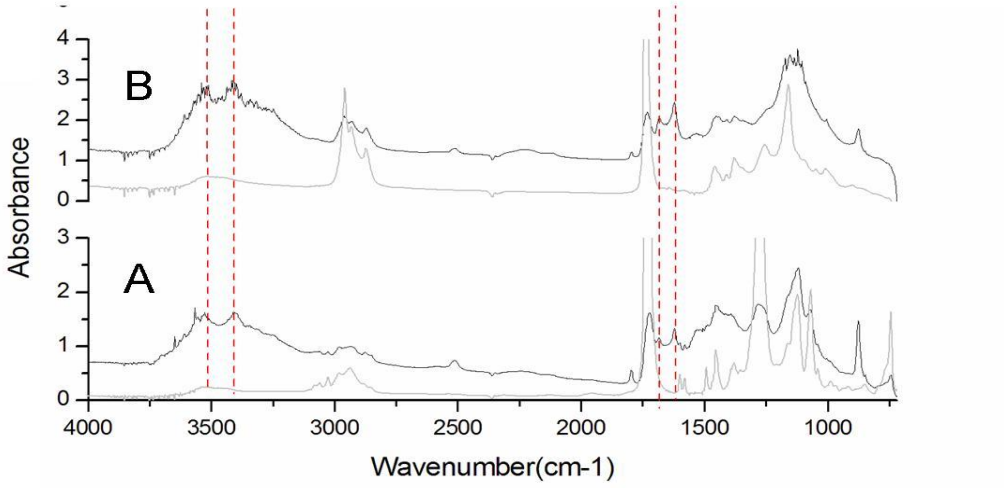

Figure 1.5. Spectra of the same sample embedded in the polyester resin (A), epoxy resin (B). Reference spectra of the resins are also reported in grey for comparison. IR peaks corresponding with the resins used as embedding medium can be observed. The absorption bands relative to some inorganic functional groups corresponding to gypsum or carbonates are the only bands different from those of the embedding resin. Peaks of the resins have been reported above in Table 1.7.

1.3.1.2.2. Lost of particles and crumbling of layers on microtoming

Particles that constitute the different painting layers are often bigger than the thickness needed for transmission experiments (4-10 μm) due to the impossibility to obtain smaller particle from the grinding process. Therefore, depending on the sample nature, it is almost impossible to obtain an entire microtomed cross-section thin enough due to the loost of inorganic material during the microtoming process. Figure 1.6. presents the

photomicrographs of the thin sections of some samples exemplifying the lost of inorganic content.

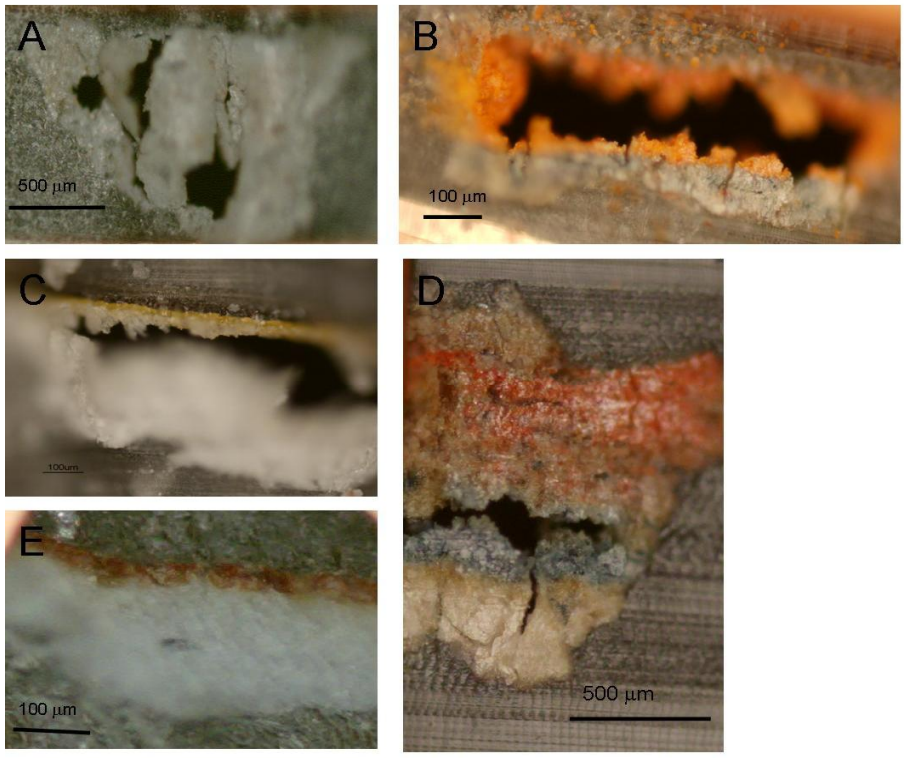

Figure 1.6. 12 µm slices of samples embedded in epoxy resin, presenting partial or complete lost of particles on microtoming: (A) SBB2; (B) SMM4; (C) VIC 7; (D) AG2 samples; and (E) P2 sample presenting all layers

As reported in the literature [5] the orientation of the sample respect to the knife can improve the results. Mainly, cutting following the layers direction usually helps in maintaining the layers, with different physical properties, together. However, each sample presented its own particularities and thus a general rule could not be established for the better microtoming of thin sections. Finally, orientation of the knife respect to the block was also considered. In our case, working with 5º to 10º was the orientation chosen.

Using a tungsten or diamond knife, thinner sections (4-6 µm) were generated more efficiently than with a glass knife and also the amount of embedding medium that could be detected in the IR spectrum was lower. That would suggest that the contamination of the embedding medium was due not only to the infiltration into the sample but also to the resin carried away when cutting that remained onto the surface

of the section. Thus, when sections thinner 10 µm were needed, a tungsten knife was used. Figure 1.7. shows the same sample cut with a glass and W knife, as well as the spectra corresponding to similar areas in the thin section obtained.

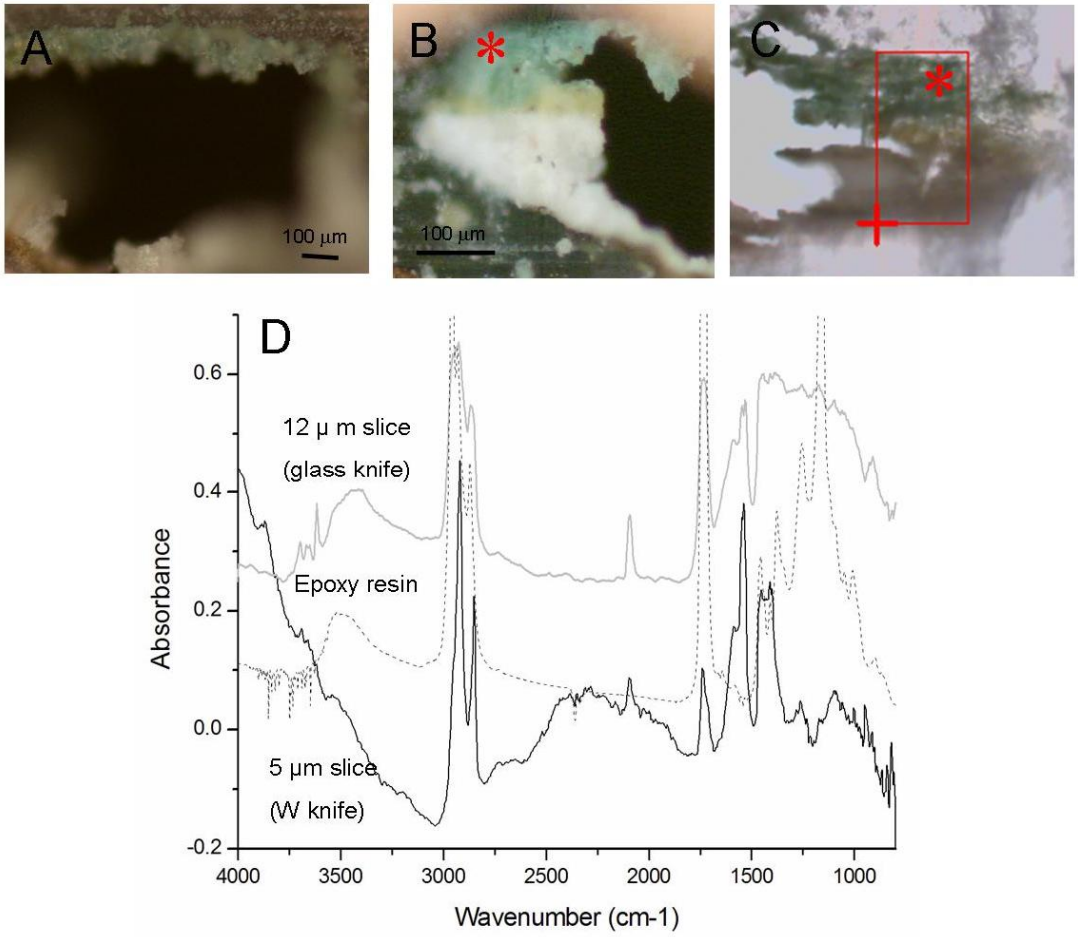

Figure 1.7. Sample VIC 5 thin sections embedded in (A) paraffin (B) epoxy resin and microtomed using a glass knife (12 µm); (C) epoxy resin and microtomimg using a W knife (5 µm); (D) comparison of the spectra spectra obtained in the point marked with at * in B(grey line) and C (black line). Epoxy bands peaks (dotted line) can be noticed in B but not in C .

Case Study I. Sample SMM4 (Sant Miquel de Montblanc, Beam)

The sample SMM4 fragment, cross-section and thin slice are reported in Figure 1.8. The sample cross-section showed three paint layers (indicated with a number in a grey square in the Figure): a blue layer on the bottom (layer 1), a red one in between (layer

2) and a red one on top (layer 2). Figure 1.8.C shows a first slice of 12 µm presenting just 2 of the layers. The red layer is almost lost and a big hole has been generated in the central part of the sample. Just some red can be appreciated on the left and right ends.

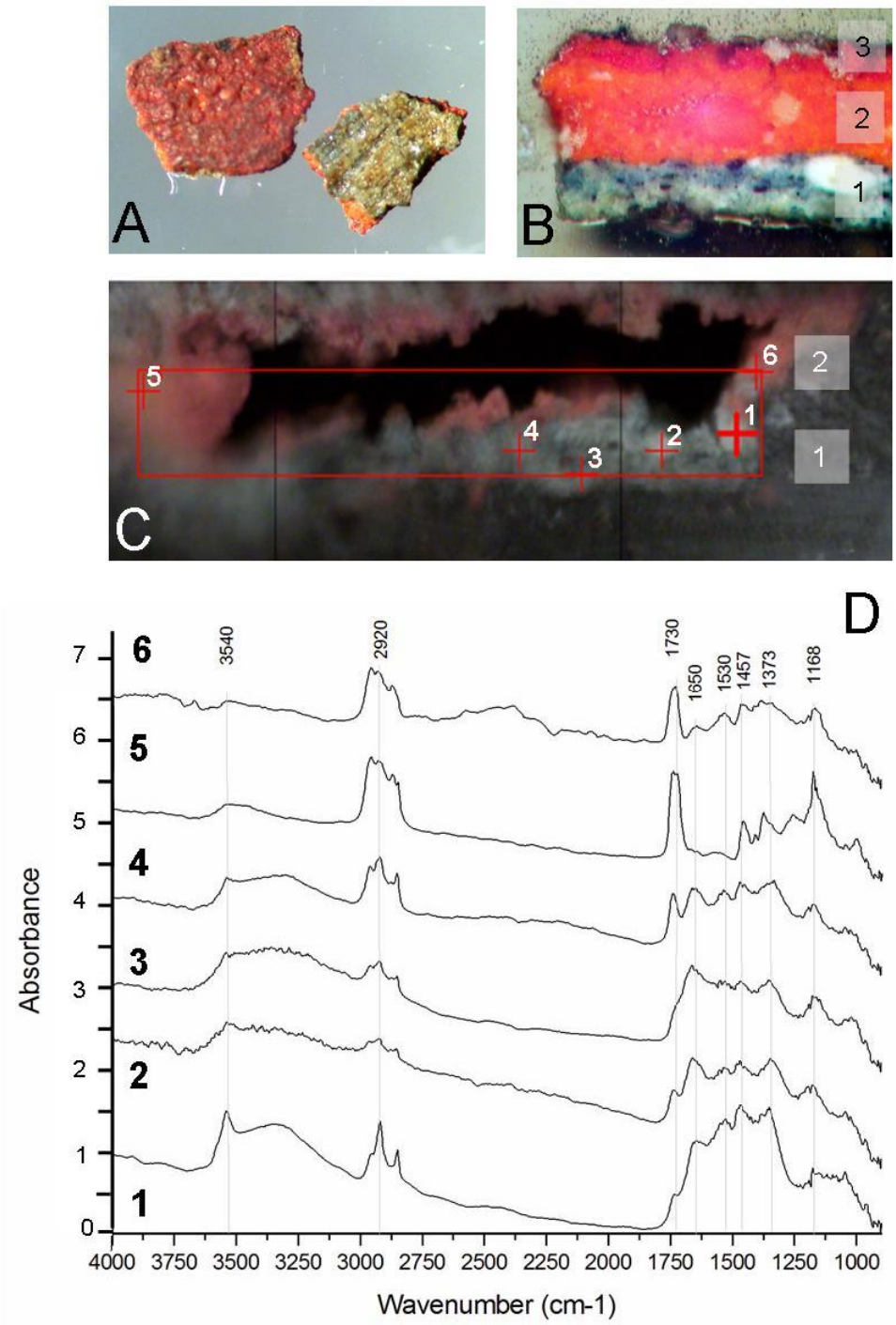

Figure 1.8. Sample SMM4 (A) stereomicroscope image of a fragment; (B) optical microscope image of the cross-section (layers indicated with a number in a grey square); (C) optical image of a 12 µm slice microtomed with a glass knife (numbers highlighted by a red square correspond to the spectra reported in D); (D) spectra of selected spots in the 12 µm slice reported in C.

Figure 1.8.D presents the spectra of selected points in the slice (numbers 1 to 6 highlighted by a red cross in the photomicrograph). Spectra are of low quality with sloping baseline and low signal-to-noise ratio. Some characteristic features of the embedding resin can be observed in almost all the spectra:

- Specra 5 and 6 (corresponding to the red areas next to the embedding resin) present mainly just the peaks of the resin (Table 1.7.).
- In spectra 1 to 4, lead white (3535 and 1400 cm^{-1}) and characteristic features of an organic material (CH st bands at 2929, 2851 cm^{-1}), can be identified.

A second slice 6 μm thick (microtomed using a W knife) is shown in Figure 1.9. presenting also the same two layers. The slice is complete thus presenting an area of the red layer to be analysed. However, the selected spectra of different areas easily highlighted the low quality of the slice. Probably the real thickness of the slice is not 6 μm and the thickness is not regular enough. Spectra intensity check shows that area 2 spectra present just 0.2 absorbance while there is no signal at all in area 3. In fact, mapping of the bands highlighted in the spectra show how all the right side of the slice is not able to be mapped. Thus mapping is not possible as not representative of the real chemical distribution of the bands. Identification of some materials is still possible mainly in the spectrum 1.

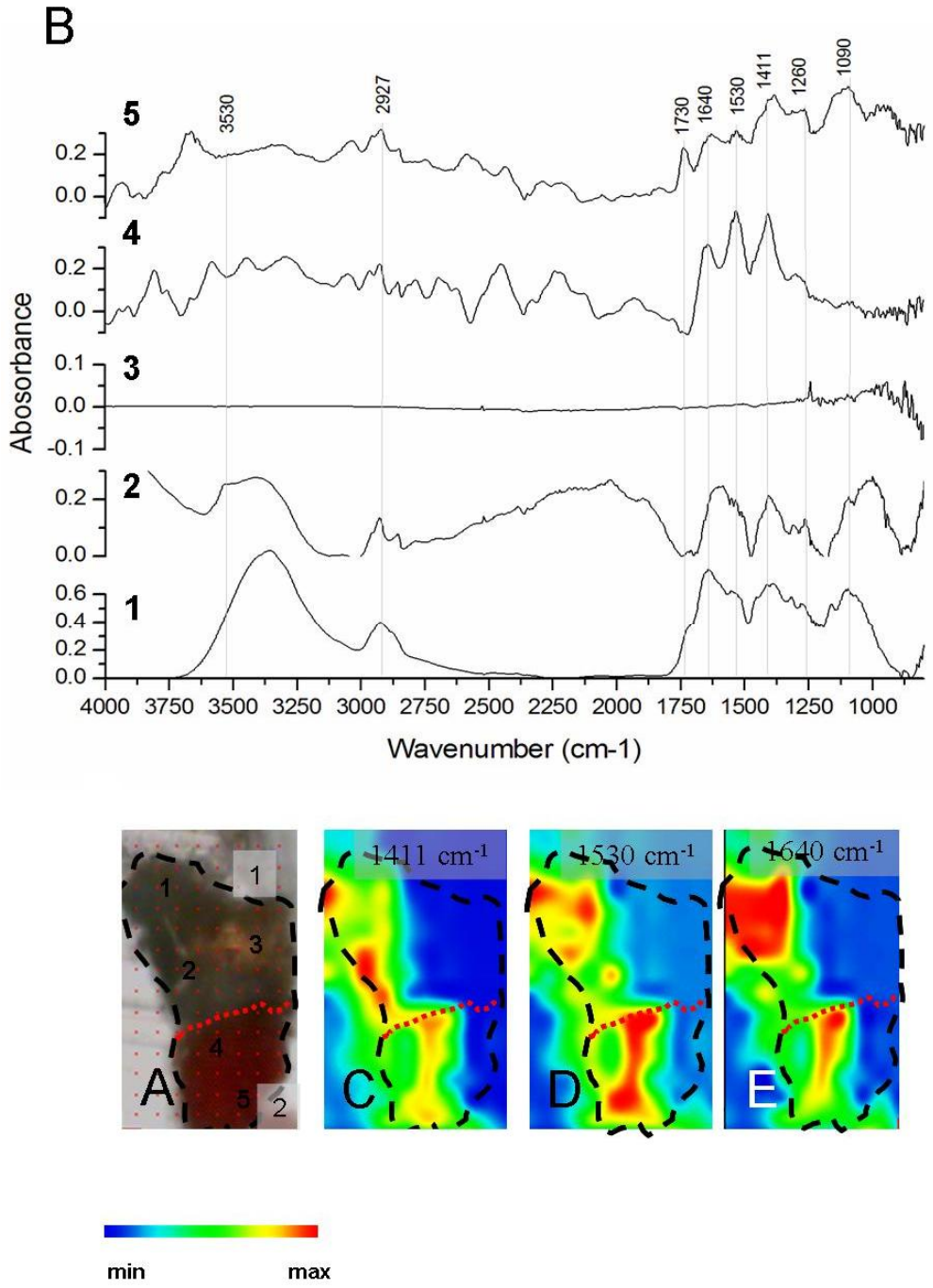

Figure 1.9. Sample SMM4 (A) 6 μm thick slice (sample layers are indicated in a grey square); (B) spectra of the selected areas in the slice photomicrograph; chemical images of (C) 1411 cm^{-1}; (D) 1530 cm^{-1}; (E) 1640 cm^{-1}.

Figure 1.10. compares the spectra of both points 1 in the slices. By the presence of the characteristic peaks at 3545, 1400, 1041 and 1630, 1480, 1315, 1073 cm^{-1} lead white and indigo blue are identified in the blue layer (layer 1 of the cross-section). A proteinaceous material seems to be indicated by the band at 3285 cm^{-1}, the characteristic shoulder at 3080 cm^{-1} and the amide bands at 1640-50, 1540 cm^{-1}. The presence of indigo has been confirmed by HPLC while the proteinaceous material has been characterized as egg by GC/MS.

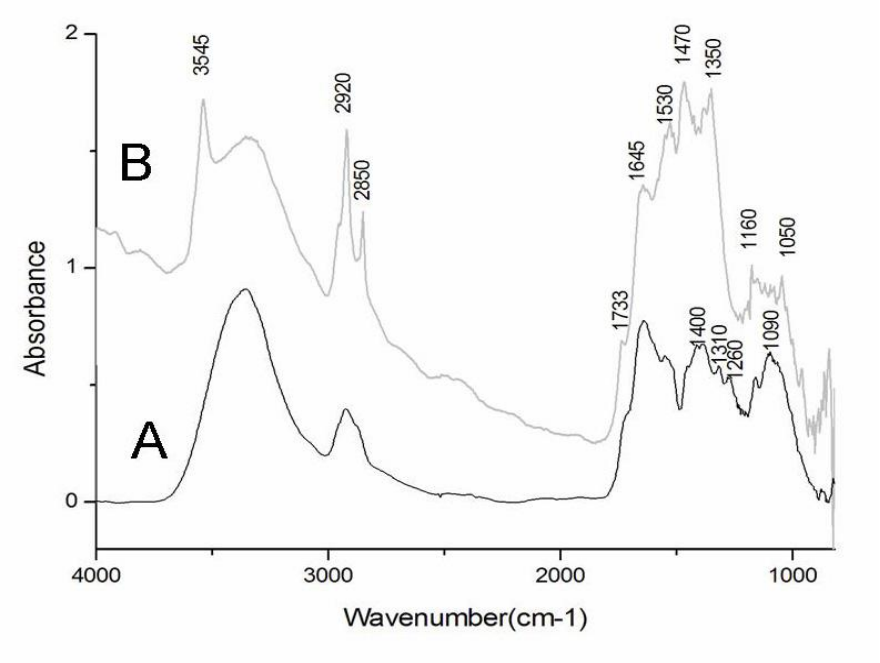

Figure 1.10. Spectra of the areas 1 of the (A) 6 μm thick slice; (B) 12 μm thick slice.

These results highlight that, although sample SMM4 characteristics allowed obtaining a thinner slice by using a W knife, the spectra quality did not improve enough to allow reliable imaging of functional groups.

1.3.1.2.3. Flattening of the slice

When slices were flat enough, they were placed directly under the FTIR microscope to be analysed. However, in some cases flattening of the slice was necessary as FTIR lateral resolution is related to the slice flatness and capacity to focus [26]. Slices were

flattened by using diamond micro compression cells. The flattened slice was directly situated under the microscope when possible. In some cases, when it remained attached to one of the diamond cells, the diamond cell itself was situated under the microscope.

Case study II. Sample B5 (Royal palace of Santes Creus, Beam)

Figure 1.11.A presents the photomicrograph of the 12µm slice of sample B5. The thin section presented the two layers also identified in the sample build-up in Figure 1.11.J. Numbers correspond to the spectra shown in Figure 1.11.I.

The sample slice was not flat at all, so it was flattened with a diamond micro compression cell. The thin section obtained was put directly under the microscope. Spectra evaluation shows that:

- the spectra of areas 2 and 3, reported in Figure 1.11. I, are not of good-quality particularly baseline is not flat nor lever but sloping. Moreover, in the spectra of these areas some infiltration of the embedding medium can be appreciated (CH st range 2950-2800 cm^{-1} and CO st 1750-1600 cm^{-1}).
- the spectrum of the preparation layer (spectra number 1) is a good quality spectrum and it allows to identify the presence of an oil as binding medium.
- similarities with the spectrum of the area 4 suggest the presence of an oil in the pictorial layer, as well. Peaks at 1019 cm^{-1} are characteristic of a clay.

Chemical images reported in Figure 1.11. B to H show that:

- infiltration in the sample is minimal: mapping of the characteristic peaks of the embedding resin (2950 and 1730 cm^{-1}) are located all around the sample.
- the characteristic peaks of carboxylates at 1630 and 1520 cm^{-1} are coincident and corresponding with the preparation layer as well as the distribution of the bands characteristic of a lipid material (2929, 1715 cm^{-1}).
- mapping of the peak at 1010 cm^{-1} confirms the presence of clay in the pictorial layer.

Thus in the case of the sample B5, information on the distribution of materials and identification of materials present (also organic materials) was possible by individual

evaluation of the spectra. Imaging of functional groups was also reliable in this case after flattening the 12 µm thin section.

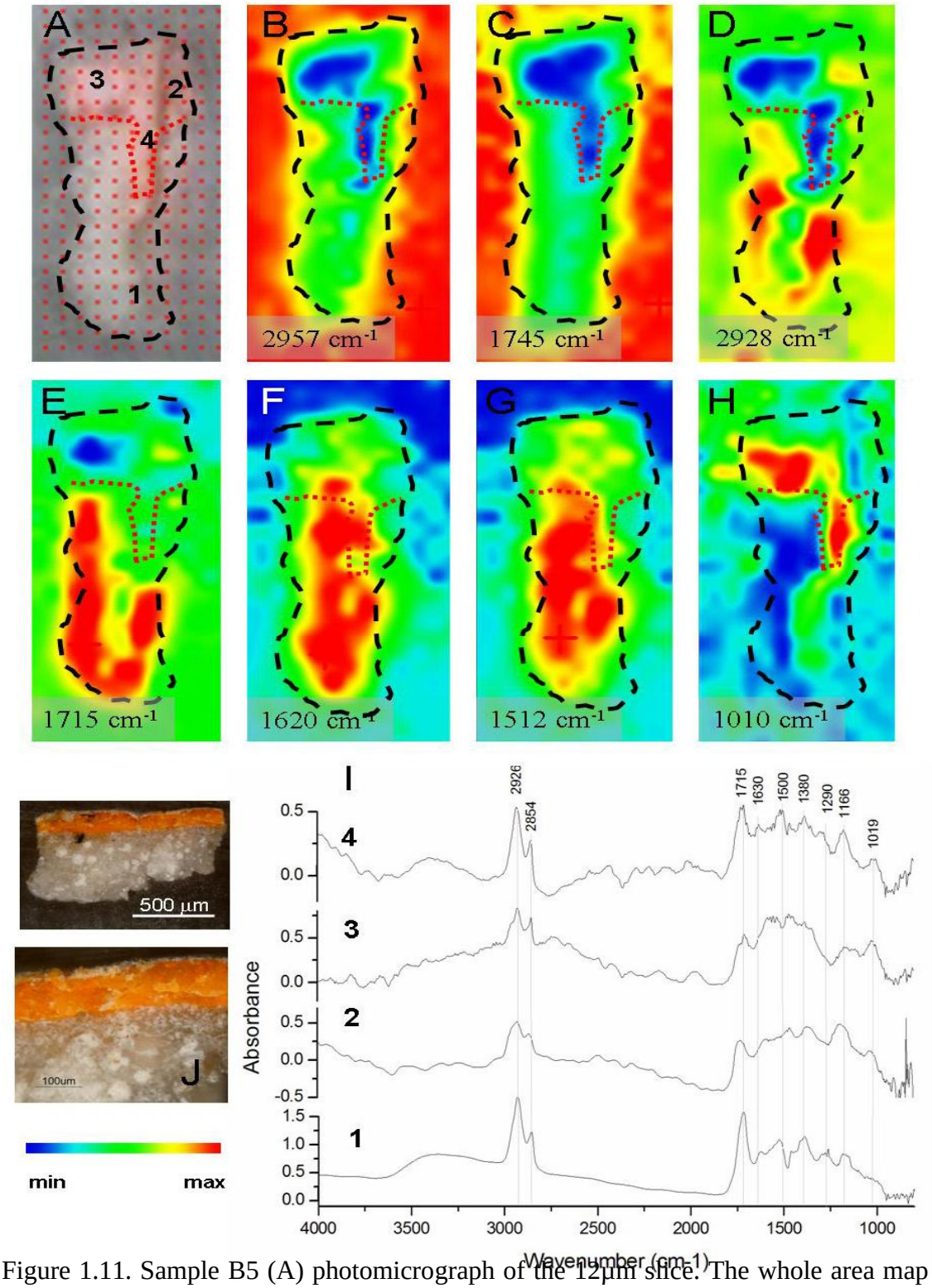

Figure 1.11. Sample B5 (A) photomicrograph of the 12µm slice. The whole area map is reported. Numbers correspond to the area where spectra shown in (I) are reported; chemical images of (B) CH st and (C) carbonyl st of the embedding resin; (D) CH st and (E) carbonyl st of the binding medium; (F) and (G) carboxylates; (H) clay; (I) spectra representative of the areas indicated by numbers in (A); (J) optical microcopic images of the sample build-up.

1.3.1.2.4. Paraffin protection of the slice on microtoming

Paraffin was directly applied on the surface of the resin block when cutting the slice, as a method to avoid the crumbling of the layers and the lost of the sample. Once the thin section was cut, paraffin was eliminated from the surface of the slice by using liquid nitrogen. In some of the samples the thin section obtained contained all the layers though improvements were not observed in all cases. Moreover, paraffin was not completely eliminated from the surface of the slice in some cases. Spectra of these samples present also the contamination of paraffin and an irregular and higher width than that theoretically obtained when microtoming. Figure 1.12. shows different slices of the sample PGe4 using different strategies.

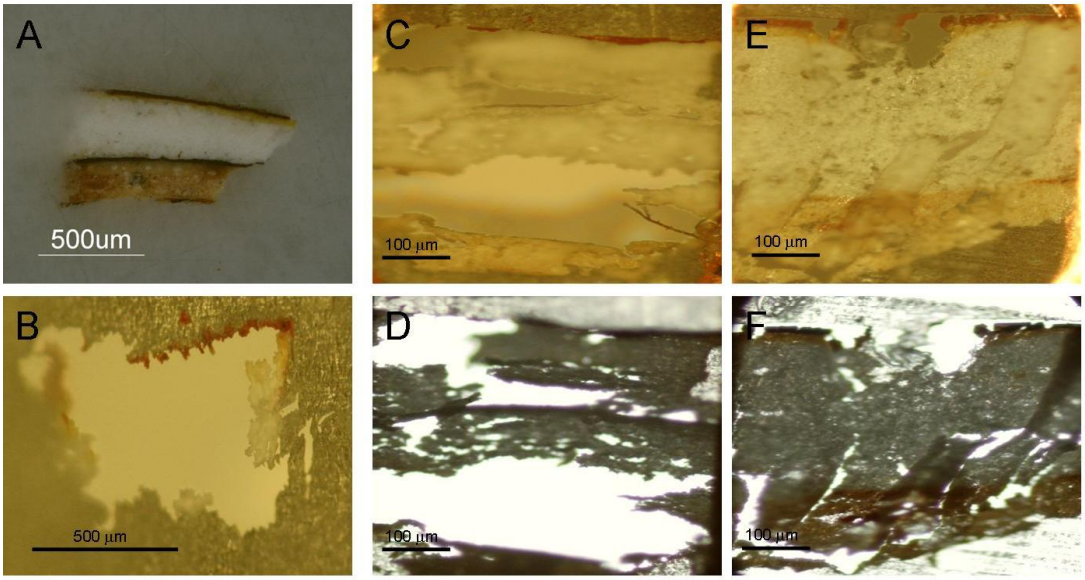

Figure 1.12. Sample PGE 4 sections: a one side polished KBr pellet (A), paraffin microtomed thin section (B), epoxy resin 14 µm slice (C, D) and epoxy embedded 14 µm slice using paraffin during the microtoming process (E,F).C, D and E,F reflected and transmitted light, respectively.

Case study III. Sample PGe2/4

Two slices of 12 µm from the same embedded fragment are reported in Figure 1.13.D. Thin sections present just the layers on top of the sample stratigraphy presented in Figure 1.13.A. and reported in Figure 1.13.B. Checking the quality of the spectra in some points of the area map demonstrates that quality is not good (low signal-to-noise ratio, absorbance lower than 0.5) and infiltration of the embedding resin occurred. However, the presence of kaolinite in the red layer by the characteristic OH st at 3715, 3650, 3626 cm^{-1} and the SiO st at 1100 and 1000 cm^{-1} and the calcium sulphate bands (3535, 3400, 1680, 1620, 1150 cm^{-1}) in the preparation layer are easily identified in both slices.

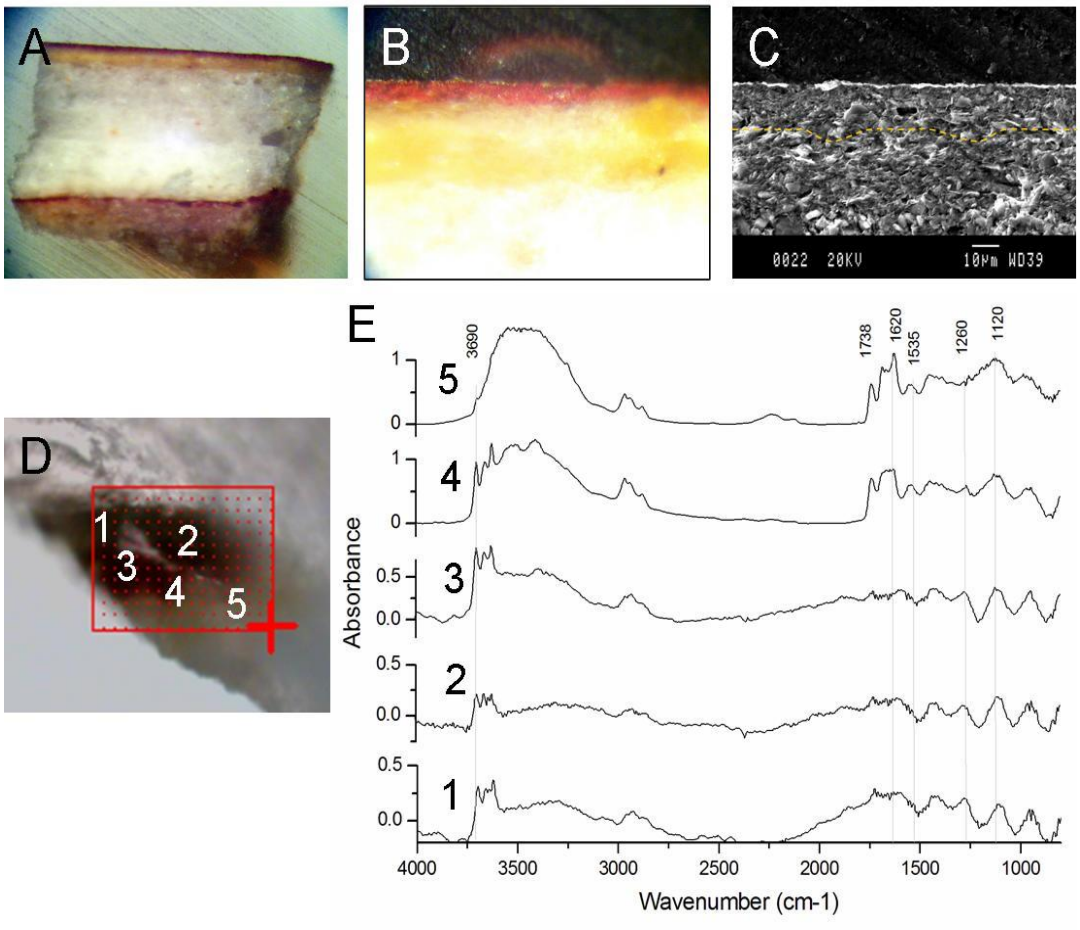

Figure 1.13. Sample PGe2/4 (A) optical microscope image of the cross-section; (B) detail of the cross-section (area on the top of A); (C) SEM image of the same area; (D) photomicrograph of the 12 µm microtomed slice (numbers correspond to the spectra in (E) spectra of different areas of the thin section.

A 10 µm slice from a different fragment embedded, showing the red layers (preparation of the gold leave) and the white preparation layer, is reported in Figure 1.14.A. the spectra in Figure 1.14.B were of good quality (no sloping baseline, high signal-to-noise ratio, intensity around 1.0 absorbance) and minimum infiltration. Interpretation of the spectra suggests:

- the presence of the clay (kaolinite) in the red layer (already identified in the 12 µm slice)
- the presence of gypsum (OH st and bending) in the preparation layer.
- the presence of a proteinaceous material: though the ratio of the Amide I: Amide II bands is not correspondent to that of a proteinaceous material due to the presence of the OH bd bands of gypsum in the same wavelength range, the proteinaceous material is confirmed by the characteristic peaks at 3280 cm-1 and a shoulder at 3080 cm^{-1}.
- an intermediate area among the red and the preparation layers presenting features of both layers.

A false colour image of the bands of kaolinite (3618 cm^{-1}), gypsum (1620 cm^{-1}) and the band at 1650 cm^{-1} (probably resulting from the amide I band plus gypsum OH bd peaks) is in agreement with what was evidenced by studying the spectra showed in Figure 1.14C, D and E.

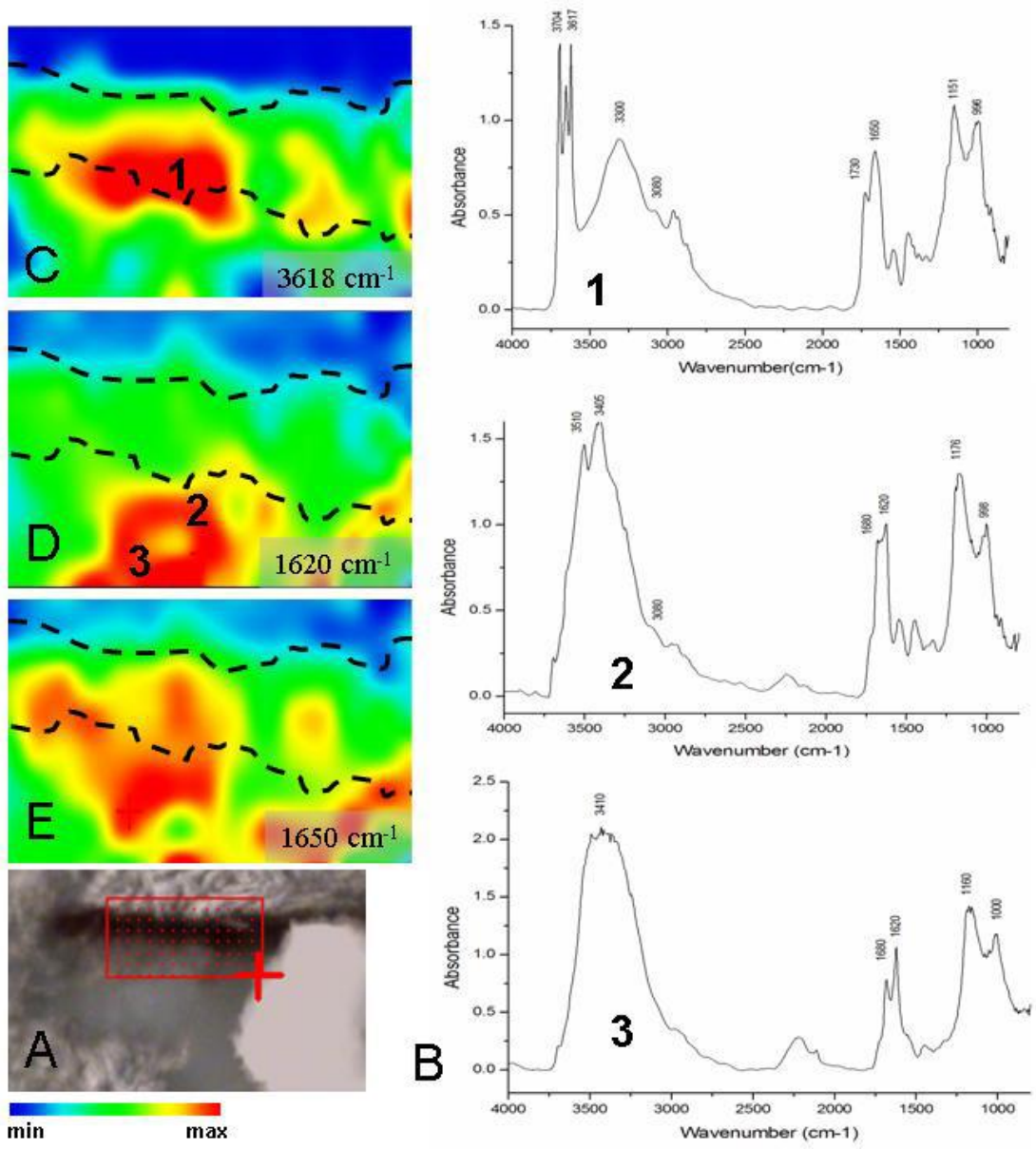

Figure 1.14. Sample Pge2/4 (A) optical microcope image of the cross-section of the 10 µm slice; (B) spectra of different areas of the thin section (indicated by numbers in the chemical images); chemical images of (C) 3618 cm^{-1}, (D) 1620 cm^{-1} and (E) 1650 cm^{-1}.

A lines can was tempted in order to highlight the main features of the sample spectra in depth. A line scan is obtained plotting the whole wavelength range of the spectrum versus position obtaining a representation of the spectra for different positions in a line on the cross-section. The line scan presented in Figure 1.15. shows :

- kaolinite features (three bands at 3700-3600 cm^{-1}) disappearing at the end of the red layer,
- the broad bands at 3500-3400 cm^{-1} of gypsum in the preparation layer,
- the band at 1650 cm^{-1} in the red layer changes to two bands (gypsum) in the preparation layer while the band around 3280 cm^{-1} disappears at the end of the red layer, confirming the localisation of the proteinaceous material in the red layer and not in the preparation layer.

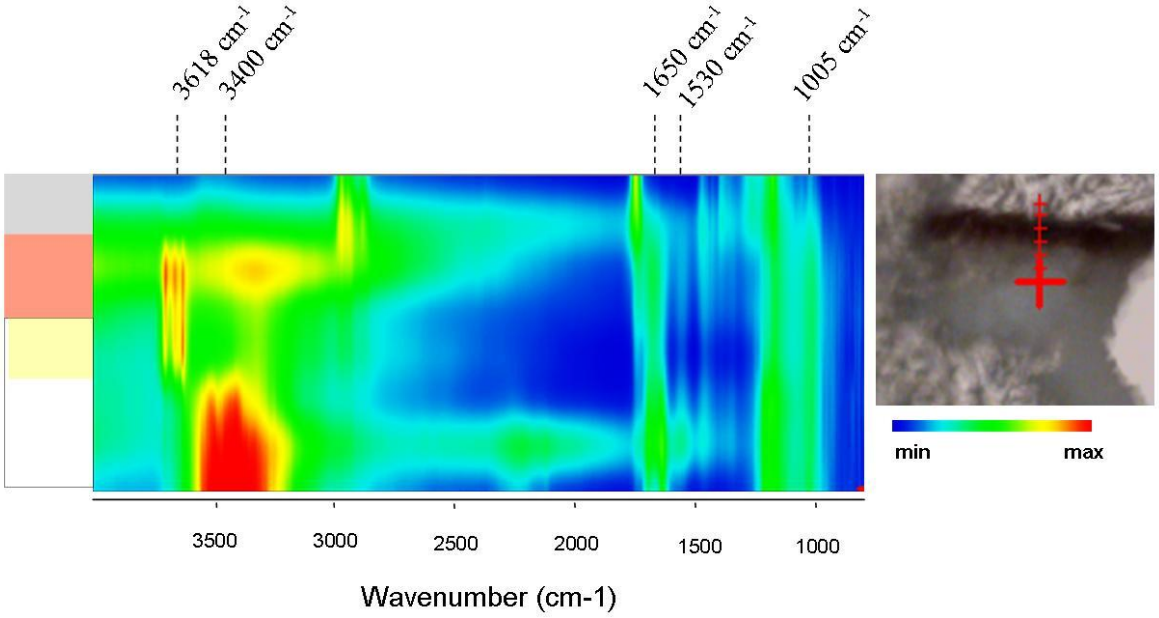

Figure 1.15. Line scan of the PGe 2/4 10 µm thick slice. The scheme of the sample stratigraphy presented on the left side of the line scan corresponds to the layers observed in Figure 1.14. B. .

Thus, line scan becomes an interesting tool to highlight the main features in the thin section spectra.

Finally, a 12 µm slice made by using paraffin in the microtoming process was flattened by pressing with the diamond micro compression cell. Sample PGe2/4 remained attached to both sides of the cell after the flattening. Figure 1.16. A and B shows both cells after the flattening. Figure 1.16 B can not be considered a reliable cross-section of the sample, while the cell shown in Figure 1.16. A contains all layers. False colour images of the distribution of gypsum (3535, 3400, 1620 cm^{-1}), kaolinite (3620 cm^{-1}) and the organic material (1650 cm^{-1}) could be generated being completely

correspondent with the layers of the sample. Spectra reported in Figure 1.17. showed the CH st bands ratio (3000-2800 cm^{-1}) altered by the presence of paraffin as well as the paraffin characteristic narrow band at 1435 cm^{-1}.

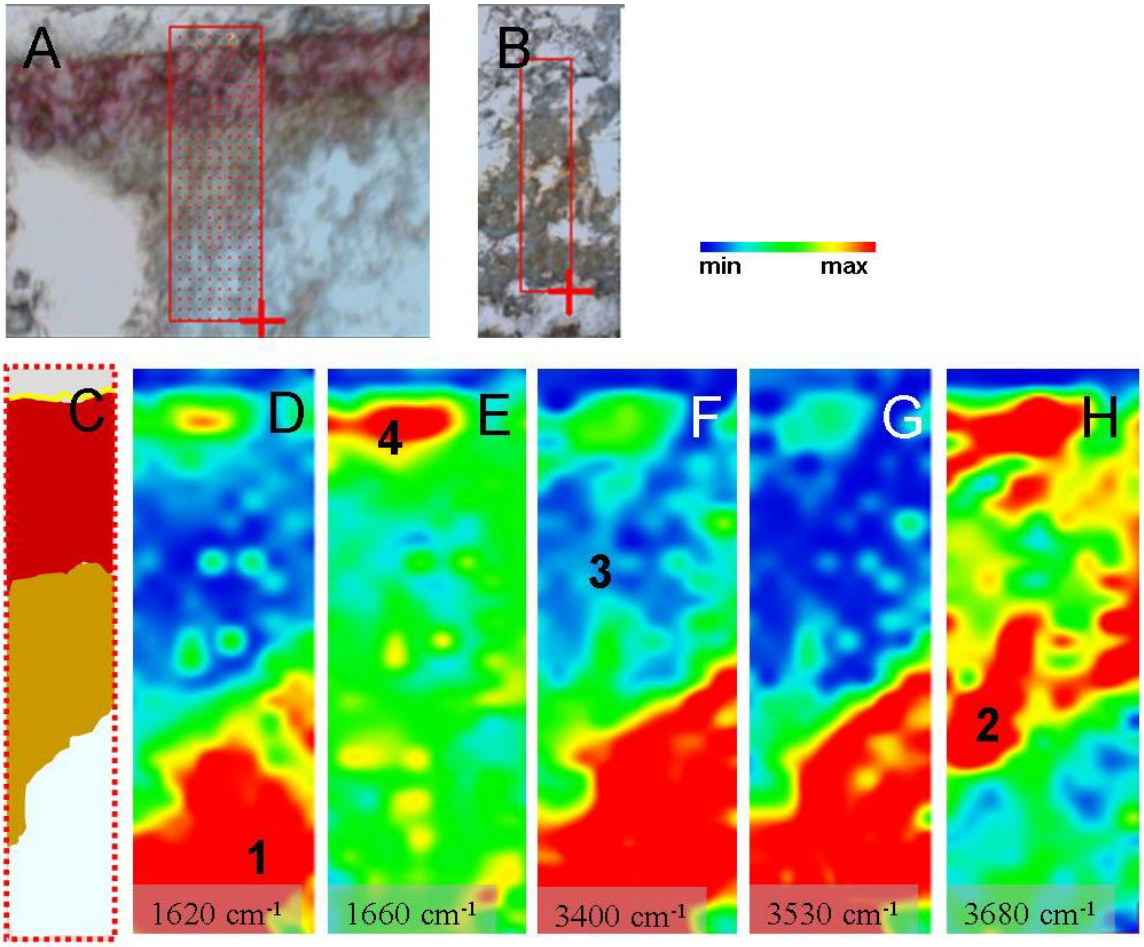

Figure 1.16. Micro compression diamond cells after the flattening of the sample PGe2/4 (A) the sample build-up can be appreciated; (B) some inorganic material; (C) scheme of the sample build-up in the area mapped from the cell reported in A (the red square highlights the area mapped); (D) to (H) chemical images of the bands identified in the spectra. Numbers indicate the areas where the spectra reported in Figure 1.17. were collected

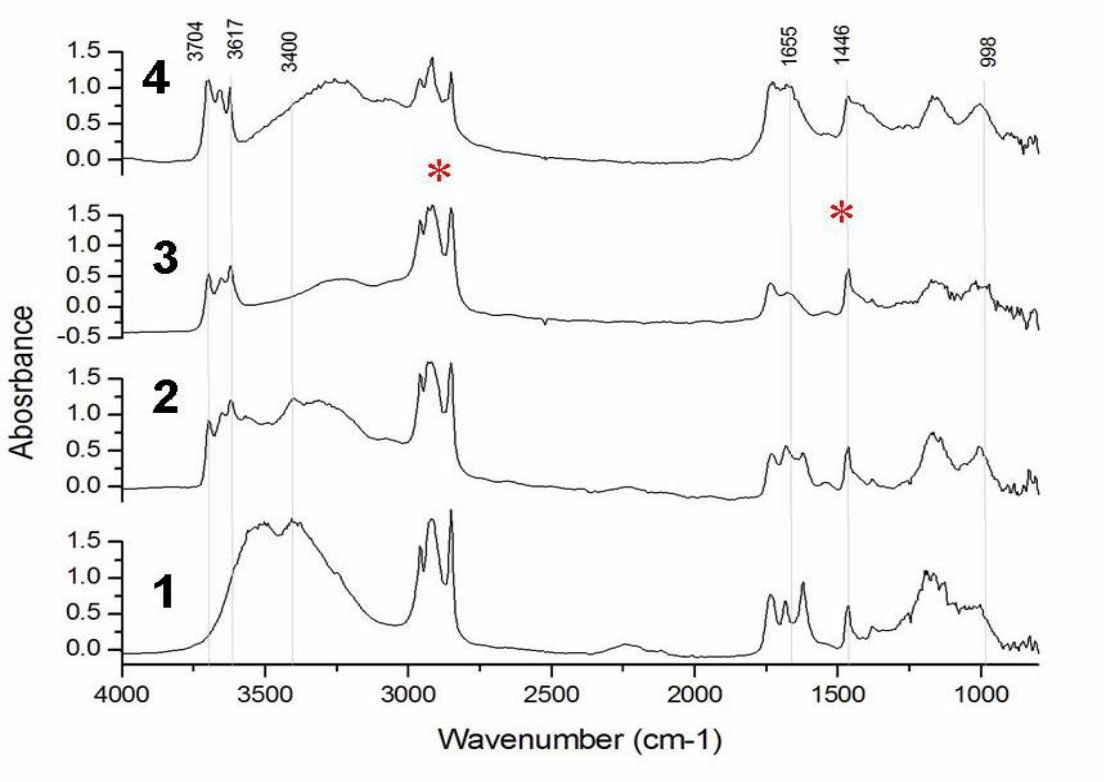

Figure 1.17. Spectra characteristic of the different areas in Figure 1.16. Bands of paraffin are indicated with a (*).

In this case study, two different strategies demonstrated were used to improve the imaging results obtained on a slice of 12 μm thickness: the preparation of a thinner section (10μm) and the combined use of paraffin (to prevent crumbling on cutting) and flattening of the slice by using a micro compression cell, being the last one the most efficient.

1.3.1.2.5. Data treating

The functional group distribution is established on the base of peak heights or areas. However, attention has to be paid when working with the software: chemical images of functional groups can be erroneous and not corresponding to the real selected peak heights due to the fact that spectra baseline is not flat. Baseline correction is compulsory for a reliable functional group mapping when uneven slices. The slice and

mapping area careful selection together with the strategies to flatten the slice are almost compulsory before the analysis. Finally, the presence of the infiltrated resin has to be considered carefully, as well. Thus, spectra should be assessed individually to be sure that chemical images correspond to real features in the spectra. An example of baseline correction effect in a sample with an sloping baseline spectrum is provided in Figure 1.18. An erroneous data interpretation is reported in Figure 1.19.

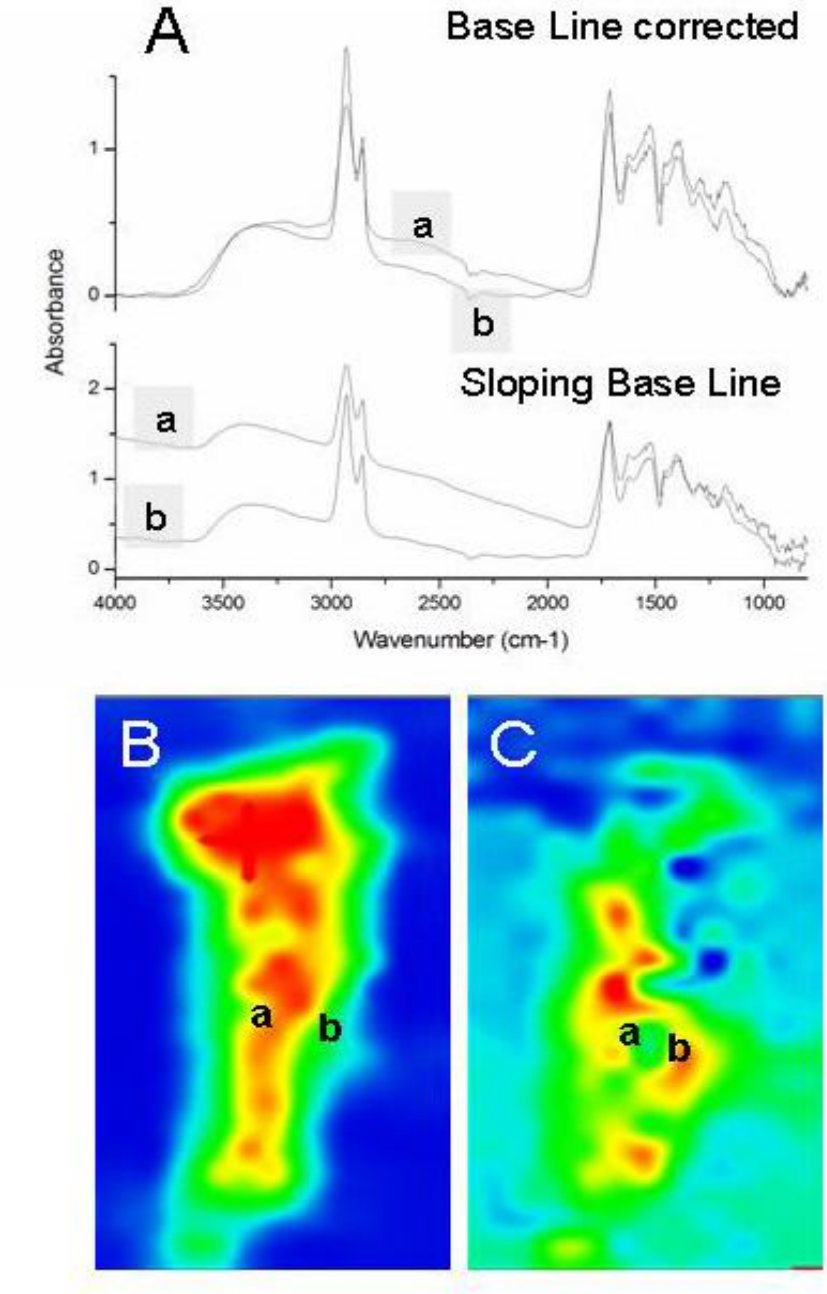

Figure 1.18. (A) FTIR transmittance spectrum of area a (grey spectrum) and b (black spectrum), close one to the other in the thin section of the sample, before and after baseline correction. Chemical image of the band at 2850 cm^{-1} before (B) and after (C) baseline correction. Areas of maximum intensity are completely changed.

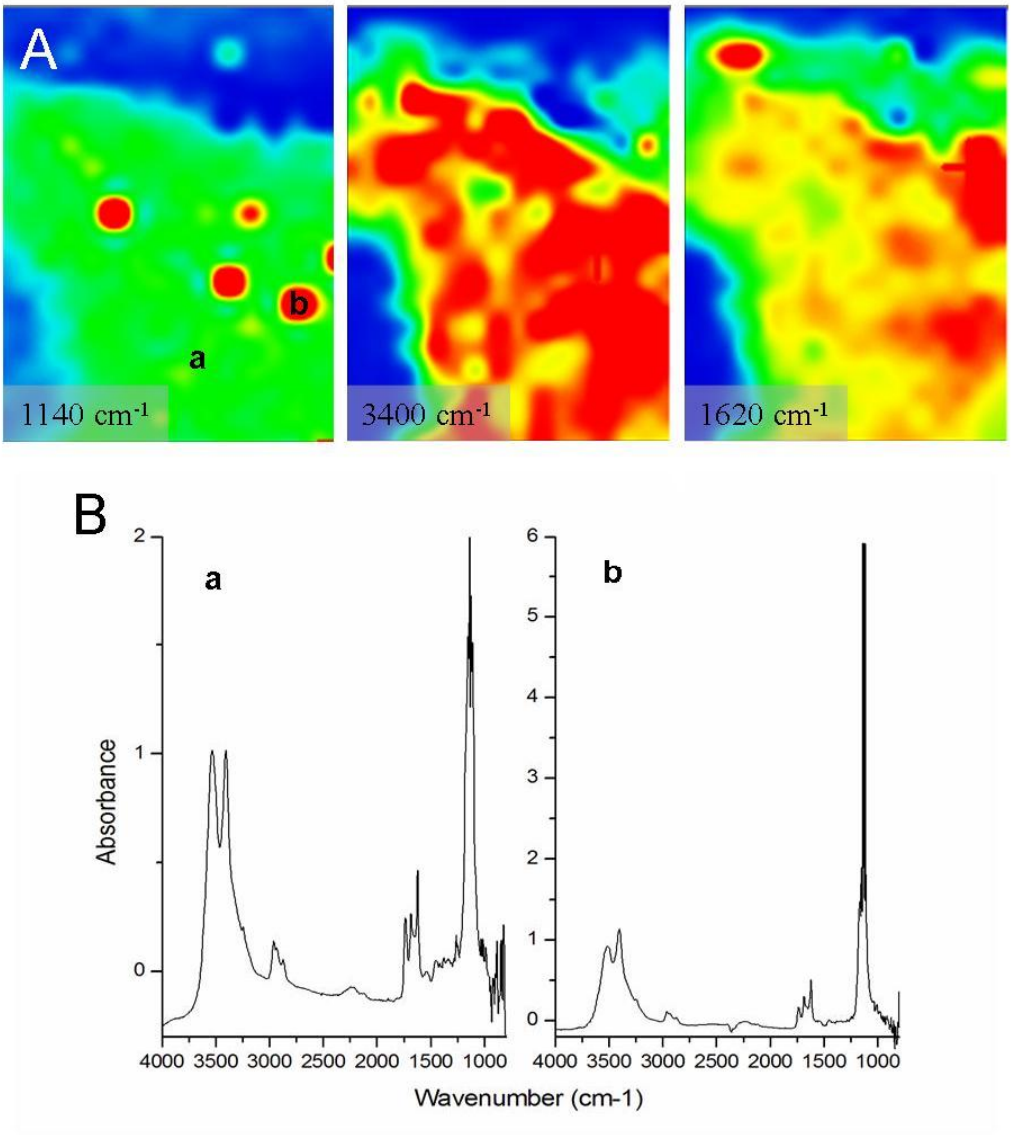

Figure 1.19. (A)Distribution of three bands characteristic of gypsum. Bands at 3400 (OH st) and 1620 (OH bd) cm^{-1} are correspondent with the preparation layer while 1140 (SO_4^{2-}) cm^{-1} shows just some areas of high intensity; (B) Spectra of area a and b. It can be easily appreciated that though the spectra of both areas correspond to gypsum, in area b specttum is saturated. Thus, the chemical image of this band do not corresponds to the real distribution of gypsum.

Case study IV. Sample AG2 (Agramunt, Romanesque door)

Figure 1.20. shows the image of a thin section of the sample AG2. The 12 µm slice presents five layers (indicated with a number in a grey square) of the layers recognisable in the sample build-up (Figure 1.20. B and C). the blue layers crumble when cutting. Spectra of some points of this thin section are reported in Figure 1.21. The selected spectra correspond to areas in the thin section that are indicated in the photomicrographs B,C and D by numbers highlighted by a red cross. The sample was too thick and not flat: spectra obtained are of bad quality and absorbencies are higher than 1.0, with sloping baseline and low signal-to-noise ratio. Moreover the infiltration of the embedding resin occurred.

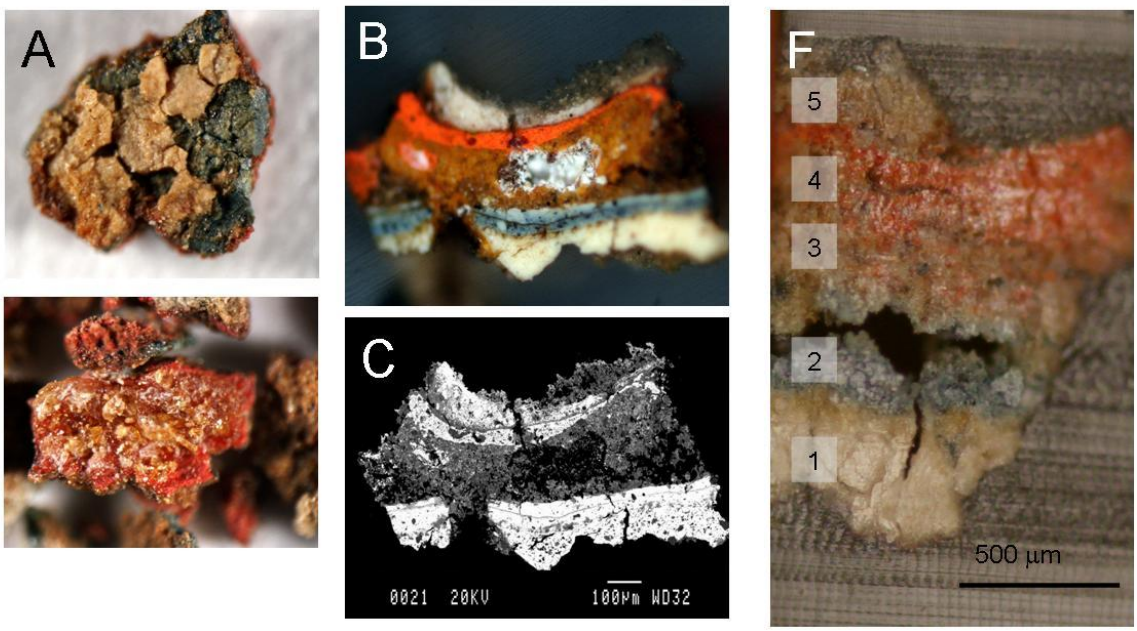

Figure 1.20. Sample AG 2 (A) stereomicroscope image of the two sides of the fragment; (B) optical image of the cross-section of the sample; (C) secondary electron image of the cross section; (D) 12 µm thin section (numbers in a grey square indicate sample layers).

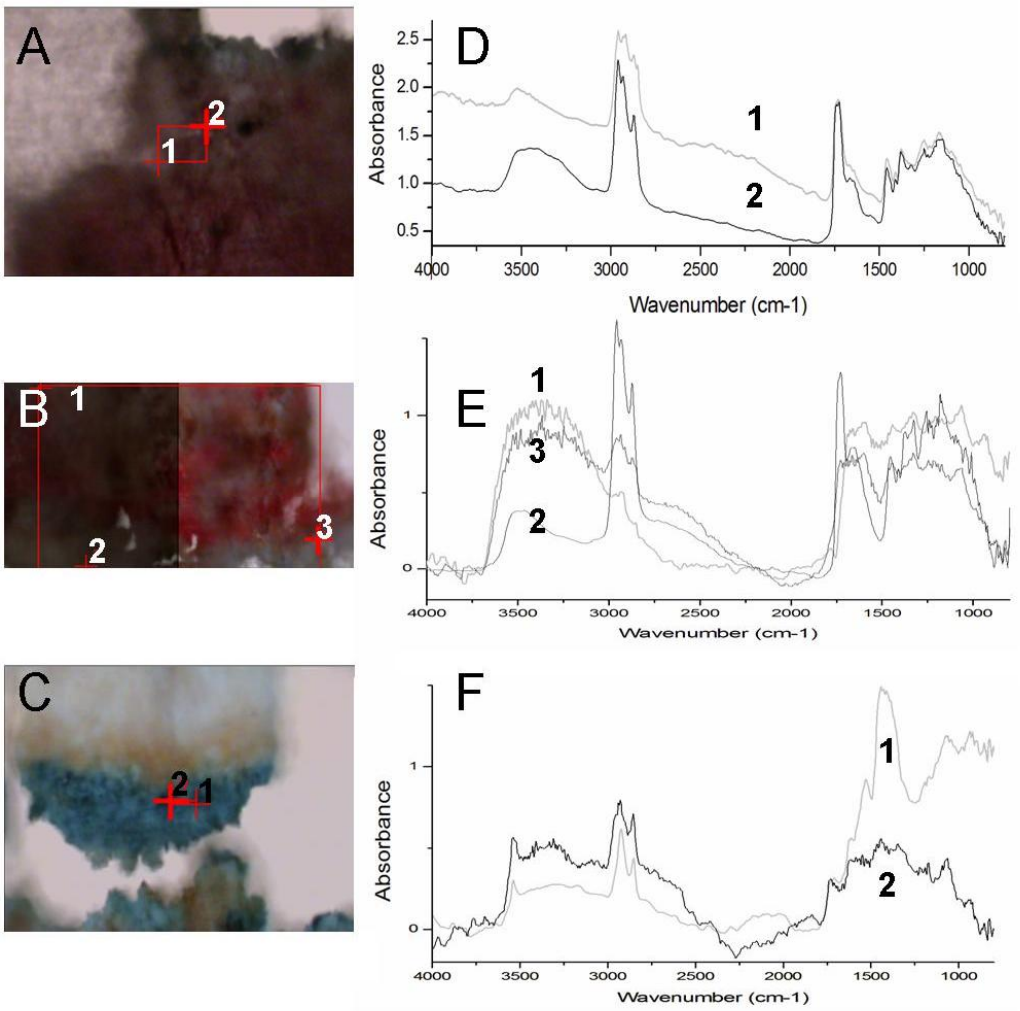

Figure 1.21. (A), (B) and (C) photomicrographs of different areas of the 12 µm thin section of AG2 (reported in Figure 1.20.D). Numbers indicate the positions where the spectra showed in (D), (E) and (F) were collected.

The slice was pressed in a micro compression diamond cell as described above. Figure 1.22. shows a photomicrograph of one of the sides of the cell. Individual spectra quality is probably better than in the original slice of 12 µm but low signal-to-noise and low absorbancies occur in some areas. As a result, though the identification of some pigments such as lead white (3545, 1400, 1044 cm^{-1}) or indigo (1621, 1320, 1176, 1099, 1073 cm^{-1}) and a lipid material (carboxylates are present at 1600 and 1540 cm^{-1}) as binding medium can be done, mapping of the bands should be carefully considered. In fact, maximum intensity in the chemical images correspond with the areas where the spectra quality is good enough.

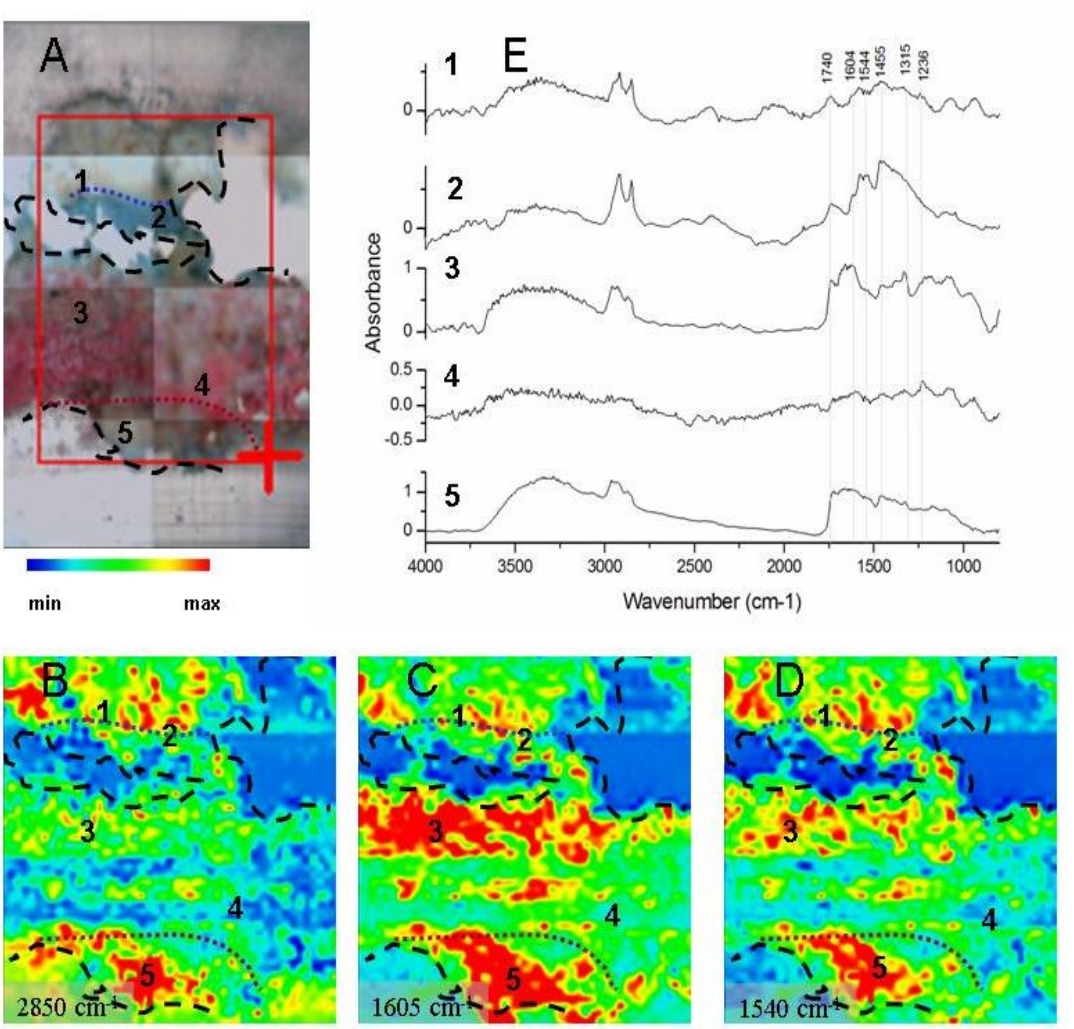

Figure 1.22. (A) Photomicrograph of one of the diamond micro-compression cells with the thin section of AG2. The red square highlights the area mapped; chemical images of (B) CH st (2850 cm^{-1}); (C) and (D) carboxylates (1600 and 1540 cm^{-1}); (E) spectra corresponding to the numbers indicated in both the photomicrograph and the chemical images

Below, a set of samples (P1 to P4) are reported in order to show some examples where the preparation method tested worked properly and imaging was successfully achieved.

1.3.2. Distribution of materials in thin sections from gypsum shield

The set of samples P1 to P4 presented a white preparation layer and one or more pigment layers on the top of it. In Figure 1.23. the build-up of the samples is reported.

Slices of less than 6 µm could be obtained for all of them without crumbling of the layers nor lost of particles. The embedding strategy, consisting in epoxy resin embedding and tungsten knife microtoming, allowed to obtain slices thin, flat and complete enough. Good quality spectra were registered, that allowed not only the identification of materials (both organic and inorganic) but also reliable images of the functional groups. Table 1.8. summarises the spectra features of the different layers. The IR absorption bands corresponding to the materials identified are reported in Table 1.6. The potomicrographs of the thin sections obtained as well as the spectra evaluated together with the chemical images performed are reported in Figures 1.23.to 1.27.

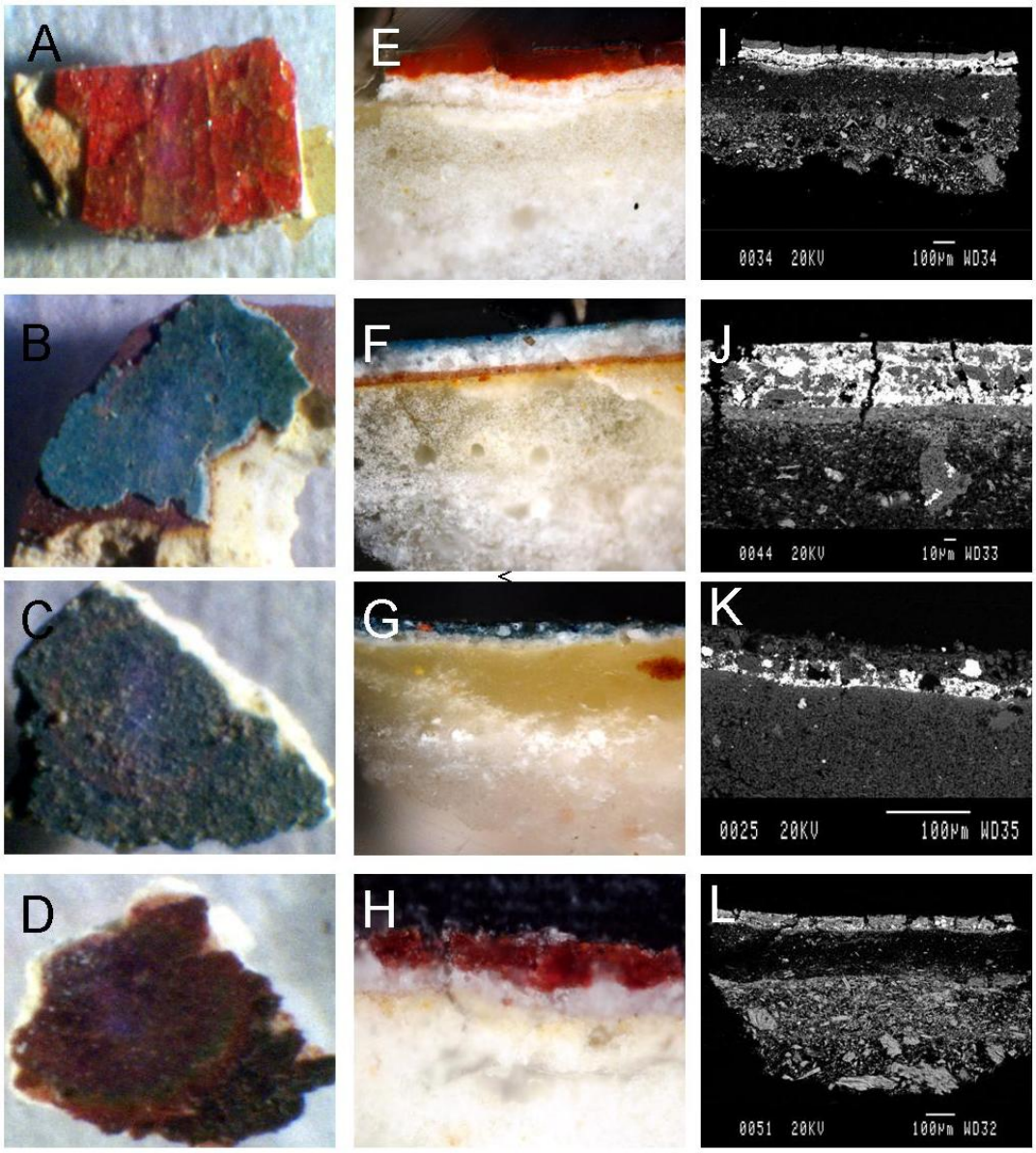

Figure 1.22. (A), (B), (C) and (D) stereomicroscope images of the pictorial layer; (E), (F), (G), (H) optical images of the cross-section, (I), (J),(K) and (L) secondary electron image of the samples P1, P2, P3 and P4, respectively. SE images highlights the presence of a layer with a heavy element. Pb was revealed by EDS in the correspondent layers.

Table 1.8. Main spectra features and results obtained for the series of samples P1 to P4

sample	*layer*	*Spectrum number*[vii]	*Material identified in the spectra*	*Mapping/cm^{-1}*
P1	superficial	5	Proteinaceous material	1650 1540
	Pigment (red)	4	Organic material ([viii]) Carbonates	1540
	preparation	3	Carbonate ([ix])	1430
		2, 1[x]	Calcium sulphate	3535 3400 1140
P2	Pigment (blue)	2	Azurite -	3420 ([xi]) 1640 ([xii])
		1	Organic material ([viii]) Carbonates	1530 1420
	preparation	-	Gypsum	3535 3400
P3	Pigment (blue)	4	Gypsum Prussian blue Calcium oxalates	1650 ([xiii]) 1324
	Preparation	1	Gypsum	3400 1140
	Brown particles	2	Gypsum Clay	990
P4	Pigment (red)	3, 4	Proteinaceous material Carbonate	1660 ([xiv])
	Preparation	1, 2	Calcium sulphate	3535 3400 1620 ([xv]) 1680

[vii] Corresponding to the numbers in the figure
[viii] Spectra would suggest the presence of a lipid material that has reacted with lead leading to the formation of carboxylates (C=O st at 1540 cm^{-1})
[ix] The band at 880 cm^{-1} in the pectra suggests the presence of calcium carbonate
[x] Infiltration of the embedding medium can be identified in the spectrum
[xi] High intensities also in the preparation layer due to the proximity of the band to the gypsum one
[xii] Not identified compound. Bands of azurite prevents the identification.
[xiii] Broad band resulting from the overlapping of the gypsum OH bd bands and oxalate ones
[xiv] The presence of this band in the spectra of the pigment layers in areas 3 and 4 justifies their high intentsity in the maps of 1620 and 1680 cm^{-1}. The presence of the band suggests the presence of a proteinaceous material confirmed by the presence of the bands at 3300 and 3080 cm-^{1}.
[xv] More intense in the spectra of area 2 and the corresponding chemical image. Differences in the spectra suggest the presence of a mixture of calcium sulfate forms, probably gypsum (Ca SO_4. H_2O)and hemydrite ($CaSO_4$. ½ H_2O)

By this way, the painting technique of the silvered gypsum shield was obtained. The shield was covered by a silver leaf and a calcium sulphate layer was applied as a preparation for the pigment layers. Blue pigments have been identified as azurite ($Cu_3(CO_3)_2(OH)_2$) and Prussian blue ($Fe_4[Fe(CN)_6]_3$), being probably the last one (first synthesized in 1709) a restoration product as the shield is dated 1640. Red pigments have been not identified. EDS results (data not shown) nor FTIR spectra showed any characteristic element or feature of an inorganic pigment. As a result a colorant is suspected. Samples P1, P2 and P4 show the absorption band at about 1420cm^{-1}, relative to the CO_3^{2-} st on the top of the preparation layer. The pigment layers show the occurrence of organic materials. P3 spectra showed calcium sulphate in all the layers and calcium oxalates in the pigment layer. The difference in the painting technique observed would be in agreement with the restoration of the shield. Finally, sample P1 presents a superficial coating layer made of a proteinaceous material.

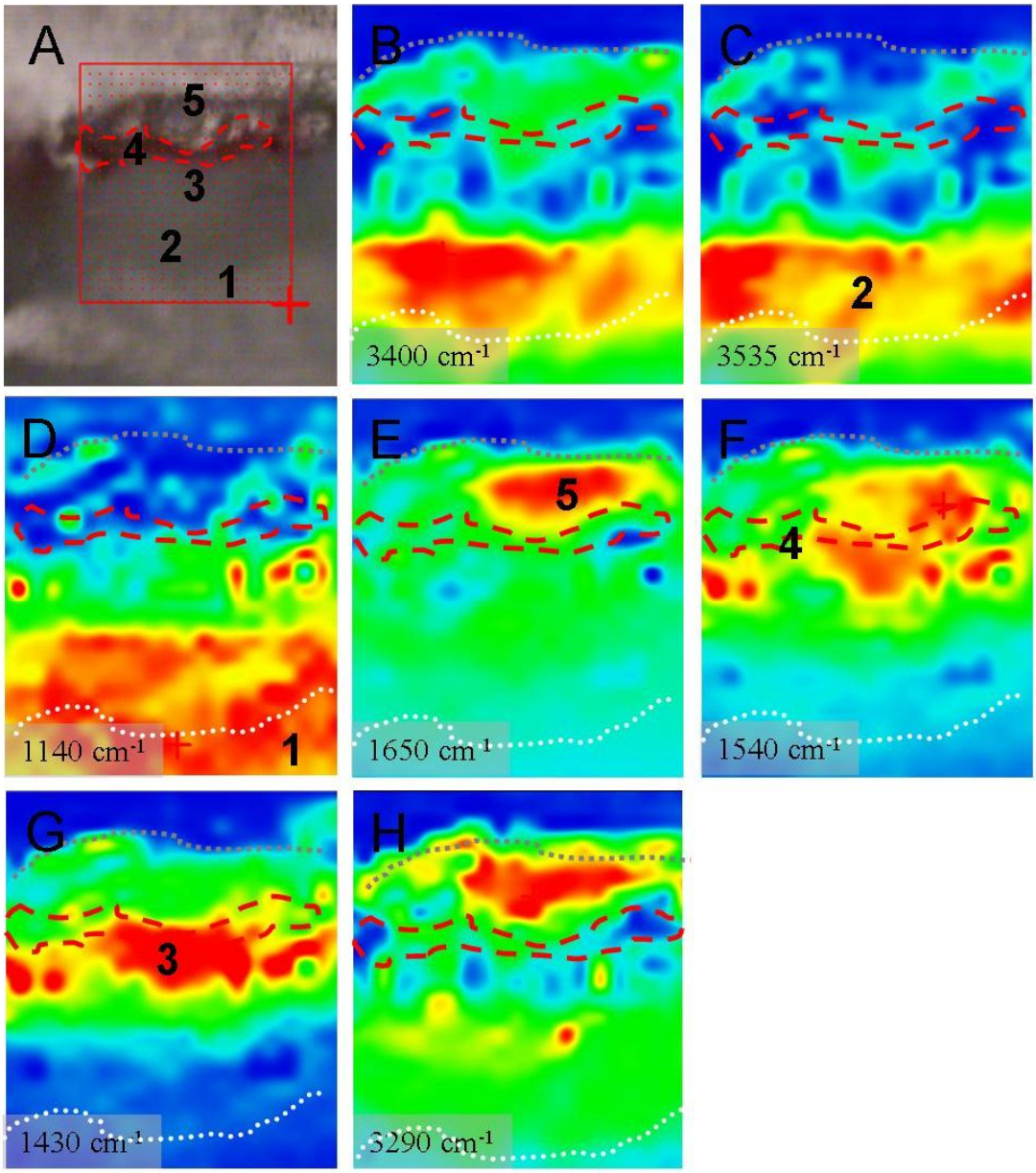

Figure 1.23. Sample P1 (A) photomicrograph of the thin section. The red square indicates the area mapped. Numbers in the photomicrograph correspond to the areas highlighted as different by the chemical images (B), (C), (D), (E), (F), (G) and (H). The bands mapped are indicated in a grey square on the bottom of the false colour map.

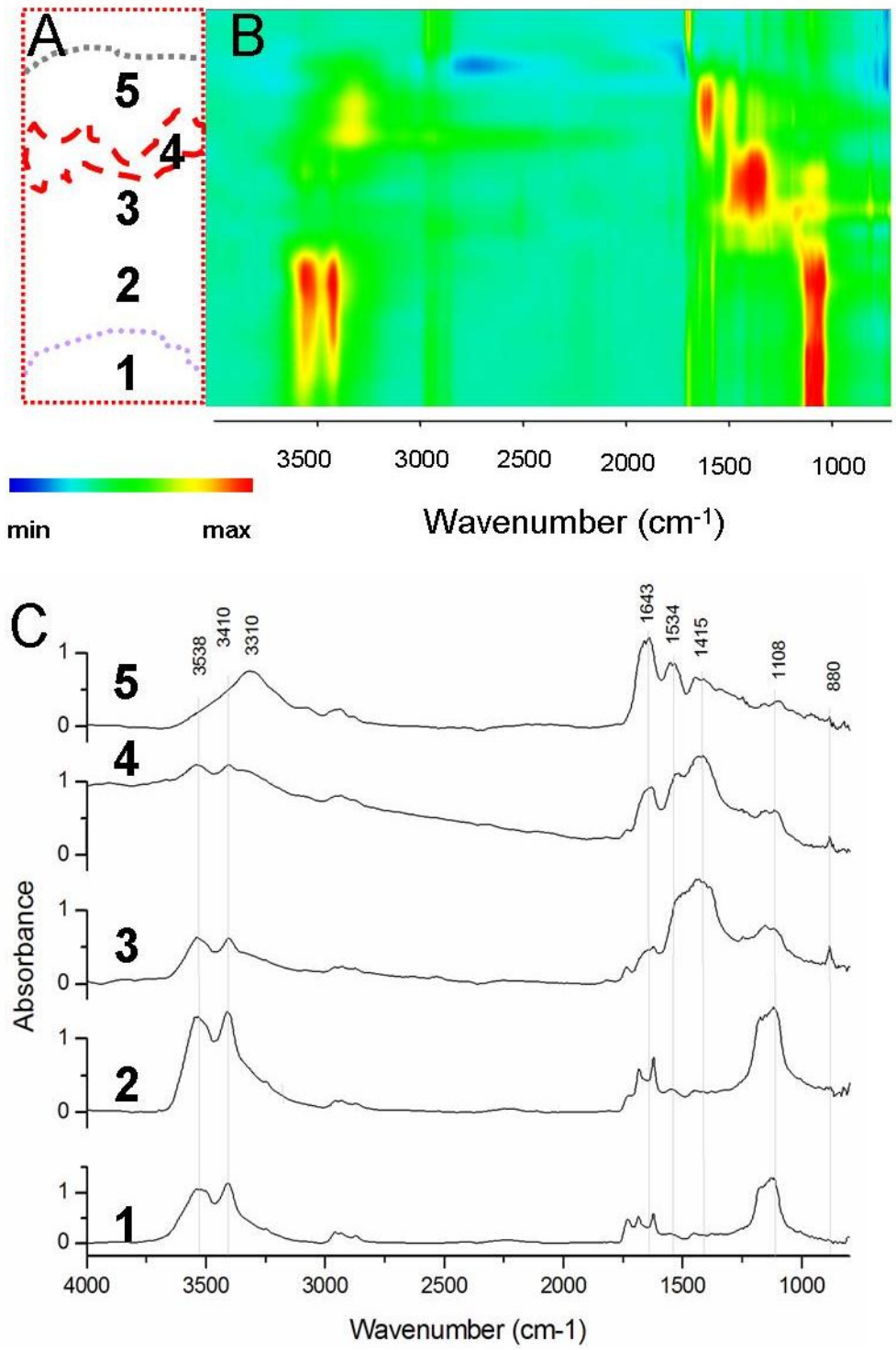

Figure 1.24. Sample P1(A) scheme of the sample build-up. The different areas evidenced by the chemical images in Figure 1.23 are indicated in the scheme ; (B) line scan showing the main features in the areas evidenced; (C) spectra of these areas. The main features in the spectra are correspondent with the line scan ones.

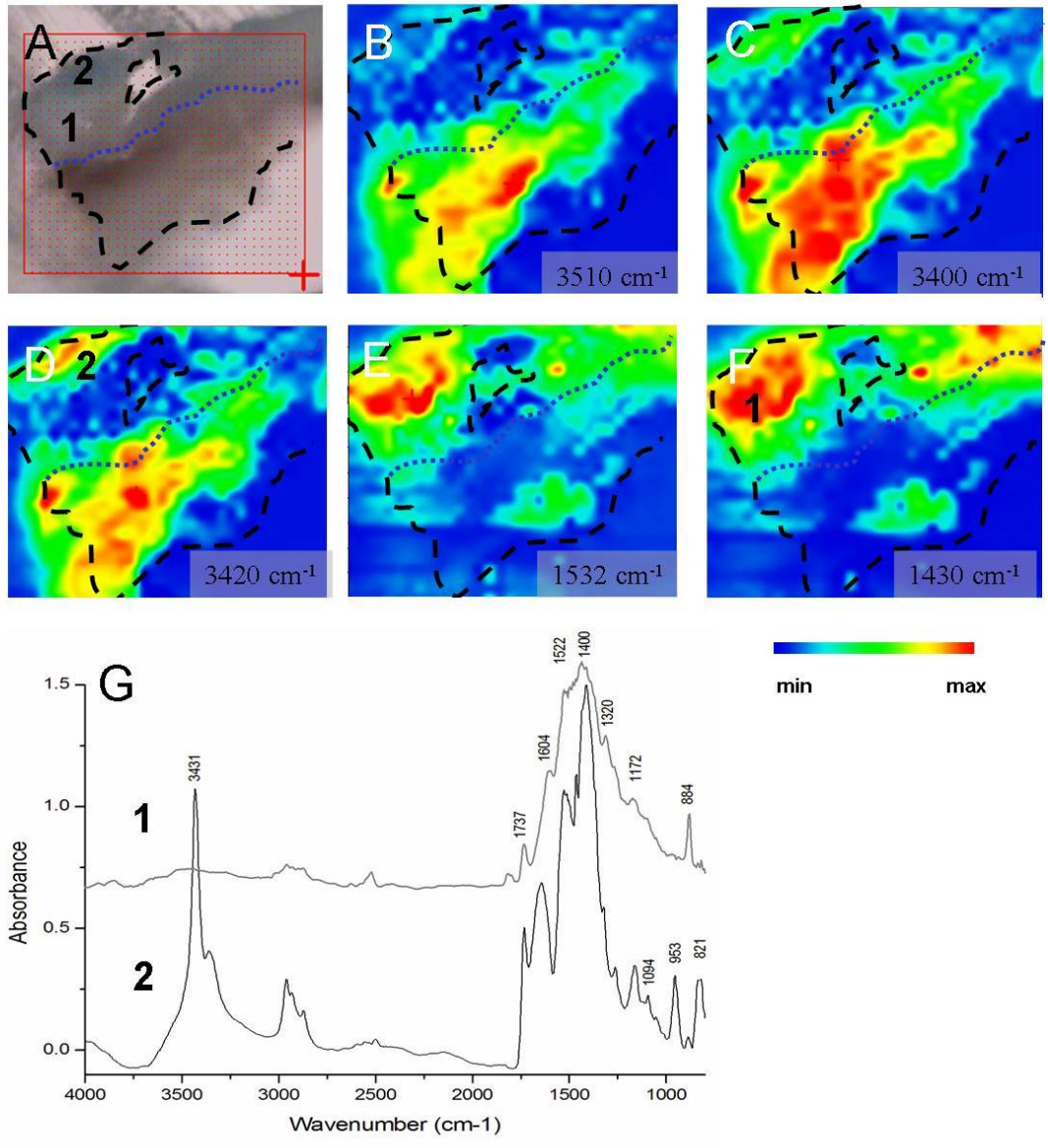

Figure 1.25. Sample P2 (A) photomicrograph of the thin section. The red square indicates the area mapped. Numbers correspond to areas highlighted by the chemical images of the bands indicated in a grey square (B), (C), (D), (E), and (F); (G) representative spectra of the areas evidenced by the chemical maps.

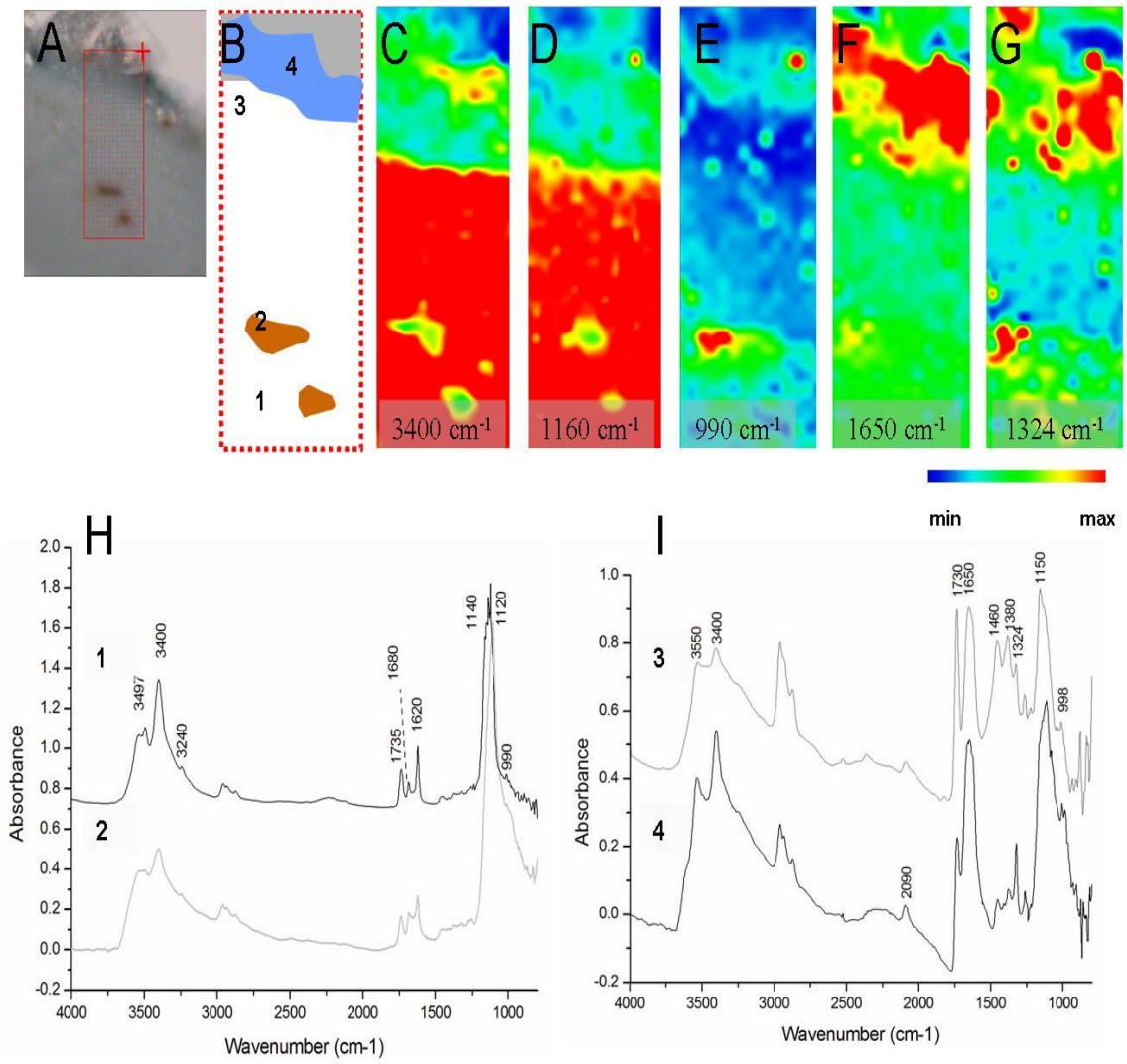

Figure 1.26. Sample P3 (A) photomicrograph of the thin section. The red square indicates the mapped area. Numbers correspond to areas highlighted by the chemical images; (B), (C), (D), (E), (F) and (G) chemical images of the bands indicates in a grey square; (H) and (I) representative spectra of the areas evidenced by the chemical maps.

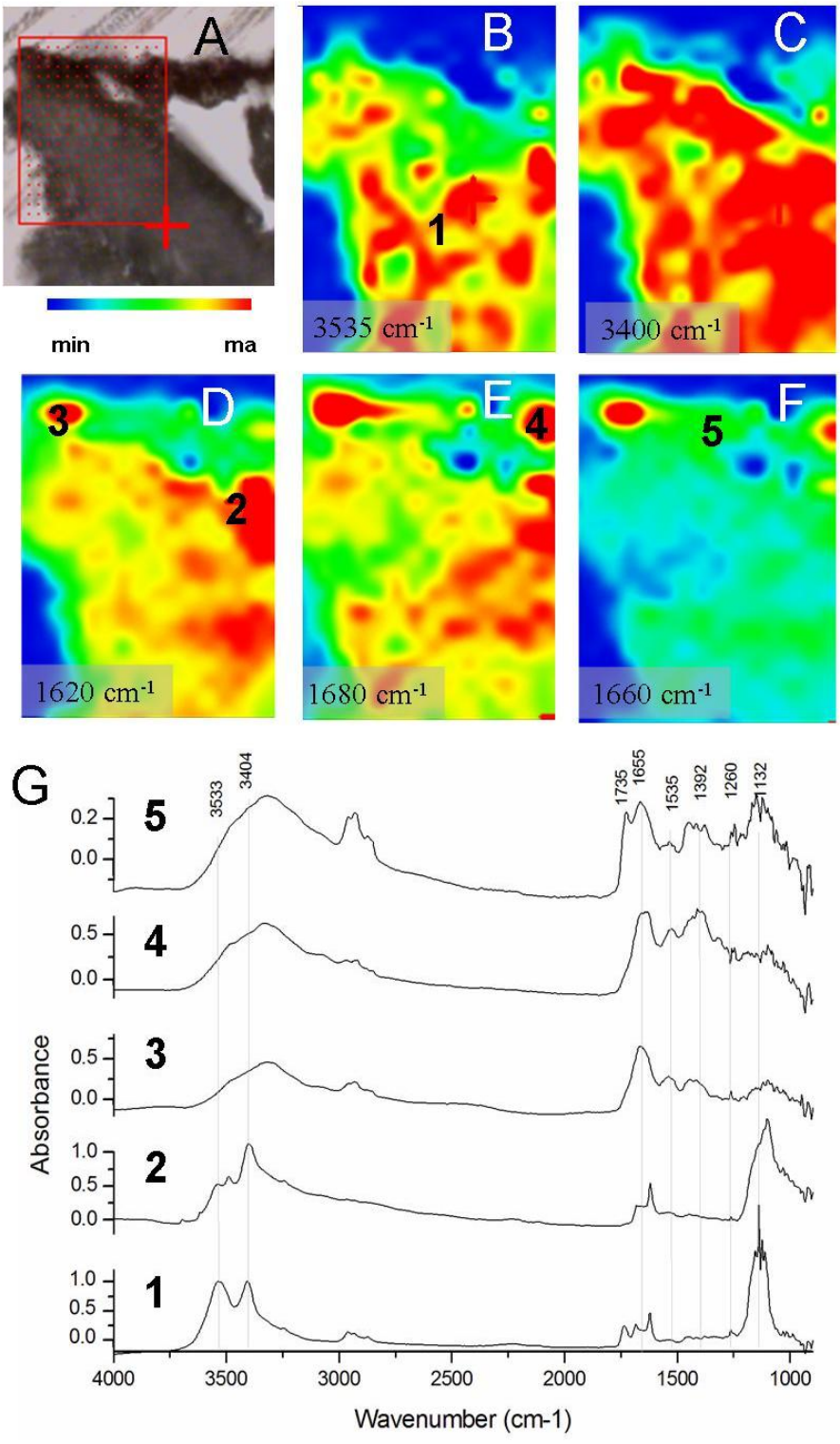

Figure 1.27. Sample P4 (A) photomicrograph of the thin section. The red square indicates the mapped area. (B), (C), (D), (E) and (F) chemical images. Numbers correspond to areas highlighted in the chemical images; (G) and (H) representative spectra of the areas evidenced by the chemical maps.

1.4. General conclusions

The sample preparation for FTIR imaging experiments is a key question. Preparation of thin sections for transmission experiments of about 10 μm thick from painting samples is quite tricky. Different methods presented in the literature were tried on decorative mural paintings characterised by a high inorganic content. Table 1.9. summarizes the strategies tested, their advantages and disadvantages.

Table 1.9. Summary of the sample embedding methods tested

Resin	*Advantages*	*Disadvantages*
paraffin	Low contamination Few bands	No control orientation Lost of sample under 15 μm
polyester	Easy embedding Transparent Curing at room temperature	Low viscosity resin (high infiltration) IR absorbing
epoxy	Easy embedding Easy slicing	Low viscosity resin (high infiltration) IR absorbing
Epoxy *Paraffin protection*	Slices with the whole stratigraphy	Adding of paraffin IR bands Lost of control of the thickness of the slice (no transmission)

In the samples showed, getting cross-sections by polishing KBr pellets in both sides resulted impossible. Highly inorganic paintings are extremely brittle and present big size pigment and filler grains. Therefore, embedding in an organic medium was demonstrated as necessary. However, infiltration, inhomogeneous thickness of the slice and complete or partial lost of the sample or sample layers were sometimes obtained.

Paraffin demonstrates not being useful due to the impossibility to control the disposition or orientation of the samples before cutting and the big difference in hardness with respect to the sample. Lost of the sample occurred in all cases.

Epoxy and polyester resins gave better results than paraffin. Infiltration occurs but at the same time allows to obtain reasonably good cross-section or partial ones. Though

both resins are strongly absorbant in the IR region, some sample functional groups can be mapped. Painting samples display different quality slices and quality spectra that not always allow reliable imaging of functional groups. Table 1.10. summarizes the ancient samples analysed and the main results obtained.

Table 1.10. Summary of the samples, strategies used and main results obtained.

Sample	*Slice width/µm([xvi]*	*Sample preparation strategy*	*Sample holder ([xvii])*	*Identification of materials*	*Distribution of materials ([xviii])*
SMM4	12	-	H	Lead white Indigo Proteinceous material	-
	6	-	H	Polysaccharide material	-
AG2	12	Pressed ([xix])	H	Lead white Indigo Carboxylates (oil)	-
PGe2/4	12	-	H	Kaolinite Gypsum Proteinaceous material	-
	10	-	H		l
	12	Paraffin ([xx]) Pressed	Dcell		m/l
B5	12	Pressed	H	Clay Lipid material	m
P1	6	-	H	Calcium carbonate Gypsum Proteinaceous mat.	m/l
P2	5	-	H	Azurite	m
P3	4	-	H	Gypsum Clay Prussian blue Calcium oxalates	m
P4	6	-	H	Gypsum proteinaceous mat.	m

When the sample slices obtained were not flat and thin enough, the characterization of the materials could only be done by the study of individual spectra but distribution of the materials in the sample build-up was not possible.

[xvi] Slices of more than 10 µm were performed with a diamond knife while less thickness slices were achieved by using a W knife.
[xvii] H : directly under the microscope; Dcell : under the microscope on a diamond micro compression cell
[xviii] general quality of the spectra allowed the mapping of functional groups (m) or at list the line scan (l).
[xix] Use of a micro compression cell to flatten the slice obtained by microtoming
[xx] Use of paraffin to avoid the crumbling of the cross-section when microtoming

Interpretation of the false colour images obtained has to be done carefully. Differences in the slice thickness or absorbing conditions, quality of the spectra and infiltration of the embedding resin should be considered individually. Chemical images can, as a result, respond to differences in the thickness of the slice or intensity of the spectra instead of real band intensity changes. In this sense, a line scan is an useful tool to highlight the main spectra features.

In some cases (by microtoming only or by using some strategies to flatten the slice) reliable maps and line scans could be obtained for inorganic and organic materials (proteinaceous and lipid materials) and decay-by-products such as calcium oxalates in the sample build-up.

A limitation of the technique is that a material can be hardly identified based on just a few IR absorption bands. Thus, additional analyses are sometimes required to complement the maps, supporting the spectra interpretation. In these cases the identification of organic materials should be previously performed by other techniques such as conventional FTIR or mass spectrometric based techniques for a reliable interpretation of the functional groups distribution. Inorganic materials would be unequivocally characterized by techniques such as SR XRD.

References

[1] J. van der Weerd, R.M.A. Heeren, J.J. Boon, 'Preparation methods for FTIR analysis' Stud. Conserv. 49, 193 (2004)

[2] JJ Boon, K Keune, J van der Weerd, M Geldof , JRJ Van Asperen de Boer, Imaging Microspectroscopic, Secondary Ion Mass Spectrometric and Electron Microscopic Studies on Discoloured and Partially Discoloured Smalt in Cross-Sections of 16th Century Paintings, Chimia 55(11): 2001, p. 952-960.

[3] I. Bonaduce, J.J. Boon, "An integrated mass spectrometric and molecular imaging analytical approach to identify and localise constituents in paintings applied to gilded multilayer structures from 14th to 16th C works of art", in New Trends in Analytical, Environmental and Cultural Heritage Chemistry, M. P. Colombini and L. Tassi editors, Research Signpost, in press

[4] C.M. de Fonjaudran A. Nevin, F. Piqué, S. Catre, 'Stratigraphic analysis of organic materials in wall painting samples using micro-FTIR attenuated total reflectance and a novel sample preparation technique', Anal Bioanal Chem (2008) 392:77–86

[5] M.R. Derrick, D. Stulik, J.M. Landry, Infrared Spectroscopy in Conservation Science (The Getty Conservation Institute Los Angeles 1999)

[6] JJ Boon, K Keune, T Learner, 'Identification of Pigments and Media from a Paint Cross-Section by Direct Mass Spectrometry and High-Resolution Imaging Mass Spectrometric and Spectroscopic Techniques'. In: ICOMCC Science symposium, Rio de Janeiro, submitted 2002

[7] MR Derrick, DC Stulik, JM Landry, SP Bouffard, 'Furniture Finish Layer Identification by Infrared Linear Mapping Microspectroscopy', Journal of the American Institute of Conservation 31: 1992, p. 225-236

[8] A Langley, A Burnstock, 'The analysis of layered paint samples from modern paintings using FTIR microscopy', ICOM committee for conservation, 12th triennal meeting, Lyon 1999, preprints, vol 1, James and James,
London, p. 234-241.

[9] RMA Heeren, JJ Boon, P Noble, J Wadum, 'Integrating Imaging FTIR and Secondary Ion Mass Spectrometery for the Analysis of Embedded Paint Cross-Sections'. In: ICOM, 12th Triennial Meeting Lyon, Lyon, 1999,
James, p. 228-233.

[10] J. van der Weerd, M.K. van Veen, R.M.Q. Heeren, J.Boon, 'Identification of pigments in paint cross-sections by reflection visible light imaging microspectroscopy, Journal of Analytical Chemistry, 75 (2003) 716-722

[11] I. Bonaduce, J. J. Boon, M. P. Colombini and G. Lanterna, "Chemical imaging techniques for the characterisation of materials and techniques in the art of gilding: a case study from a mural by F. Lippi", Proceedings of Conservation Science 2007, Milan , 10-11 May 2007.

[12] K. Keune Binding medium, pigments and metal soaps characterised and localised in paint cross-sections, , 2005. ISBN 90-77209-10-7

[13] Paints quantified: image analytical studies of preparatory grounds used by Van Gogh, Beatrice Marino, 2006. ISBN-10: 90-77209-19-0 and ISBN-13: 978-90-77209-19-6

[14] E. Dooryhee, M. Anne, I. Bardies, J.L. Hodeau, P. Martinetto, S. Rondot, J. Salomon, G.B.M. Vaughan and Ph. Walter, Non-destructive synchrotron X-ray diffraction mapping of a Roman painting, Appl. Phys., A 81 (2005) (4), pp. 663–667

[15] M. Cotte, J. Susini, V. A. Solé, Y. Taniguchi, J. Chillida, E. Checroun, P. Walter, "Applications of synchrotron-based micro-imaging techniques to the chemical analysis of ancient paintings", Journal of Analytical Atomic Spectrometry, 23, 820-828 (2008).

[16] M. Cotte, J. Susini, A. Moscato, C. Gratziu, A. Bertagnini, N. Metrich, "Blackening ofPompeian Cinnabar paintings studied by X-ray micro-spectroscopic imaging", Analytical Chemistry, 78, 7484-7492 (2006).

[17] P. Dumas, N. Jasmin, J.L. Teillaud, L.M. Miller, B. Beccard, 'Imaging capabilities of synchrotron infrared microspectroscopy', Faraday Discuss. 126, 289 (2004).

[19] P. Dumas, L. Miller, Chemical imaging of biological tissue with synchrotron infrared light, Biochimica et Biophysica Acta (BBA) - Biomembranes Volume 1758, Issue 7, July 2006, Pages 846-857

[20] L.M. Miller, R. J. Smith, Synchrotrons versus globars, point-detectors versus focal plane arrays: Selecting the best source and detector for specific infrared microspectroscopy and imaging applications', Vibrational Spectroscopy Volume 38, Issues 1-2, 29 July 2005, Pages 237-240

[21] M Cotte, P. Walter, G. Tsoucaris, P.Dumas, Studying skin of an Egyptian mummy by infrared microscopy', Vib. Spectrosc. 38, 159 (2005)

[22] E. Pantos, 'Synchrotron Radiation in Archaeological and Cultural Heritage Science' 27 (2005) 199-208 X-rays for Archaeology

[23] W.Kockelmann, E. Pantos, A. Kirfel,. (2000), Neutron and synchrotron radiation studies of archaeological objects Neutron and synchrotron radiation studies of archaeological objects. In Radiation in Art and Archaeology, Ed. D. C. Creagh & D. A. Bradley, Elsevier

[24] E. Dooryhee, P. Martinetto, Ph. Walter, M.Anne, Synchrotron X-ray analysis in art and archaeology', Radiation Physics and Chemistry 71 (2004) 863-868

[25] I. Nakai, I. Taguchi, and K. Yamasaki, (1991). Chemical Speciation of Archaeological Objects by XRF/XANES Analysis Using Synchrotron Radiation, Analytical Sciences Vol 7, supplement

[26] M. Cotte, E. Checroun, V. Mazel, V. A. Solé, P. Richardin, Y. Taniguchi, P. Walter and J. Susini, Combination of FTIR and X-rays synchrotron-based micro-imaging techniques for the study of ancient paintings. A practical point of view.

[27] Joris Dik, Koen Janssen, Geert Van Der Snickt‡, Luuk van der Loef, Karen Rickers and Marine Cotte, 'Visualization of a Lost Painting by Vincent van Gogh Using Synchrotron Radiation Based X-ray Fluorescence Elemental Mapping, Anal. Chem., 2008, 80 (16), pp 6436–6442. DOI: 10.1021/ac800965g

[28] M. Schreiner, B. Frühmann, D. Jembrih-Simbürger, and R. Linke, X-rays in art and archaeology: An overview', Powder Diffr. Volume 19, Issue 1, pp. 3-11 (March 2004)

[29] M. Cotte, E. Checroun, V. Mazel, V. A. Solé, P. Richardin, Y. Taniguchi, P. Walter and J. Susini, 'Combination of FTIR and X-rays synchrotron-based micro-imaging techniques for the study of ancient paintings. A practical point of view.'

[30] A. A. Sokolov[1] and I. M. Ternov[1], Synchrotron radiation, Russian Physics Journal 10, 10 (1967)39-47

[31] E. Koch, T. Sasaki, H. Winick, 'Handbook on synchrotron radiatio'n, North-Holland (1983)

[32] H Winick, and A Bienenstock, 'Synchrotron Radiation Research', 28(1978)33-113

[33] I M Ternov, ' Synchrotron radiation', Phys.-Usp. 38 (1995) 409-434

[34]N.Salvado´, S. Butı´, M. J. Tobin, E. Pantos, A. John N. W. Prag, and Trinitat Pradell, 'Advantages of the Use of SR-FT-IR Microspectroscopy: Applications to Cultural Heritage', Anal. Chem.2005, 77,3444-3451

[35] N.Salvadó, T. Pradell, E. Pantos, M. Z. Papiz, J. Molera , M. Seco and M. Vendrell-Saz, J Synchrotron Radiat. 9, 215 (2002)

[36] J. Roqué, J. Molera; G. Cepriá; M. Vendrell-Saz; J. Pérez-Arantegui. 'Analytical study of the behaviour of some ingredients used in lustre ceramic decorations following different recipes', Phase Transitions, Volume 81, Issue 2 & 3 February 2008 , pages 267 – 282

[37] J. Roqué, J. Molera, P. Sciau, E. Pantos and M. Vendrell-Saz, 'Copper and silver nanocrystals in lustre lead glazes: Development and optical properties', Journal of the European Ceramic SocietyVolume 26, Issue 16, 2006, Pages 3813-3824

[38] F. Casadio, F., Toniolo 'The analysis of polychrome works of art: 40 years of infrared spectrocopic investigations', Journal of Cultural Heritage2 (2001) 71-78

[39] T Learner, 'The Use of FT-IR in the Conservation of Twentieth Century Paintings', Spectroscopy Europe 8(4):

[40] RJ Meilunas, JG Bentsen and A Steinberg, 'Analysis of Aged Paint Binders by FTIR Spectroscopy', Studies in Conservation 35: 1990, p. 33-51.

[41] EH Van't Hul-Ehrnreich, 'Infrared Microspectroscopy for the Analysis of Old Painting Material's, Studies in Conservation 15: 1970, p. 175-182

[42] MJD Low, NS Baer, 'Application of Infrared Fourier Transform Spectroscopy to Problems in Conservation', General Principles, Studies in Conservation 22: 1977, p. 116-128.

[43] MR Derrick, 'Infrared Microspectroscopy in the Analysis of Cultural Artifacts. In: Practical Guide to Infrared Microspectroscopy' (Ed. Humecki HJ), Marcel Dekker, Inc, New York, 1995, p. 287-322.

[44] RTD Carbo, FB Reig, JVG Adelantado and VP Martinez, 'Fourier Transform Infrared Spectroscopy and the Analytical Study of Works of Art for Purposes of Diagnosis and Conservation', Analytica Chimica Acta 330:
1996, p. 207-215

[45] A.Rizzo, 'Progress in the application of ATR-FTIR microscopy to the study of multi-layered cross-sections from works of art Analytical and Bioanalytical Chemistry' Volume 392, Numbers 1-2 /(2998)47-55

[46] E .Abelev, et al "An alternative isolation of tungsten tips for a scanning tunnelling microscope" Revies of Scientific Instruments 76, 106105 (2005)

[47] Kushida H., 'Embedding method for electron microscopy in biology.', Tokai J Exp Clin Med. 1985 Dec;10(6):557-71

[48] AR Spurr., 'A low-viscosity epoxy resin embedding medium for electron microscopy', J Ultrastruct Res. 1969 Jan;26(1):31-43

[49] M A Wallis and R L Griffin, 'A routine method for embedding animal tissues in Spurr resin for electron microscopy' Journal of Clinical Pathology 1973;26:77-78; doi:10.1136/jcp.26.1.77

[50] S. Widåhn [a]; L. Kindblom , 'A Rapid and Simple Method for Electron Microscopy of Paraffin-Embedded Tissue', Ultrastructural Pathology, 12, 1 (1988), 131 – 136

[51] Tomita Y, Nihira M, Ohno Y, Sato S., 'Histological study of early postmortem changes in various organs: comparison of the paraffin embedding method and the epoxy resin embedding method', Nihon Hoigaku Zasshi. 1999 Jun;53(2):207-17

[52] L.Dei, A.Ahle, P.Baglioni, D.Dini, 'Green Degradation Products of Azurite in Wall Paintings: Identification and Conservation Treatment' , Studies in Conservation 43, 80-88 (1998)

[53] R. J. Gettens, M. E. Mrose, 'Calcium Sulphate Minerals in the Grounds of Italian Paintings', Studies in Conservation 1(4), 174-189 (1954).

[54] C. Genesta, 'Characterization of grounds used in canvas and sculpture' , Materials Letters 54, 382-388 (2002).

[55] I. Adrover Gracia: 'Applicazioni della spettrofotometria IR allo studio dei beni culturali' (Collana I Talenti Padova Italy 2001)

[56] S.Bruni, F. Cariati, F. Casadio, L. Toniolo, 'Spectrochemical characterization by micro-FTIR spectroscopy of blue pigments in different polychrome works of art' Vibrational Spectroscopy 20, 15 (1999) 15-25

[57] J. Madejová , 'FTIR techniques in clay mineral studies', Vibrational Spectroscopy 31,1, 1-10(2003)

Chapter 2

Characterization and distribution of oxalates in mural painting samples

This chapter illustrates the analysis by synchrotron micro-analytical techniques of mural paintings. The challenge of the experiments was to identify and to obtain the spatial distribution of the decay by- products formed. In particular, the aim of this study was to gain information on the formation mechanisms of oxalates in mural paintings. Determining the in depth distribution of oxalates respect to the organic material distribution and the nature of this oxalates would help in attributing calcium oxalates to a bio-construction or to a chemical product of degradation of binding media.

Synchrotron powder XRD investigations were performed at the station 9.6 Daresbury (UK) and Synchrotron μXRD and μFTIR experiments were carried out at the ESRF (Grenoble, France) in order to obtain information on the material distribution. To complement the information SEM-EDS, FTIR, Py/GC/MS and GC/MS techniques were applied in order to characterize the binding media and organic materials present as well as their degradation products.

Results helped to unequivocally characterize painting techniques, the inorganic crystalline products formed by the weathering processes in the different samples and also to determinate the distribution of those products along the layers.

2.1.Introduction

Calcium oxalates are often found in many cultural heritage objects exposed at the open air. They form patinas, known as “oxalate patinas”, mainly developed on marble and limestone [1,2,3,4,5]. A long and unsolved discussion arisen in the scientific community on the origin of such patinas. Some researchers claim the patinas have a biological origin by mineralisation and collapse of microorganisms, while others consider these patinas a catabolic product of micro-organisms colonisations fed by organic materials such as the remains of ancient treatments applied to the stone for protective or colouring purposes.

A third hypothesis considers a chemical origin as oxidation products of those organic substances applied as conservation treatments. It is well known that the degradation of organic compounds used as binding media and coating layers produce oxalic acid as one of the final by-products, which could react with calcium, already present in large amounts in the atmosphere, to produce calcium oxalate [2]. However, some authors believe less plausible to attribute oxalate formation to purely chemical reactions without any involvement of living-microorganism (lichens or fungi) [5].

Recent analyses showed that calcium oxalates are also present in ancient paintings though they had always been kept inside a church or a museum [6]. In some cases, any effect of an ancient or present colonisation by micro-organisms have been found on the painting layers. So that, it is really difficult to attribute the calcium oxalate to a bio-construction. Additionally, lichens produce calcium oxalate (always the di-hydrated form weddellite) that also always appears as small well-shaped crystals (tetragonal pyramid and prismatic) sized from 5 to 10 microns [1,7]. On the contrary, calcium oxalates crystals found in stone patinas and painting samples are sized under the resolution of the Scanning Electron Microscope indicating that oxalates in paintings are not micrometric but nanometric. Moreover, both crystalline forms (weddellite and whewellite) have been reported in paintings [2]. That suggests that calcium oxalate crystals are formed during the ageing process of the painting not as a metabolic product of lichens or fungi, as those products are above micrometers, but as decay product of the organic binding medium.

Experiments carried out on marble substrates to evaluate the role of organic materials in the formation of oxalate patinas by both natural ageing of organic material mixtures (indoor and outdoor) [8] and ageing tests by oxidation with reactive species (O_3, H_2O_2) [2] result in the formation of both forms of calcium oxalate or mixtures of them from all kind of organic materials (polysaccharide-glucose, arabic gum-, proteinaceous-yolk, milk- and lipidic-oil- materials) reflecting the casual and widespread of the phenomena. In the oxidation experiment [2], conditions were controlled thus, a chemical formation of oxalates from the organic material oxidation was ascertained as microorganisms were not present. Finally, it has been reported that, for some oxalate patinas studied by GC/MS [9], the quantity of oxalates is directly proportional to the amount of organic material detected.

In this chapter, the study of different samples from mural ancient paintings is presented. Samples were chosen on the bases of the results obtained by their conventional characterization (mainly FTIR) that indicated the presence of a high content of oxalates in their composition. Ten samples, grouped in three different case studies, are presented: a mural stone altarpiece from the 11th century, an azurite sample from a gypsum shield from the 17th century, and gilded samples from the ceiling of a crypt from the 17th century. Samples are illustrative of the phenomenum of the formation of oxalates in paintings, being different in period and kind of support, pigments and painting technique. Both conventional results and synchrotron investigations will be presented as not only information on oxalates was gained, but also the painting techniques and the use of pigments were studied.

The aim of the research is to study the distribution of calcium oxalates in painting samples related to the organic material in order to discern the relation among them and, by this way, understand the mechanism of formation of oxalates in the painting build-up.

2.2. Experimental section

2.2.1 Microscopy

Samples were preliminarily observed by means of a low magnification stereo microscope (Nikon SMZ 1500) in order to observe the number and sequence of painting layers including the support and the surface state.

Several fragments of the sample were embedded in polyester resin using methyl ethyl ketone peroxide as hardener (Cronolita E.I., Spain), cut with a low deformation diamond saw and polished to allow the study of the cross section under a reflecting dark field optical microscope. A Nikon Eclipse LV 100 PDL analytical microscope equipped with a Nikon Digital Camera DMX 1200 F was used for visible light microscopy of the polished cross sections.

SEM images of the same sections were acquired using a JEOL (Tokyo, Japan) JSM-840 (secondary and backscattered electron detection) with a LINK AN 10000 microanalyser for the X-ray dispersive energy. The acceleration voltage used was 20 KeV.

2.2.2.Fourier Transform Infrared Spectroscopy (FTIR)

Analyses were made with a BOMEM MB-120 Fourier transform infrared spectrometer in two transmission modes, microscope and diamond cell. All results were processed with GRAMS/32 (Galactic) software.

When working with the diamond cell, the equipment was an infrared spectrometer Bomem MB-120 equipped with a potassium bromide beamsplitter and deuterated triglycine sulfate (DTGS) detector. The spectra are the sum of 30 scans collected from 4000 to 350 cm^{-1} at a resolution of 4 cm^{-1}.

Bomem MB-120 Fourier Transform Infrared Spectrometer, equipped with a Spectra-Tech Analytical Plan microscope, was used with the diamond cell, as a sample holder. The spectrometer has a KBr beamsplitter and a Glowbar source. The microscope has a mercury cadmium telluride (MCT) detector refrigerated with liquid nitrogen. Spectrum was recorded between 4000 and 720 cm^{-1} with a resolution of 4 cm^{-1} and an accumulation of 100 scans.

2.2.3. Gas chromatographyc mass spectrometry procedures

- Pyroprobe CDS Analytical Inc. 5000 Series (Oxford, USA). It was operating with an initial temperature of 50°C, up to 550°C at 20°C/ms, then isothermal for 20 sec. (probe run time 0.33 min). The pyrolyser was coupled on-line with the injection port of a 6890N GC System Gas Chromatograph (Agilent Technologies, Palo Alto, CA, USA), coupled with a 5973 Mass Selective Detector (Agilent Technologies, Palo Alto, CA, USA) single quadrupole mass spectrometer, equipped with split/splitless injector. The interface (Py/GC) temperature was 180°C, the transfer line 300°C, the valve oven 290°C. A few µg of the samples admixed with 2 µl of hexamethyldisilazane were inserted into a quartz tube and placed into the pyrolysis chamber.
- 6890N GC System Gas Chromatograph (Agilent Technologies, Palo Alto, CA, USA), coupled with a 5973 Mass Selective Detector (Agilent Technologies, Palo Alto, CA, USA) single quadrupole mass spectrometer, equipped with split/splitless injector. The mass spectrometer was operating in the electron impact (EI) positive mode (70 eV). The MS transfer line temperature was 280 ºC; the MS ion source temperature was kept at 230 ºC; and the MS quadrupole temperature was at 150 ºC. This instrument was used for the Py/GC/MS analyses. Detailed working conditions are published elsewhere [10].
- A 6890N GC System Gas Chromatograph (Agilent Technologies, Palo Alto, CA, USA), coupled with a 5975 Mass Selective Detector (Agilent Technologies, Palo Alto, CA, USA) single quadrupole mass spectrometer, equipped with a PTV injector was used. The mass spectrometer parameters correspond to the ones reported above. This instrument was used for the analysis of samples processed with the combined analytical procedure for the

simultaneous identification of glycerolipids, proteinaceous materials, plant and animal resins, and natural waxes. The detailed operating conditions, and the analytical procedure are published in detail elsewhere [11]

- Microwave oven model MLS-1200 MEGA Milestone (FKV, Sorisole (BG,) Italy).

2.2.4. X-ray Powder diffraction

For the characterization of the crystalline phases (in the mortar support and preparation layer where there was enough amount of sample for this technique), an X-ray diffractometer SIEMENS D-500 (scintillation counter, graphite secondary monochromator, Cu Kα radiation, 20kV, 40 mA) was used.

2.2.5. Synchrotron radiation microanalysis experiments

Synchrotron radiation Fourier transform infrared microspectroscopy (SR FTIR) in transmision mode was performed at the station ID21 at the European Radiation Synchrotron Facility (ESRF, Grenoble). Maps were recorded using 4 microns step and 40 scans for each spectrum. Aperture and resolution were fixed at 8 x 8 μm and 8 cm^{-1}, respectively. In all cases the aperture and the step size chosen generates overlapping areas in order to increase the resolution of the components. A microtome Ultracut E with a glass knife was used to obtain slices around 10 μm for the FTIR analysis in transmission mode.

SR XRD (Synchrotron radiation X-Ray diffraction) patterns were acquired at station ID18F of the ESRF as well. A focal spot of 2,3 microns in the vertical direction and 11 microns in the horizontal direction was chosen with steps of 2 microns in the vertical direction and 10 microns in the horizontal. A wavelength of 0,443A (28 keV) was selected and the acquisition time was 20 seconds per pattern. The diffraction signal was recorded in transmission by means of a 2-dimensional CCD-based X-ray detector (refined detector distance 107, 26 mm). The cross-section was placed into the focused

beam with the paint layers oriented horizontally. In this position the sample was scanned both horizontally and vertically to obtain a map. Patterns were fitted with the ESRF FIT2D package [12].

Synchrotron radiation X-Ray powder diffraction was performed at station 9.6 of the Synchrotron Radiation Source at Daresbury Laboratory facilities (UK). A wavelength 0.08664 nm was used and the slits were of 200 microns. The patterns were acquired in transmission geometry by a CCD collecting plate at 150 mm and fitted with the ESRF FIT2D package [12].

2.2.6. Samples

The mural painting samples from different Catalan works of art, whose study is reported in this chapter, are briefly described in table 2.1.

Table 2.1. List of the painting samples presented in the chapter.

Sample	Painting location	Period (century)	Sample origin	Description
SPT1	Sant Pere Terrassa church	11^{th}	Mural altarpiece	mortar
SPT2				Black painting sample
SPT3				Red painting sample
SPT4				Blue painting sample
SPT5				Black painting sample
SPT6				Superficial coating
SPT7				Blue painting sample
SBB1	Sant Benet Bages church	17^{th}	Ceiling of the crypt	Gilding sample
SBB2				Blck sample
SCPRE1	Royal palace of Santes Creus Monastery	17^{th}	Gypsum shield	Blue-green sample

2.3. Results and discussion

2.3.1. Characterization of calcium oxalates in samples from a stone altarpiece: the case of Sant Pere of Terrassa

The stone altarpiece in Sant Pere de Terrassa is one of the few stone preromanesque altarpieces remaining in Catalonia. Stone altarpieces were practically inexistent during the preromanesque period and more characteristic of the gothic one, making Sant Pere's altarpiece a really singular work of art.

The church of Sant Pere, built in the Romanesque style, is one of the most remarkable monuments of Terrassa (a city 30km far from Barcelona, located in the northeastern region of Catalonia). The church is part of a monumental ensemble of three Romanesque buildings together with Sant Miquel and Santa Maria. The complex is of particular interest due to not only the beauty of the Romanesque complex but also as a representing of different historic–artistic periods in Catalonia from the Iberian culture to nowadays [13]. Churches were finished around the end of the 11th century beginning of the 12th. Thus, they present a characteristic Romanesque style although the preromanesque Visigoth structures are partially preserved in the final structure[13]. The churches were declared National Monument in 1931. Thus the study of the materials and technique used by the painters in such a unique piece is of particular interest.

The studied altarpiece (1.80 x 3.50 m) consists in a wall closing the apse of the church whose mural painting represent several figures and geometric decoration. It is made of three rows of mural paintings: the two lines on top are made of blind arches (two arches on the top row and four on the middle row) were Jesus, Saint Peter and the evangelists are represented and a bottom area with some non identified figures. An scheme of the altarpiece design and a detail are shown in Figure 2.1.A.

The original design was modified some time after being finished (probably around the 14th century when the gothic paintings were made in the church) and new figures and decoration were drawn on top of the ancient ones. Nevertheless, both designs can still be observed nowadays. Later on, several repaints, reparations and redraws were done without being documented during the different modifications of the church. Although the altarpiece has been preserved in its original position, it was covered for years and it was only found during a restoration campaign of the church in 1895.

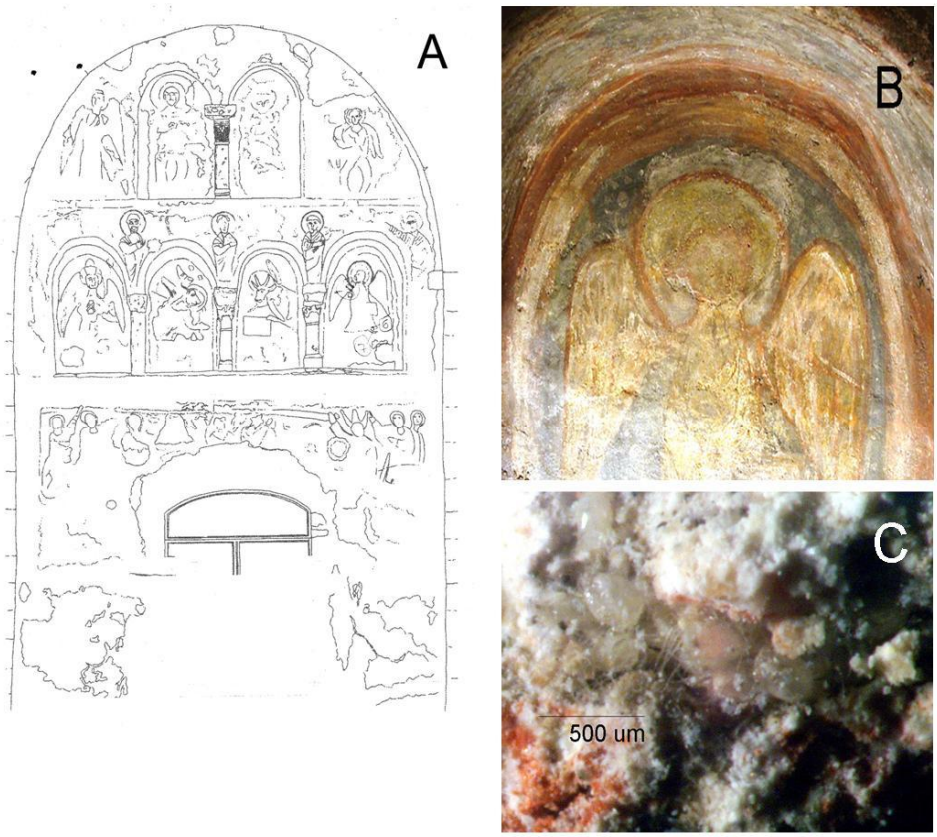

Figure 2.1.(A) Design of the altarpiece of Sant Pere of Terrassa; (B) Detail of one the pictures of the altarpiece where blue, red and ochre colors are present; (C) Presence of a biological colonization in the red sample preparation layer.

The piece looks partially deteriorated mainly because the space between the wall and the apse had been filled with different materials. Owing to that, salts had reached the painted surface, causing the decay and detachment of the painting layers. In some of the samples, the presence of biological colonization was detected mainly consisting in fungi that developed hifae penetrating trough the paint and the preparation layer (Figure 2.1.C).

Moreover, colors and design of the altarpiece are difficultly appreciable due to the application of an organic material on the surface in the restoration after being founded (20^{th} century). This layer is partially detached and the accumulation of dust in the surface is evident.

The color palette used in this piece is limited: white, black, red and several yellow colors are used the most. Blue has been applied in different background figures in the three rows of the altarpiece. Probably, a sky of stars was the background of some of the pieces. Additionally, very small blue spots can be appreciated surrounding the aureole of some figures.

2.3.1.1. Experimental Results

To characterize the materials used in this altarpiece, small samples (less than $2mm^2$) representative of each color individuated in the altarpice were collected by the restorers with the aim of determining the painting materials (pigments, filler and binder) as well as the painting technique and their state of conservation. They include some plaster substratum and chromatic layer. Samples have been described in Table 2.1.

XRD of mortar and preparation layers

The XRD pattern of the mortar under the preparation layer (sample SPT1) indicates that the main constituents are calcite ($CaCO_3$) and quartz (SiO_2), but small amounts of dolomite [$(CaMg)(CO_3)$] and clays (illite, kaolinite) were also present. These results are coherent with a lime mortar used as a substrate, which is constituted by lime (which becomes calcite after hardening) and small grains of quartz and dolomite with some contamination of clays as aggregate.

The XRD patterns of the preparation layer from pigment samples (SPT 2 to SPT7) show the same composition as the mortar and, besides, traces of calcium sodium phosphate ($NaCa(PO_4)$) which could be related to a decay by product associated to some organic additive, frequently applied to these layers.

Morphological Characterization of pigment layers

Optical Microscope observations of the samples cross-sections allowed the identification of a couple of layers (pigment layer on a white preparation layer) for all the samples but SPT 5, where two pigment layers were identified (black on top and red on the preparation layer) due to the drawing overlapping. Figure 2.2. shows some representative samples. A summary of the EDS results for the different layers is presented in Table 2.3. in the section reporting the discussion of results (see 2.3.1.3.).

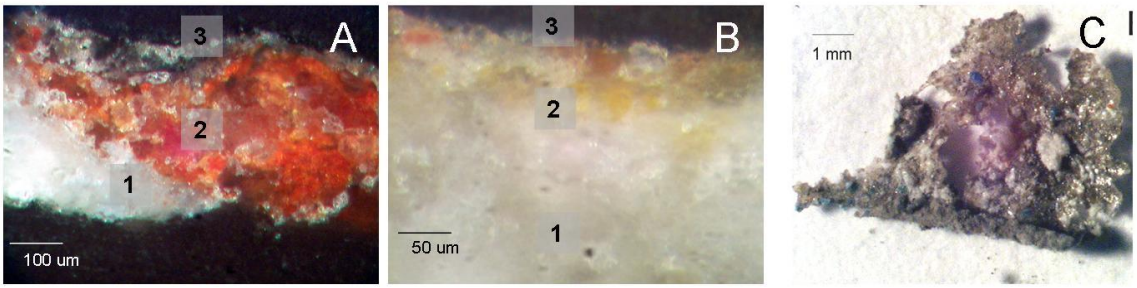

Figure 2.2.(A) Optical microscopic image of the polished cross-section of the red sample showing the three layers of the red sample: (3) top or coating layer, (2) red layer or pigment layer, (1) preparation layer; (B) surface of the sample where the top-coating layer can be clearly distinguished.

Sample SPT4 cross-section is also characterized by the presence of three layers. A cross-section of the blue painted layers is shown in Figure 2.3 where it can be seen that the blue layer (layer 3) was applied over an intermediate layer (layer 2) which is on the support (layer 1).

The main elements in the blue areas (layer 3) are Si, Ca and Cu, while other elements such as Al, S, K and Fe were found as minor components. According to the literature [14], the simultaneous identification of the three main elements (Cu, Ca and Si) would have been sufficient to indicate the presence of Egyptian blue (EB).

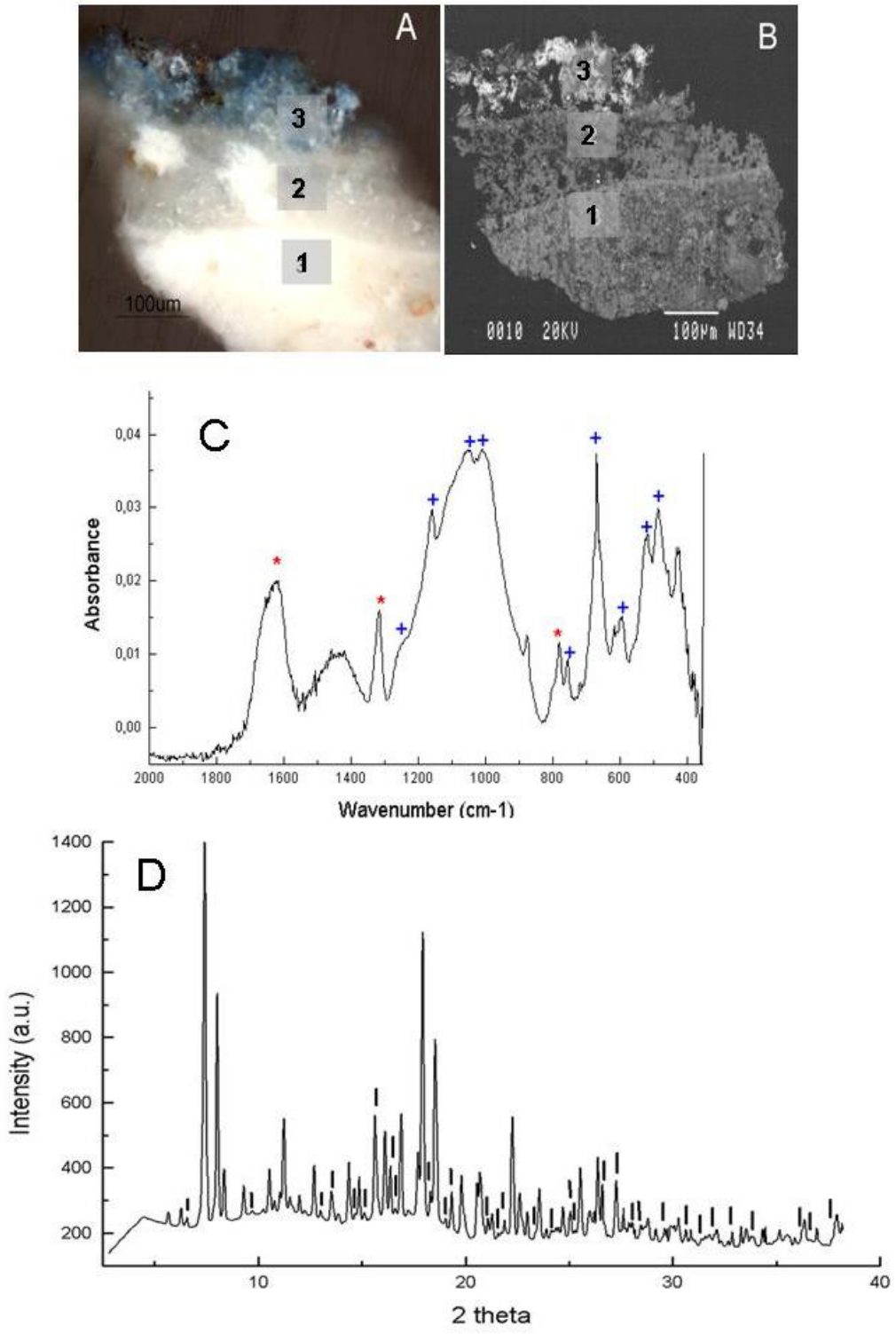

Figure 2.3. (A) Optical microscopic images of the blue sample cross-section; (B) Backscattered SEM image of a polished section of the blue sample. Three layers can be easily distinguished in both pictures; (C) FTIR spectra of the blue layer as diamond cell transmission spectrum. (+)indicate an absorption band of EB : 1230, 1160, 1051, 1008, 800, 755, 667, 595, 521 and 484 cm^{-1} .(*) indicates an absorption band of weddellite: 1640, 1322 and 790 cm^{-1}; (D) microXRD pattern of the blue sample, layer 1. Cuprorivaite (JCPDS 12-512) diffraction lines are indicated.

Fourier Transform Infrared Spectroscopy

The absorption bands found in the FTIR spectra of the different colors correspond to silicate signal (1033, 910 cm^{-1}) due to the earth pigments (clays) [15]) and peaks assigned to their crystallization water (3694 and 3617 cm^{-1}) [16]). Kaolinite seems to be present in most of the samples as a filler (1117, 1033,1010, 915 cm^{-1}) [17].

The FTIR spectra of the blue pigment layer (layer 3) in the sample SPT4 indicated the presence of bands in the characteristic region of silicates (1025-1080 cm^{-1}) ([18]) and the prominent bands of weddellite (calcium oxalate dihydrated: $CaC_2O_4 \cdot 2H_2O$) at 1640, 1322 and 790 cm^{-1} [3]). Bands at 1230, 1008 and 595, 521 and 484 cm^{-1} are peculiar to Egyptian Blue [18] . Only one of the spectra recorded showed those bands clearly enough (Figure 2.3C).

FTIR spectra also suggest the presence of organic matter highlighted by the absorption at 1727 cm^{-1}, indicating the presence of a C=O st bond, and absorptions at 3025, 2954 and 2923 cm^{-1} corresponding to the stretching vibration of hydrocarbonated chains [19]. Nevertheless, those absorption bands are in no way sufficient for a reliable identification of the organic binding medium. The FTIR spectrum of layer 2 in the blue sample suggests the use of a wax due to the characteristic CH_2 bands shown: 2915 (with a shoulder at 2950 cm^{-1}) and 2850 cm^{-1}[19]. The use of a wax as an intermediate layer is specific to the blue sample (SPT 4), as it has not been found in any other of the samples of the altarpiece. The spectrum of layer 1 contains strong carbonate absorptions due to the presence of calcium carbonate and strong calcium oxalate signal.

A protective layer coats most of the painted surfaces which, in many cases, detached part of the paint due to the retraction associated to its hardening (Figure 2.2.C). By comparison with the standards, the FTIR spectra peaks indicate the presence of a synthetic resin, probably an acrylic one [20,19].

The presence of magnesium sulphate (epsomite, $MgSO_4 \cdot 7H_2O$) has been reported in areas of the altarpiece where painting does not exist anymore and its origin has been related to the lixiviation of the mortars and other materials filling the space between

the altarpiece and the apse, heavily affected by humidity and water infiltrations. Table 2.2 summarized the band identified in the spectra of the samples.

Table 2.2. Bands identified in the spectra of samples SPT 2-7

Material	*Bands identified (cm-1)*
Clay	3694, 3617, 1117,1030, 915
Calcite	1420, 780
Epsomite	3399, 3256, 1660, 1122, 1100, 983, 623
Egyptian blue	1230, 1008, 595, 521, 484
Calcium oxalate	1640, 1322, 790
Binding media	2954, 2923, 1727
Wax	2915, 2850, 1466,1462
Acrylic resin	2985, 2929 (broad), 1733, 1280, 1240, 1162

SR X-Ray powder diffraction

Small grains of the sample were prepared to be irradiated with synchrotron radiation to acquire X-ray diffraction patterns. XRD pattern of the painting layer in SPT 4 is shown in Figure 2.3.D. XRD pattern indicates that the phases forming the sample are quartz (SiO_2), cuprorivaite ($CaCuSi_4O_{10}$) and weddellite ($CaC_2O_4{\cdot}2H_2O$), magnesium phosphate hydrate and newberyte ($MgHPO_4(H_2O)_3$). Gypsum ($CaSO_4{\cdot}2H_2O$) and cuprite (Cu_2O) were also present as minor phases.

The presence of cuprorivaite confirms the use of Egyptian blue as pigment. It has been reported [21] that quartz and other silica phases such as cristobalite are always present in Egyptian blue in high concentration. Moreover, as cuprite was found, that would mean not only that the raw mixture contained excess of copper [18], but also that pigment was synthesized under reducing conditions [22].

2.3.1.2. Discussion

Characterization of samples from the stone altarpiece of Sant Pere de Terrasa allow characterizing the pigments and the materials used as fillers. The presence of a binding media is suspected though no identification of it has been achieved mainly due to the high absorptions of inorganic compounds. Moreover, an acrylic resin as a coating material has been applied on the surface of the paintings, which now results to be deteriorated and strongly detached from the paint layers.

The pigments and other phases identified, as well as the analytical techniques used and the SEM-EDS results are shown in Table 2.3. for the different colors individuated in the samples.

Analytical investigations carried out on the painting layers of samples SPT 2, 3, 5, 6 and 7 by both EDS and FTIR determined a limited variety of pigments mostly based on clay minerals with different amounts of iron oxides (red and ochre samples), calcite (white samples) and charcoal black [23]. Blue was the only color far from the use of common pigments [24, 25].

Calcium oxalates were present in high amounts in the samples from pigment layers, presenting a high absorbance in the FTIR spectra. FTIR bands as well as SR XRD results confirmed the presence of weddellite, the dehydrated form, and not the presence of wewhellite or a mixture of them. This evidence could be indicative of the origin of this weddellite as an oxidative decay by-products of the identified organic binder [9,2] instead of a product of fungi or bacteria metabolism though in this case, some colonization have been individuated in the samples. The presence of phosphates has been reported as being related to both the degradation of organic material [7] an oxalate films formation [26]. Thus, no conclusions can be extracted on the oxalates formation mechanism.

Table 2.3. Description of the samples, and summary of the main results obtained with the different techniques.

	samples	*Elemental composition*	*Identified material*	*other phases identified*	*Analytical technique*
Mortar	SPT1	-	Calcite ($CaCO_{3)}$ Quartz ($SiO_{2)}$	Dolomite Illite Kaolinite	XRD
Preparation layers	SPT2-7		Calcite ($CaCO_{3)}$ Quartz ($SiO_{2)}$	NaCa(PO4) Dolomite Illite Kaolinite	SEM-EDS,XRD
red	SPT3 SPT5	Si, Ca, Al, Mg, Fe, P	Red earth Fe_2O_3 + clay	$CaC_2O_4.2H_2O$	SEM,EDS, FT-IR
yellow/ochre	SPT6	Si, Ca, Al, Fe, Mg, (Ti, S, K)	Yellow ochre Fe_2O_3 .H_2O + clay	$MgSO_4.7H_2O$	SEM,EDS,FT-IR
white	SPT7	Ca, Si, Mg, S	lime ($CaCO_3$)	$CaC_2O_4.2H_2O$ $MgSO_4.7H_2O$	SEM,EDS,FT-IR
black	SPT5	Ca, Si, Al, K, Mg	Coal black		SEM,EDS,FT-IR
blue	SPT4	Si, Ca, Cu K,S, Fe, Al	Egyptian blue ($CaCuSi_4O_{10}$)	$CaC_2O_4.2H_2O$	SEM,EDS, FT-IR SRXRD

In the mortar and preparation layers, calcium oxalates could not be detected by X-Ray powder diffraction though they were present in the blue sample (SPT4) by FTIR analysis. Finally, copper oxalates have not been characterized by SR XRD of the blue pigment layer meaning that Cu in cuprorivaite is not able to react with the oxalic acid like other copper-based pigments, such as azurite, can do.

Thus, SR XRD not only confirms the presence of calcium oxalates in the pigment layer and the crystalline form of calcium oxalate being weddellite, but also allow the unequivocal identification of the nature of the blue pigment. Egyptian blue was quite widely used from the third millennium B.C. to the Roman period. The use of such pigment after the Roman empire was rare but it has been reported [27] in some Italian

paintings (Church of San Clemente, Rome) and Carolingian wall paintings in Müstair (Switzerland) in the 9th century [22] , but it has never been identified in the 10th century or later. There are neither written references to the production of Egyptian blue in medieval times (in fact, scholars agree that its manufacture was lost some time in the late Roman period), nor evidences of production of this pigment in the site nor in the region.

Therefore, some hypothesis should be considered: the reuse of an Egyptian Blue pigment found nearby during an ancient restoration, the use of a modern pigment in a modern restoration and the production of Egyptian Blue during the middle ages.
However, Egyptian Blue has not been characterized in Catalan paintings of the same period nor later. Although the pigment has been characterized in Roman paintings such as Vila del Munts (Tarragona), no evidences of the production of Egyptian Blue in Catalonia during the middle ages have been found. Therefore, the use of Egyptian Blue during an ancient re-paint of the altarpiece (probably from the 12th to 14th century) seems to be possible only if the re-use of Roman pigment found by the painters, either as powder or as balls [18, Mr. Tite personal communication] has taken place. It is important to notice that the site where the church is located was formerly a Roman settlement. A later restoration process, probably after the founding of the altarpiece in 1896 using modern Egyptian Blue seems rather less plausible.

2.3.2. Distribution of weathering products of azurite in mural paintings from the Monastery of Santes Creus

Samples analysed come from a gypsum shield on top of a door in the monastery of Santes Creus (Catalonia, Spain) dating from the 1605 a.D. The shield is depicted mainly in blue and brown in order to underline the relieves with the monastery insignias. In the blue areas, green shades could easily be identified (Figure 2.4A).

Many paintings became altered by the transformation of blue areas into green and brown. Clear examples of the problematic above described are the frescoes at the Monumental Cemetery of Pisa or the Crypt of the Cathedral of Siena [28,29].

Azurite is a basic copper carbonate ($2CuCO_3.Cu(OH)_2$), a natural blue pigment used since the Fourth Dynasty in Egypt although it became the most important blue pigment during the Middle Ages and Renaissance [30].

Green shades in azurite blue paintings could be attributed to different reasons depending on their composition: natural green shades of the mineral ore, the use of synthetic green pigments obtained from copper plates exposed to vinegar, or degradation of the original pigment into green products such as copper chlorides.

Although azurite may have a natural greenish undertone due to the particles of malachite ($CuCO_3.Cu(OH)_2$) and cuprite (Cu_2O) that can be found associated in nature to the azurite ores [31], the desiderated blue tone can be obtained by purification of azurite from the other phases as it was provided by authors such as Cennino Cennini [31]. Also, though the synthesis of green pigments have been reported in Heraclius, Teophilus or Vitruvius recipies [32,25], the synthesis process products have been already characterized as mixtures of copper acetates, carbonates and hydroxychlorides [6], this is to say, a different composition from that of the degraded azurite-based paintings characterized in literature.

Thus, degradation of azurite blue pigment into a green product due to ageing seems to be the cause of the greenish areas observed in different azurite paintings. Azurite, although being stable to light and atmosphere, presents frequent chromatic alterations to greenish tonalities due to transformation into paratacamite and atacamite ($Cu_2Cl(OH)_3$) [33,34]and also malachite ($CuCO_3.Cu(OH)_2$) [31] not yet completely understood.

Synchrotron IR microscopy have been used to produce maps of high contrast chemical imaging. Results helped to determine the distribution of those products along the blue layer. To complement the information Py/GC/MS and GC/MS techniques were applied in order to characterize the binding media and organic materials present as well as their degradation products. Thus, these experiments constitute a significant contribution to better understand the chromatic degradation of azurite blue layers and the mechanism of formation of their decay by products. Moreover, experiments add information to the oxalates formation mechanisms in mural paintings.

2.3.2.1. Experimental Results

Morphological characterization

Samples (Table 2.1.) taken from the blue sampling area in the bottom right side of the shield and present different characteristics under the stereomicroscope. Some of the fragments exhibit a blue colour while others were completely greenish (Figure 2.4.B). Moreover, some of the fragments contain other layers such as a white and a brownish one (Figure 2.4.C).

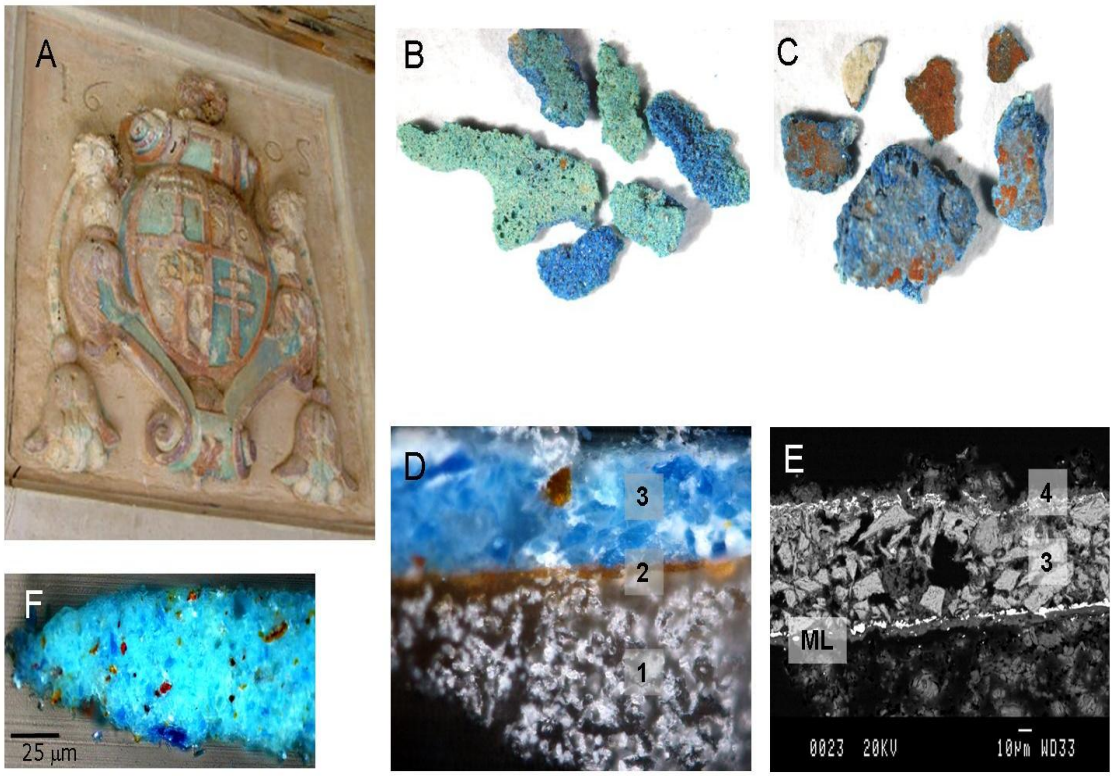

Figure 2.4. (A) Sampled shield; Several fragments of the sample of different characteristics : (B) blue and green shades; (C) a brown layer; Cross-section of the sample : (D) optical microscope image. 3 layers can be easily appreciated; (E) backscattered SEM image : a superficial layer (layer 4) and a metallic leaf between layer 2 and 3 are shown; (F) different fragment were the green shades of the matrix and the blue particles in between can be noticed.

A cross-section (figure 2.4.D) clearly evidences the presence of different layers: a white preparation layer (layer 1), a brown pigment layer (layer 2) and the blue layer of interest (layer 3), corresponding to the ones observed under the stereomicroscope. The fractured appearance and the irregular size (from 5 to 20 um) of the blue particles in layer 3 are characteristic of azurite [31]. In this sample no green shades were observed.

Figure 2.4.F shows the cross-section of another embedded fragment consisting in the blue layer (layer 3) without the rest of the layers that formed the complete stratigraphy. In this fragment it is appreciable the presence of a matrix of green shades and the existence of blue particles in between.

SEM images underline the different morphological features of the layers. The same three layers already oberved by optical microscope can be also easily identified in backscattered electron images (figure 6.4E). A metallic leaf of about 2,5 microns thick (between layers 2 and 3) and a superficial layer on top of the blue one (layer 4) can be appreciated too (figure 6.4E).

The chemical elements forming layer 1 detected by EDS (Ca, S) can be attributed to calcium sulphate ($CaSO_4$. n H_2O), which agrees with the morphology of the layer [35,36]. The main elements detected in layer 2 (Si, Al, Ca, Fe) can easily be attributed to the presence of a clay with iron oxides [15,37]. The P and S also detected in layer 2 could be attributed to an organic material present as binding media in this layer [7].

The blue pigment layer (layer 3) is characterized by the presence of Cu and by the broken appearance and the big size (from 5 to 20 μm) of some of the pigment particles. Those results are consistent with the use of a copper pigment such as azurite [31]. In other of the fragments analysed where green shades could be appreciated (figure 2.4F) the presence of Cl together with Cu was also detected in layer 3.

The metallic leave is made of silver (Ag). Finally, in the white superficial layer (layer 4) the presence of Pb can be probably attributed to the presence of a lead compound such as lead white ($PbCO_3$. $Pb(OH)_2$).

Fourier Transform Infrared Spectroscopy

Remaining fragments of the sample were analysed by Fourier Transform Infrared Spectroscopy (FTIR) in transmission mode using a diamond cell. Particles of each layer were isolated using a dissecting knife and tungsten needles under a stereo-microscope [38]. This way, information on the different layers was obtained separately. Some characteristic spectra of the different layers are presented in Figure 2.5. Table 2.4. presents the bands characteristic of each spectra obtained, while Table 2.5. shows the reference characteristic bands reported in the literature for the materials identified.

Table 2.4. FTIR bands detected in the different layers of the sample by transmission in a diamond cell.

Layer	*Bands detected (cm^{-1})*
3 blue-green	3428, 3342, 1638, 1316, 1115(b), 1034, 987, 947, 833, 779
3 blue	3428, 3309, 2557, 2505, 1638, 1464, 1403, 1370, 1329, 1115, 1095, 1034, 960, 894, 833, 773, 505, 458, 403
2	3697 , 3620, 1650 , 1540 , 1416 , 1315 , 1100, 1022, 916, 542, 472
1	1683, 1620, 1313, 1114, 1004, 779, 669, 596, 463

In layer 1, the bands at 1683, 1620, 1315, 1114 (broad), 1004, 779, 669, 598 and 463 cm^{-1} correspond to gypsum ($CaSO_4$. $2H_2O$) and calcium oxalates (CaC_2O_4. n H_2O) [37,38,39,40].

Layer 2 is characterized by the presence of the peaks at 3697 and 3620 cm^{-1} (OH st), a broad band around 1022 cm^{-1}, with a shoulder at 1100 cm^{-1} (Si-O st), and a peak at 916 cm^{-1} (Si-H bd). These peaks can be attributed to a clay, probably kaolinite by the characteristic OH st bands [41,43] .

The bands at 542 and 472 cm^{-1} can be interpreted as iron oxides characteristic peaks. The bands of iron oxides centered at 560 and 480 cm^{-1} can differ by up to 30 cm^{-1} due

to differences in particle size and shape of the pigment particles [15], the presence of Fe detected by EDS would corroborate the assignment of the bands

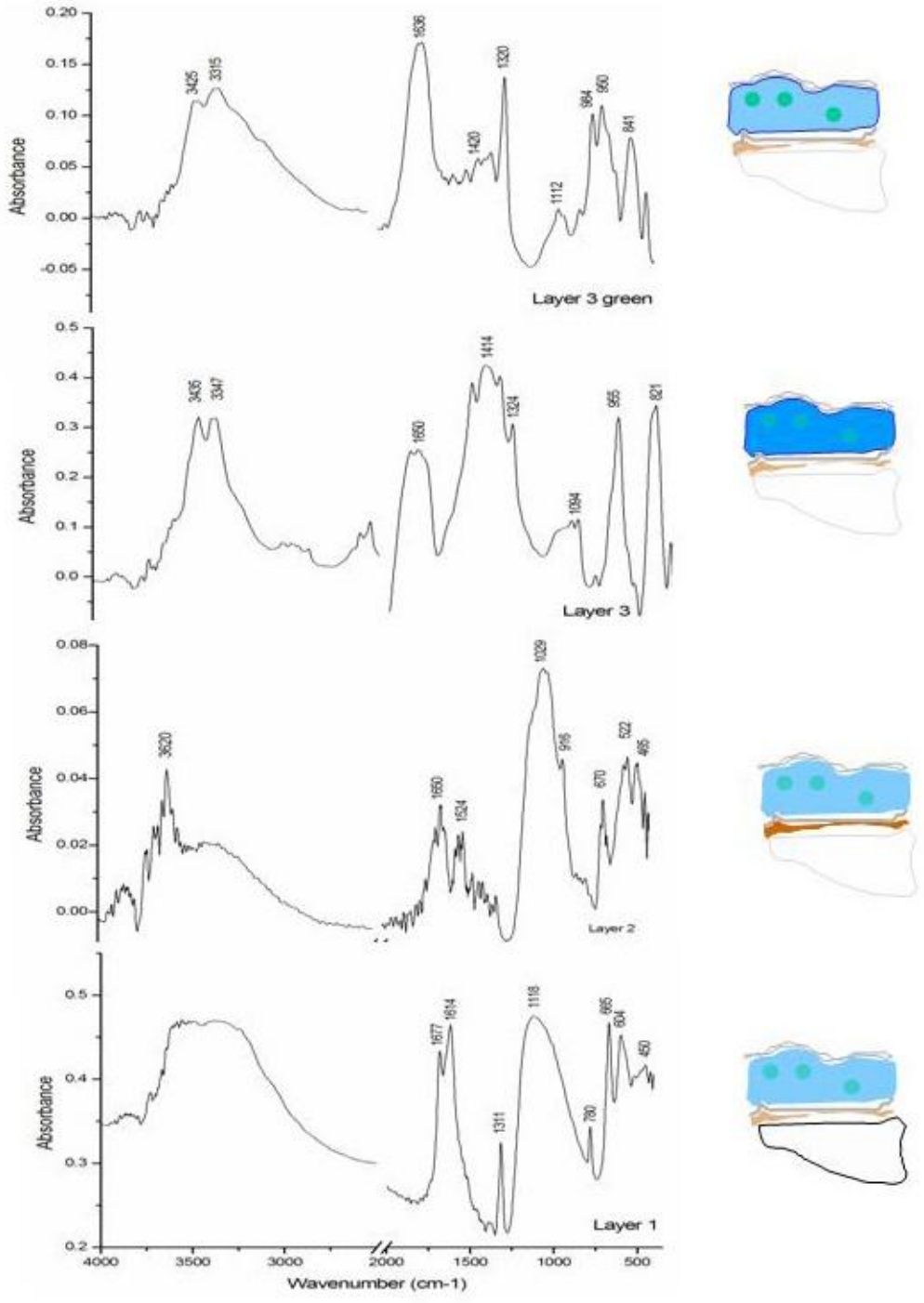

Figure 2.5. FTIR spectra in transmission mode of (A) ,(B),(C) the different layers of the sample.; (D) Selection of green particles from Layer 3. Conditions : 30 scans, 4 cm^{-1} resolution. On the right side a scheme of the cross-section of the sample indicated the layer analysed.

Table 2.5. Transmission FTIR characteristic bands of materials reported in the literature.

Azurite $2CuCO_3.Cu(OH)_2$	Atacamite $Cu_2Cl(OH)_3$	Paratacamite $Cu_2Cl(OH)_3$	Weddellite $CaC_2O_4.2H_2O$	Whewellite $CaC_2O_4.H_2O$	Copper Oxalates CuC_2O_4	Gypsum $CaSO_4$	epoxy embedding medium
						3541	3531
	3443	3448		3483			3467
3425 (s)				3425	3423	3403	
	3341	3354		3336	(w)		
		3322(sh)					
				3256			
				3061			
							2960
							2935
							2872
							1736
	1654 (w)		1645(s)			1690	1669
				1623(s)	1659	1619	
1496(s)					(vs)		
1465(m)							1457
1416(s)							1412
				1378 (vw)			1378
			1321 (s)	1321(s)			1345
					1364 (s)		1256
					1321	1169	1159
1092(m)	1089 (vw)				(m)	1089	1047
	985	986					
951	950			947 (vw)			
	915	923	920 (vw)				
	890	905		880(vw)			
	849	863					
831	818	825	780 (m)	782(m)			
769							
742				666		671	
	595	577	618	591	825 (m)	604	
	515	515	514(w)	515			
497	480						
457	448	457				462	
					502		

Oxalate peaks are also present in this layer (layer 2): C=O st at 1620 cm^{-1}, C-O st at 1320 cm^{-1} and C-C st at 780 cm^{-1} are indicative of calcium oxalates [42]. Some not well defined bands around 1650, 1530 and 1400 cm^{-1} could be indicative of the presence of a proteinaceous binder (C=O st Amide I, Amida II and C-N st, respectively) [41]. The noisy of those bands does not allow a clear identification.

Blue particles in layer 3 present the characteristic peaks of azurite confirming the identification of the pigment by means of microscope observations (optical and electronical) and EDS results [31]. Peaks at 3430 (OH st), 1460 and 1414 (CO st), 1092 (OH bd), 955 (CO bd), 837 and 769 cm^{-1}(CO bd), are clearly identifiable in the spectra of layer 3 in figure 2.5.[43]

Green particles in layer 3, however, together with azurite characteristic peaks (cited above), present the bands of copper hydroxychlorides (atacamite and paratacamite): 3440 and 3322 (OH st), 986, 948, 896, 837cm^{-1} [36]. The presence of the characteristic peaks of copper oxalates such as 1659, 1364 and 1321 cm^{-1} (reported above), can be also appreciated allowing the identification of copper oxalates together with copper hydroxychlorides.

Gas chromatography mass spectrometry techniques

For the characterization of the organic materials present in the sample, gas-chromatographic mass spectrometric techniques were applied.

Py/GC/MS results of layer 2 and layer 3 (both blue particles and green particles separately) highlighted the presence of a polysaccharide material by the identification of the characteristic markers: tri-(O-TMS)-levoglucosane and 1,2,3,5-tetrakis-(O-TMS)-xylofuranose and others unknown polysaccharides compounds. The pyrogram of the sample is shown in Figure 2.6. [44].

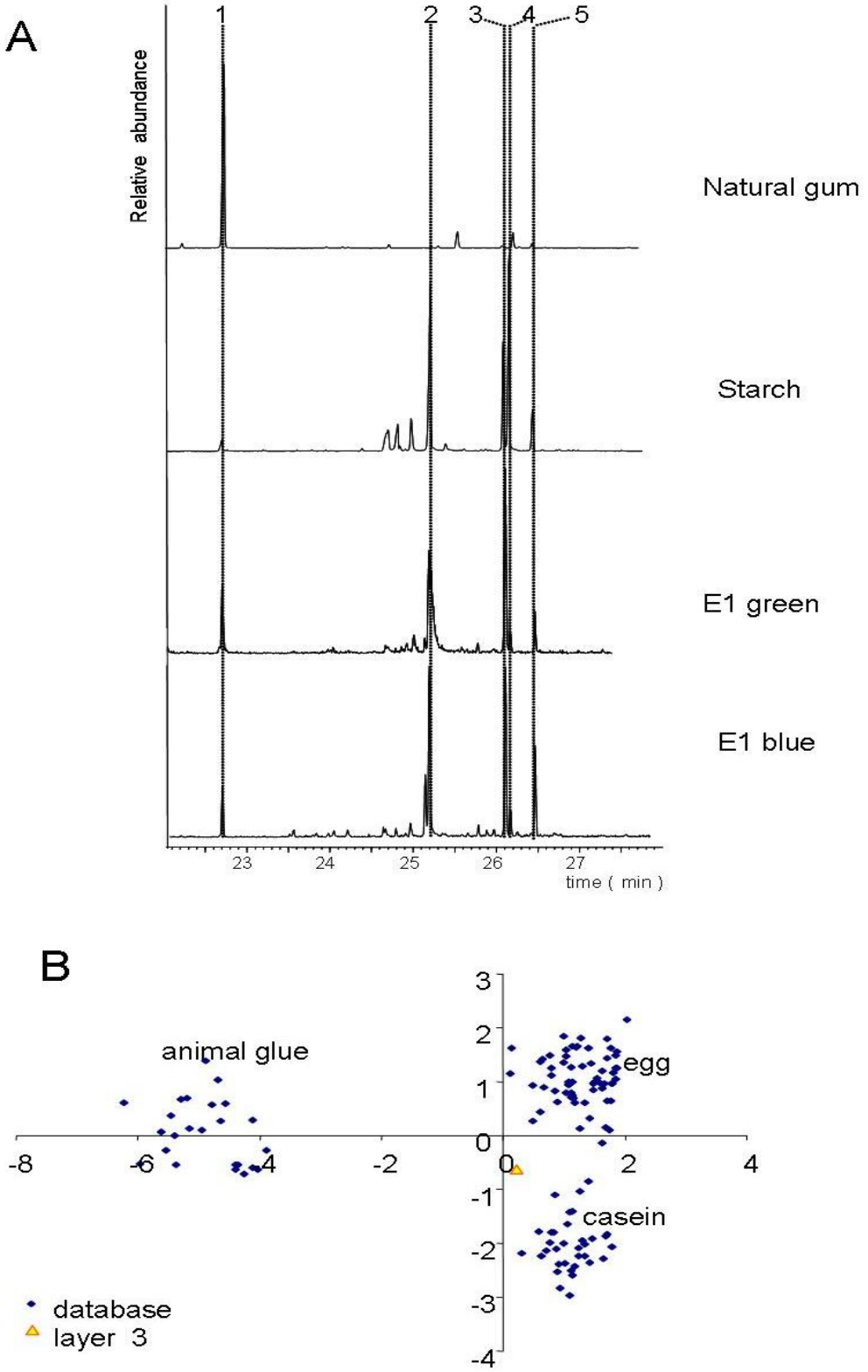

Figure 2.6. (A)Extracted chromatograms of the ions with m/z 217 of the reference materials compared with the green layer and the blue layer of sample E1: peak 1= 1,2,3,5-tetrakis-(O-TMS)-xylofuranose , peaks 2, 4 and 5= unidentified polysaccharides compounds, peak 3= tri-(O-TMS)-levoglucosane. (B) Principal Component analysis score plot of the amino acids percentage relative content in sample E1.

In Figure 2.6.A are also reported for comparison the extracted ion chromatograms of the ions with m/z 217 of the reference materials cherry gum, as an example of fruit gum, and starch. Both the green and blue samples present the main pyrolysis product of glucose based polymers (as an example starch is reported in Figure 2.5.A). Moreover 1,2,3,5-tetrakis-(O-TMS)-xylofuranose (peak 1), absent in the pyrogram of starch, has been identified in both the samples, suggesting the simultaneously presence of a fruit gum.

GC/MS results were achieved by using the combined procedure already described in the literature [10]. Layer 2 and layer 3 were again analysed separately. Purification of layer 3 fragments was necessary due to the presence of azurite. Copper based pigment can form aggregates with the proteinaceous material; in this way some derivatisation problems occur. A solid phase column was used to avoid derivatisation problems as described in the literature [45].

Layer 3 (green-blue layer) presented a proteinaceous material quantity slightly higher than the blank of the technique. The aminoacidic percentage relative content in the samples is reported in Table 2.6. The PCA treatment of the sample aminoacidic profile indicates that the sample can not be attributed to a cluster but it is situated in between the egg and the casein clusters (Figure 2.6.B). That could be attributed to the high degradation of the proteinaceous material in the sample. The high glycine content in the sample could be attributed to a bacterial attack [46]; this could have also generated the low levels of aspartic acid that would justify the sample shift towards the casein cluster.

Besides, the fatty acid composition of layer 3 highlights a profile that is not an oil nor a whole egg one. Characteristic ratios (A/P=0.15, P/S=0.8; ΣD=5.0) are not consistent with the ones of a siccative oil, but the content of dicarboxylic acids could suggest the the use of an egg undergone to deterioration as binding media. Moreover, an animal fat has been identified by the presence of linear pentadecanoic, eptadecanoic, nonanoic acids and their branched isomers.

Table 2.6. Amino acidic relative percentage content of layer 3 compared to characteristic values of egg, casein and animal glue.

sample	*Ala*	*Gly*	*Val*	*Leu*	*Ile*	*Ser*	*Pro*	*Phe*	*Asp*	*Glu*	*Hyp*
Milk(casein)	5.0	3.0	7.6	11.9	6.6	5.8	11.5	5.9	8.5	22.2	0.0
Egg	7.7	4.8	7.7	11.0	6.7	10.3	5.7	6.4	12.6	15.0	0.0
Animal glue	12.3	29.4	3.9	4.7	2.5	3.8	12.4	2.8	6.6	9.9	7.7
Layer 3	7.1	21.6	8.3	18.1	9.2	2.6	7.6	6.0	5.7	13.9	0.0

Distribution of compounds in the blue layer by SR FTIR

Remaining fragments of the blue layer were prepared for the mapping experiments performed at the ESRF in order to establish the distribution of the compounds already identified. For these experiments, sample preparation has been described in a previous chapter (see Chapter 1) and already published [47]. Sample preparation is the key point in order to be able to perform transmission experiments. [48, 16].

The embedding of the sample in an epoxy resin (spurr) and the microtoming of 10 μm slices give results good enough without loosing distribution information. The infiltration of the resin in the sample was not a real problem as organic materials were almost inexistent and the inorganic compounds to be studied present characteristic intense bands easily identifiable in the spectra with few overlappings with the embedding resin peaks. Quality of the spectra was good enough for slices from 4 to 10 μm.

The slice of 10 μm presented in Figure 2.7.B was selected for the mapping. The thin section presented some holes due to the microtoming process in the mapped area of 130 μm per 140 μm. A white area corresponding to the presence of layer 1 can be appreciated in the bottom left part of the mapped area next to the hole. The hole seems to correspond to the layers 2 and 3 that is the brown layer next to the metallic leave lost in the microtoming process. The rest of the mapped area corresponds to layer 3 (blue-green layer).

The spectra were individually evaluated considering three different wave number ranges where the embedding media characteristic bands (Table 2.5.) allow the identification of some functional groups.

Range 1 (4000-3000 cm^{-1}) allows the identification of the particularly intense stretching OH bands of copper hydroxychlorides and azurite. In this range the resin presents just a not intense resin broad band.

Range 2 (under 1000 cm^{-1}) presents no bands of the embedding media. In this range, CO bending of azurite, C-C of oxalates and C-Cl st of copper hydroxychlorides are displayed. All bands of copper hydroxychlorides occur in the ranges 1 and 2 and their characterization is completely unequivocal.

Range 3 (1700-1000 cm^{-1}) presents different characteristic bands of the embedding media which penetration can be easily noticed by the presence of the CH stretching characteristic bands at 2960, 2935 and 2872 cm^{-1} and the C=O stretching at 1736 cm^{-1}. Their presence indicates that CH stretching and C=O st can not be used for organic material identification and that bands in range 3 (1700-1000 cm^{-1}) should be considered carefully (to avoid confusion with the rest of the bands of the embedding resin in this range).

However, as it is stressed by the bands of the reference materials presented in Table 2.5., some characteristic bands of azurite and oxalates do not completely overlap with those of the embedding media. The intensities of some of the inorganic functional groups absorbencies make some of them easy to be recognized when present, also in the presence of the embedding media bands, due to their characteristic shape or the intensity changes that generate to the pure embedding resin spectrum. Moreover, some of the spectra did not present embedding media interferences at all.

On the basis of the individual evaluation of the spectra, a representative line in the mapped area was selected in order to perform a line scan. A line scan of the sample is a representation of a unique series of spectra crossing the sample , thus the wave numbers versus position plot. The lines can allows the easy identification of the main spectral features in a chosen in depth line.

The line selected for the lines can generation, as considered representative, is depicted in the microtomed section (Figure 2.7. B). Some highlighted areas, corresponding to the intense bands in the spectra of that position in the line, are the result of the absorbance of the embedding resin. Those bands (specified above and Table 2.5.) are marked with a grey dotted line on top of the line scan image in Figure 2.7.C.

The linescan starts in the area correspondent to layer 1 (position 0) and finishes at the end of the microtomed section in layer 3 (position 110). In the bottom of the linescan (spectra 0 to 30, corresponding with area 4) characteristic bands of the OH st of gypsum correspond to a highlighted broad area around 3500 cm^{-1}. Another highlighted area around 1100 cm^{-1} corresponds to the sulphate.

A broad area around 1650 cm^{-1} corresponds to the presence of both HOH st bands of gypsum (1680, 1620 cm^{-1}) and the C=O st of oxalates (1659, 1620 cm^{-1}). This broad band is not present in the scans from 30 to 110 although a narrower band corresponding to C=O st of oxalates is present in some of the spectra such as scan 80-90.

Finally, scans from 0 to 30 clearly present two narrow bands corresponding to the copper oxalate characteristic C-O st vibrations at 1359 and 1320 cm^{-1} with similar intensities consistent with the presence of copper oxalate in the spectra of these area.

From scan 30 to 110, two different highlighted bands at around 3430 and 3340 cm^{-1}correspond to the OH st of azurite and the hydroxychlorides are highlighted.

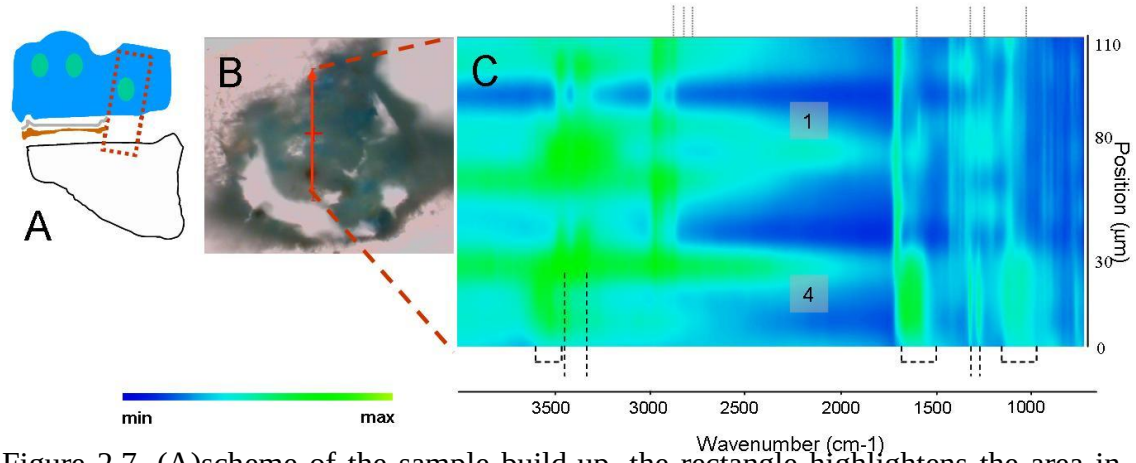

Figure 2.7. (A)scheme of the sample build-up, the rectangle highlightens the area in the slice; (B) Photomicrograph of the sample, the red line indicates the selected line to perform the linescan; (C) Linescan of the sample. Grey dotted lines on top of the linescan indicate the characteristic bands of the embedding resin while black slashed lines on the bottom evidence the bands highlighted corresponding to the main features

In Figure 2.8. the sample build-up scheme and the maps of the bands selected from the individual spectra and lines can evaluation are reported. Table 2.7. summarizes the bands mapped in Figure 2.8.

Table 2.7. Bands mapped by SR FTIR imaging experiments

Band Mapped (cm^{-1})	*Attributed functional group*	*Material*
3540	OH st	gypsum
3445	OH st	hydroxychlorides
3354-3337		
3430	OH st	azurite
1650	HOH st	Gypsum
	C=O st	oxalates
1365	C-O st	copper oxalates
1320	C-O st	oxalates
1120	SO_4	gypsum
825	C-C st	copper oxalates
780	C-C st	Calcium oxalates

In Figure 2.8. the sample build-up scheme and chemical images of the FTIR bands reported in Table 2.7. are presented.

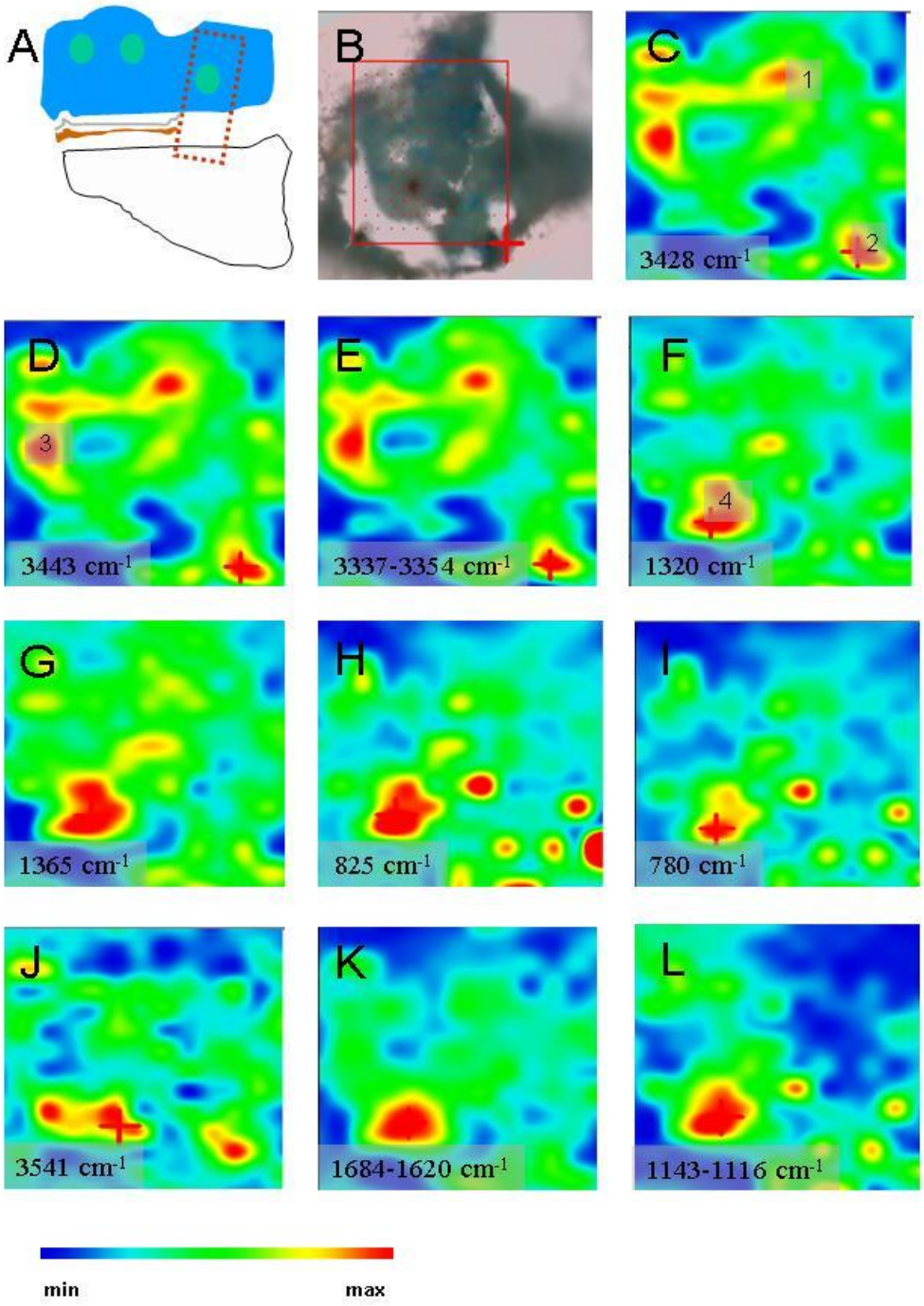

Figure 2.8. (A) scheme of the sample build-up, the rectangle highlightens the area in the slice; (B)Photomicrograph of the microtomed cross-section. The rectangle marks the area selected to perform the SR FTIR mapping; chemical image of (C) 3428 cm^{-1} (D) 3443 cm^{-1} (E) 3337-3354 cm^{-1} (F) 1320 cm^{-1} (G) 1350 cm^{-1} (H) 825 cm^{-1} (I) 780 cm^{-1} (J) 3541 cm^{-1} (K) 1620-1684 cm^{-1} (L) 1116-1143 cm^{-1}. Numbers in (C), (D) and (F) indicate the area corresponding with the spectra presented in figure 2.9. Mapped area 130 x 140 μm.

The mappings of the OH stretching bands characteristic of azurite (3430 cm^{-1}), atacamite (3445, 3353 cm^{-1}) and paratacamite (3449, 3360, 3320 cm^{-1}) indicate the same areas of occurrence (higher intensity of the characteristic bands) for all of them (areas 1,2,3 in the mappings in figure 2.8.).

The spectra of the areas underlined by the mapping are reported in Figure 2.9. Spectra present two intense bands in range 1(4000-3000 cm^{-1}). Those broad bands are centred at 3448 cm^{-1} and 3340 cm^{-1}. The resolution of the experiment of 8 cm^{-1} does not allow to distinguish between atacamite and paratacamite nor establish the presence of azurite. In fact, reference spectra of both copper hydroxychlorides mixtures give similar results.

The rest of the bands of individual spectra of areas 1,2,3 in range 2 (under 1000 cm^{-1}) are 985, 953, 919, 895 cm^{-1} and a broad band at 840 cm^{-1} with a shoulder at 820 cm^{-1}. Those bands mainly correspond to the C-Cl st of atacamite and paratacamite [41]. However, the intensity of the band at 950 cm^{-1} together with the presence of a broad band around 840 cm^{-1} was considered indicative of the presence of azurite. The shoulder at 820 cm^{-1} could also be in correspondence with the C-C bands of copper oxalates although azurite can present a less intense band also at this wavenumber.

In fact, the band at 1321 cm^{-1} of oxalates (CO st) can be easily identified in range 3 (1700-1000 cm^{-1}) together with a band at around 1650 cm^{-1} and a peak at 1365 cm^{-1}. The occurrence of those bands indicates the presence of copper oxalates in those areas.

Moreover, the features of the spectra of area 1,2 and 3 in the range 1500-1400 are not in correspondence with those of the embedding medium reference spectra but resemble those of the characteristic peaks of azurite at 1465 and 1423 cm^{-1} (CO st), in accordance with the bands at 950 and 840 cm^{-1} (CO bd) observed in the same spectra in range 3 (above mentioned). Thus, azurite is mixed together with copper hydroxychlorides and copper oxalates in those areas (areas 1 to 3).

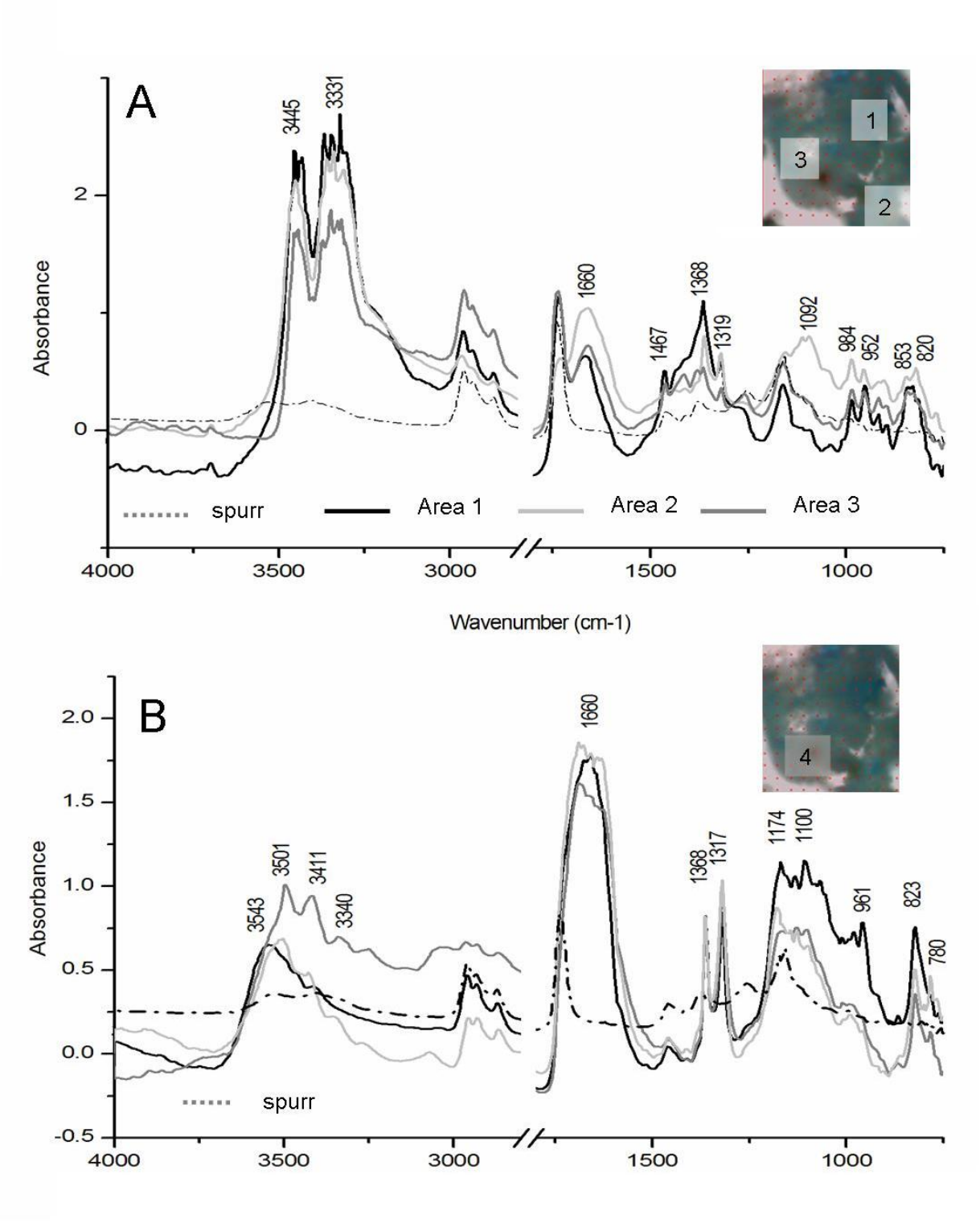

Figure 2.9. Selected SR FTIR spectra of the representative areas 1,2 and 3 (A) and different spectra from area 4 (B). Areas were also indicated in Figure 2.8.

However, when mapping the characteristic bands of oxalates, that is 1320 and 1630 cm^{-1}, a different area (area 4 in figure 6.8) presents major peak intensities. Mapping the specific peaks of copper oxalates (1365 and 825 cm^{-1}) and calcium oxalates (780 cm^{-1}) separately, major intensities coincide again in the same area (area 4). In the spectra of area 4 (figure 2.9 B) all those bands can be identified meaning that probably both kind of oxalates (calcium and copper) are present. In this area none of the peaks of azurite nor copper hydroxychlorides could be detected but other characteristic features were observed.

Range 1 (4000-3000 cm^{-1}) of the spectra of area 4 does not present the intense bands characteristic of hydroxychlorides but different bands corresponding to those of HOH st of oxalates and those of the OH st of gypsum (3540 cm^{-1}). That is in correspondence with the broad band around 1650 cm^{-1} and the presence of a band around 1150 cm^{-1} in those spectra. The broad band at 1650 cm^{-1} is the result of calcium and copper oxalate (1659 cm^{-1}) bands together with those of HOH st of gypsum (1685 and 1620 cm^{-1}) while the peak around 1150 cm^{-1} would correspond to the stretching of the sulphate group. The presence of gypsum in this area is consistent with the preparation layer (layer 1) observed in the microtomed section.

The mapping of the characteristic vibrational bands evidenced in the individual spectra of area 4 are again consistent with the higher absorbance of those vibrational bands mainly in area 4. Thus, oxalates are mainly distributed next to the gypsum layer although they were also present in the areas were azurite and hydroxychlorides were mainly present.

2.3.2.2. Discussion

The combined interpretation of results of different techniques allows to reliably characterize the samples from an organic and inorganic point of view. By this way, the composition of the different layers was established. Results of the characterization of the sample are reported in Table 2.8.

Table 2.8. Summary of the results obtained by means of FTIR, SEM-EDS, PY/GC/MS and GC/MS techniques.

Layer number	*color*	*Thickness /μm*	*Layer description*	*EDS*	*FTIR*	*PY-GC/MS*	*GC/MS*
4	Grey	5-6	Superficial patina	Pb	Lead white	-	-
3	Green-blue	50	Pigment layer	Cu, Cl	Azurite Copper Hycroxychlorides Oxalates	Polysaccharide material	Egg Animal fat
M	-	2-5	Metallic leave	Ag	-		-
2	brown	10	pigment layer Mordant (adhesive layer of metallic leaf)	Si Al Ca Fe, Ti, Cl, P, S	Clay Iron oxides oxalates	Polysaccharide material	-
1	white	100	Preparation layer	Ca, S	Gypsum Calcium oxalates	-	-

Although the organic material presents some difficulties for its reliable identification, due to its degradation and low amount, the presence of a proteinaceous material in the blue layer and polysaccharide material in both pigment layers seems clearly established. The aminoacidic profile together with acidic fraction results, allow to identify the proteinaceous material as egg. Moreover, an animal fat seems also been used as binding media.

Compounds formed as a result of the synthesis of green pigments such as copper acetates or malachite have not been identified which lead to discard the use of a synthetic green mixture of different copper compounds such as the ones described by Teophilus or Heraclius and confirm the degradation hypothesis for the green shades of the blue layer .

The presence of azurite used as blue pigment in the blue layer, and the mixture of copper hydroxychlorides and copper oxalates in the green areas of this layer was clearly established by conventional FTIR. Calcium oxalates were also identified in high amounts in layer 1.

SR FTIR experiments underlined the presence of hydroxyhlorides and copper oxalates in the blue layer. The products of degradation (copper hydroxy chlorides) look like being mainly formed on top of the blue pictorial layer far from the gypsum layer 1). Azurite is also mixed with copper hydroxy chlorides in those areas. Copper oxalates, although being also present together with azurite and the hydroxychlorides, are concentrated next to the preparation layer where their characteristic peaks are predominant in the spectra. The presence of calcium oxalates in this area may be due to its high concentration in layer 1 (characterized by conventional FTIR).

The presence of an organic material (egg) as binding medium in the blue layer has been unequivocally characterized by means of gas chromatography coupled with mass spectrometry (GC/MS). Moreover, not only calcium oxalates but also copper oxalates were founded in the samples. Copper oxalates were formed in layer 3 were copper is present due to the presence of the pigment azurite while in layer 1 (mainly calcium sulphate) calcium oxalates were formed. Thus, the formation of oxalic acid that combines with calcium or copper depending on their disponibility in the layer is clearly established. However, the degradation of the binding media by a bacterial attack would strongly suggest the formation of oxalates as a result of the action of the bacteria on the organic material used as binding media.

Finally, although Synchrotron radiation techniques add spatial information to the characterization of the blue layer, that is, to the azurite degradation products distribution, the technique presents the intrinsic difficulties that prevented the unequivocal characterization of inorganic compounds present.

2.3.3. Development and distribution of calcium oxalates in gilding decorations from the Monastery of Sant Benet del Bages

The monastery of Sant Benet del Bages was founded around 950 a.C. and its life lasted until 1835 a.C. Several transformations occurred until the abandon by the community in the 19th century. The original Romanesque crypt is allocated under the main altar and it has been deeply modified though partially preserved. During the 17th century, in 1637, some mural paintings were painted in the new vault of the crypt following the Baroque style. The mural paintings represent two shields, the shield of the monastery with the mitre and the bishop's staff, and the shield of monastery of Montserrat (Sant Benet del Bages belonged to this monastery since 1593 a.C) with the typical skyline of Montserrat mountains. The main colors of those paintings are white, yellow, green, blue and the gilding decorations of the mouldings.

Two different kinds of gilding decorations could be distinguished according to their appearance: one remain unaltered while the other look almost black. This section deals with the causes leading to the darkening of the gilding decorations resulting from their processes of decay.

Samples of both types of gilding were collected and analysed by the combined use of conventional techniques such as optical microscopy, FTIR (Fourier Transform Infrared Spectroscopy) and SEM (Scanning Electron Microscope) with a coupled Energy Dispersive X–ray Spectroscopy (EDS) facility. Since traditional techniques did not fully solve the problem in relation with the differential ageing of the gilding samples, SR techniques were used in order to obtain information on the weathering process.

It is well known that the different gilding techniques used for the application of the metallic leaves are strongly dependent on the kind of support of the painting [49]. Two main procedures are described in the bibliography mostly depending on the binding medium used [50,51]: water gilding and mordant gilding. The first one (water gilding) consists in a bolo layer (usually red earth mixed with glue) applied on a preparation layer of gypsum or calcium carbonate with glue. Over the bolo layer some water (with glue) is applied in order to improve the adhesion of the gold leaf. The mordant technique, however, consists in applying an adhesive containing drying oils (such as

linseed oil) and terpenoid resins. Some pigments (usually lead ones) could be added to both help in the drying process of the adhesive and also resemble a bolo.

When gilding was performed on a wall, it was impossible to obtain a perfectly smooth surface. Leaf was applied through the use of dense adhesives generally containing drying oils and terpenoid resins [6]. Oil gilding is also the traditional process for building exteriors. The use of gold powder has been less reported.

2.3.3.1. Experimental results

Morphological characterization

In Figure 2.10 the stereomicrocope images together with the optical and scanning electron microcope images of the samples are reported. SBB1 cross section (figure 2.10 C) shows four differentiate layers: a yellow-gold one on the top (layer 4), two layers of a red-brown color interpreted as mordant layers (2-3) and a white preparation layer (layer 1). Figure 2.10.D shows the characteristic metallic shine of the golden leaf observed in bright field illumination under the reflecting optical microscope. It can be clearly observed the use of a double leaf with probably an organic material in between interpreted also as a mordant layer.

Figure 2.10.H shows the cross section of the sample SBB3. In this case, three layers are distinguished: a brownish thin top layer (3) followed by a red - brown one (2) on a white preparation layer that resembles the SBB1 one (1). The illumination in bright field does not allow to see any metallic shine on the top layer (Figure 2.10.I).

SEM images of SBB1 cross-section showed two metallic leaves of about 1,5-2,5 microns thick each of them (Figure 2.10.F). The red layers (layer 2-3) can be also differentiate due to the different size of the filler: the layer just under the gold leaf (layer 3), it is constituted by smaller and more homogeneous grains than the lower one (layer 2). Both of them, however, showed a characteristic texture of an organic medium.

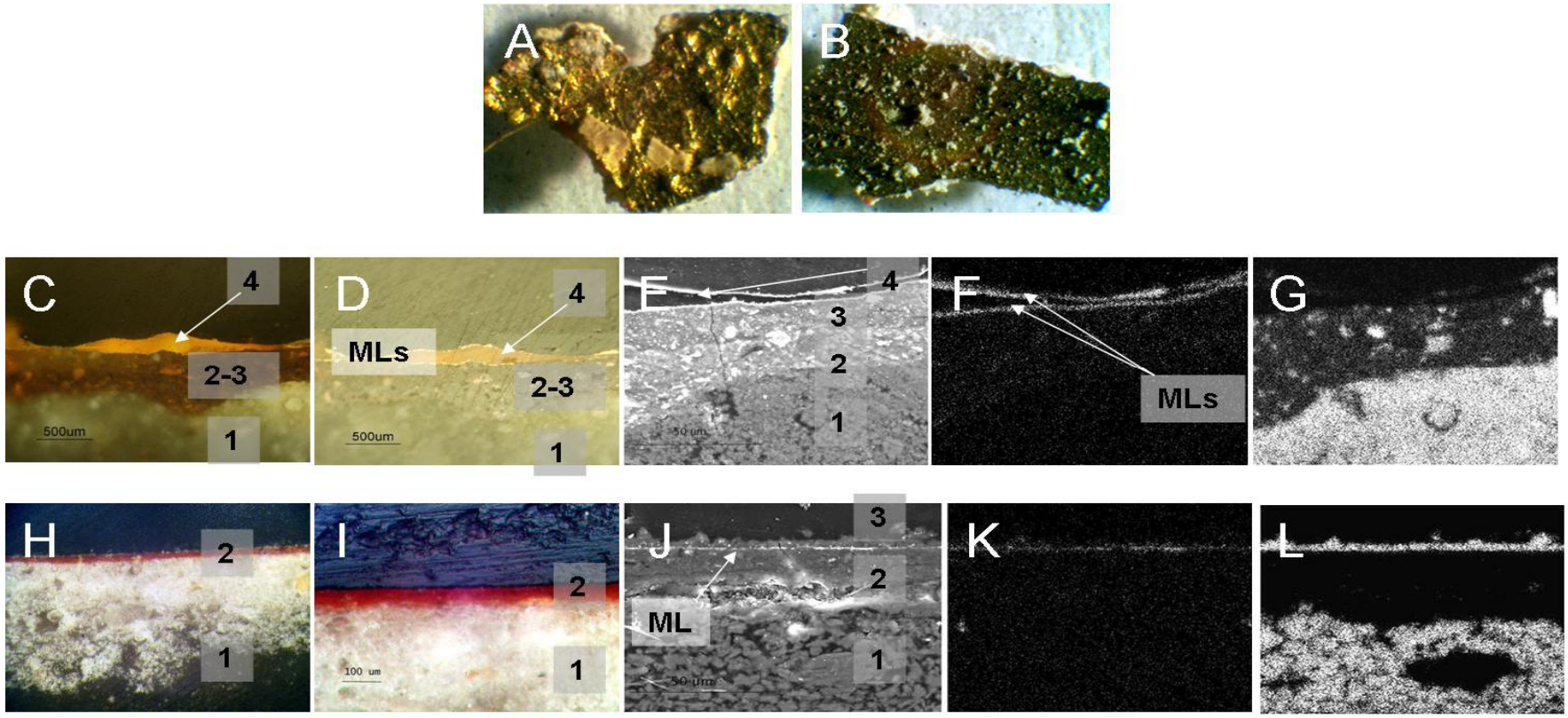

Figure 2.10. Stereomicroscope image of a fragment of (A) the unaltered and still shiny sample SBB1, and (B) the altered and almost black sample (SBB3); Images of the polished cross-section of SBB1and SBB3, respectively (C) and (H) Optical microscopic images; (D) and (I) microscopic image in bright field; (E) and (J) BSE image; elemental distribution of Au (F) and (K) and Ca (G) and (L) .

SEM images of SBB3 clearly show that layer 3 is, in fact, constituted by an irregular superficial layer on top of a discontinuous shiny leaf when observed by backscattered electrons (figure 2.10.J). The chemical elements forming the layer 2 detected by EDS (Si, Fe, Al, K, Ca and Mg) can be attributed to a clay with iron oxides. The elements detected in layer 3 are the same as in layer 2 in addition to Au. Finally, the calcium amount in layer 3 is significantly higher than in layer 2.

In Figure 2.10.F, G, K and L, the elemental distribution of Au and Ca for both samples is reported. Comparing with the distribution of the elements in SBB1 and SBB3 some differences can easily be detected. The gold layer in SBB3 is discontinuous and thinner than in SBB1, where gold leaves are visible as a thin bright line (in fact, there are two gold leaves overlapped with some kind of organic material in between forming layer 4). Besides, there is clearly an irregular layer on top of the gold one in SBB3. This layer consists of Ca without contribution of any other element above Be (EDS detection limit).

Fourier Transform Infrared Spectroscopy

FTIR analysis allow the characterization of the preparation layer of the gold leaf in SBB1. Table 2.11. summarizes the bands identified in the spectra reported in Figure 2.11.

Table 2.11. FTIR bands used for the identification of materials in SBB samples

Compound	*formula*	*Bands*
Gypsum	$CaSO_4$. $2H_2O$	601,671,1117,1138, 1620, 1680, 3403
Linseed oil + lead white	$2PbCO_3.Pb(OH)_2$	1415, 1552, 1737, 1855, 2927, 3522
Calcite	CaCO3	712, 878, 1415, 1791, 2520
Raw umber	Fe_2O_3+MnO_2+clay	457, 1035
Quartz	SiO2	797, 782
Kaolinite	$Al_2O_3.2SiO_2$. $2\ H_2O$	472, 533, 754, 798, 914, 1010, 1033, 3618, 3695
Hematite	Fe_2O_3	530-560, 450-480
Calcium oxaltes	$CaC_2O_4{\cdot}nH_2O$	1324, 780
Epoxy resin		2958, 2932, 2871, 1738, 1458, 1408, 1380, 1256, 1161

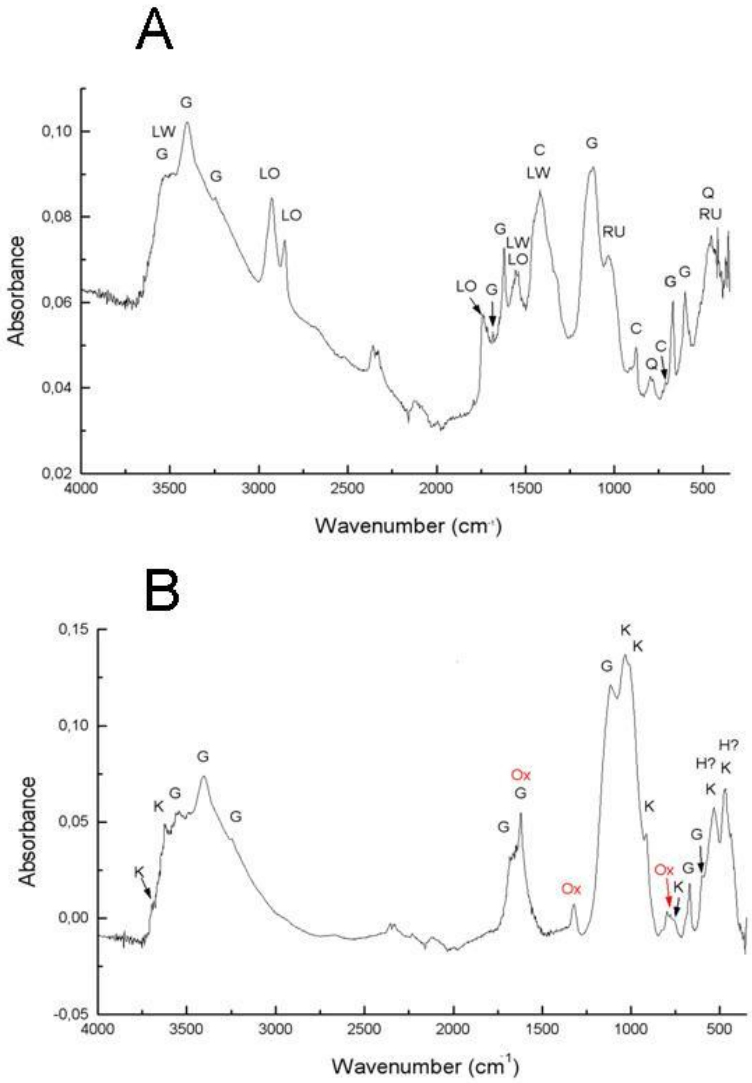

Figure 2.11. (A) SBB1 conventional FTIR spectra of the brown layers (2-3) as diamond cell transmission spectrum; (B) FTIR spectrum of the layers 3-2 of SBB3.
(*G*) indicates the absorption bands of gypsum at 601,671,1117,1138, 1620, 1680 and 3403 cm^{-1}, (*LO*) linseed oil and (*LW*) lead white (1415, 1552, 1737, 1855, 2927 and 3522 cm^{-1}), (*C*) calcite (712, 878, 1415, 1791, 2520 cm^{-1}), (*Q*) quartz (797, 782 cm^{-1}), (RU) raw umber (457, 1035 cm^{-1}), (*K*) kaolinite (472, 533, 754, 798, 914, 1010, 1033, 3618 and 3695 cm^{-1}), (*Ox*) calcium oxalates at 1320 cm^{-1} and (H) the possible peaks of hematite at 470 and 530 cm^{-1}.

SBB1 spectrum (Figure 2.1.A) shows the presence of bands corresponding to gypsum ($CaSO_4$. $2H_2O$) at 601, 671, 1117, 1138, 1620, 1680 and 3403 cm^{-1} [52] while bands at 1415, 1552, 1737, 1855, 2927 and 3522 cm^{-1} are attributed to a mixture of linseed oil with lead white ($2PbCO_3.Pb(OH)_2$) [53]. Also, characteristic bands of calcite (712, 878, 1415, 1791, 2520 cm^{-1}) [15], quartz (797, 782 cm^{-1}) and raw umber [Fe_2O_3+MnO_2+clay] (457, 1035 cm^{-1}) were identified [40]. The absorptions observed in the preparation layer correspond to gypsum due to the presence of the bands specified above. The presence of calcium oxalates can be suspected by the presence of a shoulder around 1320 cm^{-1} corresponding to the O-C-O stretching vibration.

Due to the impossibility to separate them mechanically, the first two layers of SBB3 were analyzed by FTIR together. A representative spectrum is shown in figure 2.11.B. The FTIR vibrational bands observed correspond to gypsum (bands described above) and kaolinite ($Al_2O_3.2SiO_2$. $2H_2O$). Kaolinite main peaks are 472, 533, 754, 798, 914, 1010, 1033, 3618 and 3695 cm^{-1} [39]. However, vibrational bands around 470 and 530 cm^{-1} do not keep the relative intensity of the reference materials. That is probably diagnostic for the presence of hematite (Fe_2O_3) responsible of the color of the layer 2. Hematite bands usually range between 530 and 560 cm^{-1}, and 450 and 480 cm^{-1} [19]. The absorptions observed in the white preparation layer (layer 3) correspond to gypsum as well.

Most notably, the prominent bands of calcium oxalate ($CaC_2O_4 \cdot nH_2O$) at 1324 and 780 cm^{-1} were present [39]. As gypsum is also present, the calcium oxalate band around 1640-1620 cm^{-1} can not be clearly established.

Imaging oxalate distribution by means of SR FTIR

Examination of the spectra obtained indicated that some bands (2850, 1715, 1548 cm^{-1}) ascribable to the organic materials already identified by conventional FTIR were present in addition to the embedding media ones. The bands were used in order to map the already identified materials. Also, the typical distribution of the C-H st bands (the ratio among the bands) of the epoxy resin was sometimes altered indicating the contribution of other organic materials present.

Oxalates identification and mapping was based on the presence of the characteristic peak around 1320 cm^{-1} (OCO stretching). Few compounds exhibit such band [51] nor the epoxy resin thus. In this case, to confirm the calcium oxalate identification, we could not use any other characteristic band attributed to calcium oxalate. The peak at 1620 cm^{-1} interferes with a band of gypsum and proteinaceous materials, and the characteristic band at 782 cm^{-1} was lost due to the aperture chosen .

A photomicrograph of the cross-sections of both samples after microtoming are shown in Figure 2.12 and Figure 2.13. together with some spectra corresponding to selected points in the different layers of the samples.

For SBB1, spectra established the presence of calcium oxalates just suggested by conventional FTIR. The presence of the oil (already characterized by conventional FTIR) could be indicated in layer 4 (between the gold leaves) by the appearance of the band at 2850 and a shoulder at 1715 cm^{-1} (CH stretching and C=O stretching bands characteristic of glycerolipid material, respectively) [6, 19, 54]; the disappearance of the epoxy resin peak at 2960 cm^{-1} and the increase in height of the peak at 2930 cm^{-1} (changing the resin characteristic distribution in the CH st region). Bands at 1545 cm^{-1} could be also characteristic of linseed oil with lead white as a dryer due to the formation of metal soaps. It can be assigned to the COO asymmetric stretching of the lead carboxylates [55]. Layer 2 spectrum also presents those treats. Lead white can be easily identified in some spectra of layer 3.
SBB3 spectra confirmed the presence of calcium oxalates detected by conventional FTIR, a clay in the mordant layers (Si-O st around 1100 cm^{-1}) and gypsum in the preparation layer. Characteristic peaks of the identified compounds have been already described in Table 2.11.

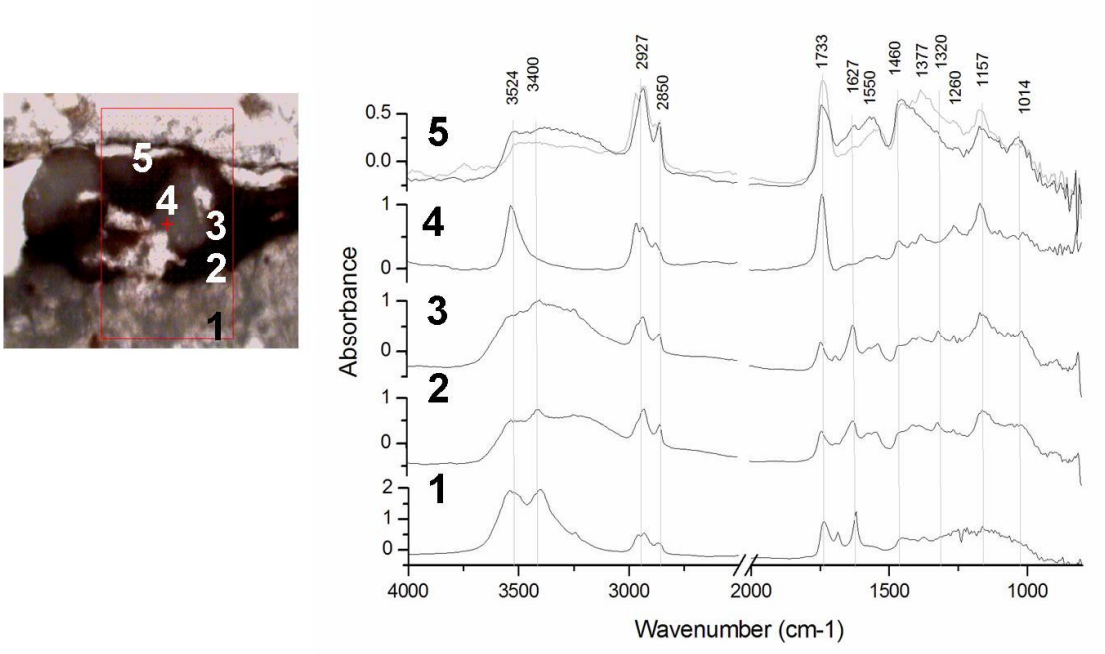

Figure 2.12. Photomicrograph of the thin section obtained for SBB1. Numbers indicate the spots corresponding to the SR transmission FTIR spectra showed on the right. Grey spectrum corresponds to the embedding media reference one.

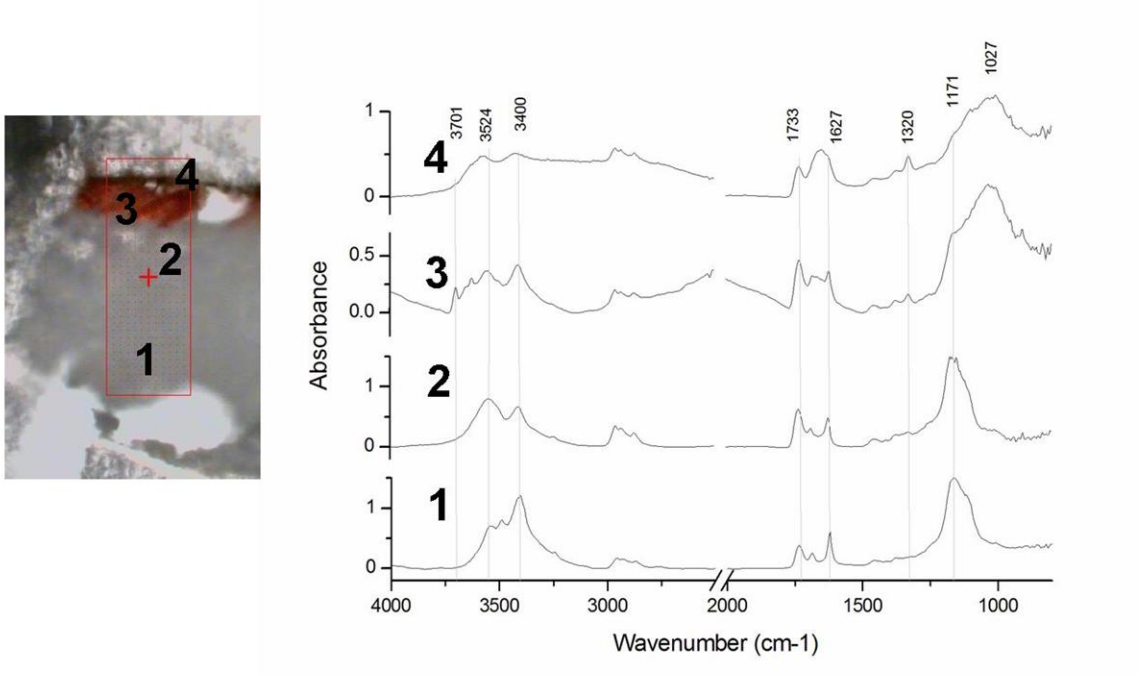

Figure 2.13. Photomicrograph of the thin section obtained for SBB3. Numbers indicate the spots corresponding to the SR transmission FTIR spectra showed on the right.

Thus, mapping of the main features highlighted by the spectra was tried. Mappings are presented in Figure 2.14. Calcium oxalates distribution in SBB1 (Figure 2.15.A) seems to be restricted to the already identified as mordant layers (layer 2,3) finishing at the beginning of the gypsum preparation layer (layer 1). For SBB3 distribution (Figure 2.15.B), calcium oxalates are mainly concentrated on the layer above the gold leaf (layer 3) and they are found in less amount in the red layer identified as a bolo (layer 2).

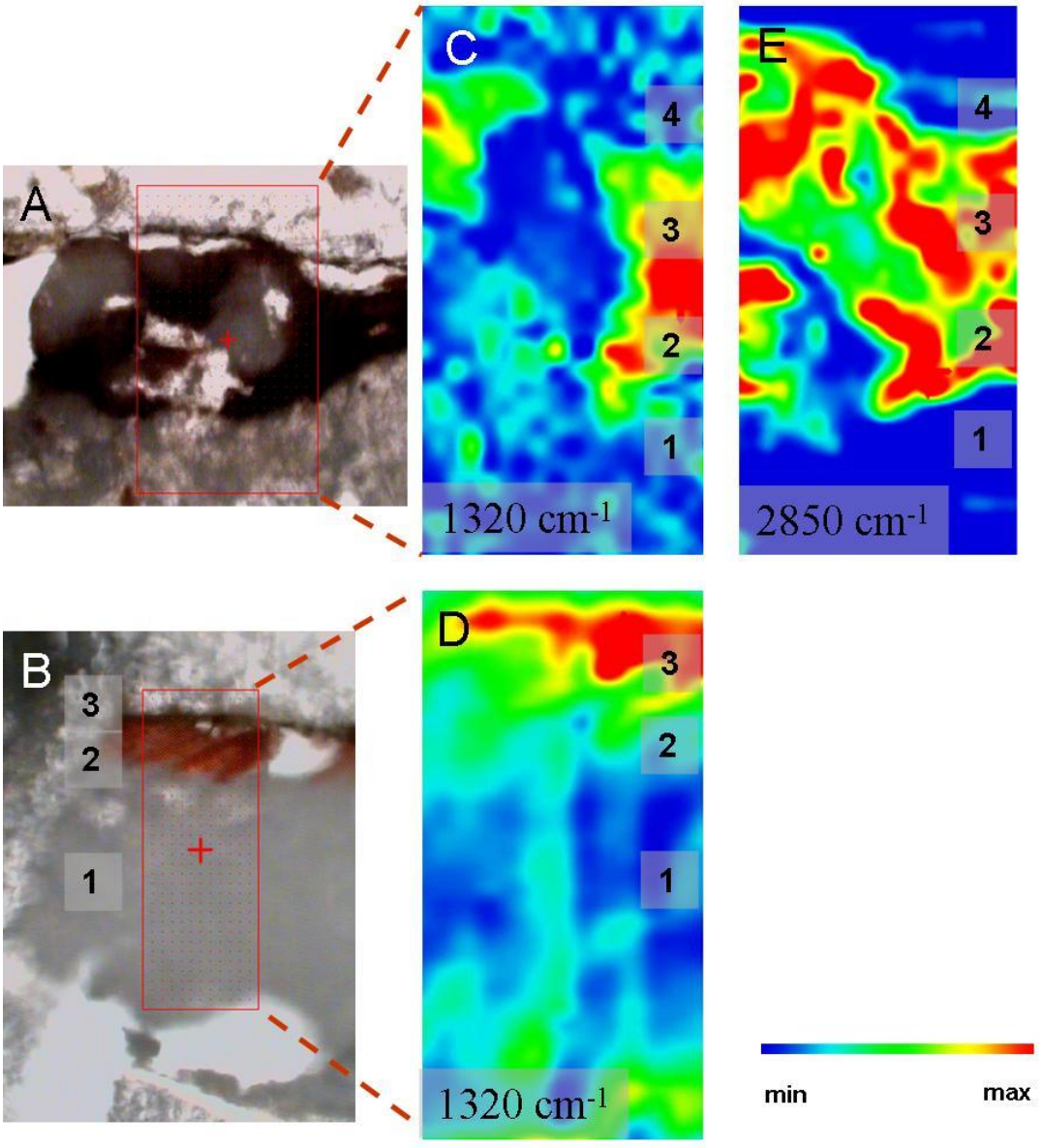

Figure 2.14. (A) and (B) Photomicrograph of the microtomed cross-sections. Rectangle marks the area selected to perform the SR FTIR mapping; chemical image of (C) and (D) 1320 cm^{-1} (O-C-O st of oxalates) and (E) 2850 cm^{-1} (CH st of organic material). Numbers in a grey square correspond to the sample layers.

Oxalate distribution in depth from SR XRD profiles

The use of SR XRD confirmed the presence of calcium oxalate in the form weddellite (calcium oxalate dihydrate [$CaC_2O_4 \cdot 2H_2O$]). In Figure 2.15., the distribution of the mineralogical phases identified in a representative vertical line scan is reported together with some patterns. Table 2.12. reports the weddellite peaks identified in each of the patters presented in Figure 2.15. Some patterns of characteristic scans of SBB1 allow to identify weddellite due to the presence of the peak 200. For SBB3, both peaks 200 and 411 of weddellite pattern could be identified in the patterns.

Peak height underlines the higher amount of calcium oxalates in the mordant layers (scan 10) of SBB1 respect to the preparation layer (scan 30). In the top gold-adhesive layer (layer 4) there is also weddellite but in less amount than in the mortdant layers, in agreement with the SR FTIR results. In SBB3, the highest amount (peak height) of weddellite can be appreciated at scan 0 which corresponds to the top dark layer (layer 3), in agreement with the SR FTIR results, as well.

Table 2.12. Measured peaks of Weddellite (JCPDF 00-017-0541)

Sample SBB1			
Scan Num	hkl	2θº JCPDF	2θº Measured
0	200	4.12	4.12
10	200	4.12	4.12
30	200	4.12	4.12
Sample SBB3			
Scan Num	hkl	2θº JCPDF	2θº Measured
10	200	4.11	4.12
	411	9.15	9.16
25	200	4.11	4.11
	411	9.15	9.15
30	200	4.11	4.11
	411	9.15	9.15

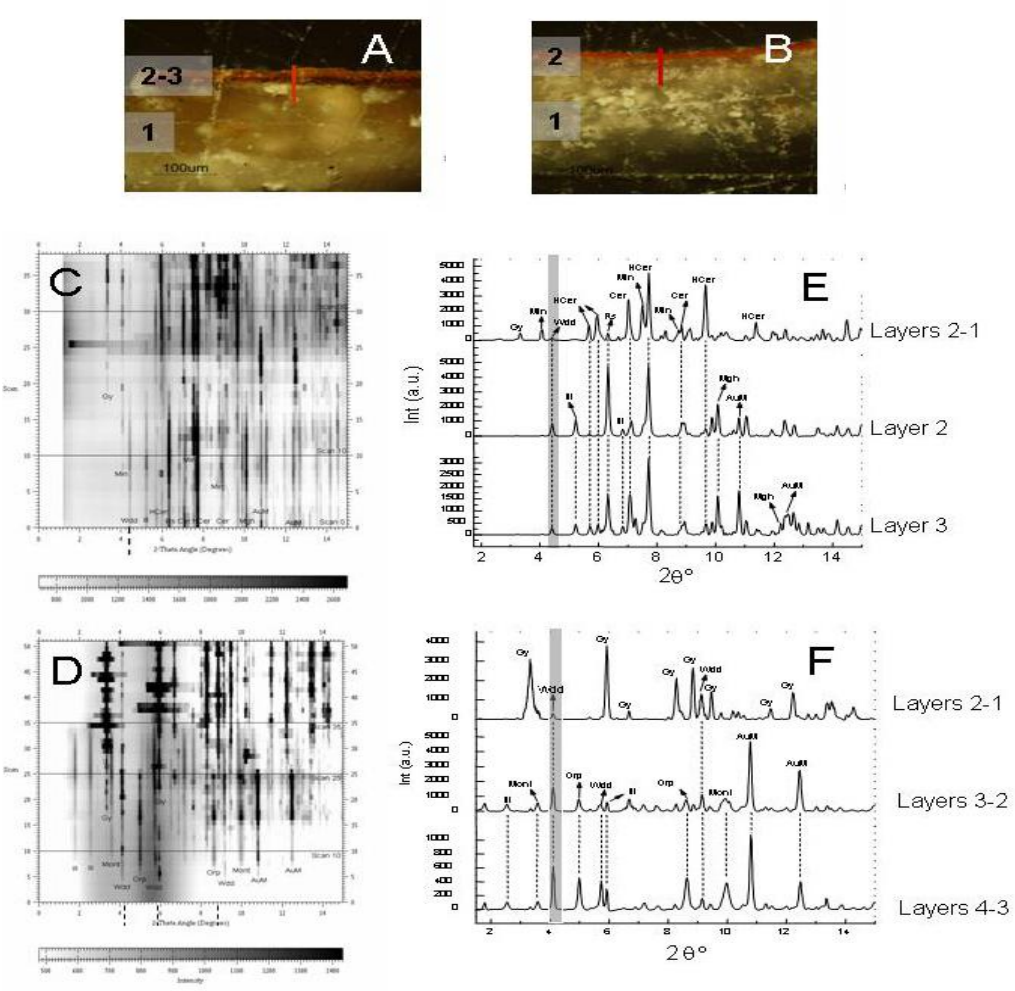

Figure 2.15. (A) and (B) optical microscope of the cross-section used for SR XRD experiments. Red line corresponds to the line scan while the numbers in a grey box indicate the sample layer; (C) and (D) mineral phases distribution and (E) and (F) XRD patterns of some scans scans for SBB1 and SBB3, repectively. (*Gy*) indicates the presence of gypsum[$CaSO_4 \cdot 2H_2O$], (*Wdd*) Weddellite [$C_2CaO_4 \cdot 2H_2O$], (*ILL*) illite [$3MgO\ Al_2O_3 \cdot 24SiO_2 \cdot 12H_2O$], (*Orp*) orpiment [$As_4S_3$] and (*AuM*) gold metal [Au].

For SBB1, the other phases identified are gypsum, gold, clays, cerussite and hydrocerussite (lead white [$2PbCO_3$ $Pb(OH)_2$]) manganese oxide (MnO_2) and maghemite (Fe_2O_3). The presence of iron oxides confirms what could just be suspected by FTIR: the use of drying pigments and red pigments added to the organic material in the mordant layer. A phase characterized by SR XRD but not reported by conventional techniques is minium (Pb_3O_4) also added to the mordant layers (2-3) as a red pigment (helping the mordant to resemble a bolo) and as a drier pigment (lead-containing) as well.

For SBB3, the other phases identified are gold, clays and gypsum (materials characterized by conventional techniques). However, dimorphite (As_4S_3) was surprisingly noticed in the brown top layer. Dimorphite is a rare form of arsenic sulfur that, however, has been already identified in the composition of the natural mineral specimen of orpiment pigment together with other phases such as alacrinite (As_8S_9), uzonite (As_4S_5), duranusite (As_4S), pararealgar (α -AsS) or realgar (β-AsS) [54]. As the presence of orpiment nor other of the substances specified above has been identified, and being pretty easy to obtain dimorphite by sublimation of compounds with S and As, dimorphite has been considered a synthetic pigment added to the glaze to help in its purposes of obtaining a gilding (looking like gold) layer.

2.3.3.2. Discussion

Data obtained, and reported in Table 2.13., by using conventional analytical methodology points out that the technique used to make the gilding decoration named SBB1 is the oil or mordant gilding. The mordant have been prepared by using a drying oil in layer 4, and an oil mixed with drying compounds, such as lead white and manganese oxides (contained in the raw umber), in layers 2 and 3. The fact that two different and consecutive layers of mordant have been applied under the second gold leaf can be interpreted as a refinement of the technique execution. The presence of two gold leaves in layer 4 can be interpreted as a repair of the first gold leaf or by the fact that the sample comes from the place where two consecutive gold leaves were overlapped in order to generate continuity in the gold top layer.
SBB3 sample, however, is characterized by a different gilding technique, probably, water gilding. Gold leaf was applied on a support layer called bolo, brown colored

mixture of clays and iron oxides. A glaze (meaning an organic layer mixed with some dimorphite) was applied on top of the gold leaf. Data for SBB3 is summarized in Table 2.14.

Table 2.13. Summary of the results obtained for the characterization of SBB1.

Layer	*Width (μm)*	*Appearance in light microscopy*	*Elements determined by EDS analysis*	*FTIR results*	*SR FTIR*	*SR XRD*
4	1,5-2,5	Gold layer	Au	Lead white ($2PbCO_3 \cdot Pb(OH)_2$) Drying oil Raw umber ($Fe_2O_3+MnO_2+nH_2O+Si+Al_2O_3$) Calcite ($CaCO_3$)	-	gold
	4-12	Yellow			Oil	-
	1,5-2,5	Gold layer			-	gold
3	11-19	Red/brown	Al, Si , Fe, Mn, Pb, Ca (K, Mg)		Oil Lead white CaOx	Minium Cerussite Weddellite
2	15-30	Red			Oil Gypsum CaOx	Maghemite Hidrocerussite Weddellite
1	35-60	White	Ca, S (Na, K)	Gypsum ($CaSO_4 \cdot 2\,H_2O$)	Gypsum CaOx	-

Table 2.14. Summary of the results obtained for the characterization of SBB3.

Layer	*Width (μm)*	*Appearance in light microscopy*	*Elements determined by EDS analysis*	*FTIR results*	*SR FTIR*	*SR XRD*
3	2-5	Black dust	Au, Ca, (Al, K, Si, Fe)	Calcium oxalates ($CaC_2O4 \cdot nH_2O$) Gypsum ($CaSO_4 \cdot 2\,H_2O$) Red Ochre ($clay+Fe_2O_3$)	CaOx	Dimorphite Weddellite
	1-2	Gold layer			-	Gold
2	20	Red/brown	Si, Fe, Al, K, (Mg, Ca)		Clay	Montmorillonite Weddellite
1	150	White	Ca, S, (Al, Si)	Gypsum ($CaSO_4 \cdot 2\,H_2O$)	Calcium sulphate	gypsum

In summary, both samples are gilding decorations with a gypsum based preparation layer but the gilding technique used turned to be clearly different. That means that, the technique used in the sample SBB3 leads to a more important degradation that ends with a complete loose of its original brightness while SBB1 has preserved its original aspect. Besides, the formation of calcium oxalate on the outermost part of SBB3 represents a difference between both samples.

SR imaging techniques highlighted that calcium oxalates are present in both samples and not only in SBB3 and also their differential distribution in each sample. For SBB1 calcium oxalates are heterogeneously distributed in the layers below the gold leaf while in SBB3 there is clearly a huge concentration of calcium oxalates (weddellite) on the surface due to the ageing of the organic material applied as a glaze. Data, included in Tables 2.13 and 2.14., highlights that calcium oxalates appear in the layers in which some organic material have been reported or at least it would be supposed to be due to the know-how on painting techniques.

It should be noticed that calcium oxalates in SBB1, though appearing heterogeneously distributed in the mordant layers where the drying oil is present (layers 2, 3 and 4), present a distribution less intense in this superficial region. Thus, the formation of oxalates is significantly higher in the mordant layers under the gold leaves (layers 2-3) than in the most superficial mordant (layer 4). The presence of the gold leaf in SBB1 prevented the normal exposition to light and oxygen of the mordant. In these conditions, the drying processes were hindered and dryers were extremely useful [6]. For the same reason (a slower ageing of the organic material present), calcium oxalates amount is lower (and not clearly detected by conventional FTIR). Moreover, that could stress that calcium oxalates are formed by using the gypsum of the ground layer and not sources of calcium external to the painting.

2.4. General conclusions

SR micro FTIR mappings and SR micro XRD profiles allowed to obtain information on the distribution of compounds but also they add information to the standard characterization in all cases. This way an almost complete characterization of the samples could be achieved by the combined interpretation of the data.

The key findings achieved by SR imaging techniques on oxalates are mainly related with the role of the organic material and the nature of the oxalates formed. Results are summarized in table 2.15.

Table 2.15. Main results obtained on oxalates formation and distribution.

Sample	*Oxalates presence*	*Type*	*Distribution layer*	*OM identified*	*remarks*	*description*
SPT1	-					
SPT2	-					Black painting
SPT3	Y	CaOx	Pigment	No id.		Red painting
SPT4	Y	CaOx	Pigment Preparation	No id.	Weddellite	Blue painting
SPT5	-					Black painting
SPT6	-					Superficial coating
SPT7	Y	CaOx	Pigment	No id.		Blue painting
SBB1	Y	CaOx	Mordant	Drying oil	Weddellite	Mordant Gilding
SBB3	Y	CaOx	Superficial varnish	Proteinaceous material	Weddellite	Water gilding
SCPRE1	Y	CuOx CaOx	Pigment	Egg Polysacch. Animal fat	CaOx next to preparation layer Bacterial attack	Blue-green

On the one hand, not only in all cases oxalates were formed in the presence of organic material could be ascertained by FTIR and GC/MS but also oxalates distribution seemed clearly concentrated in the layers where the organic material was also mainly present. Thus, oxalates formation in mural paintings is not restricted to the formation

of superficial patinas by deposition but they are formed in internal painting layers and also under coating layers of metallic leaves. This indicates the significance of the organic material role in the oxalates formation pointing to its degradation to form oxalic acid as the probable formation mechanism in painting samples.

Moreover, the characterization of the organic material allows concluding that siccative oil and egg materials are able to produce oxalates in real painting systems. Polysaccharide materials were also characterized in sample E1. However, egg and animal fat were also present. Thus, there is no way of discerning if all the organic material in the layer or which one among the organic materials identified is the origin of oxalates. In this case, amino acidic profile obtained by GC/MS indicated the biological attack of the proteinaceous material (egg). No other organic materials have been characterized in the samples described in this chapter, thus nothing can be concluded on them.

On the other hand, the presence of microorganisms in some of the samples was suspected. In Sant Pere de Terrassa the presence of microorganisms was ascertained by microscopic observation of the sample fragments and cross-sections. In the azurite sample (E1) the characterization of the binding media by GC/MS suggested a bacterial attack of the organic material. The identification of biological activity in the samples together with the characterization by SR XRD of weddellite (dehydrated form, $CaC_2O_4.2H_2O$) as the only crystalline form formed and in samples from different origin and period would be in agreement with the bacteria and fungi playing a role in the formation of oxalates, as well .

Finally, both calcium and copper oxalates are formed in painting samples. Copper oxalates had been already characterized in painting samples. In the presence of copper its oxalates are formed while calcium oxalates were concentrated in the areas next to the calcium sulphate preparation layer. This indicates the extreme facility of calcium sulphate to form oxalates and of calcium ions to migrate in the sample to the next layers to form oxalates. In the same way, copper oxalates were formed in the presence of azurite ($2CuCO_3$. $Cu(OH)_2$) but not cuprorivaite ($CaCuSi_4O_{10}$). The reason could be the different bonding of Cu in both minerals: in azurite Cu is ionically bonded while un cuprorivaite (a silicate) the bond is mainly covalent, more stable that the previous

one. Accordingly, azurite demonstrates its facility to react and thus degradation (formation of copper chlorides) while silicates remain unaltered.

The complementary results obtained from the different techniques used helped to unequivocally characterize painting techniques, the inorganic crystalline products formed by the weathering processes in the different samples and also to determinate the distribution of those products along the layers. Thus, experiments constitute a significant contribution to gain information on the chromatic degradation of azurite blue layer, gilding methods and the mechanism of formation of decay by products such as oxalates.

References

[1] M.Garcia-Vallès, M.Vendrell-Saz, J. Molera, F. Blazquez, 'Interaction of rock and atmosphere: patinas on Mediterranean monuments',.Environmental Geology , 36,137-149 (1998)

[2] F. Cariati, L. Rampazzi, L. Toniolo., A. Pozzi, 'Calcium Oxalate Films on Stone Surfaces: Experimental Assessment of the Chemical Formation', Studies in Conservation 45, 180-188 (2000)

[3] P. Maravelaki-Kalaitzaki, 'Black crusts and patinas on Pentelic marble from the Parthenon and Erechtheum (Acropolis, Athens): characterization and origin', Analytical Chimica Acta. 532, 187-198 (2005)

[4] M. T. Doménech Carbo, V. Peris Martínez, J. V. Gimeno Adelantado, F. Bosch Reig,M. C. M. Moya Moreno, 'Fourier transform infrared spectroscopy and the analytical study of sculptures and wall decoration', Journal of Molecular Structure 410-411 (1997) 559-563

[5] Alvarez de Buergo M., .Fort González R., 'Protective patinas applied on stony façades of historical buildings in the past', Construction and Building Materials 17, 83-89 (2003)

[6] N.Salvadó, T. Pradell, E. Pantos, M. Z. Papiz, J. Molera , M. Seco and M. Vendrell-Saz, 'Identification of copper-based green pigments in Jaume Huguet's Gothic altarpieces by Fourier transform infrared microspectroscopy and synchrotron radiation X-ray diffraction', Journal of Synchrotron Radiaion. 9, 215 (2002)

[7] P.V Monje, E.J Baran., 'Characterization of Calcium Oxalates Generated as Biominerals in Cacti', Plant Physiology 128 (2002) 707-713.

[8] M. Camaiti, C. Fommei, M.Giamello, G. Sabatini, A. Scala, 'Trattamenti di superfici lapidee secondo antiche ricette: primi risultati sulla formazione di ossalati di calcio' , The Oxalate Fihns in the Conservation of Works of Art, ed. M. REALINI and L. TONIOLO, Editeam S.a.S., Castello D'Argile (BO) (1996) 285-298.

[9] L. Rampazzi, A. Andreotti, I. Bonaduce, M.P. Colombini, C. Colombo, L. Toniolo, Analytical investigation of calcium oxalate films on marble monuments, Talanta, 63, (2004) 967-977.

[10] I. Bonaduce, A. Andreotti, 'Py-GC/MS of organic paint binders', in Organic Mass Spectrometry in Art and Archaeology, M.P. Colombini, F. Modugno editors, John Wiley & Sons, in press

[11] M.P. Colombini, G.Gautier, F.Modugno, E. Ribechini 'Combined GC/MS Analytical Procedure for the Characterization of Glycerolipid, Waxy, Resinous, and Proteinaceous Materials in a Unique Paint Microsample', Analytical Chemistry. 2006, vol. 78, pp. 4490-4500, ISSN: 0003-2700.

[12] A.P. Hammersley, O. Svensson, M. Hanfland, A.N. Fitch, D. Hausermann, 'Two-dimensional detector software: From real detector to idealised image or two-theta scan', High Pressure Research 14, 235-248 (1996)

[13] Ballbè i Boada, M., 1988, 'Ermites i capelles de Terrassa, Matadepera i Viladecavalls', Terrassa (Spain).

[14] G.A. Mazzocchin, D. Rudello, C. Bragato, F. Agnoli, 'A short note on Egyptian blue', Journal of Cultural Heritage, 5, (2004)129-133.

[15] D. Biakiaris, S. Danilia, S. Sotiropoulou, O. Katsimbiri, E. Pavlidou, A.P. Moutsatsou, Y. Chryssoulakis, 'Ochre-differentiation through micro-Raman and micro-FTIR spectroscopies:application on wall paintings at meteora and Mount Athos, Greece', Spectrochimica Acta A 56, 3-18 (1999)

[16] J. Van der Weerd, R.M.A Heeren, J.J. Boon, 'Preparation methods and accessories for the infrared spectroscopic analysis for multi-layer paint films', Studies in Conservation, 49, (2004) 193-210.

[17] G.E. De Benedetto, R. Laviano, L. Sabbatini, P.G. Zambonin, 'Infrared spectroscopy in the mineralogical characterization of ancient pottery', Journal of Cultural Heritage, 3, 177-186. (2002)

[18] P. Mirti, L. Appolonia, A. Casoli, R.P. Ferrari, E. Laurenti, A. Amisano Canesi, G. Chiari, 'Spectrochemical and structural studies on a Roman sample of Egyptian blue', Spectrochimica Acta A 51, 437-445. 1995

[19] M.T. Doménech Carbó, F. Bosch Reig, J.V Gimeno Adelantado, V. Periz Martínez, 'Fourier transform infrared spectroscopy and the analytical study of works of art for purposes of diagnosis an conservation', Analytical Chimica Acta, 330, 207-215, 1996,

[20] M.Derrick, L. Souza, T. Kieslich, H. Florsheim, D. Stulik, 'Embedding Paint Cross-Section Samples in Polyester Resins: Problems and Solutions ', Journal of the American Institute for Conservation 33, 227-245 (1994)

[21] J. Riederer, 'Artist's Pigments: a Handbook of their History and Characteristics vol. 3', National Gallery of Art, Washington. 1997

[22] S. Pagès-Camagna, S. Colinart, 'The Egyptian green pigment: its manufacturing process and links to Egyptian blue', Archaeometry, 45 (4), 637-658. 2003,

[23] O. Ionescu, D. Mohanu, A . Stoica, G. Baiulescu, 'Analytical contributions to the evaluation of painting authenticity from Princely church of Curtea de Arges', Talanta, 63, 815-823. 2004,

[24] Merrifield, M.P., 'The Art of Fresco Painting in the Middle Ages and Renaissance', Dover Publications, New York. 2004,

[25] A.P. Casas, J. De Andres Llopis, 'The identification of aerinite as a blue pigment in the Romanesque frescoes of the Pyrenean region', Studies in Conservation 37, 132-136. 1992

[26] J. Martín-Gil, M. C. Ramos-Sánchez , F. J. Martín-Gil, 'Ancient Pastes for Stone Protection against Environmental Agents', Studies in Conservation, Vol. 44, No. 1 (1999), pp. 58-62

[27] Lazzarini Lazzarini L., , 'The discovery of Egyptian Blue in a roman fresco of the mediaeval period (ninth century A.D.)', Studies in Conservation, 27, 84-86. 1982

[28] A. Andreotti, I. Bonaduce, M. P. Colombini, C.Baracchini, A.Caleca, A.Paolucci: Saving the Medieval Paintings by the master painter of the Triumph of Death in Pisa in 15th Triennial Conference New Delhi (Allied Publishers Pvt.Ltd. India 2008)

[29] S. Mugnaini, A. Bagnoli, P.Bensi, F.Doghini, A.Scala, G.Guasparri:, 'Thirteenth century wall paintings under the Siena Cathedral (Italy). Mineralogical and petrographic study of materials, painting techniques and state of conservation' Journal of Cultural Heritage 7, 171-185 (2006)

[30] A.Roy: Artists pigments: A Handbook of their History and Characteristics Vol 2 (National gallery of Art Oxford 1993)

[31] Cennino Cennini, 'Il libro del arte' (Akal Ediciones Madrid Spain 2002)

[32] Vitruvio, 'Los Diez Libros de Arquitectura' (Alianza Forma Editor Madrid Spain 2000)

[33] P. Vandenabeele, K. Lambert, S. Matiz, W. Schudel, A. Bergmans, L. Monees, 'In situ analysis of mediaeval wall paintings: a challenge for mobile Raman spectroscopy', Analytical and Bioanalytical Chemistry 383, 707-712 (2005)

[34] L.Dei, A.Ahle, P.Baglioni, D.Dini, 'Green Degradation Products of Azurite in Wall Paintings: Identification and Conservation Treatment' , Studies in Conservation 43, 80-88 (1998)

[35] R. J. Gettens, M. E. Mrose, 'Calcium Sulphate Minerals in the Grounds of Italian Paintings', Studies in Conservation 1(4), 174-189 (1954).

[36] C. Genesta, 'Characterization of grounds used in canvas and sculpture' , Materials Letters 54, 382-388 (2002).

[37] K. Helwig, 'The characterization of iron earth pigments using infrared spectroscopy', ' Irug postprints, IRUG at the V&A 83

[38] E. Abelev, N. Sezin, Y. Ein-Eli, An alternative isolation of tungsten tips for a scanning tunneling microscopeì', Rev. Sci. Instrum. 76, 106105 (2005)

[39] I. Adrover Gracia: 'Applicazioni della spettrofotometria IR allo studio dei beni culturali' (Collana I Talenti Padova Italy 2001)

[40] M. C. D'Antonio, D. Palacios, L. Coggiola, 'Vibrational and electronic spectra of synthetic moolooite', E. J. Baran: Spectrochim. Acta Part A: 68 (3), 424 (2007)

[41] J. Madejová , 'FTIR techniques in clay mineral studies', Vibrational Spectroscopy 31,1, 1-10(2003)

[42] R L. Frost, Y. Jing, Z. Ding, 'Raman and FTIR spectroscopy of natural oxalates: Implications for the evidence of life on Mars' , Chinese Science Bulletin 48(17), 1844 (2003)

[43] S.Bruni, F. Cariati, F. Casadio, L. Toniolo, 'Spectrochemical characterization by micro-FTIR spectroscopy of blue pigments in different polychrome works of art' Vibrational Spectroscopy 20, 15 (1999) 15-25

[44] A. Andreotti, I. Bonaduce, M. P. Colombini, F. Modugno, E. Ribechini: A. Andreotti., I. Bonaduce.b, M. P. Colombini, F. Modugno, E. Ribechini 'The diagnosis of the yellowing of the marble high-reliefs and the black decorations in the chapel of the tomb of Saint Anthony (Padua-Italy)', Journal of Mass Spectrometry, ISSN 1387-3806 (2008)accepted

[45] G. Gautier, M. P. Colombini, 'GC–MS identification of proteins in wall painting samples: A fast clean-up procedure to remove copper-based pigment interferences', Talanta 73, 95-102 (2007)

[46] I. Donati, 'Enzimi, acidi organici ed altri metaboliti coinvolti nella patogenesi di penicillium spp.', phD thesis (Universita di Bologna Italy 2008)

[47] A. Lluveras, S. Boularand, J. Roqué, M. Cotte, G. Martinez-Ruiz, P. Giráldez, M.Vendrell-Saz, 'Weathering of gilding decorations investigated by SR: development

and distribution of calcium oxalates in the case of Sant Benet de Bages (Barcelona, Spain)', Applied Physics A, 2008, 90 (1), 23-33.

[48] M. Cotte, J. Susini,V. A. Sole´, Y. Taniguchi, J. Chillida, E. Checroun, P. Walter: J. 'Applications of synchrotron-based micro-imaging techniques to the chemical analysis of ancient paintings', Analytical Atomic Spectrometry 23, 820-828 (2008)

[49] I. Bonaduce, A multi-analytical approach for the investigation of materials and techniques in the art of gilding , PhD thesis (Università di Pisa 2005)

[50] A. Villarquide Jenevois, 'La pintura sobre tela I, Historiografía, técnicas y materiales' (NEREA 2004)

[51] Doerner, Los materiales de pintura y su empleo en el arte (18ª edición Editorial Reverté Barcelona 1998).

[52] R.J. Meilunas, J.G. Bentsen, A. Steinberg, 'Analysis of Aged Paint Binders by FTIR Spectroscopy', Studies in Conservation 35, (1990) 33-51.

[53] G.C. Jones, B. Jackson, 'Infrared Transmission Spectra of Carbonate Minerals' (Chapman and Hall London 1993).

[54] R. Mayer, 'Materiales y técnicas del arte' (9ª edición. Tursen. Hermann Blume Ediciones 1993).

Chapter 3

Mass Spectrometric and SR based techniques for the identification and distribution of painting materials in samples from works of art

The complete characterization of painting samples is always a complex analytical problem due to the high number of materials present in a micro-sample, and their being heterogeneous and ageing. Thus, the identification of these materials should not be the only aim of analytical investigations. Establishing the distribution of these materials and that of their degradation products by imaging techniques is fundamental to understand the painting technique and can improve our knowledge on the conservation status of the painting and degradation pathways.

Combining the use of chromatographic-mass spectrometric techniques, such as GC/MS or Py/GC/MS, and the chemical mapping of functional groups by imaging SR FTIR in transmission mode on microtomed cross sections, can be a suitable approach to have a detailed characterisation of the organic materials in a paint sample, assuring their localisation in the sample build-up. In order to complement the information on them, SR XRD line scans have been used as the perfect tool for the inorganic materials unequivocal identification.

This analytical approach has been used to study samples from the Catalan mural paintings by Josep Maria Sert y Badía (20th century).

3.1. Introduction

Paintings are complex systems due to the fact that they are multi-material, multi-layered and that they undergo to alteration during the time as a result of both the ineractions among components and natural ageing [1]. There are several issues that need to be solved and that are related to the painting technique or the materials used by the painter, the restauration processes, the ageing mechanisms and the interaction amongst materials and layers occurred with the passing of time.

The use of conventional techniques, optical (MO) and scanning electron microscopy coupled with Electron Dispersive Spectroscopy (SEM-EDS), or microdistructive analysis such as Fourier Transform Infrared Spectroscopy (FTIR), Gas Chromatography/Mass Spectrometry (GC/MS), Pyrosis/Gas/Chromatrography Mass spectrometry (Py/GC/MS) can provide a detailed and almost complete characterization of the samples in a complementary way. Particularly, separation techniques have already showed their great suitability for the characterization of binding media as complex mixtures of different organic materials [2,3,4,5,6,7]. However, due to the heterogeneity of the paint sample and its multilayered structure, the chemical properties of the materials of adjacent areas can be completely different from on another and thus the identification is not the only point of interest: the knowledge of the distribution of paint media is fundamental to understand the technique used by the painter. Moreover, the degradation and ageing can also be considered as a three-dimensional process. Therefore a complete analysis of the painting requires both in plane and in depth information and an imaging of organic and inorganic materials of the paint cross sections is required for the characterization of painting systems. As a result, the elemental and molecular heterogeneities are resolved both within and between layers [1,8,9,10] .

In this chapter a multi-analytical approach for the complete characterisation of organic and inorganic materials in paint samples is shown. Conventional Fourier Transform Infrared Spectroscopy (FTIR) and analytical Pyrolisis in the presence of hexamethyldisilazane coupled on line with gas chromatography/mass spectrometry analysis (Py/GC/MS) have been used as screening techniques [1,7]. A GC/MS analytical procedure for the identification of lipids, waxes, proteins, and resinous materials in the same microsample was then used for the identification of organic

materials and their degradation products in the bulk sample [2]. Finally, SR FTIR in transmission mode allowed the establishment of the distribution of these materials both in depth and along the sample by the chemical images of the functional groups in a microtomed cross-section. Transmission has been chosen due to its higher spectra quality, easier interpretation and wider database. Synchrotron radiation source advantages for infrared microspectroscopy and its applications in the field of cultural heritage have been extensively and accurately described in the literature [10,11,12,13,14,15,16]. To complement the characterization of pigments, dryers and fillers, SR XRD in transmission mode was used to establish the crystalline phases present.

Seven samples from three different paintings of Josep Maria Sert y Badía, a Catalan painter from the beginning of the 20th century have been investigated. Josep Maria Sert (1876-1945) was one of the most famous mural painters of the period achieving international recognition. His work adorns the walls of such buildings as the assembly hall of the League of Nations (Geneva), the RCA Building in Rockefeller Center, and the Waldorf-Astoria Hotel (both in New York City). Sert's painting technique is of particular interest because the painter's work changed from polychrome and decorative mural paintings in his beginnings, to almost monochrome paintings (sepia, gilded and silvery tonalities) that were, in the end, considered his characteristic way of painting. In the occasion of the publication of a book on Sert paintings in the city of Vic (Barcelona), some of his paintings have been studied in detail to finally establish the artist's painting technique and the materials used. Some samples were collected and subjected to analytical investigations. Seven of these samples are here presented.

3.2. Experimental Section

3.2.1. Reagents

For the chromatographic technique all the solvents used were Baker HPLC grade. Hexadecane, tridecanoic acid and norleucine, used as internal standards, hexamethyldisilazane (HMDS), and *N,O*-bis(trimethylsilyl)trifluoroacetamide (BSTFA) containing 1% trimethylchlorosilane were purchased from Sigma (Milan, Italy). *N-tert*-Butyldimethylsilyl-*N*-methyltrifluoroacetamide (MTBSTFA) with 1%

trimethylchlorosilane was from Fluka (USA). All reagents and chemicals were used without any further purification. Standard solutions of amino acids in HCl (0.1 M), containing 12.5 µmol/mL of proline and hydroxyproline, 1.25 µmol/mL of cysteine and 2.5 µmol/mL of aspartic acid, glutamic acid, alanine, arginine, phenylalanine, glycine, hydroxylysine, isoleucine, histidine, leucine, lysine, methionine, serine, tyrosine, threonine, and valine was purchased from Sigma-Aldrich (USA). A solution containing lauric acid, suberic acid, azelaic acid , myristic acid , sebacic acid , palmitic acid, oleic acid, stearic acid (all purchased from Sigma-Aldrich, USA) in the range of 2-3 µ/g was prepared in isooctane and stored at 4°C.

A polyester resin polymerised by a peroxy organic hardener (Cronolite E.I, Plastiform, Spain) was used for the cross-section preparation.

The epoxy resin used for the SR FTIR slices was purchased by (Plastiform, Spain).

3.2.2. Apparatus

- Scanning Electron Microscope (SEM) JEOL (Tokyo, Japan) JSM-840 (secondary and backscattered electron detection) coupled with an Energy Dispersive X–ray Spectroscopy (EDS) facility LINK AN 10000 microanalyser. The acceleration voltage used was 20 KeV. EDS mappings were collected by using a Cambridge Leica Stereoscan S-360 coupled with INCA Energy Sèrie 200 microanalyser (Oxford Instruments). Conditions were as follow: filament 2,8 A, probe 3 nA and EHT 20 kV.
- Bomem MB-120 Fourier Transform Infrared Spectrometer equipped with a DTGS detector. The spectra are the sum of 30 scans collected from 4000 to 350 cm^{-1} at a resolution of 4 cm^{-1} when working with the diamond cell.
- Bomem MB-120 Fourier Transform Infrared Spectrometer, equipped with a Spectra-Tech Analytical Plan microscope, was used with the diamond cell, as a sample holder. The spectrometer has a KBr beamsplitter and a Glowbar source. The microscope has its own mercury cadmium telluride (MCT) detector refrigerated with liquid nitrogen. Spectrum was recorded between 4000 and 720 cm^{-1} with a resolution of 4 cm^{-1} and an accumulation of 100 scans.

- Pyroprobe CDS Analytical Inc. 5000 Series (Oxford, USA). It was operating with an initial temperature of 50°C, up to 550°C at 20°C/ms, then isothermal for 20 sec. (probe run time 0.33 min). The pyrolyser was coupled on-line with the injection port of a 6890N GC System Gas Chromatograph (Agilent Technologies, Palo Alto, CA, USA), coupled with a 5973 Mass Selective Detector (Agilent Technologies, Palo Alto, CA, USA) single quadrupole mass spectrometer, equipped with split/splitless injector. The interface Py/GC temperature was 180°C, the transfer line 300°C, the valve oven 290°C. The mass spectrometer was operating in the electron impact (EI) positive mode (70 eV). A few µg of the samples admixed with 2 µl of hexamethyldisilazane were inserted into a quartz tube. Detailed working conditions are published elsewhere [17].
- A 6890N GC System Gas Chromatograph (Agilent Technologies, Palo Alto, CA, USA), coupled with a 5975 Mass Selective Detector (Agilent Technologies, Palo Alto, CA, USA) single quadrupole mass spectrometer, equipped with a PTV injector was used. The mass spectrometer was operating in the electron impact (EI) positive mode (70 eV). The MS transfer line temperature was 280 ºC; the MS ion source temperature was kept at 230 ºC; and the MS quadrupole temperature was at 180 ºC. This instrument was used for the analysis of samples processed with the combined analytical procedure for the simultaneous identification of glycerolipids, proteinaceous materials, plant and animal resins, and natural waxes. The detailed operating conditions, and the analytical procedure are published in detail elsewhere [2]
- Microwave oven model MLS-1200 MEGA Milestone (FKV, Sorisole (BG,) Italy). Acis hydrolysis conditions were : power 250 W for 10 min; power 500 W for 30 min in the vapor phase with 30 mL of 6 N HCl at 160 °C for 40 min. Saponification conditions were: power 200 W with 300*i*L of KOH_{ETOH} 10% wt at 80 °C for 60 min.
- Synchrotron radiation Fourier transform infrared microspectroscopy (SR FTIR) in transmision mode was performed at the station ID21 at the European Radiation Synchrotron Facility (ESRF, Grenoble, France). Maps were recorded using 4 microns step and 40 scans for each spectrum. Beam spot and resolution were fixed at 8 x 8 µm and 8 cm^{-1}, respectively. In all cases the aperture and the step size chosen generates overlapping areas in order to increase the

resolution of the components [18]. Microtome Ultracut E with a tungsten knife for slices of less than 12 μm was used. SR XRD (Synchrotron radiation X Ray diffraction) patterns in transmission mode were acquired at the station ID18F of the ESRF as well. A focal spot of 2,3 microns in the vertical direction and 11 microns in the horizontal direction was chosen with steps of 2 microns in the vertical direction. A wavelength of 0,443Å (28 keV) was selected and the acquisition time was 20 seconds per pattern. The diffraction signal was recorded in transmission by means of a 2-dimensional CCD-based X-ray detector (refined detector distance 107, 26 mm). The cross-section was placed into the focused beam with the paint layers oriented horizontally. Samples are embedded and sectioned with a diamond saw of thickness 0,1 mm into a 200 microns thick slice.[16,17 ,18,19]

3.2.3. Samples

Seven samples were collected from six canvases painted by Josep Maria Sert y Badía in the years 1906-1926, and were named VIC 1 to VIC 7. Samples were always taken from nicks of the canvases trying to minimize the damaging to the paintings. In Table 3.1 the samples collected are summarised.

Table 3.1. Description of the paint samples

Sample name	*Painting*	*Year*
VIC 1	"Heliodor Expelled from the Temple"	1920
VIC 2	"Heliodor Expelled from the Temple"	1920
VIC 3	"The Fourth Seasons" (Winter panel)	1917-1920
VIC 4	"The Fourth Seasons" (Spring panel)	1917-1920
VIC 5	"Fight Between Jacob and the Angel"	1906
VIC 6	"Crucifixion" (central panel)	1945
VIC 7	"In Honor of the East"	1926

3.3. Results and Discussion

3.3.1. Morphological characterisation

The morphological characterisation of the samples by means of the optical and scanning electronic microscopes highlighted that two pictorial techniques can be differentiated, characterised by two different kind of stratigraphies and superficial appearances. In particular a first group, made of samples VIC 4 and VIC 5, presented few pictorial layers (mainly a preparation layer together with one or a couple of pigmented layers) with a coloured superficial appearance. A second group is made of samples VIC 1,2,3, 6 and 7, which present a dark surface with hints of golden shiny reflects. Their stratigraphies show several layers (more than 10) amongst which there is always at least a metallic layer and an alternation of pigmented and unpigmented layers. It is interesting to notice how thin some of the layers are (1-2 μm).

Figure 3.1 shows the stereomicroscope images of the samples surface and the optical and electron microscope images of their cross-sections. Table 3.2 summarizes the results of the morphological characterisation of the samples. The composition of the metallic leaves obtained with the EDS are reported as well.

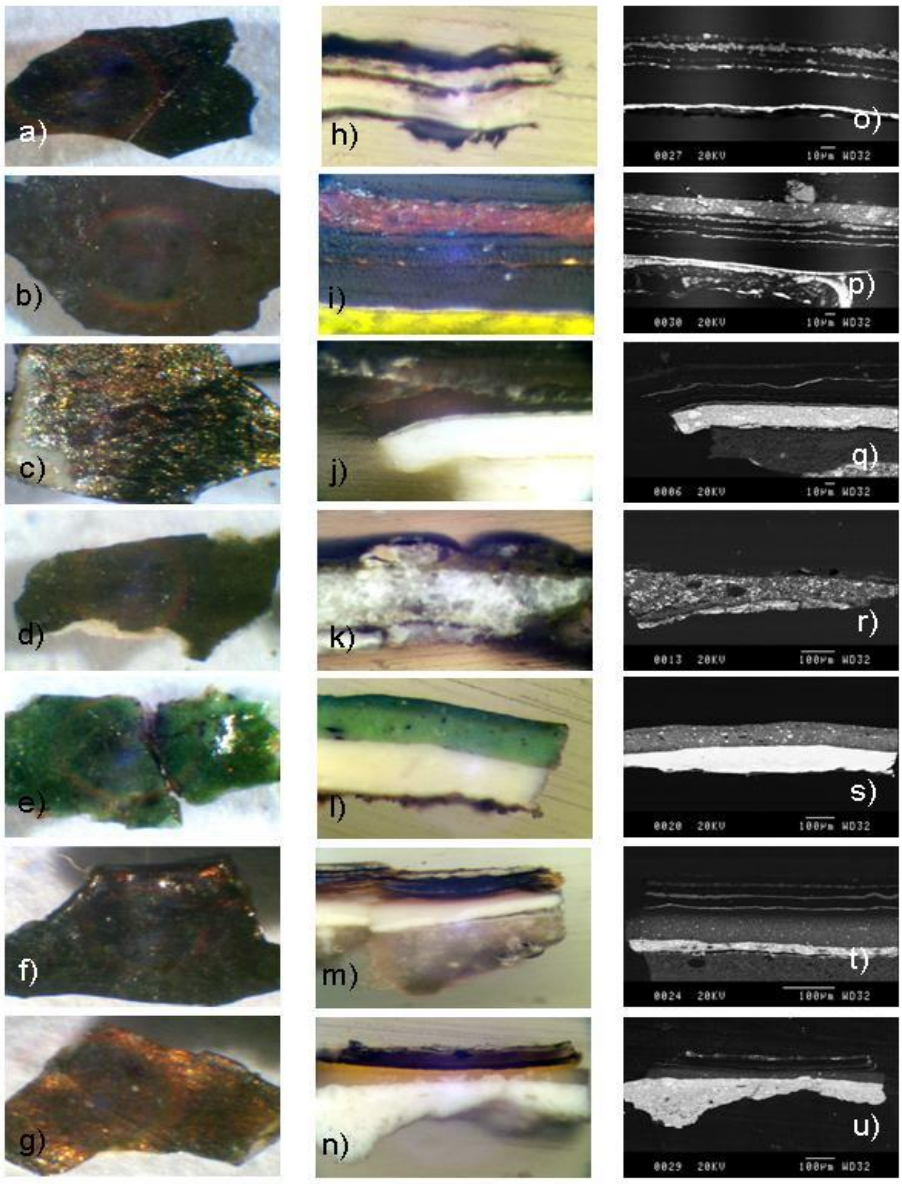

Figure 3.1. Stereomicroscope images of the surfaces of samples a) VIC 1; b) VIC 2; c) VIC 3; d) VIC 4; e) VIC 5; f) VIC 6; g) VIC 7; Optical microscopic image of the polished cross-section h) VIC 1; i) VIC 2; j) VIC 3; k) VIC 4; l) VIC 5; m) VIC 6; n) VIC 7; scanning electron microscope images of the cross-section o) VIC 1; p) VIC 2; q) VIC 3; r) VIC 4; s) VIC 5; t) VIC 6; u) VIC 7.

Table 3.2. Summary of the morphological characterization of the samples.

Sample	*Appearance of the surface*	*Total Number of layers*	*Thickness (min-max /µm)*	*Number of highly pigmented layers*	*Number of mainly organic layers*	*Number of metallic layers*	*Metallic leaves*
Vic 1	Dark blue	9	1-50	2	5	2	Au Cu-Zn
Vic 2	Dark red	13	2-20	6	4	3	Au Cu-Zn
Vic 3	Silvery	13	25-150	6	5	2	Au-Ag
Vic 4	Dark green	5		4	1	0	-
Vic 5	Green	4	25-100	4	0	0	-
Vic 6	Black - golden	10	2-200	5	3	2	Al-Pd Cu-Zn
Vic 7	golden	11	1-100	6	4	1	Au

3.3.2. Fourier Transformed Infrared Spectroscopy

Using W needles [20] under the stereomicroscope, layers were selectively sampled when possible in order to obtain some information on the distribution of both organic and inorganic materials.

The combination of bands used for the identification of the different materials in the sample spectra are specified in Table 3.3 and have been compared with reference data [18,21,22,23,24,25,26,27,28]. Figure 3.2 shows some representative spectra from different samples as examples of the materials identified.

An oil medium can be identified in the spectra by the presence of the characteristic CH st and CO st bands in Figure 3.2 a,b, in the regions, respectively 3000-2800 cm^{-1} and 1750-1650 cm^{-1}[18,21]. In almost all cases the formation of metal carboxylates could be observed in the region 1650-1500 cm^{-1}[28]. In the pigmented layers (figure 3.2 a,b), carbonyl peaks are observed at around 1740 cm^{-1} due to esters and the peak intensity is lower than that of the metal carboxylate band. This indicates the hydrolysis of the triglycerids and the reaction of the carboxylic acids to metal caboxylates. On the contrary, in mordant layers (figure 2c) the band around 1715 cm^{-1} corresponding to the carboxylic acid moieties formed upon oxidation and hydrolysis [28]. The presence of different kind of pigments and the pigment concentration in the layer, the different

coordination states of the carboxylic acid around the metal atom or the nature of the carboxylic acid justify the variations in the frequencies observed for the carboxylates [21,28]. Particularly ZnO (Zn has been detected by EDS and thus suspected in some layers) and lead carbonate lead whose C=O st bands occur at 1580-1590 and 1520-1540 cm^{-1}, respectively [28].

In figure 3.2, peaks corresponding to lead white and strontium yellow (figure 2a), calcium oxalates, quartz and iron oxides (figure 3.2b), chrome yellow and barium sulphate (figure 3.2c) bands can be identified.

Figures 3.2 d and e present some common features of a resin (CH st, C=O st and C-O st). The olefinic band at 1630 cm^{-1}, together with the bands at 945 and 930 cm^{-1} in Figure 2d suggest the occurrence of shellac [22] while a different natural resin was suspected in figure 3.2e. Finally, Figures 3.2 f and g are representative of the proteinaceous and polysaccharidic material detected in VIC 7 and VIC 5, respectively.

Data obtained are summarized in Table 3.4, with indication of the position in the sample layers. Inorganic compounds have been also included in the Table. Their identification was based on the recognition of characteristic FTIR peaks described in Table 3.3.

Results on organic materials can be summarised as follows. Natural resins were identified in all the samples, but VIC 4 and VIC 5, and seems to be concentrated in the superficial layers of the samples. The presence of a lipid material, probably a drying oil, was evidenced in all samples but VIC 1, mostly distributed in the mordant layers of the metallic leaves and pigment layers.

In sample VIC 5, a polysaccharide material was also identified on the canvas preparation layer and a proteinaceous material was identified in the superficial layers of sample VIC 7 probably as binding medium of the pigment layers alternated with the mainly organic ones.

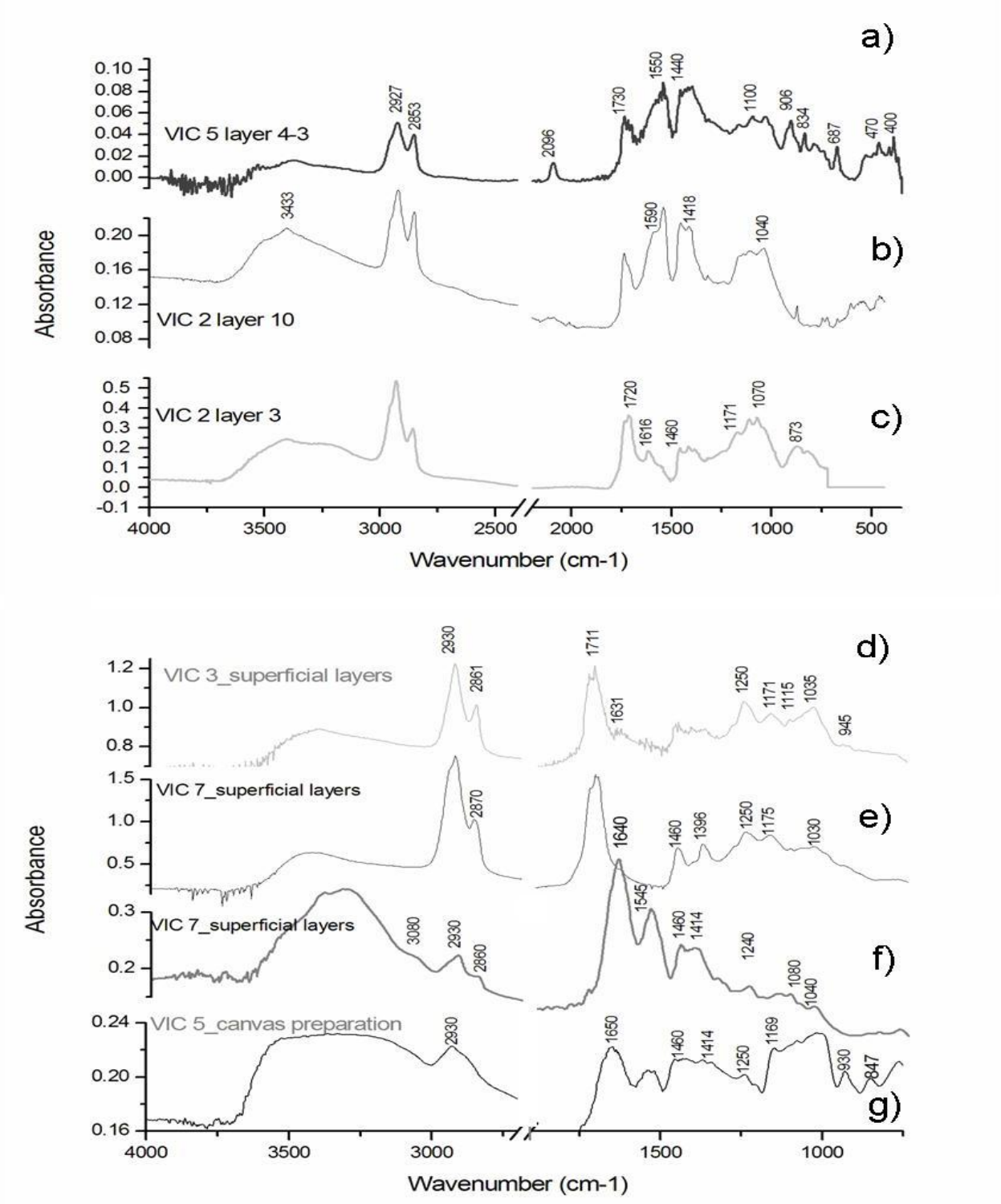

Figure 3.2. Conventional FTIR spectra of some of the samples : a), b) and c) representative spectra pigment layers where oil is detected as biding media; d to g) spectra of organic layers where different organic materials were identified : d) and e) resin, f) proteinaceous material and g) polysaccharide material. Spectra have been recorded in transmission mode at a resolution of 4 cm^{-1}. VIC 5 and VIC 2 layer 10 are the sum of 30 scans collected from 4000 to 350 cm^{-1} while the rest of the spectra are the sum of 100 scans collected from 4000 to 720 cm^{-1}.

Table 3.3. FTIR bands identified in the spectra of the samples. The bands reported correspond to the wavenumbers identified in the spectra and not to reference data.

Material	*FTIR bands*																					
	OH st H_2O idration	NH st	Amide II overtone	CH st	C=Ost	Amide I	C-O st	OH bd	MCOO	Amide II (NH bd)	CH bd	C_2O_4-	COst	PO_4^{3-}	CN	FeO	SiO_3^{2-} st	SiO_3^{2-} bd	CO_3^{2}- st	CO_3^{2}- bd	SO_4^{2-} st	SO_4^{2-} bd	CrO_4^{2-}
Oil				2927 2855	1737						1450 1380		1248 1170 1094										
Tree Resin				2930 2870	1711		-	-			1460 1396		1250 1175										
Shellac				2935 2867	1711		1640				1459 1409 1381		1250 1176 1040 947 930										
Polysaccharidic material (starch)	3350			2920	-			1640			1420 1380		1150 1070 1020 928										
Proteinaceous material (animal glue)		3310	3074			1650				1540	1450												
Calcite					1797														1420	876 710			
Lead white	3533				1737														1410	1047 683			
Zinc Oxide (*)																							
Barium sulfate																					1150 1117 1085	635 610	
Hematite																550 456							

Bone Black		2013				1090 1039 955 878					
Prussian blue							2092				
Green earth	3600 3556 3533							1074 1018 979	800 681		
Quartz								743 723			
Kaolinite	3620 3099							1030 916			
Chrome yellow											820 870
Strontium yellow											923 909 842
Ultramarine blue								1005 930			
Zn carboxylates				1588							
Pb carboxylates				1533							
Calcium Oxalates			1640		1318					790	

Note: Calcite: $CaCO_3$, Lead white: $PbCO_3.Pb(OH)_2$, Zinc Oxide: ZnO, Barium sulfate: $BaSO_4$, Hematite: Fe_2O_3, Apatite: $Ca_3(PO4)_2$, Prussian blue: $Fe_4(Fe(CN)_6)_3$, Green earth: $K[(Al,Fe^{3+})$, $(Fe^{2+,}$ $Mg)(AlSi_3$, $Si_4)0_{10}$ $(OH)_2$, Quartz: SiO_2, Chrome yellow: $PbCrO_4$, Strontium yellow: $SrCrO_4$, Ultramarine blue: $[(Na,Ca)_8(Al,Si)_{12}O_{24}$. $(S,SO_4)]$, Calcium Oxalates: $CaC_2O_4.nH_2O$)

(*) no mid IR bands

Table 3.4. FTIR results for the paint samples. Information on the layers is given when possible.

sample	*Layer*	*Llipid material*	*Natural resin*	*Proteinaceous material*	*Polysaccharide materials*	*Inorganic materials*
VIC 1	Superficial layers	-	+	-	-	Ultramarine blue
	Between metallic leaves	-	+	-	-	-
VIC 2	Superficial layers	+	+	-	-	Calcite Iron oxide Calcium oxalates Quartz
	under metallic leave	+		-	-	Barium sulphate Chrome yellow Metal Carboxylates
VIC 3	Superficial organic layers	-	+	-	-	- Calcium carbonate Barium sulphate
	Between metallic leaves	-	+	-	-	-
	Under metallic leave	+	-	-	-	Prussian blue Lead white
	Preparation	+	-	-	-	Calcium carbonate Barium sulphate Lead white
VIC 4	Pigment layers	+	-	-	-	Green Earth Bone black Barium sulphate Calcium carbonate
	Preparation	+	-	-	-	Calcium carbonate Barium sulphate Quartz
VIC 5	Pigment layers on top	+	-	-	-	Green cinnabar ([i]) Clay (kaolinite) Lead white Calcium oxalates Metal Carboxylates
	Preparation	+	-	-	-	Lead white
	Canvas prep	-	-	-	+	-
VIC 6	Superficial layers	-	+	-	-	Bone black
	mordent	+	-	-	-	Calcium carbonate
	preparation	+	-	-	-	Calcium carbonate Lead white
VIC 7	Superficial layers	-	+	+	-	-
	mordent	+	-	-	-	Lead yellow Barium sulfate
	preparation	+	-	-	-	Lead white

[i] Strontium yellow+Prussian blue

3.3.3. Pyrolysis/Gas Chromatography/Mass Spectrometry

Samples VIC 1-2-3-6 and 7 are characterised by the presence of monocarboxylic acids, a relatively high content of dicarboxilic acids attributable to a siccative oil [7]. Dehydroabietic acid together with didehydroabietic and 7-oxo dehydroabietic acid are markers of the presence of a Pinaceae resin while butolic acid is indicative of shellac [17]. Markers of a well preserved pine resin such as pimaric acid, sandaracopimaric acid or isopimaric acid were not present in any of the samples pyrograms. Levoglucosane, pyrolysis product of a glucose based polymer and xylofuranose, characteristic pyrolysis product of natural gums (fruit tree, tragacanth, arabic gums or their mixtures) [7], have been found, suggesting the presence of a mixture of polysaccharide materials. Figure 3.3 shows a pyrogram of the sample VIC 2, where peaks corresponding to the significative markers cited above are indicated.

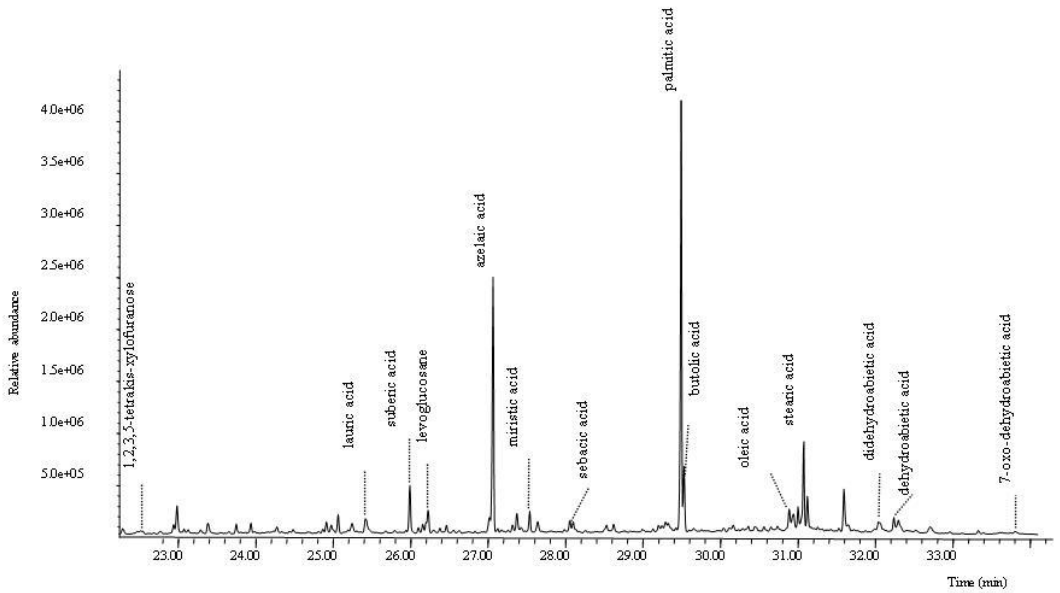

Figure 3.3. Pyrogram of sample VIC 2. Peaks are labelled with to the compounds identified.

VIC 4 and VIC 5 present similar pyrograms characterized by relatively high amounts of monocarboxylic acids, being palmitic and stearic acids the most abundant, and low amounts of dicarboxylic acids. This indicates that if a siccative oil is present, this is mixed with a non-drying lipid material. In fact in VIC 5 traces of hexadecanonitrile and octadecanonitrile, markers of egg, were found. In these two samples, markers of both plant and animal resins were absent. The markers of polysaccharide materials in sample VIC 4 and VIC 5 presented a similar profile to the other group of samples, indicating that also in this case a mixture of polysaccharide binders is present. Results are summarised in Table 3.5.

Table 3.5. Summary of results from the Py/GC/MS analysis

sample	*drying oil*	*Pinaceae resin*	*shellac*	*saccharide material*	*Proteinaceous material*
VIC 1	+	+	+	+	-
VIC 2	+	+	+	+	-
VIC 3	+	+	+	+	-
VIC 4	+	-	-	+	-
VIC 5	+	-	-	+	+ (egg)
VIC 6	+	+	+	+	-
VIC 7	+	+	+	+	-

3.3.4. Gas Chromatography/Mass Spectrometry

On the basis of the results obtained on the organic material composition of all samples by FTIR and Py/GC/MS and of the morphological observation of the sample cross sections, it was decided to proceed with the GC/MS and SR FTIR analyses of only three samples: VIC 2 and VIC 7, representing the group of samples with many layers and containing a mixture of several organic materials, and VIC 5 representing the group of samples with few layers and containing only a non drying oil and a mixture of polysaccharide materials.

The GC/MS analytical procedure for the identification of lipids, waxes, proteins, and resinous materials in the same microsample is based on a sample multistep chemical

pretreatment (solvent extractions and microwave-assisted chemolysis) that is able to separate the various organic components into three different fractions (one for the identification of proteinaceous materials and two for the identification of glycerolipis, natural resins waxes), which are suitably derivatized before analysis. The complete detailed procedure is reported in the literature [2].

First of all, hydroxyproline, marker of collagen, is present in all three samples. Most likely animal glue was the proteinaceous material used for the canvas preparation. The quantitative percentage content of amino acids of the painting samples (reported in Table 3.6) was subjected to a multivariate statistical analysis together to a data set of 121 reference samples of animal glue, egg and casein, using the principal components analysis (PCA) method [[29]] .

Table 3.6. Amino acidic relative percentage content of samples VIC2, VIC5 and VIC7

sample	*Ala*	*Gly*	*Val*	*Leu*	*Ile*	*Ser*	*Pro*	*Phe*	*Asp*	*Glu*	*Hyp*
VIC 2	8.1	21.3	5.0	9.3	4.5	8.6	2.0	3.8	18.6	18.4	0.4
VIC 5	15.0	32.3	4.8	6.8	2.9	7.1	11.4	2.0	10.2	1.0	6.6
VIC 7	12.2	21.6	4.5	6.1	3.2	4.8	10.6	3.5	9.5	12.8	11.4

The PCA score plot presented in Figure 3.4 shows that VIC 7 and VIC 5 are located in the animal glue cluster or close to it. However, VIC 5 shows a percentage content of glutammic acid (Table 3.6) quite low, this might be due to a bacterial attack [[30]] or to some complexation reaction with inorganic pigments, that has subtracted the amino acid to the derivatisation [3]. For this reason, it is not possible to exclude that another proteinaceous materials is simultaneously present. Hexadecanenitrile, marker of egg, was identified in the pyrogram of this sample (reported above). It is thus possible to hypothesize that both egg and animal glue are present in VIC 5. VIC 2 contains both egg and animal glue, as it can be assessed from its position in the PCA score plot.

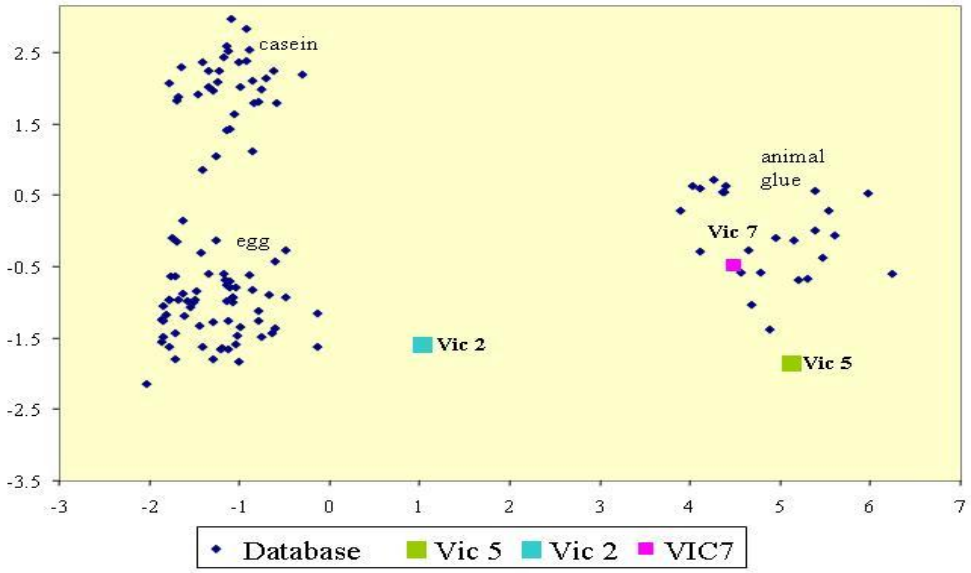

Figure 3.4. Principal Component analysis score plot of the amino acids percentage relative content in samples VIC2, VIC 5 and VIC7.

The most abundant peaks in all chromatogram of the acidic fraction (presented in Figure 3.5) are palmitic, stearic, suberic, azelaic, and sebacic acids. The calculated characteristic parameters for these acids [1] are reported in Table 3.7. The A/P ratio for samples VIC 2 and VIC 7 clearly points out to a drying oil. The P/S ratio of the samples VIC 2 and VIC 7 are consistent with the presence of a linseed oil. Moreover, sample VIC 7 presents a very high content of dicarboxylic acids that seems to suggest the use of a pre-polymerised linseed oil [1].

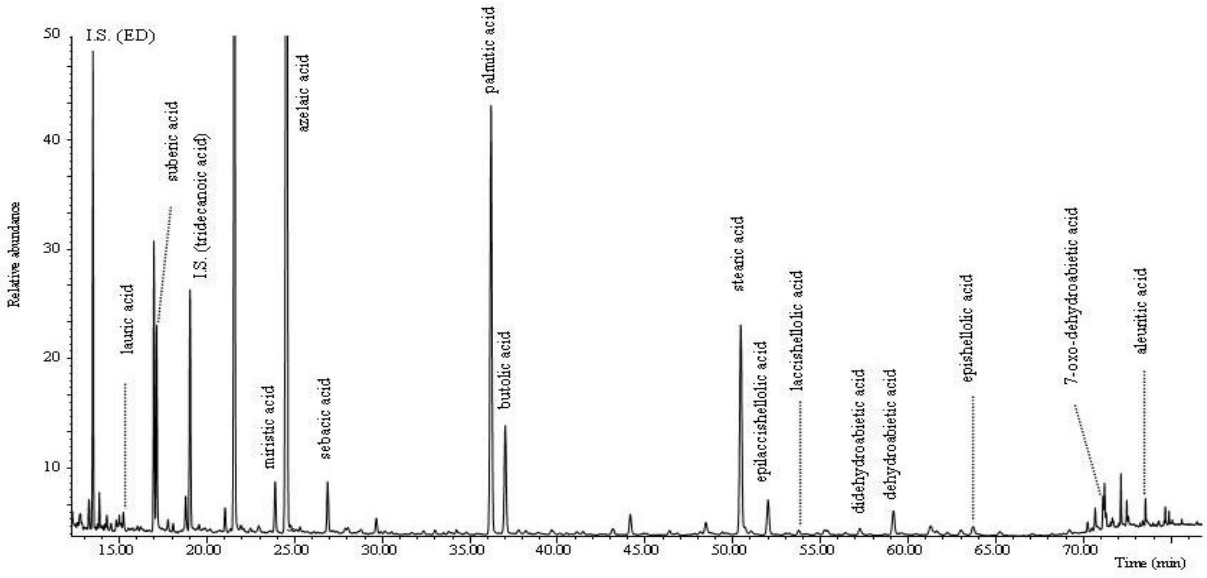

Figure 3.5. Total ion chromatogram of sample VIC 2 obtained by GC-MS procedure. Peaks are also labelled with to the markers identified

Table 3.7. characteristic ratio value of the fatty acids of samples VIC2, VIC5 and VIC7

sample	*A/P*	*P/S*	*ΣD (%)*
VIC 2	1.4	1.3	48.9.
VIC 5	0.5	1.6	23.4
VIC 7	6.0	1.1	79.7

The characteristic parameters obtained for sample VIC 2 suggest that egg (detected by analysis of the proteinaceous fraction) is present in minor amount with respect to the oil.

For VIC 5, the A/P ratio lower than 1 seems to point to a mixture of a drying oil (attested by a consistent amount of dicarboxylic acids) and a non drying fat such as egg. Egg markers were identified by pyrolisis and their presence was not excluded by the GC/MS analyses.

Finally, in the acidic fraction of VIC 2 and VIC 7 also the presence of the molecular markers of a Pinacae resin (dehydroabietic acid together with didehydroabietic and 7-oxo dehydroabietic acid) and shellac (butolic, aleuritic, epishellolic, shellolic, laccishellolic, epilaccishellolic acids) were individuated [2,3,4,5,6].

3.3.5. Synchrotron radiation FTIR

A critical point in performing SR FTIR mappings in transmission mode is the sample preparation as it is necessary to obtain very thin sample sections to avoid the complete absorption of the transmitted beam. Microtoming after embedding the sample in a epoxy resin usually causes several problems such as infiltration of the resin and crumbling and lost of particles [9,10] but it worked particularly well with VIC samples. As already evidenced, in fact, Sert painting technique uses such a high amount of organic materials that no infiltrations of the epoxy resin occurred during the embedding, avoiding the contamination of the embedding resin (an infrared absorbing media) in the spectra. Moreover, the embedded micro-samples were enough flexible, thus, they did not completely crumble on cutting, particles were not lost, and slices of an homogeneous thickness (from 5 to 12 μm) suitable for transmission experiments, were obtained. The good quality of the spectra obtained is also evidenced by a high signal-to-noise ratio that allowed the recognition of the characteristic IR features of the materials described previously. This permitted to localise in the sample cross-sections those materials that were already identified by the other spectroscopic and spectrometric techniques on the bulk of the samples.

A photomicrograph of each cross-section of the samples after microtoming is shown in Figure 3.6 (a, b, c). The microtomed thin section of VIC 2 contained only superficial layers (10 to 4). In Figure 3.6 the linescans acquired along the line depicted in the sliced cross-section for each sample are reported (Figure 3.6 d,e,f). A linescan is a representation of the spectra acquired at a sequence of points (wavenumbers vs position). A line scan permits to visualise the main spectral features of the different layers, and is useful to choose these bands to be mapped, to visualize the distribution of different functional groups. The features highlighted in the line scan can be also easily identified in the representative spectra selected and presented in Figure 3.7. In the areas between dotted lines, the linescan spectra present similar features. Figure 3.7 shows an infrared spectrum representative of these areas. Results are summarized in Table 3.8, which presents the main absorption bands recognized in the line scans of the three samples together with the absorption bands evidenced in the infrared spectra observed, and, correspondingly, the material identified. It is important to highlight that only major absorption bands are evidenced in the line scans. As a result, the features

highlighted in the linescans, correspond to CH st (2800-3000 cm^{-1}), carbonyl bands (1650-1750 cm^{-1}), CO st (1175 cm^{-1} for oils and 1260 cm^{-1} for resins) and metal carboxylates (1600-1500 cm^{-1}).

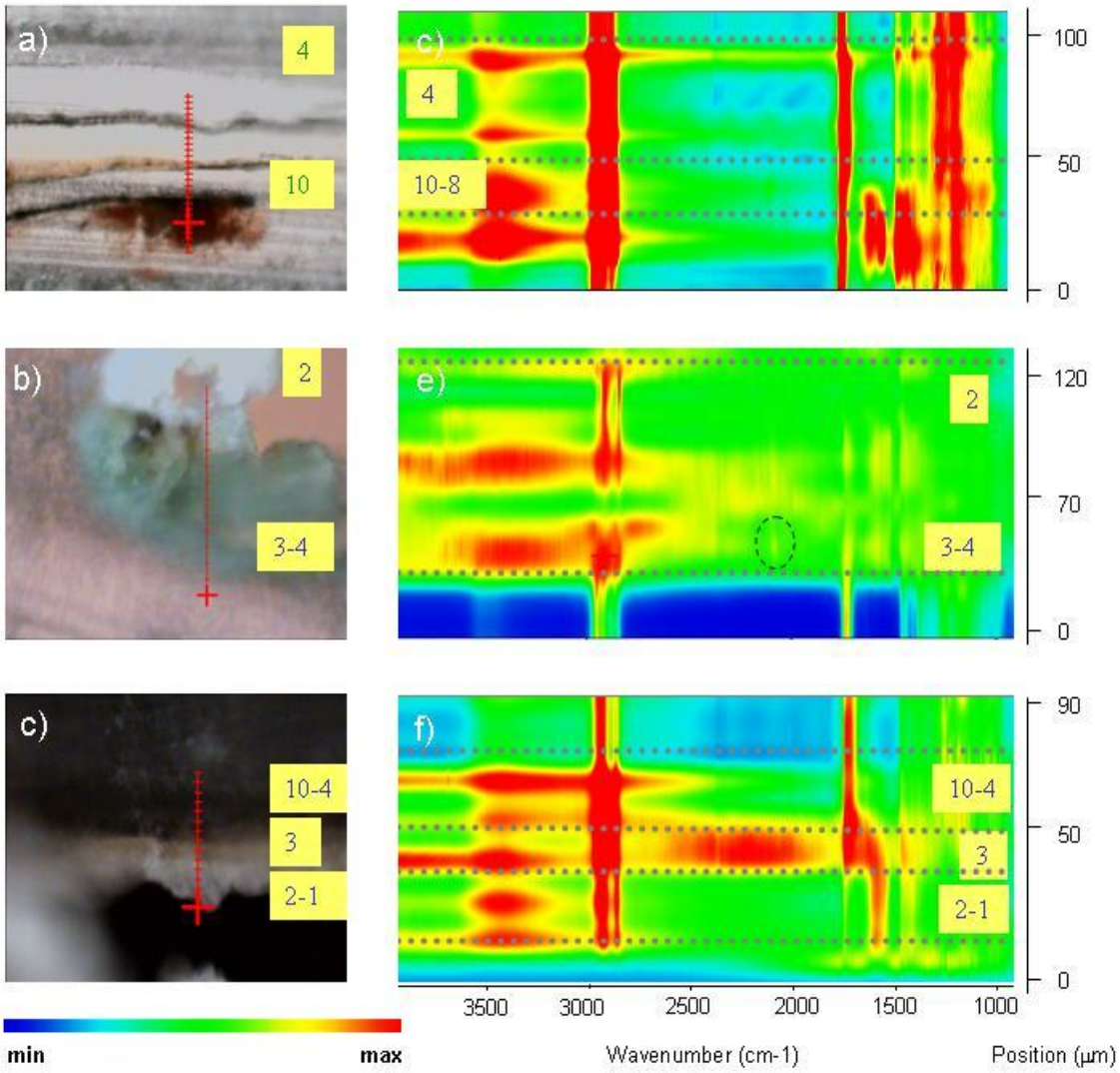

Figure 3.6. Photomicrograph of the microtomed cross-sections. The red line marks the line selected to perform the line scan a) VIC 2(12 µm); b) VIC 5(4 µm); c) VIC 7 (12 um); line scan of d) VIC 2; e) VIC 5; f) VIC 7; Grey dotted line indicates the end of the sample and the beginning of the embedding medium and the separation between layers. Squared numbers indicate some layers position.

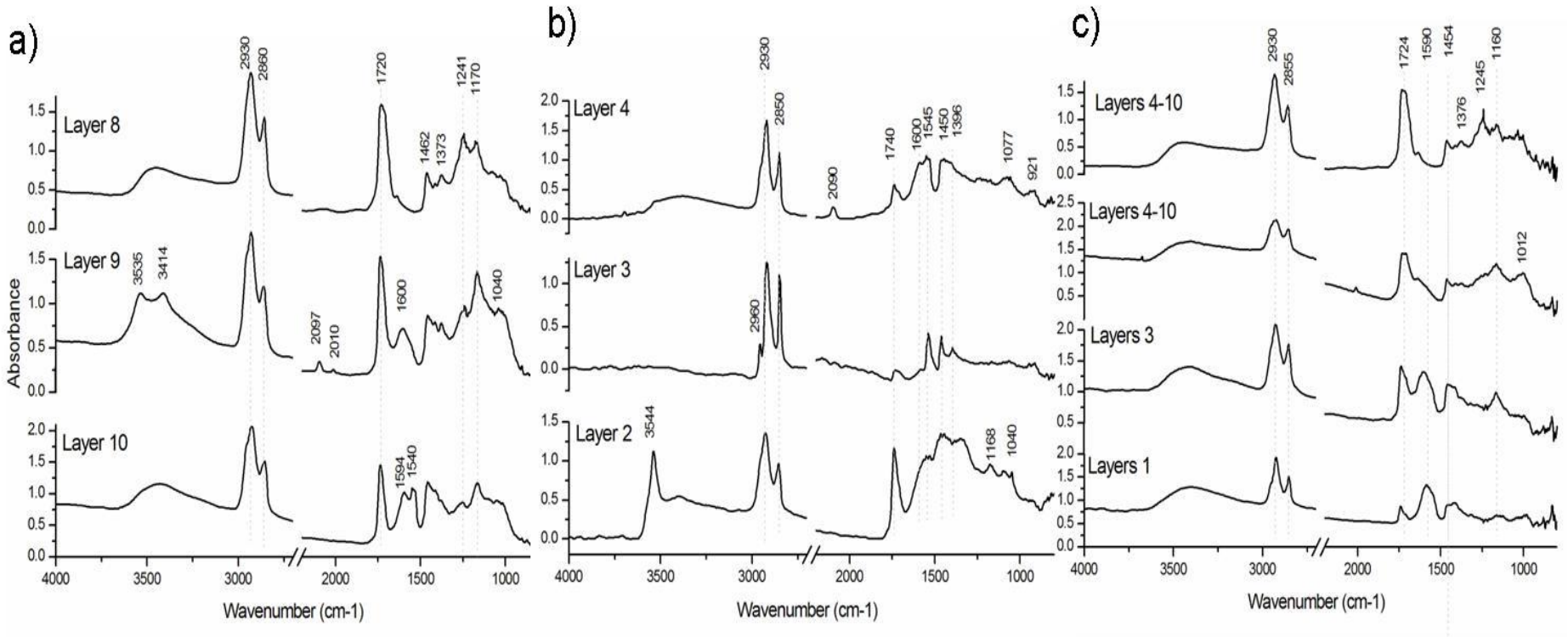

Figure 3.7. Characteristic SR FTIR spectra of some layers of the samples a) VIC 2; b) VIC 5; c) VIC 7. Spectra have been recorded with a 8x8 μm aperture, 50 scans, 4μm step and 8 cm^{-1} resolution.

Table 3.8. Correspondance of bands highlighted in the linescan, main IR bands in the spectra corresponding to the area and selected bands for mapping the material identified.

Sample	Layer	Linescan position	Highlighted feature	Spectrum bands ([i])	Material identified	Mapped bands ([ii])
VIC 2	10-9	10-45	1600 1533 1400 (ba) 1160	2930, 2850, 1730, 1590, 1530, 1462, 1415, 1387, 1240, 1167, 1040	Oil	1590 1540
	9	40-45	-	2012	Bone black	-
			-	2092	Prussian blue	2092
	8-4	50-100	1710 ([iii]) 1260 1160	2930, 2850, 1720, 1450, 1373, 1260, 1160	Resin	1715 1260
VIC 5	3-4	30-90		2930, 2850, 1730, 1580,1540, 1460, 1415	Oil	-
	4	30-45	2090	2090	Prussian blue	-
			-	1100 1050 3699 3620	Clay (kaolinite)	-
VIC 7	1-2	0-30	1580	2930, 2855, 1730, 1590, 1460, 1380,	Oil	1580
	3	30-45	1580-1730 (broad area)	2930, 2855, 1730, 1590, 1460, 1387, 1160	Oil,	-
	4-10	45-65	-	3535 1410	Lead white	-
			-	2012	Bone black	-
			1730	2930, 2855, 1720, 1632, 1460, 1376, 1245, 1160	Resin	1250

[i] Bands of an infrared spectrum from an area with similar highlighted features in the line scan.
[ii] Bands considered representative of a material and mapped to study its distribution.
[iii] Broadening of the band

By mapping the bands evidenced by the line scans, the distribution of some of the organic materials could be achieved for VIC 2 and VIC 7. False colour maps represent the distribution of specific functional group (band intensity versus position) in the cross-section: chemically specific images are obtained, where color is a function of the peak height. Mappings resulted from the accurate study of individual spectra to assure that the highlighted areas were consistent with the material real localisation.

Bands chosen are specified in Table 3.8 and the result of the mapping is presented in Figures 3.8 and 3.9 for VIC 2 and VIC 7, respectively. By mapping the bands at 1715 and 1260 cm^{-1}, considered as characteristic of a terpenoid resin, wide areas presenting the maximum intensities are coincident with the mainly organic layers on top of the stratigraphies. By mapping the carboxylate peaks (1600–1540 cm^{-1}) the oil presence in the pigmented layers is also established. Finally, mapping of the bands at 2092 cm^{-1} and 3535 cm^{-1} allows to establish the distribution of Prussian blue in layer 8 and zinc white in layers 10 to 8 in VIC 2, respectively.
VIC 5 microtomed cross-section did not allow the mapping of those bands that were identified by the study of spectra, mainly due to irregularities in the width of the slice (see Chapter 1.3.1.2.)

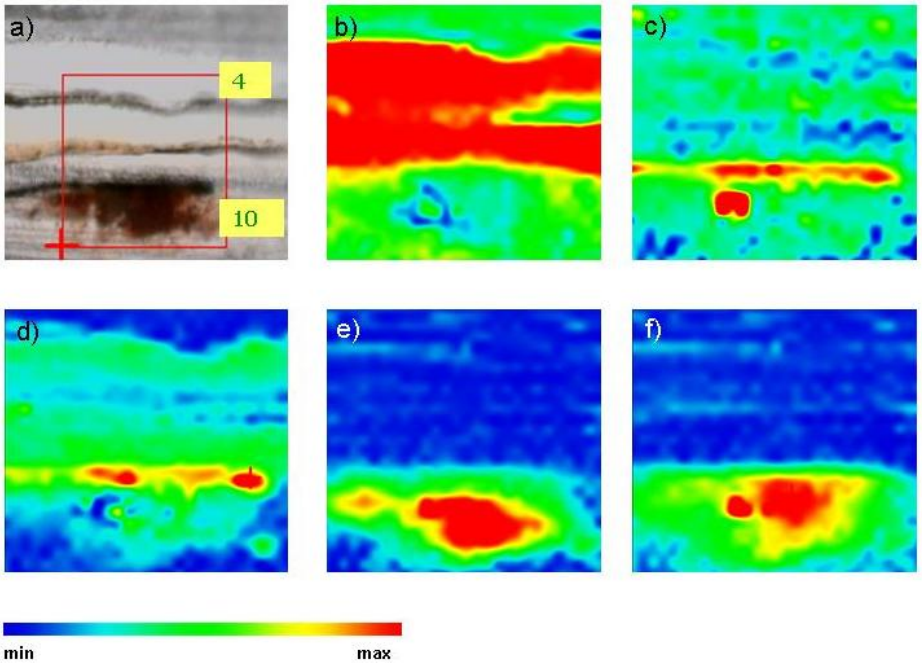

Figure 3.8. a) Photomicrograph of the microtomed cross-section of VIC 2 (width: 12 μm). The rectangle marks the area selected to perform the SR FTIR mapping ; chemical image of b) 1717, c) 2090, d)3539, e)1590 and f)1533 cm-1. Mapped area 102 x 174 μm.

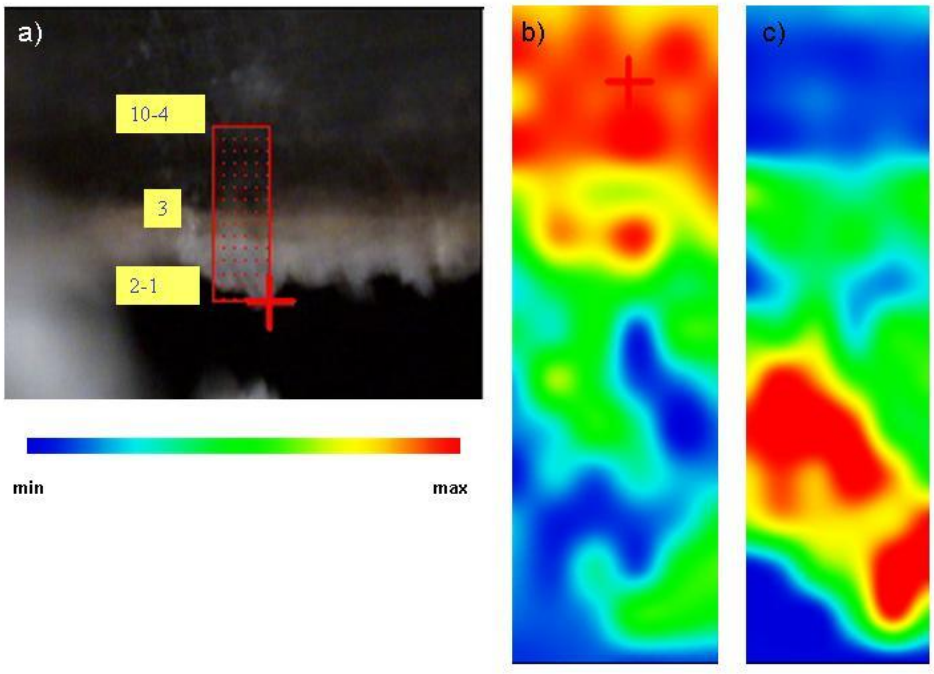

Figure 3.9. a) Photomicrograph of the microtomed cross-section of VIC 7(12 μm). The rectangle marks the area selected to perform the SR FTIR mapping ; chemical images of b) 1250 cm^{-1} and c) 1590 cm^{-1}. Mapped area is 131 x 48 μm.

3.3.6. Synchrotron Radiation XRD

Sample VIC 7 was prepared for XRD experiments in transmision mode. The sample preparation for transmission XRD experiments has been already reported in previous works [16,19]. It consists in an embedding of the fragment in polyester resin polymerised by a peroxo organic hardener under low humidity conditions and sectioned with a diamond saw of thickness 0,1 mm into a 200 microns thick slice. Patterns were fitted with the ESRF FIT2D package software [31].

A linescan was obtained. In this case the line scan consists in a 2θ versus position representation. Figure 10 b presents the linescan were the alternation of organic (non diffracting layers, white areas) and crystalline phases (grey, black areas) are easily appreciated. The line scan is acquired in the area of the cross section evidenced by a red line in the cross section image reported in Figure 3.10 a. XRD patterns of some layers are also presented (Figure 10 c). Table 3.9 reports cristallographyic phases identified in the cross-section of sample VIC 7. It is important to specify that the pattern matching process presented some difficulties due to the nature of the samples: painting cross-sections are formed by a mixture of different crystals of different size and orientation that are not powdered to obtain an statistically arranged mixture of crystals. Samples are not, thus, presenting all possible orientation under the excitation rays. Though some crystals are small enough to be considered randomly oriented, big crystals such as cerussite and hydrocerussite are bigger than the beam spot used obtaining a diffraction pattern different from that of the standards and thus difficult to be identified. SR XRD permitted the unequivocal characterization pigments and dryers (barite, apatite, cerussite, hidrocerusite, crocoite), by means of the identification of the crystalline phases. It is interesting to note the presence of lead acetate. Lead acetate is known to be a dryer for drying oils. In sample VIC 7 a prepolimerised oil was observed, as discussed in the GC/MS section. This result is in accordance with the presence of lead acetate, which could be the dryer used for the prepolymerisation process of linseed oil [32]. This is the first experimental evidence of the use of lead acetate as dryer in painting samples.

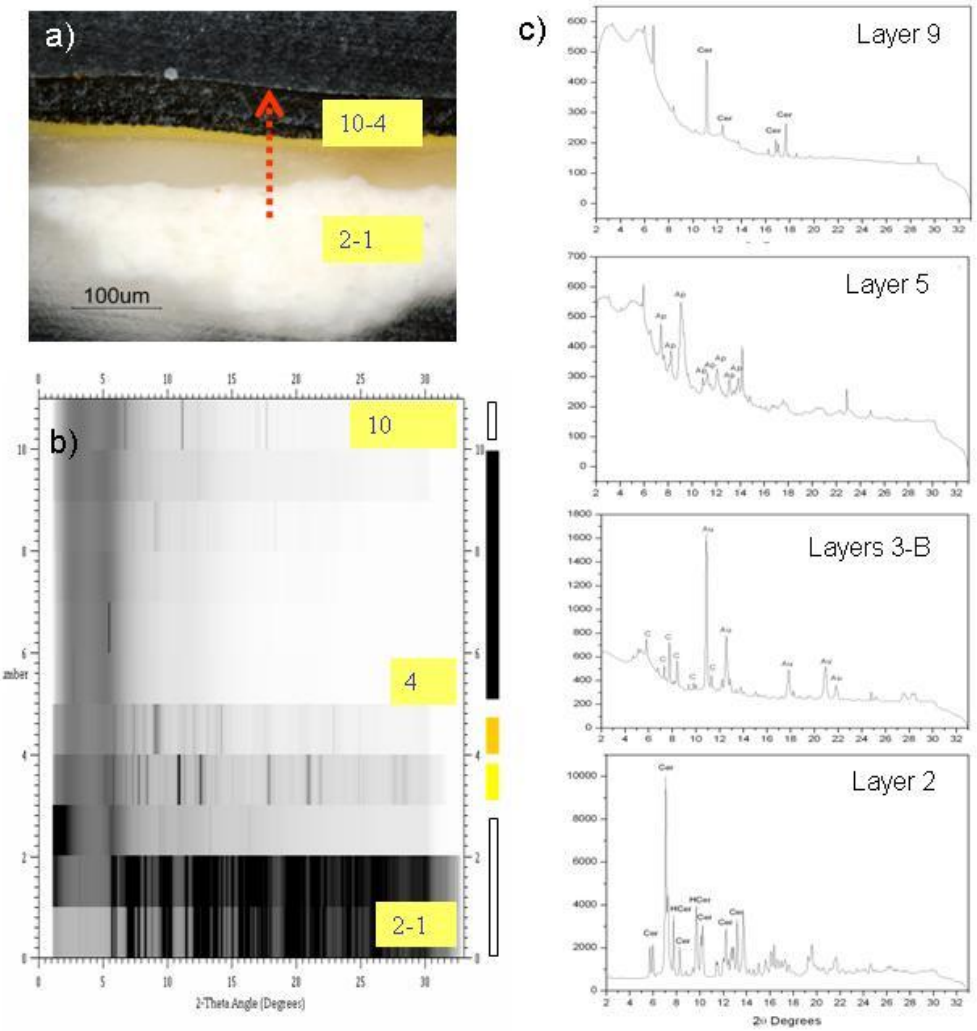

Figure 3.10. a) polished cross-section prepared for XRD anlysis (the arrow indicated the linescan position and its direction) b) XRD linescan from 0 (corresponding to layer 1-2) to 13 (corresponding to layer 10); c) XRD patterns of some of the scans corresponding to different layers. Peaks labeled with letters corresponding to: Cer (cerussite, PbCO3), Ap (Hidroxylapatite, Ca3(PO4)3(OH)), Au (gold), C(crocoite, PbCrO4) and HCer (hydrocerussite, Pb3(CO3)2(OH)2).

Table 3.9. VIC 7 XRD results : crystalline phases identified and JCPDS number.

Mineralogical phase	Chemical Formula	JCPDS number
Hydroxylapatite	$Ca_5(PO_4)_3OH$	00-009-0432
Barite	$BaSO_4$	00-024-1035
Gold	Au	00-001-1172
Crocoite	$PbCrO_4$	00-008-0210
Cerussite	$PbCO_3$	00-005-0417
Hydrocerussite	$Pb_3(CO_3)_2(OH)_2$	00-010-0401
Zinc Oxide	ZnO	00-001-1150
Lead acetate	$Pb(C_2H_3O_2)_2 \cdot 3H_2O$	00-001-0028

3.4. Conclusions

The combined interpretation of the data obtained with all the different techniques allowed the characterization of the samples layer by layer. Table 3.10 and 3.11 summarized the material identified and their distribution, inorganic and organic, repectively.

Table 3.10. Inorganic compounds identified and results of the different techniques for VIC 2, VIC 5 and VIC 7.

sample	Layer Number ([iv])	EDS results	FTIR bands ([v])	XRD crystaline phases	Inorganic compounds identified
VIC 2	10	Al, S, Si, P, Ca, Cr,Ba,Na, Fe, P	550, 456 1420, 876 1586 1318	-	Iron oxide calcite zinc compound calcium oxalates Quartz
	9	S, Al, P, Ca, Si, Na, K> Zn, Fe	2012 2092		Bone black Prussian blue
	8	Cl	-		*
	7	Cl	-		*
	6	Al, S, Si, P, Ca, Cr,Ba,Na > Fe, P			-
	5	Cl			
	A	Au >>> Ag, Cu			Gold
	4	Cl			*
	B	Cu, Zn			brass
	3	Pb, Cr, Ba	1170,1112,1072, 984, 635, 608 873,820		Barium sulphate
	2	S, Ba, P, Cr			Lead chrome yellow (PbCrO4)
	1	Fe, Mn, Pb			Clay? Iron oxide?
	C	Cu, Zn			brass

[iv] Layers have been numbered from the preparation layer to the superficial layer consecutively. Letters have been used for metallic leaves.

[v] Both conventional and SR FTIR bands

[*] The fact that shellac used as a paint varnish was probably blenched shellac that was refined by using sodium hypochlorite could explain the high concentrations of Cl observed in the resin layers

VIC 5	4	Sr, Pb, Zn, Cr, Cd, Fe, Al, Si	923, 909, 842 2092 1400, 680 3698, 3636, 1030, 1008, 916 1585	-	Strontium yellow Prussian blue Lead white Kaolinite Zinc compound
	3				
	2	Pb	3538, 1400, 1047,		Lead white
	1	-	-		-
VIC 7	10	Cl		-	
	9	Ca	2012	apathite	Bone black; prussian blue
	8	Cl	-	-	*
	7	-	-	-	-
	6	Cl	-	-	*
	5	P, Ca, Na, Al, Si, Mg	-	Apathite Hydroxyapathite barite	Bone black
	4	Cl	-	-	*
	A	Au	-	Crocoite, Au	Chrome yellow Gold
	3	Zn, P, Ca, Pb	3532, 1400 837 855, 820	cerussite hidrocerussite; Zinc oxide ; mirabilite	Lead white Zinc white
	2	Zn	-	Zinc oxide;	Zinc white
	1	Pb, Zn	3532,1420, 1052 1420, 837 1524	Cerussite hydrocerussite Lead acetate	Lead white Lead acetate

Table 3.11. Organic materials identified with the different techniques.

sample	Layer number	FTIR	Py/GC/MS	GC/MS	SR FTIR	Organic compound identified	inorganic materials (from table 9)
VIC 2	10	Natural resin Lipidic material	Drying oil Pinaceae resin Shellac Polysaccaridic material ([vi])	Linseed oil Pinaceae resin Shellac Egg Animal glue ([vi])	Lipidic material	Linseed oil	Iron oxide calcite zinc compound calcium oxalates Quartz
	9				Lipidic material	Linseed oil	Bone black Prussian blue
	8				Nat. Resin	Shellac (pine resin)	-
	7				Nat. Resin ([vii])	Shellac (pine resin)	-
	6						
	5						
	A	-			-		Gold leave
	4	-			Nat. Resin	Shellac (pine resin)	
	B				-	-	Brass leave
	3	Lipidic material			Lipidic material	Linseed oil	Barium sulphate
	2				Lipidic material	Linseed oil	Lead chrome yellow (PbCrO4)
	1				Lipidic mat.	Linseed oil	Clay? Iron oxide?
	C				-	-	Brass leave
VIC 5	4	Lipidic material	Drying oil Polysaccharidic material Egg (traces)	Drying oil Non drying fat (egg?) Animal glue	Lipidic mat.	Linseed oil(egg)	Strontium yellow Prussian blue
	3				Lipidic mat.	Linseed oil(egg)	Lead white Kaolinite zinc compound
	2	Lipidic material			Lipidic mat.	Linseed oil	Lead white
	1	Polysac.mat.				Mixture polysac mat.	
VIC 7	10	Natural resin Proteinac.mat	Drying oil Pinaceae resin Shellac Polysaccahridic material	Prepolimerized linseed oil Pine resin Shellac Animal glue	Resin	Shellac	
	9				-	-	Bone black; prussian blue
	8				Resin	Shellac (pine resin)	
	7				-	-	-
	6				resin	Shellac (pine resin)	
	5				Proteinaceous material	Animal glue?	Bone black
	4				Resin		
	A				-	-	Chrome yellow Gold
	3	Lipidic mat.			Lipidic mat.	Linseed oil	Lead white Zinc white
	2	Lipidic mat.			Lipidic mat.	Linseed oil	Zinc white
	1				Lipidic mat.	Linseed oil	Lead white Lead acetate

[vi] Polysaccharide. and proteinaceous (animal glue) materials probably used as canvas preparation.

[vii] Natural resin. In some cases a mixture of resins can be hypoyhesised by the FTIR spectra. Shellac has been surely identified in some layers in which EDS results indicated the presence of Cl. Thus, identification of the source of the resin evidenced by FTIR as shellac could be supported by the detection of Cl by EDS.

The combined use of different techniques applied on different aliquots of the same sample, and the interpretation of the results obtained, allowed us to establish the build-up of each sample, the materials used and, thus, to ascertain the painting technique of Josep Maria Sert in his paintings in the city of VIC.

In particular, Josep Maria Sert paintings presented two kind of painting techniques. That observed for samples VIC 4 and 5 is a traditional painting technique, which is based on a preparation layer plus one or more pigmented layer using mainly linseed oil as binding medium. The painting technique of samples VIC 1-2-3-6-7is based on the application of several thin layers mainly organic, with some thin pigmented layers and metallic leaves in the between. This last Sert painting technique, which is characteristic of his last works, resembles that of the Byzantine icons [33], where the color effect on the paint surface is obtained not only with pigments, but also by applying metallic leaves underneath the superficial layers, giving a metallic finishing to the painting. Through this study, the samples from the Sert paintings in the city of Vic helped to appreciate the technical evolvement of Josep Maria Sert as a painter. Sert started with the traditional painting technique (sample VIC 5 from 1906) to use contemporary both the techniques (samples VIC 3 and VIC 4 from the painting “The four seasons” from 1917-1920) and finally using extensively the complex paining technique in the last years (VIC 1 and 2 from 1920, VIC 7 from 1926 and VIC 6 from 1945).

References

[1] A. Andreotti, I. Bonaduce, M. P. Colombini, F. Modugno, E. Ribechini, 'Characterisation of natural organic materials in paintings by GC-MS analytical procedures' in New Trends in Analytical, Environmental and Cultural Heritage Chemistry, M. P. Colombini and L. Tassi editors, Research Signpost, in press

[2] A. Andreotti, I. Bonaduce, M.P. Colombini, G.Gautier, F.Modugno, E. Ribechini 'Combined GC/MS Analytical Procedure for the Characterization of Glycerolipid, Waxy, Resinous, and Proteinaceous Materials in a Unique Paint Microsample', Analytical Chemistry. 2006, vol. 78, pp. 4490-4500, ISSN: 0003-2700.

[3] G. Gautier, M. P. Colombini, 'GC–MS identification of proteins in wall painting samples: A fast clean-up procedure to remove copper-based pigment interferences', Talanta, Volume 73, Issue 1, 15, 2007, pp 95-102.

[4] M.P. Colombini, F. Modugno, 'Characterisation of proteinaceous binders in artistic paintings by chromatographic techniques', Journal of separation science, 2004, vol. 27, pp. 140-160, ISSN: 1615-9306.

[5] I.Bonaduce, Colombini M., 'The characterization of beeswax in works of art by gas chromatography-mass spectrometry and pyrolysis-gas chromatography-mass spectrometry procedures', Journal of Chromatography A, 2004, vol. 1028, pp. 297-306, ISSN: 0021-9673.

[6] M.P. Colombini, I.Bonaduce, G.Gautier, 'Molecular Pattern Recognition of Fresh and Aged Shellac', Chromatographia, 2004, vol 56 n5-6, pp. 357-364.

[7] I. Bonaduce, A. Andreotti, 'Py-GC/MS of organic paint binders', in Organic Mass Spectrometry in Art and Archaeology, M.P. Colombini, F. Modugno editors, John Wiley & Sons, in press

[8] J. van der Weerd, R.M.A. Heeren, J.J. Boon, 'Preparation methods and accessories for the infrared spectroscopic analysis of multi-layer paint films', Studies in Conservation 49, 193 (2004)

[9] C. Martin de Fonjaudran, A. Nevin, F. Piqué, S. Catre, 'Stratigraphic analysis of organic materials in wall painting samples using micro-FTIR attenuated total reflectance and a novel sample preparation technique' Analytical and Bioanalytical Chemistry (2008) 392:77–86

[10] M. Cotte, E. Checroun, V. Mazel, V. A. Solé, P. Richardin, Y. Taniguchi, P. Walter and J. Susini, 'Combination of FTIR and X-rays synchrotron-based micro-imaging techniques for the study of ancient paintings. A practical point of view.'E-Preservation Science, vol 6, 2009

[11] M. Cotte, J. Susini, V. A. Solé, Y. Taniguchi, J. Chillida, E. Checroun, P. Walter, 'Applications of synchrotron-based micro-imaging techniques to the chemical analysis of ancient paintings', Journal of Analytical Atomic Spectrometry, 23, 2008, 820-828

[12] P. Dumas, N. Jasmin, J.L. Teillaud, L.M. Miller, B. Beccard, 'Imaging capabilities of synchrotron infrared microspectroscopy', Faraday Discussions 126, (2004) 289-302

[13] M Cotte, P. Walter, G. Tsoucaris, P.Dumas, 'Studying skin of an Egyptian mummy by infrared microscopy', Vibrational Spectroscopy, 38 (2005).159-167

[14] M. Cotte, J. Susini, A. Moscato, C. Gratziu, A. Bertagnini, N. Metrich, 'Blackening of Pompeian Cinnabar paintings studied by X-ray micro-spectroscopic imaging', Analytical Chemistry, 78, 7484-7492 (2006).

[15] M. Cotte, E. Checroun, J. Susini, P. Walter, Micro-analytical study of interactions between oil and lead compounds in paintings, Applied Physics A, Volume 89,4 (2007) 841-848

[16] A. Lluveras, S. Boularand, J. Roqué, M. Cotte, G. Martinez-Ruiz, P. Giráldez, M.Vendrell-Saz, 'Weathering of gilding decorations investigated by SR: development and distribution of calcium oxalates in the case of Sant Benet de Bages (Barcelona, Spain)', Applied Physics A, 2008, 90 (1), 23-33.

[17] A. Andreotti., I. Bonaduce.b, M. P. Colombini, F. Modugno, E. Ribechini 'The diagnosis of the yellowing of the marble high-reliefs and the black decorations in the chapel of the tomb of Saint Anthony (Padua-Italy)', Journal of Mass Spectrometry, accepted

[18] M.R. Derrick, D. Stulik, J.M. Landry, 'Infrared Spectroscopy in Conservation Science' (The Getty Conservation Institute Los Angeles 1999)

[19] N.Salvadó, T. Pradell, E. Pantos, M. Z. Papiz, J. Molera , M. Seco and M. Vendrell-Saz, 'Identification of copper-based green pigments in Jaume Huguet's Gothic altarpieces by Fourier transform infrared microspectroscopy and synchrotron radiation X-ray diffraction', Journal of Synchrotron Radiaion. 9, 215 (2002)

[20] E Abelev, et al 'An alternative isolation of tungsten tips for a scanning tunnelling microscope', Reviews of Scientific Instruments 76, 106105 (2005)

[21] R.J. Meilunas, J.G. Bentsen, A. Steinberg, 'Analysis of Aged Paint Binders by FTIR Spectroscopy', Studies in Conservation 35, (1990) 33-51.

[22] M. R. Derrick D.C. Stulik, 'Infrared mapping microspectroscopy for identification of furniture finish layers', 1990 WAG Postprints

[23] I. Adrover Gracia: 'Applicazioni della spettrofotometria IR allo studio dei beni culturali' (Collana I Talenti Padova Italy 2001)

[24] K. Helwig, 'The characterization of iron earth pigments using infrared spectroscopy', ' Irug postprints, IRUG at the V&A 83

[25] D. Biakiaris, S. Danilia, S. Sotiropoulou, O. Katsimbiri, E. Pavlidou, A.P. Moutsatsou, Y. Chryssoulakis, 'Ochre-differentiation through micro-Raman and micro-FTIR spectroscopies:application on wall paintings at meteora and Mount Athos, Greece', Spectrochimica Acta A 56, 3-18 (1999)

[26] S Bruni, F Cariati, F Casadio, L Toniolo, 'Spectrochemical characterization by micro-FTIR spectroscopy of blue pigments in different polychrome works of art', Vibrational Spectroscopy 20 (1999) 15-25

[27] J. Madejová , 'FTIR techniques in clay mineral studies', Vibrational Spectroscopy 31,1, 1-10(2003)

[28] J. van der Weerd, 'Microspetroscopic analysis of traditional oil paint', Thesis, Amsterdam,2002. Down loadable from www.amolf.nl/publications.

[29] R. G. Brereton, 'Chemometrics.Data Analysis for the Laboratory and Chemical Plant', J. Wiley & Sons Ltd, West Sussex, England, 2004,chapter 4, ISBN 0-471-48978-6

[30] I. Donati, 'Enzimi, acidi organici ed altri metaboliti coinvolti nella patogenesi di *penicillium spp*. dottorato di ricerca patologia vegetale' (2008) Università di Bologna

[31] A.P. Hammersley, O. Svensson, M. Hanfland, A.N. Fitch, D. Hausermann, 'Two-dimensional detector software: From real detector to idealised image or two-theta scan', High Pressure Research 14, 235-248 (1996)

[32] L. Carlyle, ' Paint dryers discussed in 19th century british oil painitng manuals', jaic online 38 , 1 (1999) 69-82

[33] M. Doerner, 'Los materiales de pintura y su empleo en el arte' (18ª edición Editorial Reverté Barcelona 1998).

Chapter 4

GC/MS characterisation of saccharide materials in samples from works of art

Since the 3rd millennium B.C., polysaccharides have been widely used as binding media and sizing agents. Polysaccharide materials, such as plant gums, sugar, flour or honey are considered in ancient artistic recipes and they have also been widely employed for restoration and consolidation processes. Analytical problems such as low purity and small sample amount have to be taken into account. Furthermore, organic materials can undergo ageing and degradation processes that can have changed their chemical composition and properties.

A GC/MS analytical procedure for the identification of polysaccharide materials present in painting samples has been optimised. The procedure is based on the silylation of aldoses and uronic acids, released from the sample by a microwave assisted acidic hydrolysis, and previously converted into the corresponding diethyl-dithioacetals and diethyl-dithioacetal lactones. Using this method only one chromatographic peak for each compound is obtained, providing simple and highly reproducible chromatograms. Purification from inorganic pigments, which can strongly interfere in the derivatisation step, is performed by using ion exchange resins. The polysaccharide material is then identified from the profile of aldoses and uronic acids through a decisional scheme.

Chemical characterization of samples from mural paintings of the Mediterranean area dating back from the 4th century B.C. to the 19th century A.D. will be presented. Possible contamination of biological origin and polysaccharide degradation in painting samples will be also discussed.

4.1. Introduction

Polysaccharide materials have been used in works of art since antiquity. Egyptian mummification processes, ancient Egyptian paintings in tombs, Macedonian mural paintings and Mycenaean wall paintings in the Palace of Nestor are some examples of their widespread use [1, 2, 3, 4,5, 6]. During the middle ages, polysaccharide materials were used for gilding purposes and in illuminated manuscripts [7, 8]. Ancient texts on painting techniques cite polysaccharide materials such as honey, plant gums or common sugar for different purposes [9, 10, 11, 12].

In painting samples, the low amount of the sample (often less than 1 mg) and the low purity of the organic materials present (mixed together in different proportions to obtain the wanted visual effects), as well as the complexity of the matrix (made of several layers with several materials mixed together, organic and inorganic) and the heterogeneity of the ageing requires the use of sensitive and specific techniques.

Chromatographic/mass spectrometric techniques (HPLC/MS, HPAEC, GC/MS, Py/GC/MS) have demonstrated their suitability for the characterization of organic materials used in the production and restoration of works of art [13,14,15,16,17, 18,19,20,21,22]. Some analytical procedures for the characterization of polysaccharide materials based on High Performance Anion Exchange Chromatography (HPAEC) [23] and Pyrolysis/Gas Chromatography/ Mass Spectrometry [24,25,26] have been developed and applied to painting samples. GC/MS provides the sensivity and low detection limits necessary for the analysis of organic materials in works-of-art. GC/MS procedures for the characterization of polysaccharide materials in works of art have been developed [2,4,8,27, 28, 29, 30,31].

Recently, a GC/MS procedure for the characterisation of plant gums based on the mercaptalation of the sugars, freed by hydrolysis from the matrix, prior to sylanization of the diethyl mercaptal derivatives of the parent sugars was set-up. By this way, a single chromatographic peak was obtained for both aldoses and uronic acids present in plant gums identified in just one single chromatographic step [1, 28].

However, the procedure presents some issues. Drying the derivatised solution prior to the injection can be quite tricky, and sometimes not achievable at all. Moreover, the formation of unwanted products during the derivatisation step sometimes also occurred, strongly reducing the reproducibility of the chromatograms. Moreover, mural painting samples with their high inorganic content are not derivatised properly due to analytical interferences by the inorganic species from pigments and fillers occurring in the derivatisation step.

In this chapter, an analytical procedure for the analysis of polysaccharide materials present in works of art is presented. The procedure is still based on the acidic hydrolysis assisted by microwaves to free the sugars, a clean-up step of the samples to eliminate the inorganic material and a derivatisation consisting in a mercaptalation followed by sylilation. Important modifications have been introduced in the clean-up and derivatisation steps of the previously published procedure to avoid the above mentioned problems. Identification of the problems and discussion of the improvements introduced in the clue points will be presented.

Finally, the optimized procedure has been employed in the characterization of reference raw material and reference painting samples, in order to establish a database of saccharide materials, and to samples from works-of-art, to understand the painting techniques. The results obtained from the characterisation of ancient painting samples open for debate on their possible contamination by other saccharide sources or the degradation of the polysaccharide material present in the sample.

4.1.1. Use of saccharide materials in works-of-art

Several saccharide materials are known to have bee used extensively as a binding media for painting and adhesives for gilding [12,32,33]. During the Middle Ages, illuminated manuscripts were using plant gums as binding medium. The watercolour and gauche techniques assured the use of gums (mainly arabic gum) as binding media until now [32].

In the medieval manuscripts, recipe books where experienced painters described the most usual techniques and materials and their uses, several references to saccharide materials can be found to different purposes. In the Codees Lucensis (8th century) the use of almond gum for gilding on wood or house walls, and of a 'liquid gum' as painting binder, is described [9,10]. The Diversis Artibus written by Teophilus Presbyter in the 12th century reports the application of pigments binded with a medium made of a mixture of oils and gums [10].

In the Bolognese manuscript (15th century) different references to candied, rose or white sugar, white gum, gummed water and honey are done, related mainly to the gilding art [10]. In the Strasburg Manuscript (15th century), the preparation of gum solutions for illuminated manuscripts is described extensively [10]. Honey is also indicated as gold sizing agent and during the grinding process of gold [9]. Cennino Cennini in Il libro del'Arte (also 15th century) describes the use of honey, sugar, gum (arabic gum is specified) and fig latex [34]. Vasari cites arabic gum solutions as being used in retouching fresco paintings [11]. Finally, Jean Le begue and the Alcheriuous manuscripts (15th century) mention frankincense, a gum resin, to obtain a mordant which is not suffering from humidity [9].

However, interpretation of recipe books is not easy and usually the correspondence between the material used and the name given in the manuscript is not obvious. Table 4.1. summarizes the polysaccharide materials cited in Il Libro del'Arte [34].

Table 4.1. Polysaccharide materials and related mentions in Il Libro del Arte (Cennino Cennini).

Chapter	*Title*	*Polysaccharide material*			
		gum	honey	sugar	Other related mentions
X	El modo e l'ordine del disegnare in carta pecorina e in bambagina, e aombrare di acquerelle	x			acquerello d'inchiostro
XLIV	Della natura di un rosso il quale vien chiamato lacca	x			
XXXI	Come tu di disegnare e aombrare in carta tinta di acquerelle, e poi biancheggiare con biacca	x[i]			acquerello d'inchiostro
LXVII	Il modo e ordine a lavorare in muro, cio in fresco, e di colorire o incarnare viso giovenile				acquerelle
LXXII	El modo di colorire in muro in secco, e sue tempere				cime di fico
XC	Per che modo dei cominciare a lavorare in muro ad olio				lattificio del fico
CLVIII	Un altro modo per mettere d'oro in carta			x	
CLIX	Di un colore simile all'oro, il quale si chiama porporina; e in che modo si fa	x[i]			
CLX	In qual modo si macina l'oro e l'argento, e come si tempera per far verdure e adornamenti, e come si pu˜ invernicare il verdeterra	x[i]			
CLXI	Dei colori che si adoprano in lavorare in carta	x			
CLXV	Del lavorare in zendado palii, gonfaloni, stendarli o altri lavori, e del mettere d'oro diademe o campi			x	
CLXXVII	Del lavorare camere o logge a verdeterra in secco		x		acquerella

[i] Arabic gum

Polysaccharide materials have been already identified in works-of-art. Gum arabic, has been found in the painted decoration of the marble throne in the Tomb of Eurydice while a vegetable gum has been also identified mixed with egg in the wall paintings of the Tomb Ayios Athanasios (Thessalonike, Greece) and the Tomb Finikas. This is the first identification of a gum in Greek painting around 300 BC although it was extensively used in Egyptian painting of the Dynastic period [3,4]. The analysis of the cartonage coffin of an Egyptian mummy from the collection of the Museé de Chateaudun (transitory period between 21^{th} and 22^{th} Dinasty) confirmed the use of a gum in its elaboration [26]. In wall painting samples from the 17th century taken at different sites in South India also gums have been identified [2]. Recently, in the preparation layer of painting Bamiyan Buddha polysaccharide materials have been also identified [35]

4.1.2. Saccharide materials composition

Saccharides are widespread in nature. Cellulose is the main component of cotton and wood, and glycogen and starch are the reserves of energy of animals and plants respectively [32,36]. Sucrose and lactose are the main components of sugar and milk and monosaccharide such as ribose and deoxyribose are part of the ribonucleic acids (ADN and ARN). Another natural product occurring as derivative of carbohydrates is ascorbic acid (vitamin C) [36].

Chemically, polysaccharide materials are polymers with a high molecular weight consisting of monosaccharides and uronic acids, that is polyhydroxyaldehides and polyhydroxyketones and their derivatives, held together by a glycosidic bond.

Table 4.2. summarizes the polysaccharide materials used in works-of-art as well as their sugar composition [32,33].

Table 4.2. Polysaccharide materials used in works-of-art found in the literature

		xylose	*arabinose*	*ramnose*	*fucose*	*galcturonic acid*	*glucoronic acid*	*glucose*	*mannose*	*galactose*	*fructose*	*others*
Plant gums	arabic	-	x	x	-	x	x	-	-	x	-	-
	tragacanth	x	x	-	x	x	-	-	-	x	-	-
	Locust bean	-	-	-	-	-	-	-	x	x	-	-
	Fruit tree	x	x	-	-	-	-	-	x	x		
	Guar	-	-	-	-	-	-	-	x	x	-	-
	Karaya	-	-	x	-	x	-	-	-	x	-	-
	Ghatti	x	x	-	-	-	x	-	x	x	-	-
mucilagine	Tamarind see	x	?	-	-	-	-	x	-	x	x	inositol
	Japanese lacquer	-	-	-	-	-	-	-	-	-	x	-
	starch	-	-	-	-	-	-	x	-	-	-	-
Gum-resin	Myrrh	-	x	-	-	-	(4-O-methyl)	-	-	x	-	-
	Olibanum	-	x	-	-	-	(4-O-methyl)	-	-	x	-	-
	Gamboges	x	x	x	tr	-	x	x	x	x		
Cellulose								x				
honey								x			x	

4.1.2.1. Plant gums

Plant gums are naturally occurring water-soluble exudates from several species of plants or extracted from the endosperm of some seeds [32,37]. Plant gums used as binders are high molecular weight polysaccharides made of nine sugars: two aldopentoses (xylose, arabinose), three aldohexoses (mannose, glucose, fructose), two methylhexoses (rhamnose, fucose) and two uronic acids (glucuronic and galaturonic acids). The relative content of each sugar is reported to change with the source of the gum [38]. The chemical structures of the gum monosaccharides and uronic acids are

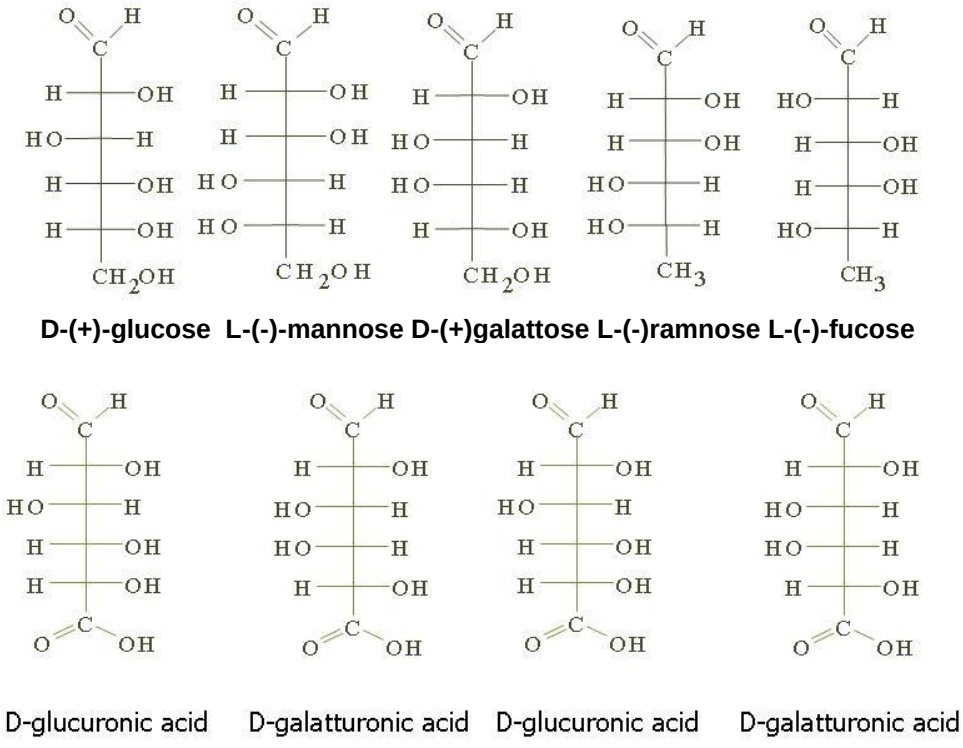

Figure 4.1. Chemical structure of the sugars composing plant gums.

In the Mediterranean basin, the gums traditionally used are arabic gum (from *Acacia Senegal*) from Sudan, India or Australia, tragacanth gum (from *Astragalus leguminosae*) from Asia minor and near east (Iran), fruit tree gums such as cherry, almond, apricot, plum and peach tree, and locust bean or carob gum (from *Ceratonia siliqua, leguminosae*). Table 4.3 summarizes other gums reported in the literature [37,39].

Table 4.3. Summary of gums from different origins

Continent of origin	*Gum*	*Plant family*
Indian sub-continent	Guar	Cyanaposis tetragonolobus (Leguminosae)
	Karaya	Sterculia urens (Sterculiaceae)
	Ghatti	Anogeissus latifolia (Combretaceae)
	Tamarind seed	Tamarindus indica
Mexico	Mesquite	Propolis juliflora
	Nopal (Cholla)	Opuntia fulgida
West Africa	Khaya	Khaya grandifolia (mahogany tree)

Properties and structure of exudated gums have been referred in literature [37, 40].

4.1.2.2. Other saccharide materials used as paint materials

4.1.2.2.1. Honey

Honey polysaccharide content is of about a 70% among monosaccharide (glucose) and disaccharide (sucrose). Sucrose is made of glucose (aldohexose) and fructose (ketohexose) bond together.

4.1.2.2.2. Gum resins

Gum resins are a family of triterpenoid resins (*Burseraceae family*) with a percentage of polysaccharide content in their composition including myrrh (*Commiphora species*) and olibanum (*Boswellia carterii* and *Boswellia fiereana*) [32,39]. Olibanum (or frankincense) presents a compositions of 2-7% of essential oil, 50-64 % of resin, and a polysaccharide content of about 25-40 % [33] though it has been also written a 5-10% of polysaccharide content [39]. Myrrh composition is reported as follows : 2-10% essential oil, 30-40 % resin, and 50-0% gum [33].

Gamboge (gutte gum) from *Garcinia genere* comes from Siam, Cambodge and Sri-lanka. Its composition is referred as being 70-80% resin and 20-30% polysaccharide content [33].

4.1.2.2.3. Cellulose and derivatives

Cellulose and starch are made of units of glucose linked in different ways. They are abundant organic materials: wood, paper and textiles are cellulose based materials. In this group are included cellulose nitrate and cellulose acetate that are products resulting from different treatments of cellulose [32].

4.1.2.2.4. Other materials

Japanese Lacquer (or urushi) from *Rhus verniciflua* presents a 60 % of resin and 7% of saccharide content [32,33].
Luo Han Guo (*luohanguo*) refers to the fruit of *Siraitia grosvenori*, formerly called *Momordica grosvenori*, a member of the Curcubitaceae. *Luohanguo* is primarily grown in southern China, mainly in Guangxi Province, with most of the product from the mountains of Guilin. The story told in China is that knowledge of this fruit first emerged from monks who were using it during the 13th Century. [41]

4.1.3. Analysis of saccharide materials

Qualitatively, different methods have been proposed for the analysis of saccharide materials: precipitation with specific salts or dyes, color or gel formation with specific reagents have been proposed for food analysis. However, those methods are usually aimed at the identification of the presence or absence of a polysaccharide material [37,38].

The identification of polysaccharide materials can be achieved by the use of spectroscopic techniques such as FTIR (Fourier Transform Infrared Spectroscopy) but it unlikely enable distinguishing the various polysaccharide materials among them[42, 43].

Good review on the use of chromatography on sugars on food has been published recently [38,44]. Techniques mainly used are size exclusion chromatography (SEC) [38] , HPLC (High-Performance Liquid Chromatography) [45], HPAEC (High Performance Anion-Exchange Chromatography) [46], Size-Exclusion Chromatography (SEC) [38], GC/MS (Gas Chromatograhy/Mass spectrometry) and Py/GC (Pyrolysis/Gas Chromatography) [47,48,49,50]. Also CE (Capillary Electrophoresis) has been applied for the characterization of polysaccharide materials [51,52]. Table 1.4. shows a comparison of the different techniques and detectors used in food, bacteria analysis and Cultural Heritage.

Table 4.4. Techniques used for the characterization of carbohydrates

Techniques	*Detection limit*	*Detector*	*Food/environment*	*Biochemistry*	*Cultural heritage*
HPLC	mg	UV	+	-	-
		RI (refractive index)	+	-	-
		ELSD (evaporative light scattering detection)	+	-	-
		IR-ELSD	+	-	-
		PAD (pulsed amperometric detection)	+	-	-
		MALDI-MS	+	-	-
		ESI-MS	+	-	-
HPAEC	ng	PAD	+	+	+
CE		UV	+	-	+
GC/MS	ng		+	+	+
PyGC MS	ng		+	-	+
FTIR			-	-	+

4.1.3.1. Analysis of samples from works of art

Different methodologies have been used from spectroscopic techniques to chromatographic ones for the analysis of saccharide materials from works of art. FTIR and Raman present the advantage that sample preparation is almost non-existent. However, they usually allow just general identification of the presence of a saccharide

material without identification of its source [53]. Moreover, the presence of inorganic compounds (highly infrared absorbing) can prevent the identification of the organic materials present in painting layers. Moreover, in painting analysis field, the presence of high amounts of inorganic compounds (pigments and fillers) that are highly IR absorbing and the presence of mixtures of organic materials make difficult the identification of the polysaccharide material and usually practically prevents its characterization [38, 54].

Thin Layer Chromatography (TLC) [55], Pyrolysis/Gas Chromatography (Py/GC) [24,56], High Performance Anion Exchange Chromatography (HPAEC) [23] and Capillary Electrophoresis (CE) [57] analytical procedures have been settled up for the analysis of polysaccharide materials in works-of-art. However, Gas chromatography (GC) has first appeared as a technique able to provide the necessary resolution for the reliable identification and quantification of sugars [27,28,29,30,31]. Table 4.5 summarizes some the literature on the characterization of polysaccharide materials in works-of-art in the last 50 years.

Table 4.5. Characterization of polysaccharide materials in works of art an archaelogical findings.

technique	*method*	*sample*	*results*	*ref*
GC TLC	TMS derivatives -	Surface coating and paint from wooden Egyptian sarcophagus (21st Dinasty)	Tragacanth gum honey	5
TLC	-	16th century manuscript	Arabian gum	58
TLC	-	3 ancient Egyptian epitaphal stelae	Tragacanth gum	59
GC		Wallpaintings in Kerala and Karnataka (South India)	Karaya, Arabic, neem gums	2
GC		Nefertari thomb paintings		6
GC/MS	TMS derivatives	Ink samples from a manuscript and a printed book from 1778 and 1540	Arabic gum (traces)	8
FTIR	-	Bamiyan Buddha		35
HPAEC	-	Macedonian tombs (4th-3rd century B.C.)	Starch fruit tree and tragacanth gums	23

GC/MS	TMS mercaptal derivatives	Macedonian tombs (4^{th}-3^{rd} century B.C.) Myceanean Palace of Nestor (13^{th} century B.C.)	fruit tree and tragacanth gums	1
GC/MS	TMS	William Blake temperas	Mixtures of plant gums and sugar	4
GC/MS	Methoxylamine acetate	Teracotta statue, Greece (400 BC)	Tragacanth + guar ?	17

It should be noticed that the identification of polysaccharide materials has been done, in all cases, on the basis of presence/absence of the sugars and that the quantification of the sugar content is reported in just one case [8].

4.1.3.2. GC/MS analysis of sugars

The analysis of sugars by GC/MS entails some difficulties [4,37,44]. The preparation of carbohydrates for chromatographic analysis have been reviewed [60].The main processes in carbohydrate sample preparation are extraction, clean-up, hydrolysis and derivatisation.

First of all, monosaccharide must be freed by hydrolysis prior to derivatisation. Different strategies have been tried in the literature, mainly conventional acid-catalyzed hydrolysis and methanolysis. The most representative conditions reported in the literature are presented in Table 4.6.

Table 4.6. Hydrolysis treatments summary

method		*reagents*	*product*	*conditions*	*reference*
chemolysis	Acid hydrolysis	HCl	Freed sugars	80ºC 12 h	30
		H_2SO_4 1N		100ºC ;10-12 h	37
		TFA		2 h 120 ºC	4, 28, 30
	Methanolysis	HCl in methanol	Methyl glycosides	90ºC 24 h	27
Enzymatic depolymerization					38
Chemical + enzymatic hydrolysis					38

The primary goal in defining the optimum conditions for hydrolyzing a polysaccharide is to found the conditions in which maximum completeness of hydrolysis and minimum degradation of the components are obtained. Quantitative determination of polysaccharide materials can only be reached if the hydrolysis yield is reproducible. Uronic acids and ketoses easily decompose during hydrolysis [4,38]. Moreover, humins can be formed in the presence of large amounts of inorganic material [37] and browning reactions (Maillard) are reported to take place in the presence of amino compounds and reducing sugars [61].

Microwave have demonstrated giving short reaction times and good reaction yields. Conditions for plant gums have been optimized elsewhere and the procedure applied to painting samples for both HPAEC and GCMS analysis [1,23].

Another problem arising when the analysis of monosaccharides is performed comes from the fact that, in water solutions, monosaccharides undergo intramolecular reactions to form cyclic hemiacetals and hemiketals, either five and six-membered rings that are in equilibrium one with the other. This means that more than one chromatographic peak per analite (from 1 to 6) can be obtained if just silylation is performed [5, 27]. The acquisition of highly complex chromatograms implies that irreproducible quantification, loss of sensitivity, and a limited possibility to identify the various polysaccharide materials may occur. Different strategies have been described to overcome this problem:

- reduction of carbonyl moieties to hydroxymethyl groups followed by acetylation [2, 62]
- conversion of the parental monosaccharides into the acyclic oxime followed by sylilation or acetylation. [44, 30,31,63]
- mercaptalation of the parental sugars followed by silylation [28, 1, 64]

However, each strategy presents its own disadvantages:

- some of the monosaccharides result in just one derivative (compromising the correct interpretation of the sugar profile obtained) during the reduction of the carbonyl moieties (for instance mannitol is fromed from the reduction of both

mannose and fructose) and ketoses generate two isomers (for instance mannitol and sorbitol are formed from fructose) [36].

- more than one peak (syn and anti forms) is obtained in the oxime formation.
- variable yields and by-products formation occur in the mercaptalation-silylation procedures

In Table 4.7. a summary of the polysaccharide derivatisation methods reported in the literature is presented.

Table 4.7. Summary of the derivatisation procedures

method	*strategie for the reduction of the number of chroamtographic peaks*	*reagent*	*products*	*Chracteristics of the method*
Acylated derivatives	Reduction	$NaBH_4$	Alditol acetates	1 peak /Neutral sugars
		NH_4Cl :pyridine	Aldonitrile acetate	1 peak /sugar No ketose
Sylaltion	-	-	TMS derivatives	5 to 6 peaks /sugar
	Conversion of free carbonyl groups into oxime	Hydroxyalamine chorihidrate :pyridine	TMS Oxime derivatives	2 peaks /sugar
	Mercaptalation	ETSH:TFA	TMS diethyl dithioacetal derivatives	1 peak /sugar no ketose

4.2. Experimental Section

4.2.1. Reagents

Monosaccharides and uronic acids d-(+)-galactose, l-(−)-fucose, l-(+)-arabinose, l-(−)-ramnose, l-(−)-mannose, d-(+)-xylose, d-(+)-glucose, d-glucuronic acid, d-galacturonic acid monohydrate, d-allose, d-glucuronic acid lactone, 2-deoxy-d-ribose, d-psicose, d-tagatose, myo-inositol and mannitol, used as an internal standard, purity 99%, were obtained from Sigma–Aldrich (Milan, Italy).

Trifluoroacetic acid 99% purity, and anhydrous pyridine were from Fluka (Milan, Italy), ethanethiol (ETSH) 99.5%, sodium azide (NaN_3) 99.5% and *N*,*O*-bis(trimethylsilyl) trifluoroacetamide (BSTFA) with and without 1%

trimethylchlorosilane (TMCS), were from Sigma–Aldrich. The cation/anion exchange resin Zerolit DMF, with the inclusion of an indicator and granulometry comprised between 14 and 52 mesh, was supplied by BDH Chemicals Ltd (UK).

Standard solutions of monosaccharides with concentrations of about 100 ppm were prepared in bidistilled water and 1% of sodium azide was added to prevent microbial growth. The solutions were stored at 4 °C.

4.2.2. Raw materials and reference solutions

Arabic, locust bean and tragacanth gums were purchased from Sigma–Aldrich. Cherry gum, frankincense, myrrh, mastic resin, oliban, beeswax and propolis were kindly provided by the Opificio delle Pietre Dure (Florence, Italy). Honey (acacia, milefiori and chestnut types) were provided from local markets and Luohanguo was kindly provided by Catharina Blaensdorf, bought at a local market in Xi'an (China). Materials were analysed from the uniformly grinded solid but for Luohango (a solution was prepared from the grinded dried fruit) and honey (appplyed in a glass support and dried before analysis).

Solutions (about 4000 ppm in bidistilled water) were prepared in the Laboratory in Pisa for the analysis of reference plant gums and are reported in Table 4.8.

Table 4.8. Summary of the solutions prepared from raw gums.

Sample name	*gum*	*Other binder*	*pigment*	*NaN_3* [ii]	*Preparation data*	*ageing*
GA sol. Sigma A	arabic	-	-	+	11/07	natural
GA sol. Sigma B	arabic	-	-	-	11/07	natural
TG sol. Sigma A	tragacanth	-	-	+	11/07	natural
TG sol. Sigma B	tragacanth	-	-	-	11/07	natural
Ft sol. Sigma A	fruit tree	-	-	+	11/07	natural
Ft sol. Sigma B	fruit tree	-	-	-	11/07	natural
TG 06	tragacanth	-	-	-	09/06	natural

[ii] indicate the addition (+) or not (-) of NaN3 as biocide after the preparation.

4.2.3. Reference Painting samples

Reference paint layers containing arabic, tragacanth and fruit tree (cherry) gum have been prepared on different supports. The paint layers were prepared both with and without some common inorganic pigments, namely ultramarine (la, SiO_2, Al_2O_3,Na_2O,S), bolo (b, SiO_2, $Fe^{3+}O(OH)$), copper acetate (CuAc, $Cu(CH_3COO)_2.2Cu(OH)_2$) and red lead (mi, Pb_3O_4). Gums were finely grinded, solubilised in water and filtered prior to the application on the support by using a brush and left to dry at room temperature. Mixture with pigments was performed by grinding the pigment in a glass mortar with the filtered gum solution.

Reference paint layers of proteinaceous binders were analysed, as well. Finally, paint layers containing both polysaccharide and proteinaceous binders were prepared. A detailed description of the layers is presented in Table 4.9.

Table 4.9. Description of the reference paint layers analysed.

Sample name ([iii])	*Gum*	*Other binder*	*pigment*	*support*	*NaN3*	*data*	*ageing*
GA (UniPi)	Arabic	-	-	Glass	+	02/08	solar box[iv]
TG (UniPi)	Tragacanth	-	-	Glass	+	02/08	solar box
Ft st (UnPi)	Fruit tree	-	-	Glass	+	02/08	solar box
GA v (OPi)	Arabic	-	-	Glass	-	05/08	natural
TG v (OPi)	Tragacanth	-	-	Glass	-	05/08	natural
FtG v (OPi)	Fruit tree	-	-	Glass	-	05/08	natural
GA i (OPi)	Arabic	-	-	plaster	-	05/08	natural
TG i (OPi)	Tragacanth	-	-	plaster	-	05/08	natural
FtG i (OPi)	Fruit tree	-	-	plaster	-	05/08	natural
GA Pb v (OPi)	Arabic	-	mi	Glass	-	05/08	natural
TG Pb v (OPi)	Tragacanth	-	mi	Glass	-	05/08	natural
FtG Pb v (OPi)	Fruit tree	-	mi	Glass	-	05/08	natural
GA Cu v (OPi)	Arabic	-	CuAc	Glass	-	05/08	natural
TG Cu v (OPi)	Tragacanth	-	CuAc	Glass	-	05/08	natural

[iii] Reference paint layers were prepared in collaboration with Gianni Caponi, restorer of the laboratories of the Opera Primaziale Pisana (OPi) and at the laboratory of the University of Pisa (UniPi) by the authors.
[iv] see 4.2.5

FtG Cu v (OPi)	Fruit tree	-	CuAc	Glass	-	05/08	natural
GA Si v (OPi)	Arabic	-	ma	Glass	-	05/08	natural
TG Si v (OPi)	Tragacanth	-	ma	Glass	-	05/08	natural
FtG Si v (OPi)	Fruit tree	-	ma	Glass	-	05/08	natural
GA b v (OPi)	Arabic	-	b	Glass	-	05/08	natural
TG b v (OPi)	Tragacanth	-	b	Glass	-	05/08	natural
FtG b v (OPi)	Fruit tree	-	b	Glass	-	05/08	natural
GA int (OPi)	Arabic	-	-	Plaster	-	05/08	natural
TG int (OPi)	Tragacanth	-	-	Plaster	-	05/08	natural
FtG int (OPi)	Fruit tree	-	-	plaster	-	05/08	natural
Egg st (UniPi)	-	Egg	-	glass	-	05/04	Natural
Animal glue st (UniPi)	-	Animal glue	-	glass	-	05/04	Natural
Casein st (UniPi)	-	casein	-	glass	-	05/04	Natural
GA egg	arabic	egg	-	glass	-	09/06	Natural
TG egg	Tragacanth	egg	-	glass	-	09/06	Natural
Ft egg	Fruit tree	egg	-	glass	-	09/06	Natural
GA aglue	arabic	Animal glue	-	glass	-	09/06	Natural
TG aglue	Tragacanth	Animal glue	-	glass	-	09/06	Natural
Ft aglue	Fruit tree	Animal glue	-	glass	-	09/06	Natural
GA milk	arabic	milk	-	glass	-	09/06	Natural
TG milk	Tragacanth	milk	-	glass	-	09/06	Natural
Ft milk	Fruit tree	milk	-	glass	-	09/06	Natural

4.2.4. Samples from works-of-art

Samples from mural paintings, coating layers and restoration patinas, coming from different locations and periods, were analysed. A list and description of the samples are reported in Table 4.10.

Table 4.10. Description of the samples from works-of-art

Sample name	*Description*	*Age/century*	*Location*	*Sample weight/mg*
VP 75	Red mural painting	20th	Verdala Palace (Malta)	1.2
Camp	Coating layer on mural paintings	20th	Camposanto Pisa (Italy)	0.6
105.65-46 pi	Pictorial layer of mural painting			10.0
105.65-46 prep	Preparation layer of mural painting			17.2
158.16 NWS	Pictorial layer of mural painting			14.3
179.268 NWS	Pictorial layer of mural painting			9.7
135.43-64	Mural painting sample			27.2
007.15-1	Pictorial layer of mural painting			1.8
004.5-1	Pictorial layer of mural painting			7.1
105.66-46	Pictorial layer of mural painting			4.2
112.93-46	Pictorial layer of mural painting			3.5
065.77-31	Pictorial layer of mural painting			2.3
083.07-43	Pictorial layer of mural painting	13th (AD)	Palace of Nestor (Pylos, Greece)	514.4
076.105	Pictorial layer of mural painting			4.2
006.04-1	Preparation layer of mural painting			265.9
006.02-1	Mural painting sample			2.7
Dr17 R3/4	Pictorial layer of mural painting			2.6
080.09-43	Mural painting sample			1.52
179.122	Pictorial layer of mural painting			1.6
P118	Mural painting sample			340.2
026.13-5	Mural painting sample			8.9
021.75-5	Mural painting sample			11.1
075.105 prep 1	Preparation layer of mural painting			10.4
075.105 prep 2	Preparation layer of mural painting			27.7
Dr201	Mural painting sample			9.2
Met2rosso	Plasters samples		Mausoleo of Mitridate I (Nisa Partica, Turkmenistan)	16.7
Met1base				21.5
Met2pois				20.4
Met1ros				16.9
Bcn e 18	Mural painting	IV BC – I AD	Villa Bicentenario (Ercolano, Italy)	1.0
Bcn w 17	Mural paining		Villa Bicentenario (Ercolano, Italy)	1.8

VP superficial	Superficial layer on mural painting		Villa Papiri (Ercolano, Italy)	0.6
VP intonaco	Preparation layer of mural painting		Villa Papiri (Ercolano, Italy)	9.6
Pdv 3	Black decoration in marble panel	16^{th}	Sant Antonio da Padova (Padova, Itlay)	21.5
Pdv 4	Black decoration in marble panel		Sant Antonio da Padova (Padova, Italy)	-
Pdv 6	Black decoration in marble panel		Sant Antonio da Padova (Padova, Italy)	-
OSM-P	superficial scratched material of the darked area on the marble statue 'San Pietro' by Donatello	15^{th}	OrSanMichele(FLorence, Italy)	16.9
OSM-C	Superficial bronzing on the marble statue 'Quattro Santi Coronati' by Nanni di Banco		OrSanMichele (Florence, Italy)	

Sample VP 75 was collected in the vault of the Main Room of the Verdala Palace in Malta. It was suspected that the painter, Cali (1908-1912) used the gouche technique instead of his oil based characteristic technique.

The sample Camp coming from the superficial patina on the Storia dei Santi (Il Camposanto, Pisa) belongs to a restoration product applied probably during the 50's.

The four plaster samples named met2rosso, met2pois, met1ros and met1base come from the Mausoleo of Miridate I from Nisa Partica (Tukmenistan). The Palace dates back to the 1^{st} century BC.

Twenty samples of mural paintings from the Mycenaean "Palace of Nestor" (Pylos, Greece) from the 13^{th} century BC were studied [65].

Four samples were collected at the roman city of Ercolano: two from the Villa del Bicentenario (called bcn w3 17 and bcn e 18) and two from the Vila dei Papiri (VP superficial and VP intonaco) mural paintings.

The tomb of Saint Anthony in Padua (Italy). The chapel containing the "Ark", that is the Saint's tomb, is located in the Northern part of the Basilica of Saint Anthony from Padua. Since 1300 when it was built, the humidity has caused severe damages so that in the 1500 the original frescoes were substituted with marble high relieves and bronzes. Nine high relieves representing the Saint's miracles and life, made by Sansovino, Lombardo and other '500 masters, decorate the walls behind the tomb. Samples from Sant Antonio da Padova corresponds to black decorations scraped of the marble. Three different samples coming from different panels were analysed.

Analyses have been done on samples from the brownish patina of the statues from Orsanmichele (Florence, Italy). The church of Orsanmichele was a lodge built in the 1290 by Arnolfo di Cambio as a market for the grain, and between the 1337 and the 1400, transformed in church of the ancient Florentine Corporations of Arts. The Corporations of Arts placed on the external facade the sculptures of the Saint Patrons, made by the most famous artists of the period such as Donatello, Lorenzo Ghiberti, Andrea del Verrocchio, Nanni di Banco and Gianbologna. An extended diagnostic campaign [66] has been carried out in the occasion of the restoration of the sculptures in the 1990. The sculptures have been cleaned by using different classical and innovative methods such as the laser cleaning, removing old restoration materials and also the bronzing of the 18 th century, and finally the sculpture have been copied in 2002. Nowadays the original sculptures present a widespread browning of the marble surfaces though being preserved inside the church.

4.2.5. Apparatus and chromatographic conditions

A microwave oven MLS MEGA Milestone 1200W (Milestone Microwave Laboratory System, Monroe, CT, USA) was used.

Two GC/MS systems were used to perform the analyses: a Thermoquest Trace GC system equipped with a programmed-temperature vaporizer (PTV) injector and coupled with an ion trap mass spectrometer PolarisQ (Finnigan, USA) and a 6890N GC System Gas Chromatograph (Agilent Technologies, Palo Alto, CA, USA), coupled with a 5975 Mass Selective Detector (Agilent Technologies, Palo Alto, CA, USA)

single quadrupole mass spectrometer, equipped with a PTV injector. The injector was used in the constant temperature splitless mode at 250 ºC, with a purge time of 0.87 s. The mass spectrometer was operating in the electron impact (EI) positive mode (70 eV). The MS transfer line temperature was 280 ºC; the MS ion source temperature was kept at 230 ºC; the MS quadrupole temperature was at 150 ºC. The MS ion trap temperature was 250 ºC and the MS ion trap temperature was 230 ºC.

In both instruments, chromatographic separation was performed on an HP-5MS silica capillary column (J&W Scientific, Agilent Technologies, USA), 30m×0.25mm I.D. (5% phenyl-/95% methylpolysiloxane). The carrier gas (helium, 99.995% purity) flow was kept at 1.0 ml/min. The chromatographic oven was kept at 50 ºC for 2 min, then from 50 ºC to 190ºC at 5ºC/min, 20 min at 190 ºC, from 190 ºC to 280 ºC at 5ºC/min, and 280 ºC for 15 min. Mass spectra were recorded both in total ion chromatogram (TIC) mode (*m*/*z* 50–650) and selected ion monitoring (SIM) mode (*m*/*z* 249 and 319 for xylose and arabinose; *m*/*z* 249 and 333 for ramnose and fucose; *m*/*z* 135 and 305 for galacturonic and glucuronic acids; *m*/*z* 307, 319 and 331 for glucose, mannose, and galactose; *m*/*z* 319 for mannitol).

A HP-19091G-B233 chiral column (J&W Scientific, Agilent Technologies, USA), 30m×0.25mm I.D. (20% Permethylater B-Cyclodextrin) was also used for chromatographic separation in the 6890N GC System Gas Chromatograph (Agilent Technologies, Palo Alto, CA, USA).

Drying of samples proceed with a RC10-22 speed vacuum system with a refrigerated trap RCT 90 from Thermo Electron Corporation (St. Herblain, France).

A Solarbox 1500e RH (Erichsen, Milano, Italy) with a solar filter 280 nm was used for the ageing of the reference paint layers.

4.2.6. Analytical Procedure

Figure 4.2. reports the whole analytical procedure is schematised, followed by the description of the single steps:

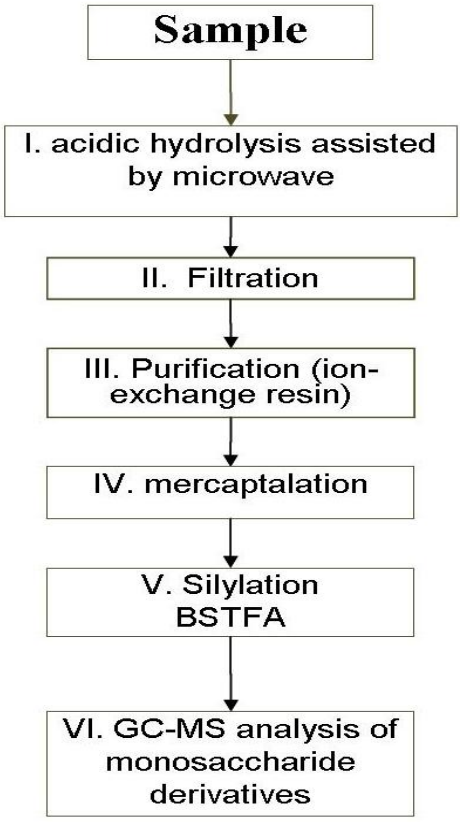

Figure 4.2. Scheme of the analytical procedure.

I) A weighed amount of the sample was admixed with 0.5 ml of trifluoroacetic acid 2M in PTFE closed conic vials, and subjected to microwave assisted acid hydrolysis. Hydrolysis conditions were as follows : power 500 W, temperature 120 °C, duration 20 min.

II) After hydrolysis, the sample was filtered with a PTFE membrane filter and then dried in the rotatory evaporator.

III) Once reconstituted in 100 µl of bidistilled water, the freed sugars are purified on a Zeolit DMF double-exchange resin, packed on a 0.5 cm diameter glass column. Sugars were eluted with 2 ml of bidistilled water. This way cations and anions are retained in the staionary phase.

IV) An aliquot of the solution containing monosaccharides and uronic acids was added with the derivatisation internal standard solution, evaporated to dryness in the rotary evaporator and subjected to mercaptalation. Admixing 25 µl of ethanethiol/trifluoroacetic acid (2/1,v/v), and keeping at room

temperature for 10 min with sporadic shaken, the corresponding diethyldithioacetals and diethyl dithioacetal lactones are formed.

V) The mercaptalation mixture is then subjected to silylation reaction prior to GC/MS analysis. The silylation is performed in two steps. In the first step, 100 µl of BSTFA are added to the mercaptalation mixture and the mixture is kept 15 minutes at 60ºC. This way, the mercaptalation reaction is interrupted, avoiding the formation of unwanted products from mercaptalation. Drying under nitrogen flow, the derivatised TFA and ethanthiol are easily eliminated. In the second step 50 µl BSTFA (1% TMCS) as derivatising agent and 100 µl pyridine as solvent were added and kept at 60ºC for 45 min to complitely sylilate the mercaptal derivatives of the parental sugars.

VI) The reaction mixture was then dried under nitrogen flow and redissolved in 50 µl of hexane: 2 µl of this solution, containing diethyl-dithioacetal trimethylsilyl derivatives of the parental sugars, were thus injected into the gas chromatograph.

Laboratory blanks were run to determine the detection limit (LOD) and the quantitation limit (LOQ) of the analytical procedure. At a statistical significance level of 0.05, the LOD and LOQ obtained for each sugar are reported in Table 4.11. Results highlighted the low levels of contamination of almost every sugar but glucose.

Table 4.11. Detection and quantitation limits for pentoses, hexoses, methyl hexoses and uronic acids.

Sugar	*Detection limit/µg*	*Quantitation limit/µg*
Arabinose	0.07	0.17
Xylose	0.02	0.04
Rhamnose	0.00	0.00
Fucose	0.00	0.00
Galacturonic acid	0.00	0.00
Glucuronic acid	0.00	0.00
Glucose	0.20	0.42
Mannose	0.01	0.02
Galactose	0.01	0.02

Retention times and mass spectra were established for the trimethylsilyl diethyl dithioacetals of monosaccharides and TMS diethyl dithioacetals lactone of the uronic acids. Some ketoses (fructose, myoinositol, tagatose, psicose) were also analysed[v]. Results are presented in table 4.12.

Table 4.12. Retention times for trimethylsilylated diethyldithioacetals of the monosaccharides analysed.

Sugar	*Derivative Formula ([vi])*	*Rt (min) ([vii])*	*RMM ([viii])*
Mannitol	$C_{24}H_{62}O_6Si_6$		614
Psicose	n.d.	33.828 (1.7)	-
	n.d.	35.019 (1)	
Fructose	n.d.	33.176 (1)	-
	n.d.	34.113 (3.3)	
	n.d.	35.050 (3)	
	n.d.	41.652 (1.8)	
	n.d.	49.709 (1.7)	
Tagatose	n.d.	33.227 (1)	-
	n.d.	34.145 (8)	
	n.d.	36.902 (1)	
Deoxyribose	$C_{18}H_{44}O_3S_2Si_3$	34.286	456
Ribose	$C_{21}H_{52}O_4S_2Si_4$	39.415	544
Xylose	$C_{21}H_{52}O_4S_2Si_4$	39.428	544
Arabinose	$C_{21}H_{52}O_4S_2Si_4$	39.547	544
Myoinositol	n.d.	34.561(1)	-
	n.d.	35.925 (1)	
	n.d.	39.760 (8500)	
Ramnose	$C_{22}H_{54}O_4S_2Si_4$	43.168	558
Fucose	$C_{22}H_{54}O_4S_2Si_4$	44.725	558
Galacturonic acid	$C_{19}H_{42}O_5S_2Si_3$	50.707	498
Glucuronic acid	$C_{19}H_{42}O_5S_2Si_3$	53.012	498

[v] several chromatographic peaks are obtained when analysing ketoses which do not correspond to the silylated sugars. It is known that dialkyl dithioacetals of ketoses are not obtained directly from the parent sugar but ketoses undergo decomposition reactions during mercaptalation [69].

[vi] n.d. not determined (ketose)

[vii] Rt = retention time (relative intensity of the peaks are in parentheses for ketose)

[viii] RMM = relative molecular mass

Acido Lactone	$C_{19}H_{42}O_5S_2Si_3$	53.143	498
Glucose	$C_{25}H_{62}O_5S_2Si_5$	54.117	646
Mannose	$C_{25}H_{62}O_5S_2Si_5$	54.379	646
Galactose	$C_{25}H_{62}O_5S_2Si_5$	55.437	646
Allose	$C_{25}H_{62}O_5S_2Si_5$	54.177 (1)	646

4.3. Results and Discussion

4.3.1. Optimisation of the analytical procedure

4.3.1.1. Clean-up-step

When analysing samples from paintings by GC/MS, a clean up procedure prior to chromatographic analysis is necessary to suppress interferences due to inorganic components [60]. In the analytical procedure previously published, a cation-exchange resin was used to suppress interferences from cations[(ix)] [1,23]. Actually, the analyses of samples with a high content of sulphates and silicates (data not shown) presented derivatisation problems evidenced by very low intensity chromatographic peaks of all sugars including mannitol (internal standard of derivatisation), highlighting that anions can interfere as well. Thus, the use of a double exchange resin has been introduced to eliminate simultaneously both cations and anions from the solution containing the sugars freed from the hydrolysis step.

4.3.1.2. Derivatisation procedure

The derivatisation procedure previously published [1] can be summarised as follows: 25 µl of a mixture 2:1 ETSH:TFA were added to the dried sample; after 20 minutes, 80 µl of BSTFA and 50 µl of pyridine were added; after 45 minutes the solution was dried under nitrogen flow, redissolved in hexane and injected into the GC/MS. Although the

[ix] A cation exchange OMIX monolithic sorbent tip SCX (Strong cation exchange) that offers a simple and efficient solution for the removal of detergents and salts, used in the proteomics field, was tested. Though the tips demonstrated their ability to separate cations from the saccharide material, their capacity was not enough to purify mural painting samples with their high inorganic content.

procedure demonstrated its suitability to avoid the formation of more than one peak for analyte when aldoses and uronic acids are analysed, drying the mixture prior GC injection could be problematic. In fact the drying itself would take long time (30-45 minutes), in some cases precipitates would be observed or the solution would not dry at all. In these last cases the derivatisation could, occasionally be ineffective, leading to irreversible contaminations of the chromatographic system. A possible explanation could be the formation of pyridine trifluoroacetate (PyTFA) in the reaction mixture. To find out if the formation of PyTFA takes place, FTIR spectrum of a mixture of 8 µl of TFA with 50 µl pyridine (ratio correspondent with the derivatisation mixture) was recorded. It presented all characteristic bands of pyridine (600, 705, 740, 990, 1025, 1070, 1145, 1215, 1435, 1480, 1580, 1600, 1875, 1923, 1995, 3010, 3035, 3060, 3085 and 3150 cm^{-1}) plus some bands non correspondent to the pyridine nor to the TFA spectra (580, 675, 780, 1120, 1200, 1250 sh, 1840, 3650 cm^{-1}). These bands are in agreement with the reference spectra for pyridine trifluoroacetate (1680, 1645, 1560, 1490, 1460, 1420, 1384, 1260, 1195, 1180, 1070, 1040, 990, 950, 840, 802, 760, 722, 683, 604 cm^{-1}). Moreover, drying this mixture under nitrogen flow (30 minutes) produces a white solid. The FTIR spectrum of this solid presented all the chraracteristic peaks of pyridine trifluoroacetate confirming that the formation of this compound during the reaction occurs. Finally, also in the case of the complete reagents mixture (that is 25 µl EtSH:TFA (2:1), 50 µl pyridine, 80 µl BSTFA) the peaks characteristic of pyridine trifluoroacetate were identified in the FTIR spectra. Figure 4.3. shows the FTIR spectra obtained from the mixtures cited above.

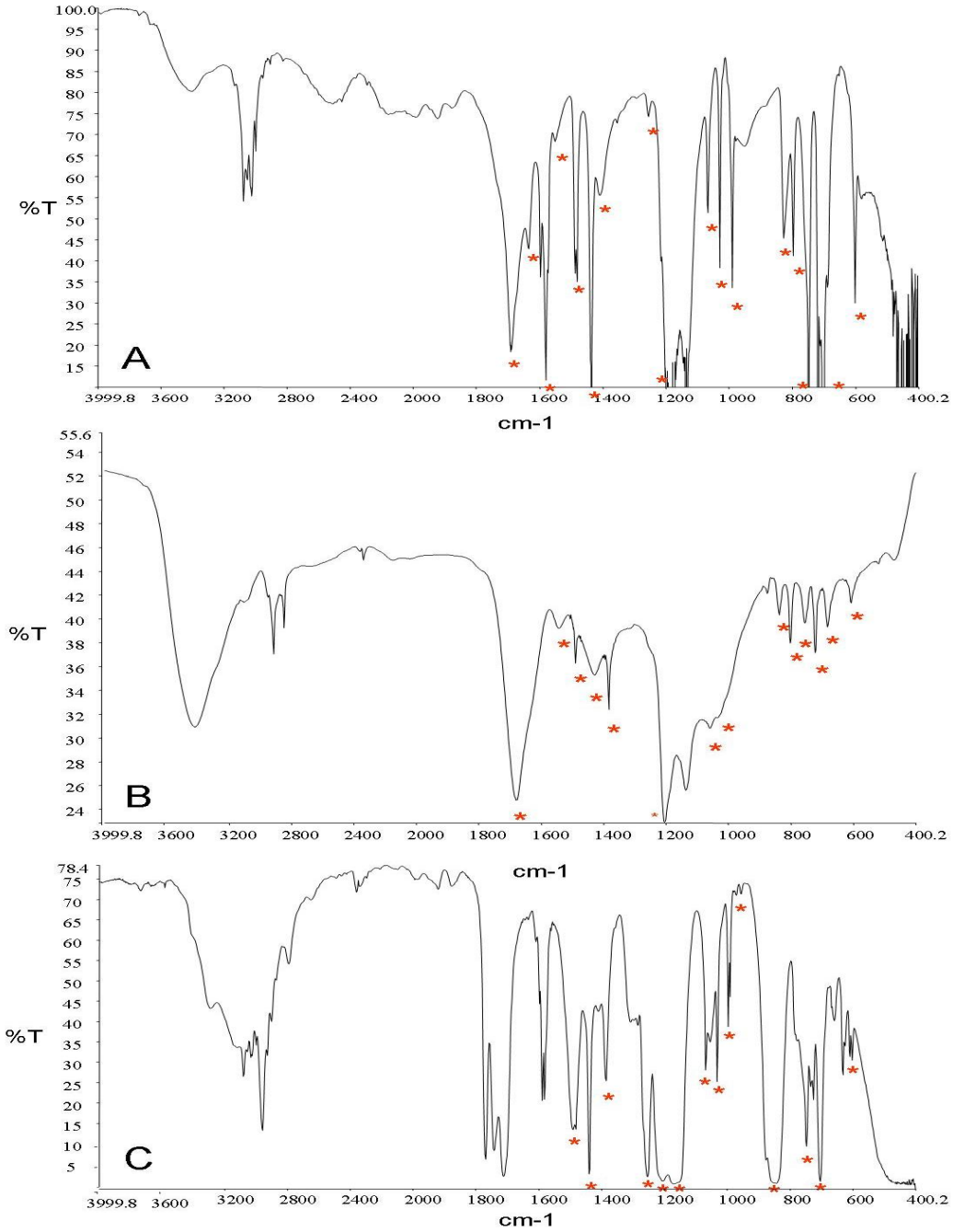

Figure 4.3. Spectra obtained for (A) mixture of pyridine and TFA acid; (B) solid after drying the mixture pyridine-TFA; (C) mixture of pyridine, TFA and BSTFA. (*) indicate the characteristic bands of pyridine trifluoroacetate.

The occurrence of pyridine trifluoroacetate in the final reaction mixture can explain the difficulties observed in the drying processes, and the chromatographic problems arising when the solution was injected into the GC. In fact, the temperature, the drying speed and the sample composition could all influence the equilibrium (pyridine + TFA↔ pyridine trifluoroacetate). As a result, when drying, the removal of pyridine and TFA from the reaction mixture could not be enough to assure the displacement of the equilibrium to the left and thus the formation of TFA and pyridine from the pyridine trifluoroacetate. The occurrence of the salt in the mixture is therefore responsible of the incomplete reaction yields in the subsequent silylation step.

However, as reported in the literature, pyridine is fundamental to assure the completeness of the silylation reaction [1,67, 68]. The role of pyridine was tested. An average relative standard deviation of the sugar peak areas of 9% was obtained when pyridine was used, versus 20% when pyridine was not used. Therefore, TFA and ETSH must be removed from the reaction mixture prior to the addition of pyridin, to avoid the co-existance of TFA and pyridine in the reaction mixture. As a result, a derivatisation in three steps was proposed. The best mercaptalation yields are obtained after short reaction times at room temperature [69]: in fact, after 20 minutes, secondary products of the mercaptalation of sugars, such as glycosides, can be formed [64]. By adding BSTFA to the mercaptalation mixture after 20 minutes, the mercaptalation reaction is suddenly stopped, and TFA and ETSH are derivatised (15 minutes at 60°C). This way, TFA-trimetylsilyl ester and ETSH trimetylsilyl ether are easily eliminated by drying under nitrogen flow the reaction mixture. To assure the complete sylilation of the mercaptal derivatives of the parental sugars another silylation step using pyridine as solvent is thus proposed.

Using a mixture of BSTFA/Py > 1 [1] shows that only aldo pentoses (xilose and arabinose) generate just one peak, while chromatograms of methyl hexoses, hexoses and uronic acids presented from 2 to 5 peaks being the main peaks correspondent to the trimethylsylilated diethyl dithioacetal of the parental sugar and the others unidentified.

To understand the nature of the unidentified compounds and thus to understand if the mercaptalation or the silylation steps were showing low reaction yelds, different strategies were tried:

- Longer mercaptalation times (40 minutes) shoed the formation of the same unwanted products.
- Shorter mercaptalation times (10 minutes) were not giving better reaction yields nor reproducibilities (RSD < 10% in both cases) and secondary chromatographic peaks were also present. Therefore, 10 minutes for the mercaptalation was the reaction time adopted in order to shorten derivatisation time. In figure 4.4. a chromatogram of a standard solution mercaptalated 10 and 20 minutes is reported for comparison.
- peaks corresponding to the trimethylsilylated derivatives of the parental sugars were never observed. This indicates that the mercaptalation reaction is efficient and quantitative. Figure 4.5. and figure 4.6. show the chromatogram obtained for a deoxy hexose (fucose) and an uronic acid (glucuronic acid) both mercaptalted and after silylation and silylated only. It can be observed that the peaks corresponding to unidentified compounds are not corresponding to the persilylated derivatives of the parental sugar.

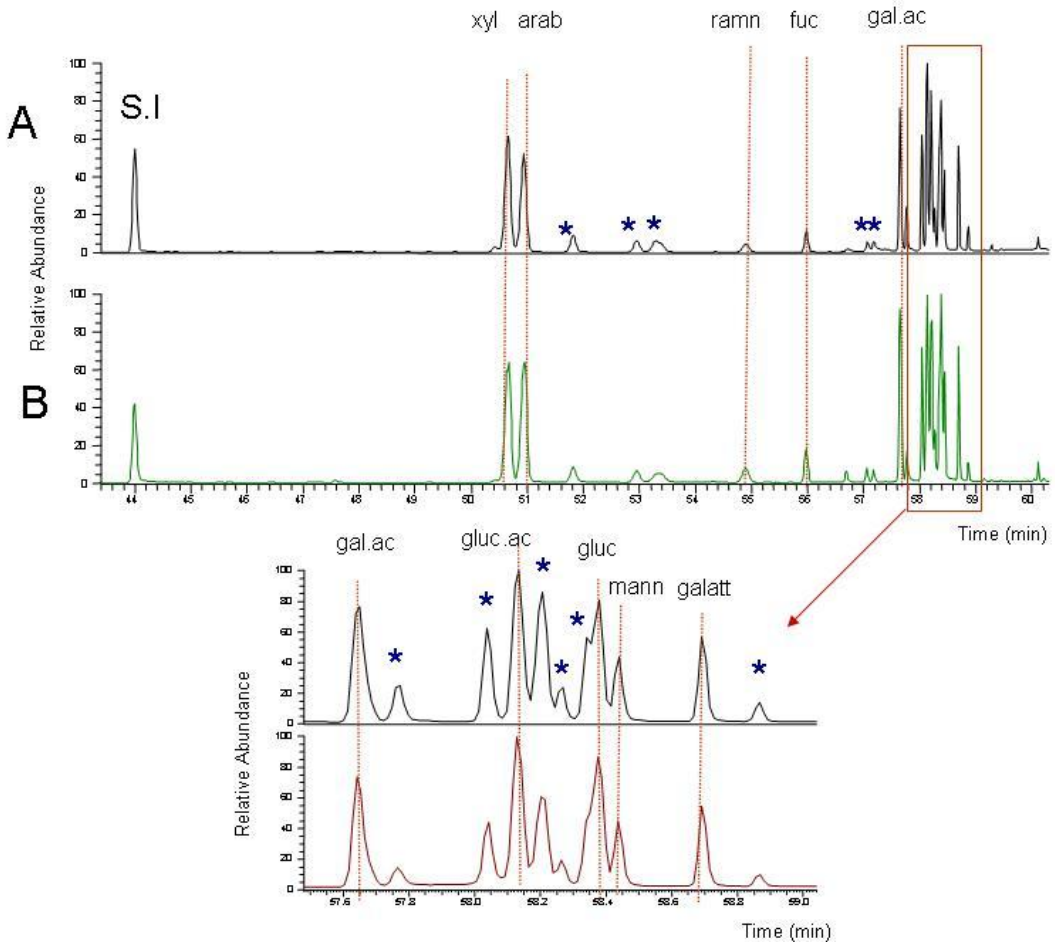

Figure 4.4. Chromatogram of a solution standard of the 9 monosacharides present in plant gums. Main peaks correspond to TMS diethyl dithioacetal of the parental sugars while peaks indicated with * correspond to the products generated due to derivatisation problems. A) 20 minutes of mercaptalation, B) 10 minutes mercaptaltion. Silylation conditions in both cases were as follows: 45 min 60 oC 100 ul BSTFA 50 ul Pyridine.S.I. corresponds to internal standard (mannitol).

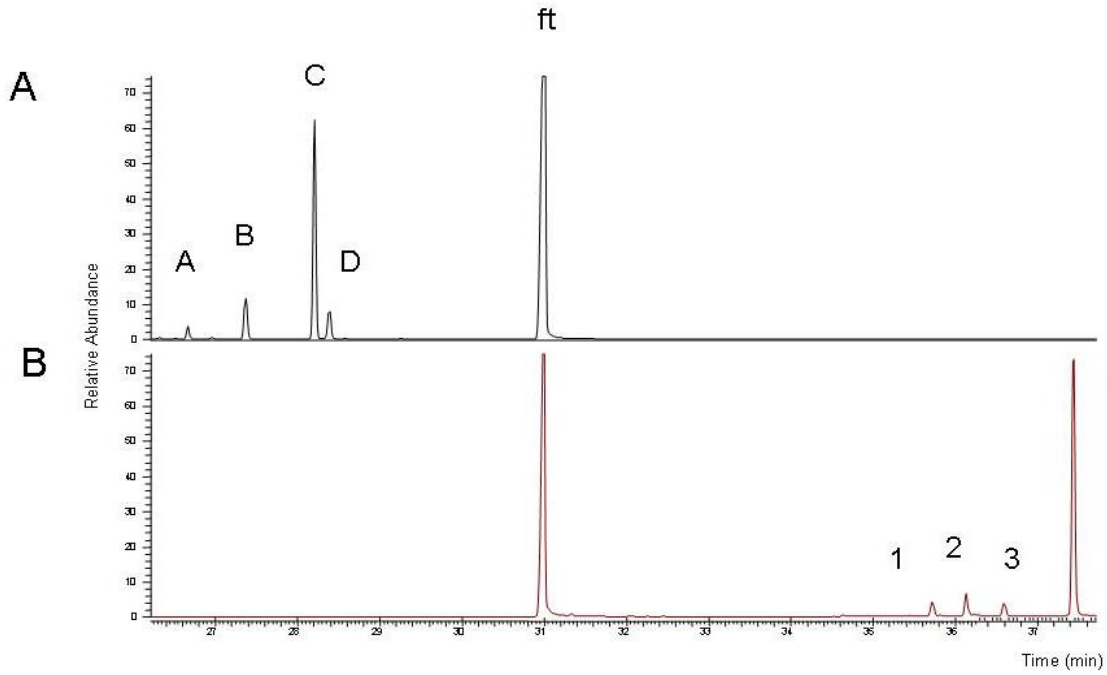

Figure 4.5. Fucose (deoxy hexose) derivatised by (A) persilylation; (B) mercaptalation and silylation. From the silylation 4 peaks corresponding to the 4 forms of the sugar in equilibrium in solution can be observed (peaks A-D). From the mercaptalation followed by silylation, the main peaks corresponding to the trimethylsylilated diethyl dithioacetal of fucose are identifiable. Peak A-D and 1-3 are not correspondant thaus mercaptalation is taking place properly. Silylation conditions in both cases were as follows: 45 min 60 °C 100 µl BSTFA 50 µl Pyridine.

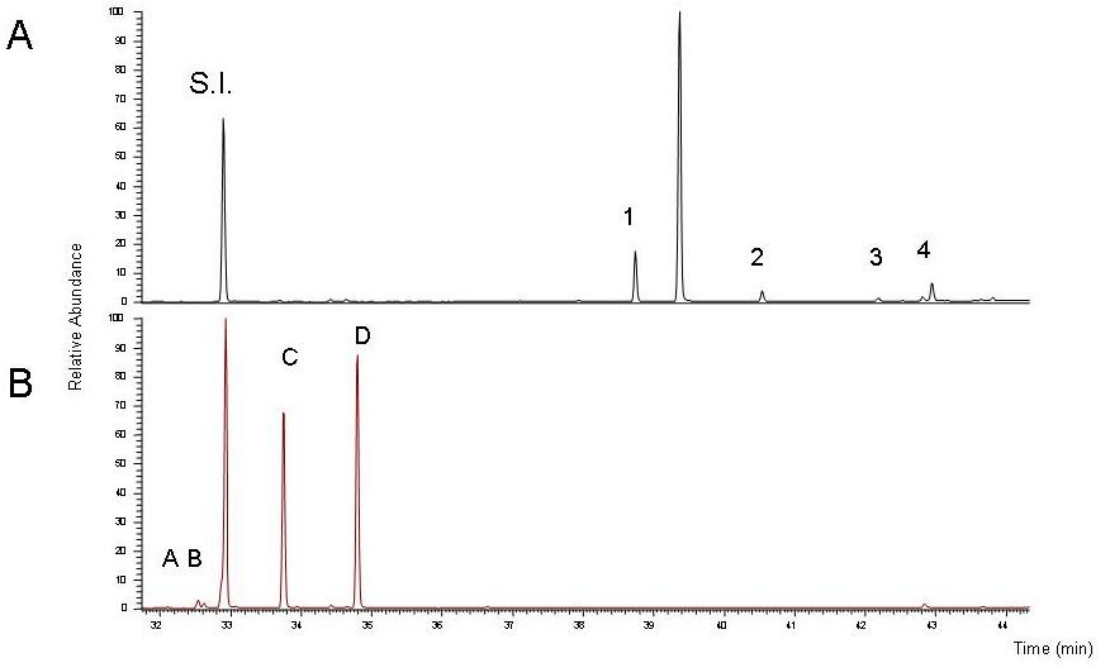

Figure 4.6. Glucuronic acid derivatised by (A) mercaptalation and silylation; (B) silylation only. From the silylation four peaks corresponding to the four forms of the sugar in equilibrium in solution can be observed (peaks A-D). From mercaptalation and silylation it is identifiable the main peak corresponding to the trimethylsylilated diethyl dithioacetal lactone of glucuronic acid and three peaks (1-4) corresponding to the Dithyl diethiocetal of fucose non trimethylsylilated properly. Silylation conditions in both cases were as follows: 45 min 60 °C 100 µl BSTFA 50 µl Pyridine.

Results showed that the silylation of mercaptalated sugars is the step to be improved. Conditions of silylation were modified as follows:

- Modification of the temperature (70 ºC) and time (30 and 60 minutes) did not produce any improvement
- The ratio between BSTFA and pyridine (BSTFA : pyridine) was modified from 2:1 to 5:1, 3:1 and 1:1 not improving results.

- by using 100 µl pyridine with 50 µl BSTFA (2:1) and 1% TMCS [(x)]as catalyst just one peak is present in the chromatogram of all pentoses, hexoses and methyl hexoses. Chromatograms of the uronic acids still present some smaller peaks of the above mentioned unidentified compounds, but in this case the ratio uronic acid : derivatisation by-products is ≥10.

The procedure was modified accordingly. Figures 4.7. and 4.8. show different chromatograms obtained after the modification of the second silylation step for fucose and glucuronic acid.

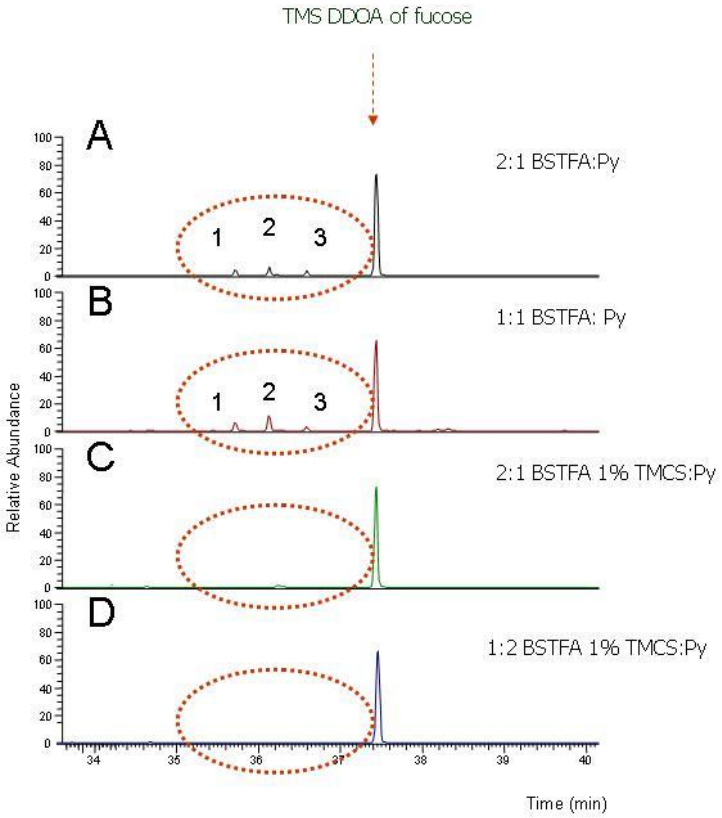

Figure 4.7. Chromatograms obtained by modification of the conditions of the second step of silylation for fucose (45 minuts 60 ºC). (A) 100 µl BSTFA and 50 µl Pyridine (2:1), (B) 50 µl BSTFA, 50 µl Pyridine (1:1); (C) 100 µl BSTFA 1 % TMCS, 50 µl Pyridine, (D) 50 µl BSTFA 1% TMCS), 100 µl Pyridine. Last conditions were adopted as giving better results. In all cases 20 minutes of mercaptalation, 15 minutes of a first silylation step at 60 ºC with 100 µl BSTFA were performed.

[x] The use of 1% TMCS acting as catalysts is reported in the literature as improving the silylation yields [67, 68].

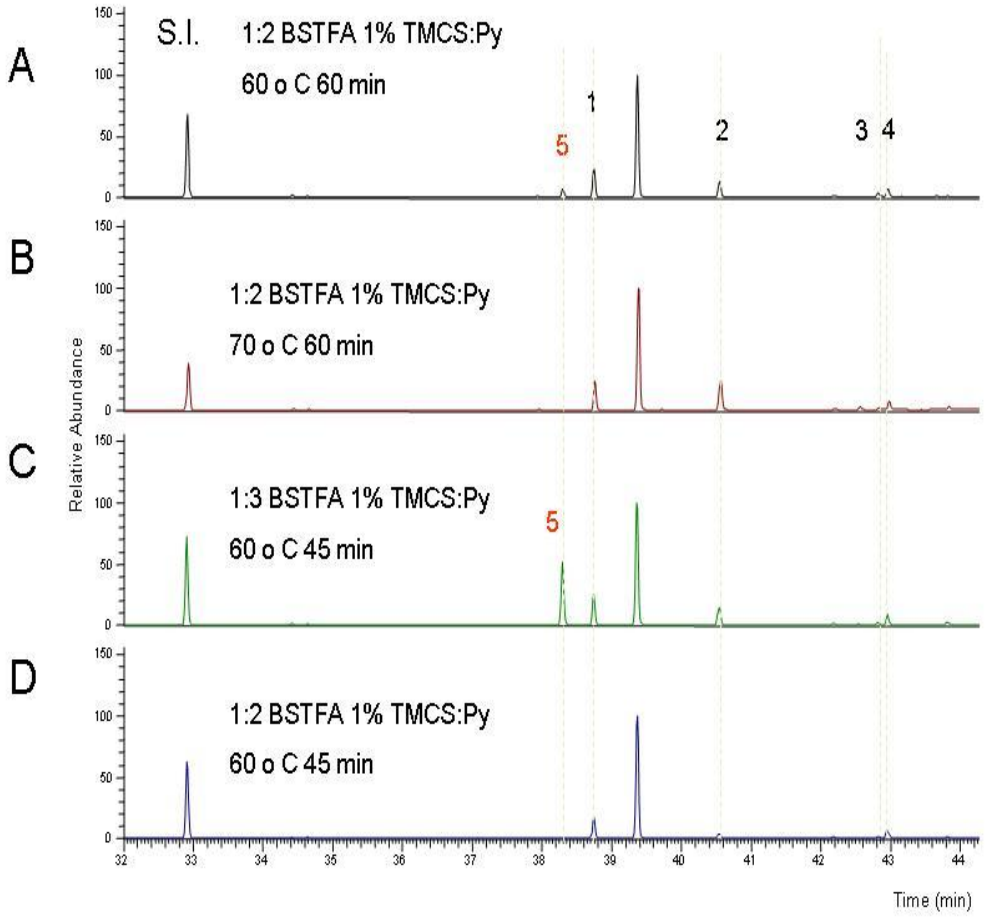

Figure 4.8. Chromatograms obtained by modification of the conditions of the second step of silylation for glucuronic acid. (A) time 1 hour 60 ºC (1:2 BSTFA 1%TMCS: Pyridine); B) Temperature 70 ºC (1:2 BSTFA 1%TMCS: Pyridine); (C) 1:3 BSTFA 1%TMCS: Pyridine (60 ºC, 45 min); (D) 50 µl BSTFA 1% TMCS), 100 µl Pyridine. Last conditions were adopted as being better results and being conicident with the better conditions established for the monosaccharides. In all cases 20 minuts mercaptalation, 15 minutes of a first step silylation at 60 ºC with 100 µl BSTFA were performed. The numbers indicate the peaks formed due to uncomplete silylation of the mercaptalated derivative of the parental sugar.

The reproducibility of the derivatisation procedure was tested analysing five replicates of a sugar standard solution. A RSD < 10% was observed for each sugar. Calibration curves for aldoses and uronic acids were performed obtaining a linear response in the range 0.1 to 2 µg/g (R^2 >0.99).

To evaluate the stability of the derivatised solutions, a sugar standard solution was derivatised and injected repeatedly and stored at -18°C in the between. A RSD lower than 14% was obtained for the first 270 minutes.

The lifetime of the hydrolysed solution obtained for arabic, tragacanth and fruit tree gum was established. The glycosidic composition of the gums is maintained for 150 hours with a deviation standard lower than 13 % for the three gums tested.

In Figure 4.9 the chromatogram of a standard solution of the seven monosaccharides and the two uronic acids (concentration 100 ppm) is reported, showing only one peak for each sugar.

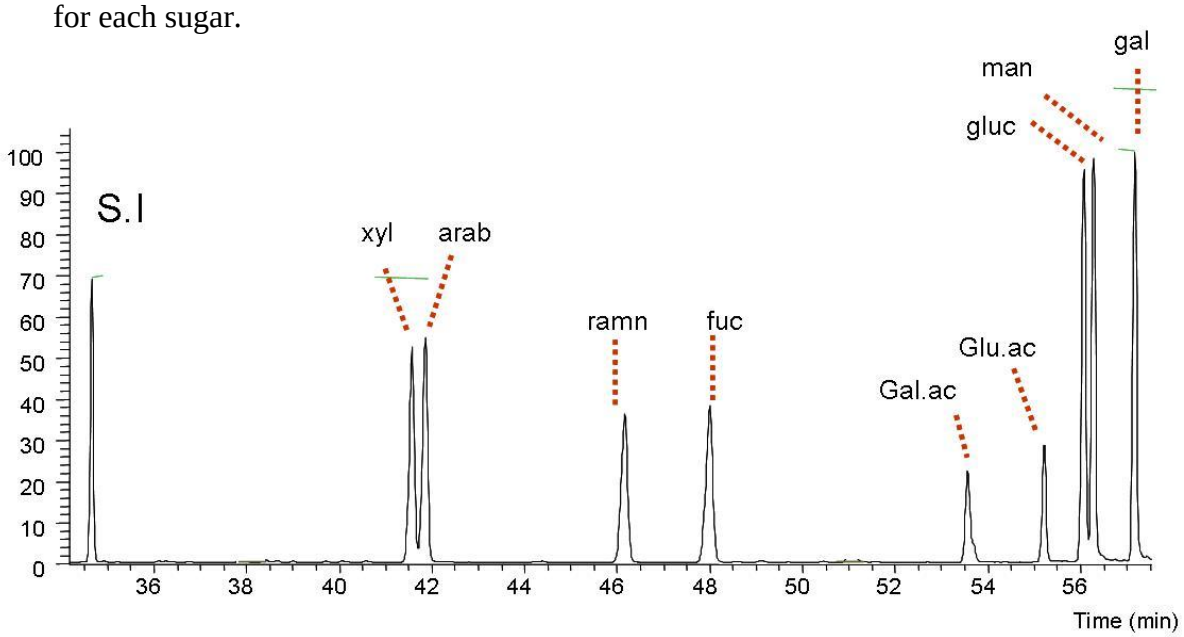

Figure 4.9. Chromatogram of the standard solution of TMS mercaptal derivatives of the nine sugars[xi].

The procedure described, is not the best suited for the analysis of the ketoses. In fact, several chromatographic peaks are obtained when analysing ketoses which do not correspond to the persilylated sugars. It is in fact known from the literature that dialkyl dithioacetals of ketose are not obtained directly from the parent sugar but ketoses undergo decomposition reactions during mercaptalation [69]. Figure 4.10. presents the chromatogram of fructose (ketohexose) both mercapatalated and silylated and silylated only.

[xi] S.I. internal standard (mannitol)

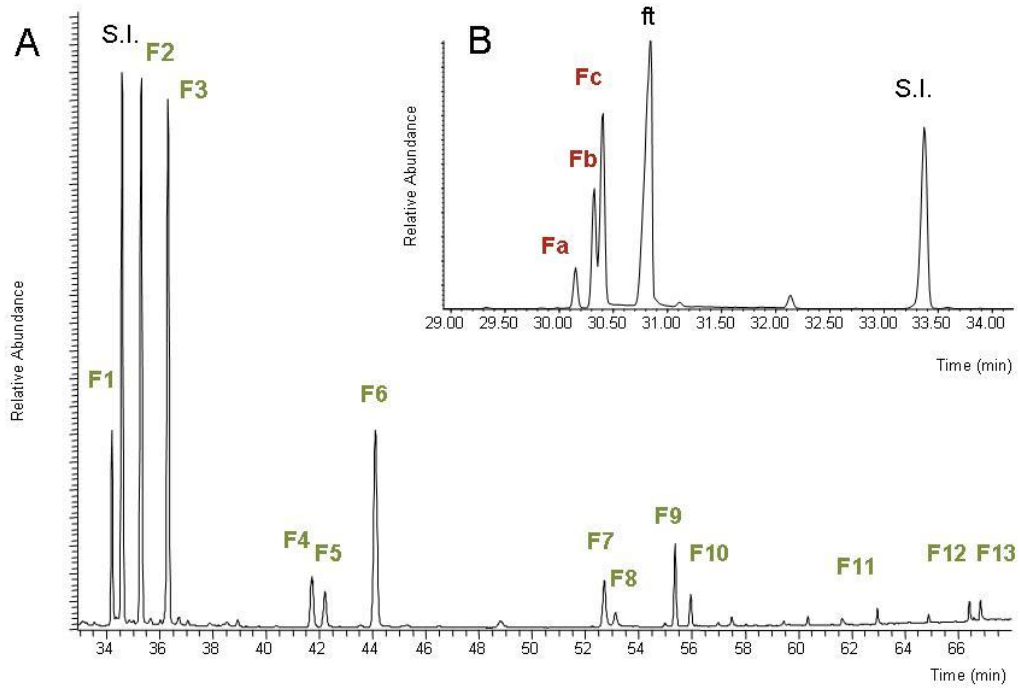

Figure 4.9. (A) fructose mercaptalated and silylated and (B) fructose sylilated only. In both cases more than one peak is generated.

4.3.2. Reference materials and painting samples

4.3.2.1. Reference raw materials

The overall procedure was checked by analysing three sample replicates of the available raw plant gums, gum solutions and reference painting layers. Other materials used as binding media in works of art were analysed to widen our knowledge on their polysaccharide content and glycoside profile: honey, propolis, pine and mastice resins, beeswax, oliban, myrrh, animal glue, casein and egg were analysed. Their glycosidic

profiles and percentage content of polysaccharidic material[xii] are reported in Table 4.13.

Table 4.13. Average relative percentage sugar composition of the raw materials

material	*description*	*Sugars*										*Glyc mat %*
		Xyl	Arab	Ramn	Fuc	Gal Ac..	Gluc. Ac.	Gluc	Mann	Galact	Fructose [xiii]	
GA st [xiv]	sigma	0.0	25.6	13.2	0.0	0.0	11.7	0.0	0.0	49.1	0.0	65
GA sol.	Sigma	0.0	26.6	11.1	0.0	0.0	12.1	0.0	0.0	48.4	0.0	70
GA raw	sigma	0.0	25.6	13.2	0.0	0.0	11.7	0.0	0.0	49.1	0.0	90
TG st	sigma	21.3	36.4	2.1	7.2	12.8	0.5	11.4	0	10.2	0.0	23
TG sol.	sigma	18.6	33.7	2.1	7.6	12.8	0.7	11.6	0.0	12.8	0.0	62
TG raw	sigma	19.4	30.9	2.1	5.9	16.7	0.8	11.8	0.0	12.2	0.0	50
Ft st	cherry	7.0	48.7	2.1	0.0	0.0	5.9	0.0	1.8	34.4	0.0	62
Ft sol.	cherry	10.0	44.1	2.3	0.0	0.0	5.7	0.0	2.5	34.3	0.0	45
Ft raw	cherry	5.2	35.0	1.6	0.0	0.0	3.5	0.0	2.3	52.0	0.0	95
LB sol	sigma	0.0	0.0	0.0	0.0	0.0	0.0	0.0	79.5	20.5	0.0	87
LB raw	sigma	0.0	0.0	0.0	0.0	0.0	0.0	0.0	62.4	37.6	0.0	30
Egg		0.0	0.0	0.0	0.0	0.0	0.0	0.0	83.2	16.8	0.0	0.79
Animal glue		0.0	0.0	0.0	0.0	0.0	0.0	35.6	0.0	64.4	0.0	0.14
milk		0.0	0.0	0.0	0.0	0.0	0.0	39.1	0.0	60.9	0.0	12.46
beeswax		0.0	0.0	0.0	0.0	0.0	0.0	100	0.0	0.0	0.0	0.02
Propolis		9.0	15.5	13.3	0.0	0.0	1.0	39.0	13.2	7.6	0.8	1.8
Honey [xv]	Acacia	0.0	0.0	0.0	0.0	0.0	0.0	95.6	0.0	0.0	4.4	20
	Milefiori	0.0	0.0	0.0	0.0	0.0	0.0	95.8	0.0	0.0	4.1	18
	chesnut	0.0	0.0	0.0	0.0	0.0	0.0	95.0	0.0	0.0	5.0	18
mastice		0.0	51.1	2.1	1.3	0.0	2.3	0.0	3.3	39.9	0.0	0.7
myrrh		2.8	43.4	1.4	1.4	0.0	2.3	0.0	3.8	46.3	0.0	7
oliban	Oman	0.0	21.3	8.5	0.4	0.0	6.2	0.0	1.0	62.3	0.0	5.34
	somalia	0.0	23.0	0.5	1.0	0.0	2.7	0.0	1.2	71.5	0.0	11.75
Luohanguo	china	0.0	0.0	0.0	0.0	0.0	0.0	100	0.0	0.0	0.0	n.d. [xvi]

[xii] % content of glycoside material is the percentage of glycoside material calcolated as the sum of the content determined for each sugar with respect to the weighted amount of raw material analysed

[xiii] Fructose % calculated on the base of peak at Rt 34.113 in table 3

[xiv] st= reference paint layer; sol = solution; raw= raw material.

[xv] Glucose peak area is 30 times bigger than fructose peak area for the three types of honey. The percentage of saccharide material in ancient painting samples would not allow to determine fructose presence.

[xvi] not determined (solution of unknown concentration).

%RSD calculated for the solution, painting layer and grinded raw material of each gum for all sugars but galactose is less than 20 % for arabic gum and fruit tree gum and 12% for tragacanth gum. Only galactose presents higher RSD (40%) for fruit tree and locust bean gums. This indicates that working with solutions or reference painting layers is almost indistinctive in terms of sugar percentage sugar content. It also highlights that the amount of glycoside material that can be encountered in a painting is strongly dependent on the nature of the sample, and the way the painter has processed the gum for the preparation of the binder (solution followed by decantation or direct grinding of the raw material with the pigment).

Data in the table highlight that several materials, which are not saccharide binders, such as milk or oliban, have a considerable saccharide content. Therefore, the detection of sugars in a painting sample could be ascribable to different kind of binders, not necessarily plant gums, and a mixture of organic materials can lead to chromatograms difficult to be interpreted when the organic material composition

4.3.2.2. Data Interpretation/Identification of gums

Each of the gums studied showed a very specific sugar composition. It is quite easy to identify each one in a sample of unknown composition, with the aid of a decisional scheme such as the one reported in literature [1] when only one plant gum is present. The propose decisional scheme for the identification of arabic, tragacanth, fruit tree, karaya, locust bean and guar gum is reported in Figure 4.11.

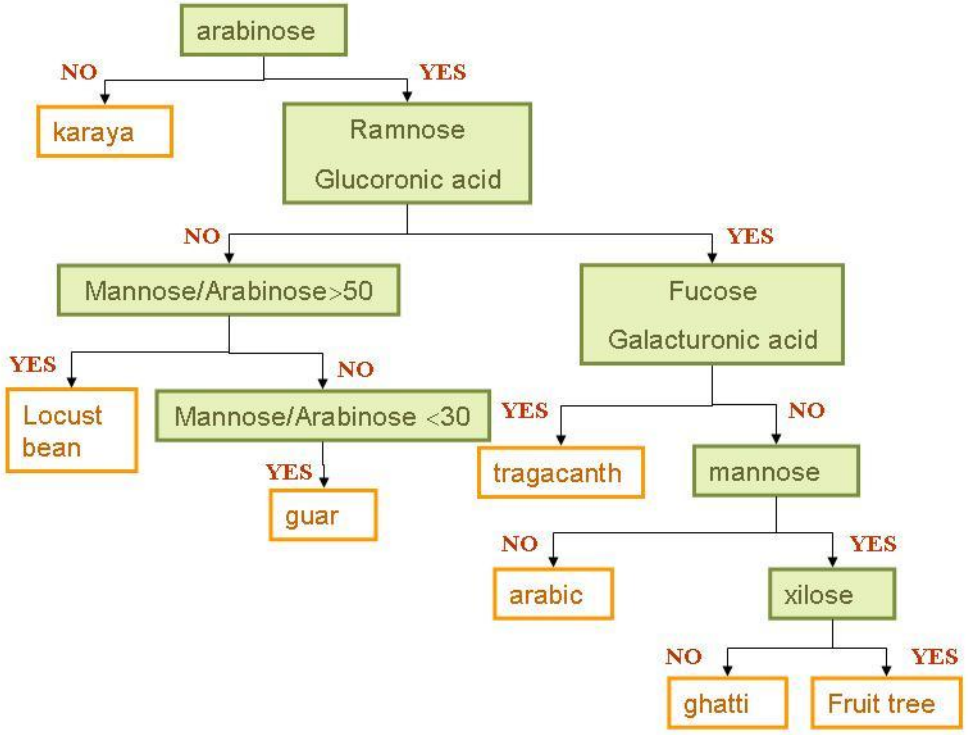

Figure 4.11. Decisional scheme for the identification of agum(arabic, tragacanth, fruit tree, ghatti, karaya, locust bean and guar) on the basis of its sugar composition.

Glucose was excluded from the scheme, since it could have arisen from several external sources that may have contaminated the sample: it would thus be impossible to correctly identify the source of the gum. In fact, glucose is one of the products of photosynthesis in plants and some prokaryotes, in addition to being present in animals and fungi (resulting from the breakdown of glycogen) and in plants (starch and cellulose). However, it is also the main component in honey, as reported in Table 4.13.

4.3.3. Ancient painting samples

Results of the analyses of samples from works-of-art are presented below grouped by origin. Their glycoside molecular profile is presented calculated both with and without glucose. Samples were summarised in Table 4.10.

4.3.3.1. Verdala Palace (Malta)

The glycoside profile of the sample is reported in Table 4.14. Figure 4.12. presents the chromatogram of sample VP 75. Peaks corresponding to several monosaccharides can be identified.

Table 4.14. Glycosidic profile of sample VP75.

Sample	*sugars*									*Sugar content /µg* (xvii)	*%sugar content (xii)*	*Result of the decisional scheme*
	Xyl	Arab	Ramn	Fuc	Gal Ac.	Gluc. Ac.	Gluc	Mann	Galact			
VP 75	7.9	58.8	2.5	0.0	0.0	5.6	4.5	1.7	19.0	9.52	0.8	Fruit tree
	8.3	62.5	2.7	0.0	0.0	6.0		0.8	19.8			

By using the decisional scheme, the absence of fucose and galacturonic acid together with the presence of mannose, fruit tree is identified as the gum present in the sample (arabinose/yes; ramnose and glucuronic acid/yes; fucose and galacturonic acid/no; mannose/yes; xylose/yes→fruit tree). However, the galactose relative content is lower than the reference fruit tree values reported in Table 4.13. Glucose is present in the sample indicating that another source for this sugar must be hypothesised.

[xvii] µg of polysaccharides material in the sample as the sum of the µg of each of the monosaccharides and uronic acids obtained from chromatographic peak areas by using the calibration curves.

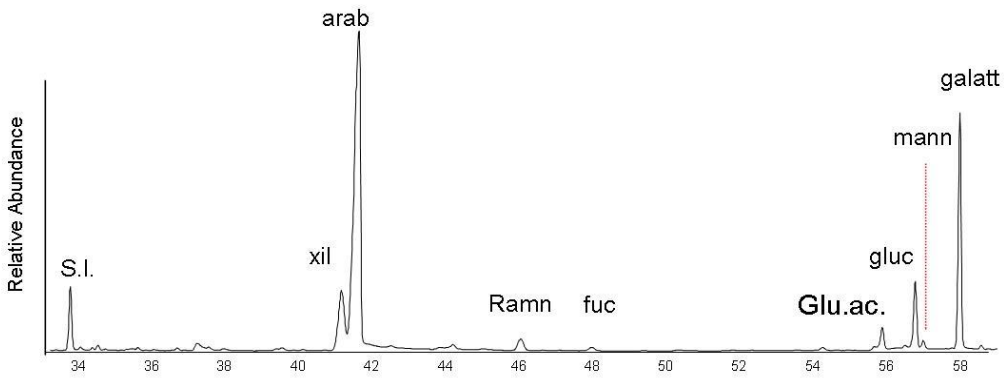

Figure 4.12. Chromatogram of sample VP75.

4.3.3.2. Camposanto Monumentale di Pisa (Italy)

Cchromatogram is shown in Figure 4.13 and data are presented in Table 4.15.

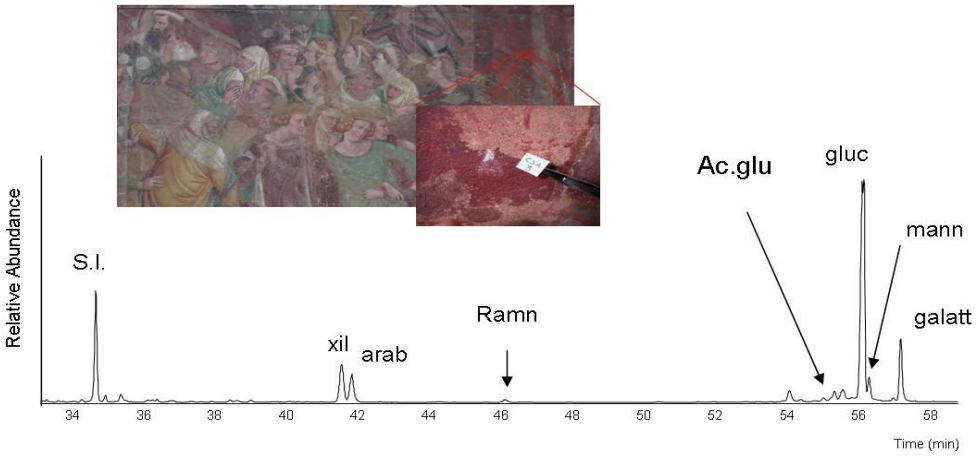

Figure 4.13. Chromatogram of sample Camp.

Table 4.15. Glycosidic profile of sample Camp.

Sample	*sugars*									*Sugar content /µg*	*%sugar content*	*Decisional scheme*
	Xyl	Arab	Ramn	Fuc	Gal Ac.	Gluc. Ac.	Gluc	Mann	Galact			
Camp	12.2	8.7	2.2	0.0	0.0	1.5	56.2	7.0	12.4	2.7	0.5	Fruit tree
	27.9	19.9	5.0	0.0	0.0	2.9	-	15.9	8.4			

In this case, by using the decisional scheme the presence of mannose, glucuronic acid and ramnose and the absence of galacturonic acid and fucose also suggests the presence of a fruit tree gum (arabinose/yes; ramnose and glucuronic acid/yes; fucose and galacturonic acid/no; mannose/yes; xylose/yes→fruit tree). However, the glycosidic profile is not correspondent with characteristic values of a fruit tree gum mainly due to the fact that the xylose relative amount is higher than that of arabinose (xyl/arab >1). It has to be noticed that all reference plant gums studied present a xylose/ arabinose ratio lower than 1 though this inversion phenomenum has been already noticed in ancient sample [1,8]. Moreover, glucuronic acid, mannose and galactose percentage content are different from the ones reported in Table 4.13.
A high content of glucose (56%) is highlighted. A source for glucose, such as starch or honey, must be hypothesized.

4.3.3.3. Mausoleum of Mitridate I (Turkmenistan)

In the case of the plaster samples from the Mausoleum of Mitridate I from Nisa prtica (Turkmenistan) just one of the four samples analysed presented a content of saccharide material at the blank level (sample met2pois). The other three samples presented a saccharidic content higher than the quantification limit. Glycoside profiles are presented in Table 4.16.

Table 4.16. Glycoside profiles of samples from Mausoleum Mitri.

Sample	*sugars*									*Sugar content /µg*	*%sugar content*	*Decisional scheme*
	Xyl	Arab	Ramn	Fuc	Gal Ac.	Gluc. Ac.	Gluc	Mann	Galact			
Met 2 rosso	23.5	21.9	6.7	1.4	1.5	6.7	21.5	9.9	6.9	2.11	0.013	-
	29.9	27.9	8.5	1.8	1.9	8.6		12.6	8.8			
Met 1 base	18.7	16.5	3.2	0.0	0.0	2.8	39.1	10.3	9.5	0.85	0.004	Fruit tree
	31.8	28.2	5.4	0.0	0.0	4.7		17.5	16.2			
Met 1 ros	20.6	14.9	3.0	1.5	2.1	5.2	37.1	8.4	7.2	3.01	0.018	-
	32.7	23.7	4.8	2.5	3.3	8.3		13.4	11.5			

Also in this case the saccharide profile of the three samples present all the monosaccharides in a percentage higher than 1 and glucose in a percentage ranging from 20 to 40. This can be interpreted as originated by a mixture of gums. However, sample Met 1 base profile without glucose would resemble that of a fruit tree (arabinose/yes; ramnose and glucuronic acid/yes; fucose and galacturonic acid/no; mannose/yes; xylose/yes→fruit tree). To note that also in these samples the xyl/arab ratio is similar to 1.

4.3.3.4. Palace of Nestor (Pylos, Greece)

The samples from palace of Nestor (Pylos) could be grouped in three different sets based on their glycoside content:

a) samples with a content of saccharide material at the blank level (samples 105.65-46, 158.16 NWS, 179.268 NWS, 007.15-1, 112.93-46, 006.02-1 all, Dr17 R 3/4 , Dr 201)
b) samples with a content of polysaccharide material between the quantification and detection limit (105.66-46, 179.122, p118, 026.13-5)
c) samples with a content of polysaccharide material superior to the quantification limit (105.65-46, 135.43-64, 004.5-1, 065.77-31, 083.07-43, 076.105, 006.04-1 prep, 080.09-43, 021.75-5, 075.105 prep1, 075.105 prep2).

The glycoside profiles of the samples are reported in Table 4.17. All samples but 105.65-46 and 021.75-5 present glucose in % from 30 to 70%. All samples with a sugar content between the DL and QL have a glucose level under the detection level but Dr 201. All samples presented mannose but P118.

Table 4.17. Glycoside profile of the samples from Pylos.

Sample	*sugars*									*Sugar content /µg*	*%sugar content*
	Xyl	Arab	Ramn	Fuc	Gal Ac.	Gluc. Ac.	Gluc	Mann	Galact		
105.65-46 pi	49.6	13.9	1.56	0.4	2.03	9.29	0	8.89	14.23	1.49	0.015
105.65-46 prep										-	-
158.16 NWS pi										-	-
179.268 NWS pi										-	-
135.43-64all	27.1	21.2	0.9	0.5	0.8	0.0	35.1	4.2	10.2	2.10	0.008
	41.7	32.7	1.4	0.7	1.2	0.0	-	6.5	15.8		
007.15-1 pi										-	-
004.5-1 pi	22.7	21.1	1.5	0.6	3.6	1.6	30.7	5.4	12.9	1.70	0.024
	32.7	30.5	2.2	0.9	5.1	2.3	-	7.8	18.6		
105.66-46 pi	y	y	y	-	y	y	-	y	y	0.36	0.009
112.93-46 pi										-	-
065.77-31 pi	25.1	5.0	0.7	0.4	2.7	5.8	44.6	4.1	11.5	1.30	0.056
	45.3	9.1	1.3	0.8	4.9	10.4	-	7.4	20.8		
083.07-43 pi	7.9	10.5	7.3	1.8	1.3	0.7	40.3	13.3	16.8	2.41	0.000
	13.3	17.6	12.2	3.0	2.1	1.2	-	22.3	28.2		
076.105 pi	8.2	7.7	1.4	0.7	1.5	2.2	62.2	7.0	9.0	1.18	0.028
	21.8	20.4	3.8	1.9	3.9	5.9	-	18.5	23.9		
006.04-1 prep	22.5	9.8	2.2	0.9	1.6	4.0	44.7	7.1	7.1	0.95	0.000
	40.7	17.7	4.0	1.7	3	7.3	-	12.8	12.9		
006.02-1 all										-	-

Dr17 R3/4 pi										-	-
080.09-43 all	9.0	18.5	2.5	1.7	0.0	0.4	29.8	7.3	30.8	1.52	0.102
	12.8	26.4	3.5	2.4	0.0	0.5	-	10.4	43.9		
179.122 pi	y	y	y	-	-	-	-	y	y	0.37	0.023
P118 all	-	y	y	y	-	-	-	-	y	0.38	0.001
026.13-5 all	-	y	y	-	-	-	-	y	y	0.35	0.004
021.75-5 all	26.1	24.1	6.1	2.0	1.7	2.2	0.0	15.2	22.6	0.57	0.005
075.105 prep 1	16.7	10.2	1.9	0.6	1.0	1.2	53.3	7.6	7.6	5.08	0.049
	35.7	21.9	4.2	1.2	2.1	2.5	-	16.2	16.2		
075.105 prep 2	22.4	19.7	3.3	1.0	1.4	1.2	36.4	5.8	8.8	1.10	0.004
	35.2	31.0	5.2	1.6	2.2	1.9	-	9.1	13.9		
Dr201 all	-	-	-	-	-	-	y	-	-	0.44	0.005

None of the samples with a saccharide content between the detection and quantification limits could be characterised by using the decisional scheme.

The glycoside profiles and chromatograms of the samples with a saccharide content higher than the quantification limit present mainly differences based on the xylose/arabinose ratio. On the basis of the ratio three sub-groups can be distinguished.

- Group A: xyl/arab less than one (samples 083.07-43, 080.09-43)
- Group B: xyl/arab ratio almost one (samples 135.43-64, 004.5-1, 076.105, 021.75-5, 075.105 prep2)
- Group C: xyl/arab higher than one (samples 105.65-46, 065.77-31, 006.04-1 prep, 075.105 prep1)

Figure 4.14. presents three chromatograms representative of the three glycoside profiles described above. As discussed before, any reference natural gum analysed presents a xylose/arabinose ratio higher than one.

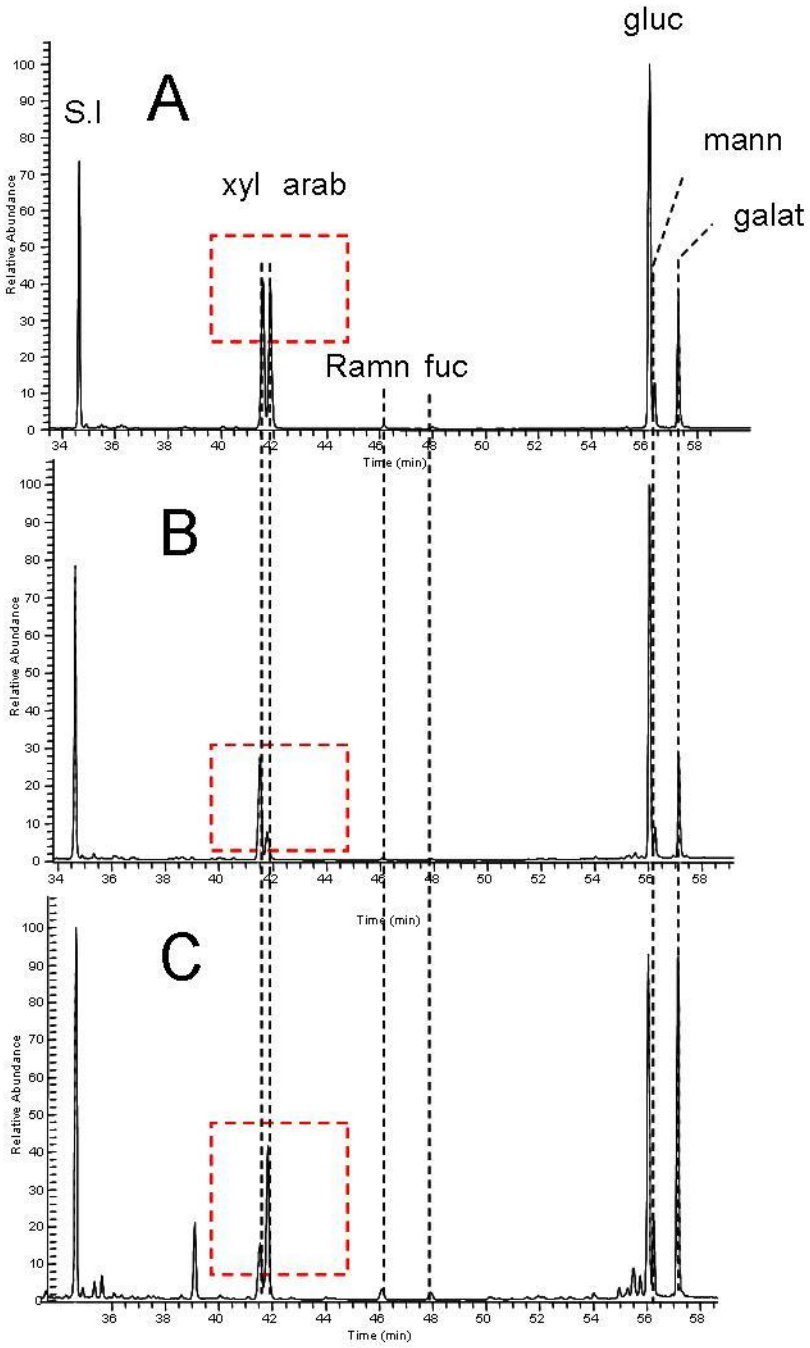

Figure 4.14. Chromatograms representative of the three types of profiles detected in Pylos samples, depending on the ratio xylose/arabinose. (A) sample 131.43-64 containing all layers (xyl/arab=1); (B) sample 065.77-31 corresponding to the pictorial layer (xyl/arab> 1); (C) sample 080.09-43 corresponding to all layers (xyl/arab <1).

The evaluation of the glycoside profile of the samples one by one indicates that with the exception of samples 105.65-46 , 021.75-5 and 080.09-43 all samples present all

sugars. Thus, a mixture of polysaccharide materials can be suggested, which could be in accordance of a mixture of fruit tree and tragacanth gum.

4.3.3.5. Roman city of Ercolano (Naples, Italy)

All samples from Ercolano from Villa del Bicentenario present the occurrence of saccharide materials between the detection and quantification limit. Profiles are reported in Table 4.18. The use of a decisional scheme on bcn w3 17 indicated the presence of fruit tree gum (arabinose/yes; ramnose and glucuronic acid/yes; fucose and galacturonic acid/no; mannose/yes→fruit tree) while it could not be used for the sample Bcn e 18.

Table 4.18. Glycoside profile of samples from Ercolano.

Sample	*sugars*									*Sugar content /μg*	*%sugar content*	*Decisional scheme*
	Xyl	Arab	Ramn	Fuc	Gal Ac.	Gluc. Ac.	Gluc	Mann	Galact			
bcn w3 17	y	y	y	-	-	y	y	y	y	0.77	0.043	Fruit tree
Bcn e 18	y	y	y	-	-	-	y	-	y	0.52	0.052	-
VP superficial	17.7	5.9	0.0	0.0	0.0	0.0	65.7	7.0	3.6	0.67	0.112	-
VP intonaco	21.8 45.4	6.1 12.6	1.1 2.3	1.0 2.0	1.3 2.7	1.2 2.6	52.1 -	9.5 19.9	6.0 12.5	0.94	0.010	-

VP samples show a saccharide content over the quantification limit. However, in VP intonaco sample all sugars are present with a percentage higher than 1, thus a mixture of polysaccharide materials can be suggested. Moreover, xyl/arab ratio is again higher than 1. 50 % of glucose is detected in these samples suggesting the occurrence of a material such as starch or honey (Table 4.13.). VP superficial presented only xylose, arabinose and glucose. This profile is not coincident with the profile of any gum nor polysaccharide material analysed.

4.3.3.6. Basilica of Sant' Antonio da Padova (Italy)

All samples showed the occurrence of saccharide materials. The profiles of samples 3, 4 and 6 are summarized in Table 4.19.

Table 4.19. Glycosidic profiles of samples from Sant Antonio di Padova.

Sample	*sugars*									*Sugar content /µg*	*%sugar content*	*Decisional scheme*
	Xyl	Arab	Ramn	Fuc	Gal Ac..	Gluc. Ac.	Gluc	Mann	Galact			
Pdv 3	32.5	11.4	2.8	0.0	0.0	20.2	0.0	22.0	11.1	1.16	0.005	Fruit tree
Pdv 4	23.7	11.5	0.0	0.0	0.0	0.0	55.7	0.0	9.2	0.64	-	-
	53.4	25.9	0.0	0.0	0.0	0.0	-	0.0	20.7			
Pdv 6	58.8	6.1	0.0	0.0	0.0	0.0	28.9	0.0	3.4	1.30	-	-
	86.0	8.9	0.0	0.0	0.0	0.0	-	0.0	5.0			

Xylose, arabinose, ramnose, glucuronic acid, mannose and galactose are present in sample Pdv 3. By means of a decisional scheme, fruit tree gum can be identified as the source of the sugars present in the sample but glucose. However the ratio xyl/arab is higher than one, mannose and glucuronic acid are present in a percentage higher than the one reported for the reference fruit tree gum while galactose is in lower amounts than the reference values (Table 4.13.).

Sample Pdv 4 and Pdv 6 presented again a xylose/arabinose ratio higher than 1. In this case both acids and deoxy hexoses together with mannose are not present while glucose is in a content between the detection and quantification limits. Galactose, xylose and arabinose are the only sugars over the quantification limit making the identification of the saccharide material impossible.

4.3.3.7. Orsanmichele (Florence, italy)

In this case just xylose (30-40%) and glucose (60-70%) are present in the samples. Thus the identification of the polysaccharide material is not possible since it is not coincident with any of the profiles reported above nor in the literature. Data is presented in Table 4.20.

Table 4.20. Glycoside profiles of the samples from Orsanmichele.

Sample	*sugars*									*Sugar content /µg*	*%sugar content*
	Xyl	Arab	Ramn	Fuc	Gal Ac.	Gluc. Ac.	Gluc	Mann	Galact		
OSM-P	32.2	0.0	0.0	0.0	0.0	0.0	67.8	0.0	0.0	0.84	0.005
OSM-C	36.5	0.0	0.0	0.0	0.0	0.0	63.5	0.0	0.0	1.50	0.094

4.3.4. Degradation of polysaccharide materials and changes in the glycoside profiles

The analysis of painting samples gave quantitative glycosidic profiles that can not be ascribed to any of the gums nor materials known with the exception of the sample from Malta. Though a mixture of materials could be hypothesised in some cases, the xylose/arabinose ratio higher than 1 suggested a change in the glycoside profile of the polysaccharide binders. Moreover, in almost all cases glucose was present and, although the simultaneous presence of both a plant gum and a glucose containing material, such as starch or honey, can be hypoyhesised, it is quite unlikely that this was the case with all samples. The evolution of the profiles of the polysaccharide materials during ageing had already been observed in the literature without giving an explanation: an increase of the galactose content and a lowering of the arabinose and rhamnose content, as well as the presence of mannose that was not present in the original composition were observed [1, 8]. The inversion of the ratio Xylose/arabinose was also observed [8].

Analysis of plant gums is of interest in the alimentary and medic field. However, in these cases the ageing of the material is never the matter of interest. Thus, although some studies on the degradation of saccharide materials have been done on thermal and photooxidative degradation, mainly assessing the changes on the physical properties of the polysacaridic material [70], little attention has been paid to the chemical changes undergone by saccharide materials nor to the results of a biological attack [63, 71, 72].

The analysis of painting samples thus showed that, though saccharide binders are found, their identification is not straightforward. To try to better understand this phenomenum three different aspects were investigated: the effect of the simultaneous presence of inorganic materials, including metal contained in pigments, the effect of simultaneous presence of proteinaceous binders and the effect of biological attacks.

4.3.4.1. Artificial Ageing

Reference paint layers of arabic, tragacanth and fruit tree (cherry) gums were artificially light aged for 3 weeks (outdoor filter $\lambda < 280$ nm). This artificial ageing has commonly been successfully employed to the study of the behaviour of paint materials such as drying oils, leaning the basis for a better understanding of their ageing behaviour. Although polysaccharide materials do not present double bonds, with this test the combined use of light, oxygen and water was investigated to highlight eventual modifications of the molecular profile and of the solubility of the plant gum occurring in the normal, conservation conditions of a work-of-art.

Table 4.21. presents comparison of the data obtained for reference paint layers of gums before and after ageing in the solar box for three weeks. RSD for the different monosaccharide and uronic acids is similar to the one for non aged gums and lower than 20 % for all sugars and gums. Results showed that the molecular profile of each gum is maintained. Moreover, if modifications of the macromolecular structure of the polysaccharide fraction occurred, in terms of both hydrolysis with subsequent molecular weight decrease, or cross-linking, with subsequent molecular weight

increase, it has not altered the recovery of sugars after the microwave assisted hydrolysis step, with the exception of Arabic gum where better recoveries are obtained.

Table 4.21. Relative percentage content of sugars, average percentage recovery and relative standard deviation on three replicate analyses of painting layers of raw plant gums on a glass slide aged for 3 weeks in a solar box.

Paint layer	*Sugars*									*Recovery%*
	Xyl	Arab	Ramn	Fuc	Gal Ac..	Gluc. Ac.	Gluc	Mann	Galact	
GA non aged	0.0	36	17.7	0.0	0.0	11.2	0.0	0.0	35	65
GA aged	0.0	25.2	14.0	0.0	0.0	16.7	0.0	0.0	48.7	95
TG non aged	21.3	36.4	2.1	7.2	12.8	0.5	11.4	0.0	10.2	23
TG aged	20.2	35.1	3.1	7.5	13.6	0.4	10.0	0.0	10.0	23
Ft non aged	7.0	48.7	2.1	0	0	5.9	0	1.8	34.4	62
Ft aged	6.1	43.1	2.1	0	0	9	0	2.7	36.8	62

These results would suggest that natural ageing of polysaccharide binders should not compromise the possibility of identifying plant gums in paint samples.

4.3.4.2. Simultaneous presence of inorganic compounds

Some reference paint layers containing plant (tragacanth, arabic, and cherry) gums and pigments (Table 4.9) were analysed after six months of natural ageing (no NaN_3 added). Results showed that none of the pigments generate analytical interferences during the derivatisation when using the clean-up step (Zeolit column).

It is important to note that glycoside profiles presented some changes. Glycoside profiles of the reference paint layers are presented in Table 4.22.

Table 4.22. Relative percentage content of sugars of painting layers containing a mixture of plant gums and pigments.

Paint layer	*Sugars*								
	Xyl	Arab	Ramn	Fuc	Gal Ac..	Gluc. Ac.	Gluc	Mann	Galact
GA Pb v	0.0	30.0	13.0	0.0	0.0	8.8	0.0	0.0	48.2
GA Cu v	0.0	40.7	10.9	0.0	0.0	8.2	0.0	0.0	40.2
GA Si v	0.0	37.2	13.3	0.0	0.0	6.8	0.0	0.0	42.7
GA b v	0.0	32.4	13.9	0.0	0.0	7.5	0.0	0.0	46.1
TG Pb v	17.7	34.1	4.3	8.7	2.5	0.0	12.0	0.0	20.5
TG Cu v	4.6	29.2	12.8	1.9	1.3	3.7	7.2	0.0	39.3
TG Si v	15.0	23.6	4.4	7.3	2.1	0.6	24.8	6.0	16.4
TG b v	12.6	26.9	3.5	11.7	1.6	0.0	27.6	0.0	16.1
FtG Pb v	4.4	48.7	1.8	0.0	0.0	4.0	0.0	2.8	38.3
FtG Cu v	4.3	62.6	0.7	0.0	0.0	6.5	1.2	3.1	21.7
FtG Si v	5.5	57.9	1.2	0.0	0.0	3.0	1.8	1.6	28.9
FtG b v	4.1	47.7	1.8	0.0	0.0	4.0	1.7	2.6	38.2
GA i	0.0	32.9	13.8	0.0	0.0	10.	0.0	0.0	43.3
TG i	25.2	48.9	1.4	6.4	0.4	0.9	8.2	0.0	8.4
Ft i	4.3	67.2	0.6	0.0	0.0	2.1	0.0	0.7	24.8

Changes can be summarised as follows:

- Arabic gum does not present significative changes in the percentage of the different sugars.
- Tragacanth gum presents a lower amount of galacturonic acid in all cases, higher percentages of glucose (Si, Fe) and galactose (Pb, Cu) , and lower amounts of xylose (Cu). Moreover, in the presence of ultramarine blue (Si) mannose was also detected.
- Fruit tree presents higher percentages of arabinose for the Si and Cu based pigments. Glucose is over the quantification limit in the Si, Cu and Fe containing samples. A low content of glucuronic acid is observed for the plaster reference layer.

Though in most of the cases the presence/absence of monosaccharides and uronic acids remains unaltered, data in Table 4.22. highlights the occurrence of changes in the

glycoside profile in the reference layers in the presence of inorganic materials of different types. Moreover, changes do not occur for all the gums nor in the presence of all pigments in the same way. Thus, identification of the gum in these cases is not straightforward. Artificial ageing of these reference layers must be performed to evaluate the role played by inorganic materials in the interconversion of sugars under light ageing.

4.3.4.3. Simultaneous presence of proteins

Reference painting layers prepared with mixtures of gums (arabic, tragacanth and cherry) and proteinaceous materials (egg, animal glue, casein) were analysed after two years of their preparation. Data arepresented in Table 4.23.

Table 4.23. Relative percentage content of sugars of painting layers containing a mixture of plant gums and proteinaceous materials.

Paint layer		*Sugars*								
		Xyl	Arab	Ramn	Fuc	Gal Ac.	Gluc. Ac.	Gluc	Mann	Galact
GA	Egg	0.0	36.1	13.8	0.0	0.0	7.9	0.0	2.0	39.7
	Glue	0.0	37.1	14.3	0.0	0.0.	10.5	0.0	0.0	38.1
	Milk	0.0	30.9	10.8	0.0	0.0	9.0	2.7	0.0	46.4
TG	Egg	18.5	30.8	1.5	4.2	2.3	1.2	13.4	17.3	10.7
	Glue	18.6	40.2	2.0	7.6	0.5	0.4	12.8	0.0	17.8
	Milk	1.9	4.7	0.0	0.0	0.0	0.0	26.9	0.0	64.3
Ft	Egg	16.1	42.9	2.4	0.0	0.0	6.3	1.0	8.7	23.8
	Glue	13.1	43.3	1.2	0.0	0.0	5.5	1.4	2.3	33.2
	Milk	9.2	30.6	1.2	0.0	0.0	2.1	14.9	2.5	39.7

Results show that the molecular pattern is manteined for all gums though browning reactions [61,**Errore. Il segnalibro non è definito.**] could be visually observed after the hydrolysis in almost all cases. However, some changes in the glycoside profile can be observed, mainly due to the contribution of the polysaccharide content of egg, animal glue and milk (Table 4.13.) [73, 74]. In the presence of milk the glycoside profile of the gums presents higher percentage of glucose and galactose and in the

presence of egg higher percentage of mannose while almost no change can be observed in the presence of animal glue due to its low saccharide content.

Moreover, the fruit tree profile presents higher percentage of xylose while tragacanth gum shows lower percentages of galacturonic acid in all cases (from 12 % for the reference material to less than 2% in the presence of proteins) which can not be explained on the basis of the simple contribution of the saccharide content of the proteinaceous binder. It has to be stressed that the modification of the sugar profile is obviously dependent on the relative amount of the different binders.

These results show that the sugar profile of a plant gum can appaear modified when a proteinaceous binder is present, not only as a result of its saccharide content contribution but also because the Maillard reaction, occuring when hydrolysis is performed, selectively substract different sugars to the analysis. It can not be excluded that this effect is also influenced by the ageing and the organic and inorganic materials simultaneously present. This aspect needs further investigations.

4.3.4.4. Biological attack

The ageing of the reference paint layers, the presence of egg, animal glue or milk, nor the simultaneous presence of pigments, resembles the alteration of the pentoses ratio observed in paint samples. Since glucose, together with galactose and rhamnose, is present in animals, microorganisms and as product of the methabolism of some prokaryotes, the effect of a biological attack on the gums was considered [75, 76].

Solutions of the gums tragacanth, locust bean, arabic and cherry tree were prepared and analysed (Table 4.8.). Fraction A was admixed with NaN_3 to prevent biological attack while fraction B was not. The solutions were sigilated with parafilm and left at room temperature. After two months at room temperature the formation of fungi for the tragacanth gum was evident. After a year, arabic gum solutions A and B were still clear as well as locust beam, fruit tree and tragacanth gums solution A. Solutions B of locust bean and cherry tree gum presented the occurrence of fungi, and tragacanth gum

solution B presented a clear increasing of the phenomenum. Figure 4.14 shows the tragacanth solutions A and B after a year from their preparation.

Figure 4.14. Solutions A and B of tragacanth gum after one year from their preparation. The presence of fungi in the solution B (right side) is clearly observable.

The analysis of both fractions were done after two months and after a year of their preparation. Glycosidic profiles of the solutions are presented in Table 4.24.

Table 4.24. Glycosidic profile of the solutions A and B.

Solution ([xviii])	*Biological attack observation* ([xix])	*sugars*								
		Xyl	Arab	Ramn	Fuc	Gal Ac.	Gluc. Ac.	Gluc	Mann	Galact
GA sol fresh	-	0.0	26.6	11.1	0.0	0.0	12.1	0.0	0.0	48.4
GA sol A 2 month	-	0.0	31.6	16.6	0.0	0.0	11.2	0.0	0.0	40.5
GA sol A 24 month	-	0.0	35.7	15.7	0.0	0.0	6.9	0.0	0.0	41.8

[xviii] Sol A : 4000 ppm solution with NaN_3 added as biocide ; Sol. B : 4000 ppm solution without NaN_3; Fresh solution common for both A and B
[xix] Visual observation of the formation of fungi

GA sol B 2 months	-	0.0	27.3	15.9	0.0	0.0	9.1	0.0	0.0	41.4
GA sol B 24 month	-	0.0	36.2	13.7	0.0	0.0	6.9	0.0	0.0	43.1
TG sol fresh	-	18.6	33.7	2.1	7.6	12.8	0.7	11.6	0.0	12.8
TG sol A 2 month	-	21.5	34.2	2.2	6.1	16.9	0.4	10.6	0.0	8.5
TG sol A 24 month	-	20.1	34.0	1.5	6.3	10.6	0.0	14.1	0.0	13.4
TG sol B 2 months	y	24.0	16.8	4.0	9.1	23.5	0.6	12.1	0.0	10.0
TG sol B 2 years	y	39.8	7.6	2.7	14.3	21.6	0.0	10.8	0.0	3.2
TG 2006	y	41.3	10.2	2.2	16.9	23.7	0.0	0.0	0.0	5.9
Ft sol fresh	-	10.1	44.1	3.0	0.0	0.0	6.0	0.0	2.5	34.3
Ft sol A 2 month	-	8.4	40.5	2.3	0.0	0.0	5.7	0.0	3.8	39.3
Ft sol A 24 month	-	6.9	48.3	1.5	0.0	0.0	3.5	0.0	1.4	38.3
Ft sol B 2 months	-	6.5	36.6	1.6	0.0	0.0	14.1	0.0	3.6	37.7
Ft sol B 24 month	y	7.9	39.9	1.8	0.0	0.0	5.2	0.0	2.0	42.6
LB sol fresh	-	0.0	0.0	0.0	0.0	0.0	0.0	0.0	79.5	20.5
LB sol A 2 month	-	0.0	0.0	0.0	0.0	0.0	0.0	0.0	79.7	20.3
LB sol A 24 month	-	0.0	0.0	0.0	0.0	0.0	0.0	11.7	73.0	15.3
LB sol B 2 months	-	0.0	0.0	0.0	0.0	0.0	0.0	6.9	71.7	21.4
LB sol B 24 month	-	0.0	0.0	0.0	0.0	0.0	0.0	13.6	68.7	17.7

GC/MS analyses highlighted that:

- Arabic gum profiles were maintained for both A/B solutions though a decreasing in the glucuronic acid content seems to take place.
- Fruit tree presented an almost constant glycoside profile
- Locust bean gum experimented some slightly changes in its sugar profile though the ratio mannose/galactose remained unaltered.
- Tragacanth gum solution A presented the same profile than the fresh solution after 24 months. However, the solution B profile showed several changes :
    - the change of the ratio xylose/arabinose from less than 1 to almost 1 after 2 months and more than one after 24 months, resembling the results observed for ancient painting samples.
    - the content of fucose and galacturonic acid seems to increase while galactose percentage diminishes.
- Tragacanth gum solution prepared in 2006 profile resembles that of TG solution B 24 months though glucose is under the detection limit in this case.

The presence of ribose, (chromatographic peak overlapped with xylose, table 4.) in the sample was discarded by using a chiral column that allowed the chromatographic separation of ribose and xylose.

Since these results showed very interesting and promising results further investigations were tried. Reference paint layers with and without pigments (described in Table 4.13) were cut in a half and the first half was introduced in a physiological solution containing bacteria (Sol. B), while the second half in a physiological solution containing fungi (Sol.F). By this way, two analyzable fractions were created in each case: one corresponding to the gum solubilised in the physiological solution and the other corresponding to the material remained on the glass support.

The activity of the solutions was measured after 1 month being compared with the activity of the solutions before the immersion (Sol. B and F). Results highlighted an increase in the activity of the solutions in all cases, also when pigments were present. This indicates that both bacteria and fungi were feeding with the solubilised gum.

GC/MS analyses were performed on both an aliquot of the solution where the reference layer was immersed, and the material scratched from the surface of the reference layer. Results presented in Table 4.25. highlighted several compositional changes in both fractions (the solutions and the reference layers).

To evaluate the contribution of the initial solutions, solutions of bacterial (Sol Bacteria) and fungi (Sol. Fungi) were also analysed as blanks. Results are also presented in Table 4.25. Though both solutions presented some polysaccharide material content, the percentage (calculated as reported above) is really low: 0.001 % for bacterial and 0.0009 % for fungi.

Table 4.25. Results of the solutions and reference paint layers treated with bacteria and fungi inoculate.

Sample([xx])	*sugars*								
	xyl ([xxi])	arab	ramn	fuc	Galac.ac	Gluc.ac	gluc	mann	galact
Sol. Bacteria	0.0	0.0	40.5	0.0	0.0	0.0	14.9	7.9	36.7
Sol. Fungi	0.0	0.0	0.0	0.0	0.0	0.0	48.7	34.0	17.3
Sol GA F	0.0	47.1	8.4	0.0	0.0	6.3	0.0	0.0	38.2
Sol. GA B	0.0	9.4	10.4	1.8	0.0	3.5	21.1	15.6	38.1
GA st F	0.0	81.5	14.8	0.0	0.0	0.0	0.0	0.0	4.0
GA st B	0.0	15.9	5.4	0.0	0.0	12.9	17.1	9.1	39.6
Sol. TG F	9.4	27.2	6.3	2.4	0.0	3.1	16.3	8.6	26.7
Sol. TG B	0.0	36.1	13.5	0.0	0.0	6.6	0.0	0.0	43.8
TG st F	15.2	54.4	0.0	30.3	0.0	0.0	0.0	0.0	0.0
TG st B	21.3	38.1	4.5	5.7	3.6	1.8	6.1	0.0	18.9
Sol. Ft B									
Sol. Ft F	10.4	0.0	0.0	0.0	0.0	0.0	58.4	20.0	11.2
Ft st F	0.0	100.0	0.0	0.0	0.0	0.0	0.0	0.0	0.0
Ft st B	5.5	63.2	1.0	0.0	0.0	6.2	0.0	1.1	23.0

[xx] Sol indicates analysis of the solution fraction while st indicates the analysis of the reference paint layer fraction. F and B that the attack has been performed with fungi or bacteria, respectively.
[xxi] Also in this case the absence of ribose was ascertained by using a chiral column.

The analysis showed that changes (in some cases very significant) of the glycoside profile and the molecular patterns of the gums is taking place in the presence of bacteria and fungi. Establishing a general scheme of the changes that occurred for each gum was not possible. Though xylose/arabinose ratio higher than one has not been obtained with these investigations, data highlighted that if a biological attack is taking place, the identification of the binder can be completely compromised. A systematic approach to the issue of the biological attack should be tried.

4.4 General conclusions

A procedure for the characterization of polysaccharide materials in painting samples has been settled. The use of a double-exchange resin for the purification of the samples has allowed to remove analytical interferences in the derivatisation of highly inorganic samples. Modifications in the derivatisation step ensured the reproducibility of the reaction yields, and prevented chromatographic problems due to unwanted secondary products of the deriviatisation reactions.

The derivatisation procedure is based on mercaptalation followed by silylation. Two steps of silylation are required to avoid the coexistance of TFA and pyridine. In the first step mercaptalation is interrupted by the derivatisation of TFA and EtSH by BSTFA and drying under nitrogen flow. In the second step the complete derivatisation of the mercaptal derivatives of the parental sugars takes place. Conditions have been optimized to avoid secondary chromatographic peaks due to reaction by-products. Final conditions are as follows: BSTFA as derivatiser with 1% TMCS as catalayser and pyridine as solvent in a ratio 1:2 . By this way, just one peak per analite is obtained. The procedure works for aldoses and uronic acids, which are the main components of gums and most saccharide materials used as binding media, adhesives and varnishes in paintings. Although mercaptalation of ketoses leads to the formation of several reaction products, fructose peaks are not overlapped with the aldoses and uronic acids ones. Thus, presence of honey can be also evidenced in paint samples.

The application of the procedure to reference painting samples permitted the characterisation of the glycoside profile of gums and other materials. A database of the glycoside profiles of several organic materials have been built by using the procedure.

The application of the procedure to ancient painting samples showed, in all cases but one, that glycoside profiles obtained did not strictly correspond to any of the reference materials investigated. A mixture of polysaccharide materials was suspected in some cases. The xylose/arabinose ratio observed in most cases, the widespread presence of glucose, and the unassigned quantitative glycoside profiles, stimulated further investigations.

The study of mixtures of polysaccharide binders and proteinaceous ones, the study of pigments containing reference layers, and the study of fungi and bacteria attack were taken into account. The results of these preliminary investigation highlighted that modification can occurr in the quantitative but also qualitative profile of plant gums. As a result, it is possible to affirm the following:

1) caution must be paid when other saccharide containing materials are present in the sample, because their contribution to the glycoside profile, if they are not known, prevents the identification of the saccharide binder present.
2) the proteinaceous binders, in addition to their contribution to the glycoside profile due to their saccharide content, give rise to modifications of the quantitative molecular profile as an effect of reactions (such as Maillard) occurring during the sample preparation and possibly as an effect of time.
3) some pigments and inorganic materials in general seem to act as catalysers of isomerisation of some sugars, producing a modification of the quantitative and qualitative profiles of polysaccharide binders. Further investigations are needed to fully understand this phenomenon.
4) bacteria and fungi can produce modifications of the glycoside profiles to such an extent that makes the polysaccharide binder identification impossible. Further systematic investigation is needed to better understand this phenomenon but when a polysaccharide binder is investigated in a paint sample, the presence of a biological attack should be ascertained with the suitable techniques.

These results indicated, as it has never been done in the literature, that the identification of a polysaccharide binders can not just be performed on its qualitative evaluation. Several factors need to be taken into account, which still need to be studied, since they are far from being completely understood. Further investigations are needed to find out if these changes can be somehow stigmatised, allowing a reliable identification of saccharide binders in a paint sample.

References

[1] Bonaduce I., Brecoulaki H., Colombini M.P., Lluveras A., Restivo V., Ribechini E., 'Gas chromatographic-mass spectrometric characterisation of plant gums in samples from painted works of art', *Journal of Chromatography A 1175 (2007) 275–282*

[2] Birnstein V.J., 'On the technology of central asian wall paintings : the problem of binding media', Studies in Conservation 20 (1975) 8-19

[3] Kakoulli, I. Late Classical and Hellenistic Monumental Paintings: A review of the technical literature , reviews in conservation number 3 (2002)56-67

[4] Vallance S.L., Singer B.W., Hitchen B.W., Towsend J.H., 'The development and initial applications of a gas chromatographic method for the characterization of gum media', Jaic online 37 nº3 art 4 (1998) 294-311

[5] Masschelein-Kleiner L., Heylen J., Tricot-Marckx F., 'Contribution à l'analyse des liants, adésifs et vernis anciens', Studies in Conservation 13 nº 3 (1968)105-121

[6] Mora P., Mora L., Porta E., 'Conservation de la tombe de Nefertari dans la vallée des reines', 9th Triennal meeting of the ICOM Comité for Conservation, Dresden (1990) 518-523

[7] Bonaduce I., Boon J.J., 'An integrated mass spectrometric and molecular imaging analytical approach to identify and localise constituents in paintings applied to gilded multilayer structures from the 14th to 16th C works of art', in New trends in analytical, environmental and cultural heritage chemistry, M.P. Colombini, L. Tassi editors, Transworld research Network (2008) 345-388

[8] Bleton J., Coupry C., Sansouet J., 'Approche d'etude des encres anciens', Studies in conservation 41 nº 2 (1996) 95-108

[9] Bonaduce I., 'A multy-analytical approach for the investigation of materials and techniques in the art of gilding', PhD thesis, Università di Pisa(2005)

[10] Doerner, 'Los materiales de pintura y su empleo en el arte' (18ª edición Editorial Reverté Barcelona 1998).

[11] Merrifield M. P., 'The Art of Fresco Painting in the Middle Ages and the Renaissance', Courier Dover Publications, 2004, ISBN 0486432939

[12] Cennino Cennini, in F. Frezzato (Editor), Il libro dell'Arte, Neri Pozza Editore, Vicenza, 1st ed., 2003.

[13] Bonaduce, I.; Colombini, M. P., 'Gas Chromatography/Mass spectrometry for the chracterization of organic materials in frescoes of the Monumental Cemetery of Pisa (Italy) ', *Rapid Commun. Mass Spectrom*. 2003, *17*,2523-2527.

[14] Colombini, M. P.; Modugno, F.; Giacomelli A., 'Two procedures for suppressing interference from inorganic pigments in the analysis by gas chromatography-mass spectrometry of proteinaceous binders in painting' *J. Chromatogr. A* 1999, *846*,101-111.

[15] de la Cruz-Canizares, J.; Domenech-Carbo, M. T.; Gimeno-Adelantado, J.V.; Mateo-Castro, R.; Bosch-Reig, F. *J. Chromatogr. A* 2004, *1025*, 277-285.

[16] van den Berg, J. D. J.; van den Berg, K. J.; Boon, J. J. 'Identification of non-cross-linked compounds in methanolic extracts of cured and aged linseed oil-based paint films using gas chromatography – mass spectrometry', *J. Chromatogr. A*2002, *950*, 195-211.

[17] Chiavari, G.; Gandini, N.; Russo, P.; Fabbri, D. 'Characterisation of standard tempera painting layers containing proteinaceous binders by pyrolysis (/methylation)-gas chromatography/mass spectrometry' *Chromatographia* 1998, *47*,420-426.

[18] Gimeno-Adelantado, J. V.; Mateo-Castro, R.; Domenech-Carbo, M. T.; Bosch-Reig, F.; Domenech-Carbo, A.; Casas-Catalan, M. J.; Osete-Cortina, L. *J.Chromatogr. A* 2001, *922*, 385-90.

[19] Colombini, M. P.; Bonaduce, I.; Gautier, G. 'A diagnosis of the yellowing of the marble high reliefs and the black decorations in the chapel of the tomb of Saint Anthony (Padua, Italy)', *Chromatographia* 2003, *58*,357-364.

[20] Bonaduce, I.; Colombini, M. P., 'The Characterization of Beeswax in works of Art by Gas Chromatography-Mass Spectrometry and Pyrolysis-Gas Chromatography-Mass Spectrometry Procedures', *J. Chromatogr. A* 2004, *1028*, 297-306.

[21] Regert, M.; Colinart, S.; Degrand, L.; Decavallas, O., 'Chemical Alteration and use of beeswax through time: accelated ageing tests and analysis of archaeological samples from various environmental contexts', *Archaeometry* 2001,*43*, 549-569.

[22] Andreotti A., Bonaduce I., Colombini M.P, Gautier G., Modugno F., Ribechini E., 'Combined GC/MS Analytical Procedure for the Characterization of Glycerolipid, Waxy, Resinous, and Proteinaceous Materials in a Unique Paint Microsample', Anal. Chem. 2006, 78, 4490-4500

[23] Colombini M.P, Ceccarini A., Carmignani A., Ion chromatograhy characterization of polysaccharides in ancient wall paintings, Journal of Chromatography A 968 (2002) 79-88

[24] Chiavari G., Montalbani S., Prati S., Keheyan Y., Baroni S., 'Application of analytical Pyrolysis for the characterisaton of old inks', J.Anal. Appl. Pyrolysis 80 (2007) 400-405

[25] Chiantore O., Riedo C., Scalarone D., 'Gas chroamtographic/mass spectrometric analysis of products from on-line pyrolyis-silylation products of plant gums used as binding media', Iternational Journal of Mass Spectrometry (2008), doi: 10.1016/j.ijms.2008.07.31

[26] Wright M.M., Pyrolysis_mass spectrometry of natural gums, resins and waxes and its use for detecting such materials in ancient Egyptian mummy cases, Journal of Analytical and Applyed Pyrolysis, 11 (1987) 195

[27] Mejanelle,P., Bleton J., Tchapla A., Goursaud S., Gas Chromatography_Mass Sepctrometric Analyis of Monosaccharides afte rmethanolysis and Trimethylsilylation. Application to the study of museum objects. Chapter 24 Carbohydrate analysis by modern chromatography and electrophoresis, Journal of Chromatotgraphy library vol 66 (2002) Elsevier Science Editor Ziad El Rassi.

[28] Pitthard V., Finch P., GC-MS analysis od monosaccharide mixtures as their diethyldithioacetal derivatives: application to plant gums used in art works, Chromatographia Supplement vol 53(2001), p317-321

[29] Schneider U., Kenndler E., Identifiaction of plant and animal glues in museum objects by GC-MS, after catalytic hydrolysis of the proteins by the use of a cation changer, with simultaneous separation from the carbohydrates,Fresenius J Anal Chem (2001)371, 81-87

[30] Pitthard V., Griesser M., Stanek S., Bayerova T., Study of complex organic binding media on artworks applying GC-MS analysis: selcted examples from the Kunsthistorisches Museum, Viena, nacromolecular Symposium (2006) 238, 37-45

[31] Pitthard V., Griesser M., Methodology and application of GC_MS to study altered organic binding medi from objects of the Kunsthistorches Museum, Viena, S. Stanek, Ann. Chim. (Rome) 96 (2006) 561.

[32] Mills J., White R., The organic chemistry of museum objects, 2nd edition (1994) Butterworth Heineman (London)

[33] Jones J.K.L., Nunn J.R., 'The structure of frankincense gum', Journal of the American Chemical Society 77(1955) 5745-5746

[34] Cennino Cennini: Il libro del'arte (Akal Ediciones Madrid Spain 2002)

[35] Cotte M., Susini J., Sole V.A., Taniguchi Y., Chillida J., Checroun E., Walter P., ' Applications of synchrotron based micro imaging techniques to the chemical analysis of ancient paintings', Journal of Analytical Atomic Spectrometry 23 (2008) 820-828

[36] Griffin R.W., Química Orgánica Moderna, Ed. Reverté , Barcelona, 1969

[37] Wiliams P.A., Philips G.O., Stephen A.M., Churms S.C., Gums and Mucilage, Food Polysaccharides and Their applications chapter 13 p.455-495 2nd edition

[38] BeMiller J.N., Gums and Hyrocolloids (chapter 6), Carbohydrates in Food, 2nd edition 2006 Taylor and Francis, Editor Anne-Chalotte Eliasson

[39] Ribechini E., Study of amorphousorganic residues in archaeological findings by MS techniques (2005) University of Pisa

[40] Verbeken D., Dierckx S., Dewettinck K., ' Exudate gums: occurrence, production, and applications', Appl Microbiol Biotechnol 63 (2003) 10-21

[41] Xia Y., Rivero-Huguet M.E., Highes B.H., Marshall W.D., Isolation of the sweet components from Siritia grosvenorii, Food chemistry 107 (2008) 1022-1028

[42] Kuhn L.P., 'Infrared spectra of carbohydrates', Analytical Chemistry 22 nº2 (1950) 276-283

[43]. Prado B.M, Kim S.,. Ozen B. F, Mauer L.J., ' Differentiation of carbohydrate Gum mixtures using Fourier Transform Infrared Spectroscopy and Chemometrics', Journal of agricultural and Food Chemistry 53 (2005) 2823-2829

[44] Molnár-Perl I., Role of chromatography in the analysis of sugars, carboxylic acids and amino acids in food, Journal of chroamtography A, 891 (2000) 1-32

[45] Cheetman N.W.H., Sirimanne P., 'High-performance liquid chromatographic separation of carbohydrate oligomers', Journal of Chromatography 207 (1981) 439-444

[46] Talaga V., Vialle S., Moreau M., 'Development of a HPAEC with PAD based quntification assay for pneumococcal polysacahrides and conjugates', Vaccine 20 (2002) 2472-2484

[47] Scalarone D., Chiantore O., Riedo C., 'Gas chroamtographic/mass spectrometric analysis of on-line pyrolyis-silylation products of monosaccharides', J.Anal.Appl.Pyrolysis 83 (2008) 157-164

[48] Chiantore O., Riedo C., Scalarone D., 'Gas chroamtographic/mass spectrometric analysis of products from on-line pyrolyis-silylation products of plant gums used as binding media', Iternational Journal of Mass Spectrometry (2008), doi: 10.1016/j.ijms.2008.07.31

[49] Fabbri D., Chiavari G., 'Analytical Pyrolysis of carbohydrated in the presence of hexamethyldisilazane', Analytica Chimica Acta 449 (2001) 271-280

[50] Sanders E.B., Goldsmith A.I., Seeman J.I., 'A model that distinguishes the pyrolysis of D-glucose, D-fructose and sucrose from that of cellulose. Application to the understanding of smoke formation', J.Anal. Appl. Pyrolysis 66 (2003) 29-50

[51] Soga T., Serwe M., 'Determination of carbohydrates in food samples by capillary electrophoresis with indirect UV detection', Food Chem. 69 (2000) 339

[52] Carvalho A.Z., da Silva J.A.F., do Lago C.L., 'Determination of mono- and disaccharides by capillary electrophoresis with contactless conductivity detection', Electrophoresis 24 (2003) 2138

[53] Vandenabeele, Wehling B., Moens L., Edwards H., De Reu M., Van Hooydonk G., Analysis of micro-Raman spectroscopy of natural organic binding media and varnishes used in art, Analytical Chimica Acta 407 (2000) 261-274

[54] Derrick M. M.R. Derrick, D. Stulik, J.M. Landry, Infrared Spectroscopy in Conservation Science (The Getty Conservation Institute Los Angeles 1999)

[55] Kharbae B.V., Joshi G.P., Thin layer chromatographic and hydrolysis methods for the identifiaction of plant gums in art objets, Studies in Conservation 40 (1995) 93-102

[56] Derrick M.R., Stulik D.C., Identification of natural gums in works of art pyrolysis gas chromatogrpahy, 9th Triennal meeting of the ICOM Comitteé for Conservation, Dresden (1990)

[57] Grobl M., Harrison S., Kaml I., Kenndler E., Characterisation of natural polysaccharides (plant gums) used as binding media for artistic and historic works by capillary zone electrophoresis, Journl of Chromatogrpahy A 1077 (2005) 80-89

[58] Fliedered F., Mise au point des techniques d'identification des pigments et des liants inclus dans la couche picturale des enluminure de manuscrits. Studies in Conservation 13 (1968) 49-86

[59] Sziszko W., Technological investigations of the three Egyptian epitaphial stelae on wood supports now preserved in national museum, (1972)

[60] Sanz M.L., Nartínez-Castro I., Recent developement in sample preparation for chromatoraphic analysis of carbohydrates (review), Journal of Chromatography A 1153 (2007) 74-89

[61] Daniels V., Lohneis G., Deterioration of sugar artifacts, Studies in Conservation, 42 (1997) 17-26

[62] Blakeney A.B., Harris P.J., Henry R.J., Stone B.A., A simple and rapid preparation of alditol acetates for monosaccharide analysis, Carbohydrate Research 113(1983) 291-299

[63] Newman R., in: V. Dorge, F.C. Howlett (Eds.), PaintedWood: History and Conservation, J. Paul Getty Trust, Williamsburg, VA, 1994, p. 33.

[64] Honda S., Yamaochi N., Kakehi K., Rapad Gas chromatographic análisis of aldoses as their dethyl dithioacetal trimethylsilylates, J. Chromatogr. 169 (1979) 287.

[65] M.L. Lang, The Palace of Nestor at Pylos in Western Messenia. Vol. II. The Frescoes, Princeton University Press, Princeton, 1969.

[66] Giusti A.M., Lalli C., Lanterna G., Matteini M., Porcinai S., Rizzi M., Siano S., '*Indagini storiche e diagnostiche per il restauro dei "Santi Quattro Coronati" dalla facciata di Orsanmichele a Firenze*, in OPD Restauro Rivista dell'Opificio delle Pietre Dure e Laboratori di Restauro di Firenze, Firenze, Centro Dì, n. 13, 2001, pp. 143-150.

[67] Hsu C., Cheng C., Lee C., Ding W., Derivatisation procedures and determination of levoglucosan and related monosaccharide anhydrides in atmospheric aerosol by GCMS, Talanta 72 (2007) 199-205

[68] Evershed R. P., Advances in Silylation, in Handbook of Derivatives for chromatography (Second Edition); K Blau and J. Halket (Eds) John Wiley & Sons, Chichester, England, 1993.

[69] Horton D., Norris P. 'Preparative Carbohydrates Chemistry', Ed.S. Hanessian CRC Press, 1997, p. 35-53 ISBN 0824798023

[70] Wang Q., Ellis P.R., Ross-Murphy S.B., The stability of guar gum in an acqueous system under acidic conditions, Food hydrocolloids 14 (2000) 129-134

[71] Tiano P., Biodegradation of Cultural Heritege : Decay Mechanisms and Control methods

[72] Ciferri O., Microbial degradation of Paintings, Applyed and environmental microbiology (1999) 879-885

[73] Cataldi T.R.I., Angelotti M., Bianco G., Determintion of mono nd disaccharides in milk and milk products by HPAEC with PAD, Analytica Chimica Acta 485 (2003) 43-49

[74] Troyano, E., Olano A., Fernández-Díaz M., Sanz J., Martínez-Castro I., Gas chromatographic Anaysis of free monosaccharides in milk, Chromatographia 32 nº 7/8 (1991) 379-382

[75] Fox K.F., Complementary of GCMS ans LCMS análisis for determination of carbohydrate profiles of vegetative cells and spores of bacilli, Journal of Microbiological Methods 33 (1998) 1-11

[76] Rizzo A.F., Korkeala H., Mojonen I., Gas chromatography análisis of cellular fatty acids and neutral monosaccharides in the identification of Lactobacilli, Applyed and environmental microbiology, (1987) 2883-2888

Chapter 5

A GC/MS analytical procedure for the characterization of glycerolipids, waxes, terpenoid resins, polysaccharide and proteinaceous materials in the same micro sample avoiding interferences from interfering inorganic materials

A procedure for the analysis of the whole content of organic materials present in painting sample has been settled. The GC/MS procedure allows the identification of glycerolipids, waxes, proteins, resinous and polysaccharide materials in the same micro sample from painted works of art. It is based on a sample multy- step chemical pre- treatment consisting in the ammonia extraction of proteins and polysaccharide materials, to separate them from lipid and resinous materials. The extraction is followed by the separation and purification of proteinaceous and polysaccharide materials before the hydrolysis, based on the use of the monolithic sorbent tip technology with a C4 stationary phase. Lipids and resins are saponified/salified separately. Three fractions are generated and analysed separately by GC-MS allowing the quantitative analysis of monosaccharides and uronic acids, aminoacids and lipid material, and molecular patter recognition of resin and wax components.

The procedure was applied to ancient painting samples from a Greek icon. Proteinaceous, lipid and polysaccharide materials were characterized in the samples. The results obtained will be discussed in details.

5.1. Introduction

Samples from painted works-of-art are characterized by the presence of several different organic materials together with pigments, extenders and dryers. GC/MS techniques have demonstrated their suitability for the analysis of samples from works-of-art. Several GC/MS procedures for the characterization of organic materials present in painting samples as binders and varnishes have been developed in the last years [1,2,3,4,5, 6,7,8,9,10,11].

Painting samples are small due to the uniqueness of the work-of-art and the organic materials are minor component. Thus, the optimisation of the procedures in order to obtain maximum information from less amount of sample is a step forward . Recently a GC/MS analytical procedure for the characterization of lipids, waxes, resinous and proteinaceous materials in the same paint micro-sample from a unique painting sample has been described [12]. The procedure is based on a combination of previously published methods [1, 2,7, 8,10] involves a multistep chemical pretreatment of the sample that achieves the separation of an aqueous fraction containing amino acids and of two organic fractions (acidic and neutral), which are both submitted to derivatization by silylation reactions prior to GC/MS analysis. Finally, a clean up procedure has been developed for the elimination of the strong analytical interferences generated by the high amount of inorganic pigments, dryers and fillers in the determination of proteinaceous binders [13]. This procedure has been integrated on the previous one [12], allowing the identification of lipid, resinous and proteinaceous materials in the same paint sample, avoiding interferences from inorganic materials [14]. However, by this procedure polysaccharide materials analysis must be performed on a different sample aliquot [11].

On the basis of the previous studies, a novel GC/MS analytical procedure for the determination of lipids, waxes, resins, proteins and polysaccharide materials in the same paint micro sample in the presence of interfering inorganic materials has been set-up. With this analytical procedure the separation between polysaccharide and

proteinaceous materials is achieved, and purification of proteinaceous binders is simultaneouly performed. This analytical procedure allows:

- to identify proteinaceous binders (egg, collagen, casein, garlic) on the basis of the quantitative determination of the amino acid profile processed by principal component analysis;
- to identify glycerolipids (linseed oil, poppy seed oil, walnut oil and egg) on the basis of the quantitative determination of fatty and dicarboxylic acids, plant resins (Pinaceae resins, sandarac, mastic and dammar), animal resins (shellac), tar or pitches and natural waxes (beeswax, carnauba wax), on the basis of the molecular pattern recognition of long chain alcohols, mid- long-chain acids, hydrocarbons and terpenic molecular markers;
- to identify polysaccharide binders (starch, honey, tragacanth, arabic, fruit tree, guar, and karaya gums) on the basis of the quantitative/qualitative determination of ocurring sugars processed with a decisional scheme.

The characterisation of samples from a Greek Icon of the 15th century will be presented, and the identification of organic components carefully discussed.

5.2 Experimental Section

5.2.1 Reagents

All the solvents were Baker HPLC grade and used without any further purification. Trifluoroacetic acid 99% purity, and anhydrous pyridine were from Fluka (Milan, Italy), ethanethiol (ETSH) 99.5%, sodium azide (NaN3) 99.5% *N*,*O*bis(trimethylsilyl)trifluoroacetamide (BSTFA) with and without 1% trimethylchlorosilane and *N*-*tert*-butyldimethylsilyl-*N*-methyltrifluoroacetamide (MTBSTFA) with 1% trimethylchlorosilane and triethylamine were purchased from Sigma-Aldrich (USA).

The following solutions, apart from those for the amino acids, were prepared by weighing pure substances and were used as standards: (i) amino acids solution in 0.1 N HCl, purchased from Sigma-Aldrich (USA) and containing 12.5 *í*mol/mL of proline (Pro) and hydroxyproline (Hyp) and 2.5 *í*mol/mL of aspartic acid (Asp), glutamic acid

(Glu), alanine (Ala), arginine, cysteine, phenylalanine (Phe), glycine (Gly), hydroxylysine, isoleucine (Ile), histidine, leucine (Leu), lysine (Lys), methionine (Met), serine (Ser), tyrosine (Tyr), threonine, and valine (Val); (ii) fatty acids solution in acetone, containing lauric acid (0.24 mg/g), suberic acid (0.27 mg/g of Su), azelaic acid (0.28 mg/g of A), myristic acid (0.25 mg/g of My), sebacic acid (0.3 mg/g of Se), palmitic acid (0.25 mg/g of P), oleic acid (0.51 mg/g of O), stearic acid (0.51 mg/g of S). All acids, purity g 99%, were purchased from Sigma-Aldrich (USA); (iii) norleucine solution in bidistilled water (Sigma-Aldrich (USA), purity 99%), 138.66 μg/g, was used as derivatisation internal standard for amino acids; (iv) tridecanoic acid solution of isooctane (Sigma-Aldrich (USA), purity 99%), 135.48 μg/g, was used as acidic and neutral fraction derivatization internal standard; (v) hexadecane solution in isooctane (Sigma-Aldrich (USA), purity 99%), 80.34*í*g/g, was used as injection internal standard.; (vi) monosaccharides and uronic acids solution in bidistilled water containing about 100 ppm of d-(+)-galactose (4.8 mg/g), l-(−)-fucose, l-(+)-arabinose, l-(−)-ramnose, l-(−)-mannose, d-(+)-xylose, d-(+)-glucose, d-glucuronic acid, d-galacturonic acid monohydrate and (xi) mannitol in bidistilled water , used as an internal standard. All monosaccharides and uronic acids (purity 99%) were obtained from Sigma–Aldrich (Milan, Italy). All standard solutions were used to derive calibration curves, and were stored at 4°C

5.2.2 Apparatus

- A microwave oven model MLS-1200 MEGA Milestone (FKV, Sorisole (Bergamo), Italy) was used for hydrolysis of proteins and peptides, and saponification/salification of glycerolipid, waxy and resinous materials. Operating conditions will be given in details in paragraph 2.4..
- 6890N GC System Gas Chromatograph (Agilent Technologies), coupled with a 5975 Mass Selective Detector (Agilent Technologies) single golden quadrupole mass spectrometer, equipped with PTV injector. The mass spectrometer was operated in the EI positive mode (70 eV). The MS transfer line temperature was 280°C; the MS ion source temperature was kept at 230°C and the MS quadrupole temperature at 150°C. The mass spectrometer operated in the EI positive mode (70 eV). For the gas chromatographic separation an HP-5MS fused silica capillary column (5%diphenyl-95%dimethyl-polysiloxane, 30m x

0.25mm i.d., 0.25 μm film thickness, J&W Scientific, Agilent Technologies, Palo Alto, CA, USA) coupled with a deactivated silica pre-column (2m X 0.32mm i.d., J&W Scientific Agilent Technologies, Palo Alto, CA, USA) using a quartz press fit was used. The carrier gas was used in the constant flow mode (He, purity 99.995%) at 1.2 ml/min for the proteinaceous and the lipid-resinous fractions, and at 1.0 ml/min for the polysaccharide fraction.

For the analysis of the lipid resinous fraction the PTV injector was used in splitless mode at 300°C and the chromatographic oven was programmed as follows: 80° C, isothermal for 2 minutes, 10°C/min up to 200° C, 200°C, isothermal for 3 minutes, 10°C/min up to 280°C, 280° C, isothermal for 3 minutes, 20°C/min up to 300 °C, 300°C, isothermal for 30 minutes. The For the analysis of silylated amino acids the PTV injector was used in splitless mode at 220 °C and the chromatographic oven was programmed as follows: initial temperature 100°C, isothermal for 2 min, then 4°C/min up to 280 °C, and isothermal for 15 min. For the anlysis of derivatised monosaccharides and uronicn acids, the chromatographic oven was kept at 50ºC for 2 min, then from 50 ºC to 190ºC at 5◦C/min, 20 min at 190ºC, from 190ºC to 280ºC at 5ºC/min, and 280 ºC for 15 min.

Ionisation was performed in electron impact mode at 70 eV.

- A RC10-22 speed vacuum system with a refrigerated ion trap RCT 90 from Thermo Electron Corporation (St. Herblain, France) was used for the drying of the samples.
- The OMIX C4 pipette tips were purchased from Varian (Milan, Italy). They consist of pipette tips 100 μl capacity, containing a miniaturised solid phase extraction bed of functionalised monolithic sorbent, inserted inside the tips. Purification is performed by cycles of loading-unloading of the solution containing the proteins to be purified.
- The cation/anion exchange resin Zerolit DMF, with the inclusion of an indicator and granulometry comprised between 14 and 52 mesh, was supplied by BDH Chemicals Ltd (UK).
- The Solarbox (1500e RH), purchased from Erichsen (Germany), was used for artificial aging of the painted replicas. The conditions of exposure were 572 h at 20°C, 50% relative humidity (RH), and a wavelength range of 280-400 nm.

5.2.3 Samples

a) reference painting layers.

Reference paint layers on glass support and solutions (about 4000 ppm) of arabic, tragacanth and fruit tree gums were prepared at the Laboratory of Pisa. NaN_3 was admixed as biocide.

b) Painting samples from works-of art

Four samples from the Greek Icon Panagia Kardiotissa (15^{th} century) were collected trying to sample the different layers selectively. The painting buil-up presented six pictorial layers applied on a wood support consisting in : (2) ground layer; (3) original paint layer; (4) original varnish; (5) blue/white overpainting; (6) overpainting varnish; (7) superficial layer. Description of the samples is provided in Table 5.1.

Table 5.1 Description of the painting samples analysed.

sample	*description*	*mg*
pK2	Blue overprinting (5), the original varnish (4) and traces of the original paint layer (3)	0,1
pk4	Fragments containing all layers, from the preparation (2) to the final varnish (7). The sample contains also Paraloid B72, used by a restaurer as consolidant.	3,5
pk8	The sample was taken from the mantle of Maria. Wood, ground (2), original paint layer/(s) (3) and some varnish (4).	2,9
pk9	The sample was taken from the halo of Maria. Dark varnish (7) for the determination of the last varnish. The sample also contains a little of the original varnish layer (6).	0,1

5.2.4. Analytical procedure

The overall combined analytical procedure for the determination of glycerolipids, resins, waxes, proteinaceous and polysaccharide materials, also in the presence of high amounts of interfering inorganic pigments dryers and extenders is presented in Figure 5.1 and can be schematised as follows:

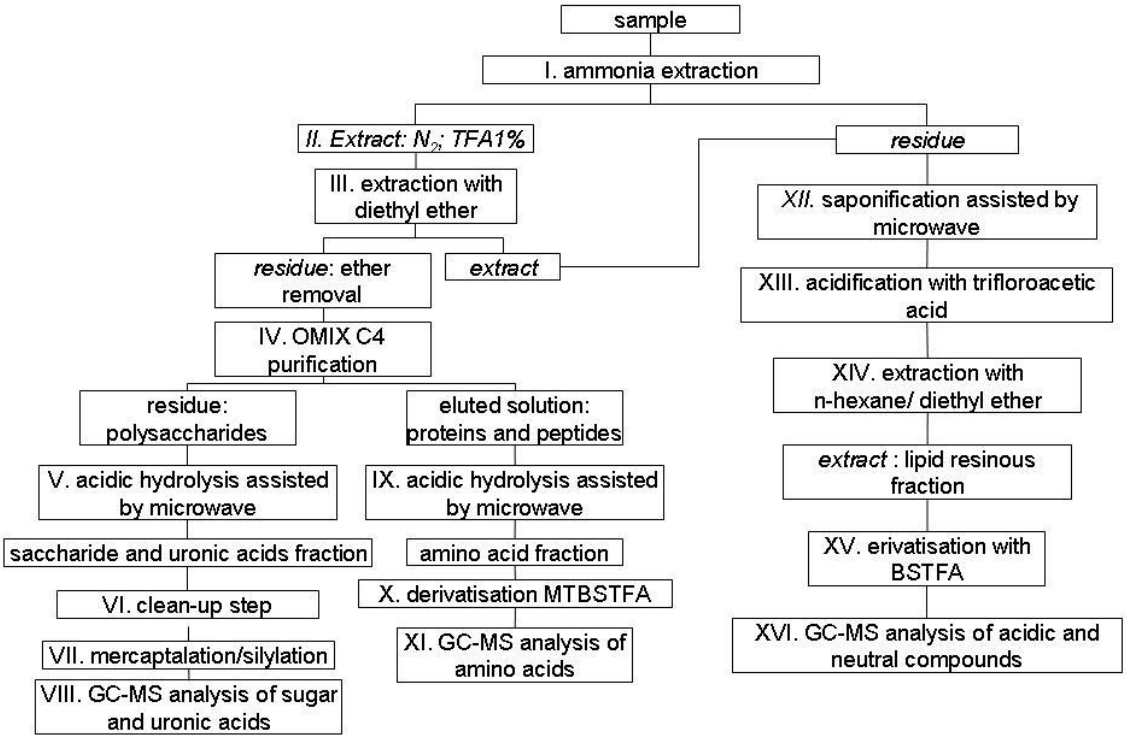

Figure 5.1. Scheme of the GC/MS combined analytical procedure.

I. The sample is subjected to ammonia extraction. To solubilise proteins and polysaccharide and to separate them from insoluble inorganic salts, 200-400 μL of 2.5 N NH_3 are added to the sample in an ultrasonic bath at 60 °C for 120 min, twice. During this step, free organic acids with a certain solubility in ammonia are extracted together with the proteinaceous matter. The residue containing insoluble organic and inorganic species is kept for step XII.
II. The extracted ammonia solution (containing proteinaceous and polysaccharide matter [15,16]) is evaporated to dryness under a stream of nitrogen and redissolved in 100μl of TFA 1%.

III. The acidic solution, containing proteins, saccharides, peptides, soluble salts, and free organic acids, is subjected to extraction with diethyl ether (200 μl, three times). Free organic acids extracted together with proteins and polysaccharides by ammonia in step I are solubilised in ether. The ethereal extracts combined with the residue of the ammonia extraction derived from step I are kept for step XII.

IV. The acidic solution containing proteins, peptides, polysaccharides and soluble organic salts is fluxed with nitrogen to remove the excess of ether and then subjected to the clean up step with a Omix C4 tip [14], using formic acid (0.1 %)/MeOH (75 %)/H_2O (25 %) as eluting solution (100μl, twice) and ten aspirating/dispensing cycles. The rinsing solution admixed with the residue of the purification step are kept for steps V. The purified solution is kept for step XII.

V. The residue admixed with the rinsing solution of the OMIX C4 purification is a solution of soluble inorganic salts, proteinaceous materials that exceed the capacity of the tip, and the polysaccharide material. It is dried under nitrogen stream, admixed with 0.5 ml of trifluoroacetic acid 2M in PTFE closed conic vials, and subjected to microwave assisted acid hydrolysis. Hydrolysis conditions were as follows : power 500 W, temperature 120 ºC, duration 20 min [11].

VI. After hydrolysis, the sample was filtered with a PTFE membrane and then dried in the rotatory evaporator. Once reconstituted in a 100 μl of bidistilled water, the solution of the freed sugars is purified on a Zeolit DMF double-exchange resin, packed on a 0.5 cm diameter glass column. Sugars are eluted with 2 ml of bidistilled water. The aqueous phase is an aqueous solution containing purified monosaccharides and uronic acids: *saccharide and uronic acid fraction.*

VII. An aliquot of the solution containing monosaccharides and uronic acids is added with the derivatisation internal standard solution, evaporated to dryness in the rotary evaporator and subjected to a three step derivatisation: a step of mercaptalation and two steps of silylation (see Chapter 4.3.1.2.). By a mercaptalation step admixing 25μl of ethanethiol/trifluoroacetic acid (2/1,v/v), and keeping at room temperature for 10 min with sporadic shaken, the

corresponding diethyldithioacetals and diethyl dithioacetal lactones are formed. In the first step of silylation, 100 μl of BSTFA are added to the mercaptalation mixture and the mixture is kept 15 minuts at 60 ºC. After drying under nitrogen flow, the second step of silylation consits in admixing 50 μl BSTFA (1% TMCS) as derivatising agent and 100 μl pyridine as solvent. The reaction mixture is kept at 60ºC for 45 min to complitely silylate the mercaptal derivatives of the parental sugars.

VIII. The reaction mixture was then dried under nitrogen flow and redissolved in 50 μl of hexane: 2μl of this solution, containing diethyl-dithioacetal trimethylsilyl derivatives of the parental sugars, were thus injected into the gas chromatograph.

IX. The solution of highly purified proteins and peptides in formic acid (0.1 %)/MeOH (75 %)/H_2O (25 %) is dried under a stream of nitrogen and subjected to acidic hydrolysis assisted by microwaves (power = 250 W for 10 min; power = 500 W for 30 min) in the vapor phase with 30 ml of 6 N HCl at 160 °C for 40 min. After the hydrolysis, bidistilled water (200-400 μl) is added to the acidic hydrolysate. The aqueous phase is an acidic solution containing highly purified amino acids: *amino acid fraction*.

X. An aliquot of the amino acid fraction, admixed with 5 μl of norleucine solution and 10 μl of hexadecane solution, is evaporated to dryness under a stream of nitrogen and is subjected to derivatization with 20 μl of *N-tert*-butyldimethylsilyl-N-methyltrifluoroacetamide (MTBSTFA), 40 μl of pyridine (solvent), 2 μl of triethylamine (catalyst), and at 60 °C for 30 min.

XI. At total of 2 μl of the pyridine solution of derivatised amino acids is analyzed by GC-MS.

XII. The residue of the ammonia extraction, combined with the ethereal extracts, is subjected to saponification/salification assisted by microwaves with 300 μl of KOH_{ETOH} 10% wt at 60 °C for 120 min.

XIII. After saponification, the hydroalcoholic solution is diluted in bidistilled water and acidified with trifluoroacetic acid (aqueous solution 1:1).

XIV. The acidic solution is then extracted with hexane (200 μl, three times) and, afterwards, with dieyhyl ether (200 μl, three times). The extracts are dried under nitrogen flow (to remove trifluoroacetic acid, which is partially soluble

in the organic phase) and redissolved in acetone and hexane (300µl 1:1) : *lipid resinous fraction.*

XV. An aliquot of the lipid resinous fraction is admixed with 5µl of tridecanoic acid solution, evaporated to dryness under nitrogen flow and subjected to derivatization with 20 µl of *N,O*-bis(trimetilsilil)trifluoroacetammide (BSTFA), 200 µl of isooctane (solvent) at 60 °C for 30 min. Finally 5 µl of hexadecane solution are added.

XVI. A total of 2 µl of the isooctane solution of acidic and neutral compounds, eventually derivatized, is analyzed by GC-MS. The analysis of this fraction allows acidic and neutral terpenoid compounds, sterols, alcohols, alkanes, monocarboxylic acids, dicarboxylic acids, and hydroxyacids to be determined.

5.3. Results and Discussion

The combined analytical procedure was tested by using standard solutions and reference materials. Running blanks of the procedure highlighted a low level of contamination of amino acids, monosaccharides, uronic acids and fatty acids. As a result, the detection limit and the quantitation limit were calculated. At a statistical significance level of 0.05, the LOD and LOQ of the proteinaceous, glycerolipids and saccharide materials is reported in Table 5.2.

Table 5.1. Detection and Quantitation Limits of Fatty Acids, Dicaboxylic Acids, Amino Acid, monosaccharides and uronic acids Standard Compounds

compound	*Detection limit /μg*	*Quantitation limit /μg*
Ala	0.01	0.01
Gly	0.03	0.05
Val	0.01	0.01
Leu	0.01	0.02
Ile	0.01	0.01
Ser	0.01	0.01
Pro	0.01	0.01
Phe	0.01	0.01
Asp	0.02	0.03
Glu	0.03	0.05
Hyp	0.01	0.01
lauric acid, suberic acid, myristic acid, sebacic acid, oleic acid	0.1-0.3	0.3
azelaic	0.3	0.5
palmitic	0.6	1.6
stearic acid	1.0	2.5
xylose	0.13	0.27
arabinose	0.02	0.05
ramnose	0.01	0.01
fucose	0.01	0.01
galacturonic acid	0.00	0.00
glucuronic acid	0.00	0.00
glucose	0.44	0.85
mannose	0.11	0.20
galactose	0.03	0.06

It is important to highlity the higher level of contamination of glycerolipids and saccharide material components, with respect to proteinaceous materials: the sum of acids at the LOD level for glycerolipids components is in fact 2.4 μg, that of saccharide components is 0.75μg, and that of proteinaceous is 0.14μg.

To perform the analysis of polysaccharide, proteinaceous, and lipid resinous materials in the same sample requires the separation of three different fractions, to be chemically processed in different ways:
-proteinaceous materials require hydrochloric acid 6M as hydrolysing agent, being the microwave assisted hydrolyses performed in open glass conic vials (power 250W, temperature 160°C, duration 40 minutes)
-polysaccharide materials require trifluoroacetic acid 2M as hydrolysing agent, being the microwave assisted hydrolysis performed in closed PTFE conic vials (power 500 W, temperature 120 ºC, duration 20 min).
-lipid resinous materials require salification/saponification with KOH10% in ethanol, being the microwave assisted reaction performed in closed PTFE conic vials (power 200 W, temperature 80°C, duration 60 min).
This indicates that to determine saccharide material in the same sample used for the determination of proteinaceous and lipid resinous materials, it is necessary to evaluate the behaviour of plant gums when subjected to the ammonia extraction used to separate proteins from lipids and resins, and when subjected to the C4 purification procedure, used to eliminate inorganic materials from the proteinaceous fraction.

5.3.1 Settling up of the analytical procedure

5.3.1.1 Ammonia extraction of polysaccharides.

Analysis of reference painting samples of plant gums were done with and without ammonia extraction in order to evaluate the % of gum recovered. The ammonia extraction of arabic gum, fruit tree gum and tragacanth gum were performed as follows : 200-400 μL of 2.5 N NH_3 were added to the sample in an ultrasonic bath at 60 °C for 120 min, twice. After the extraction, the dried ammoniacal fraction was hydrolysed and the procedure followed as described in literature for the analysis of polysaccharide materials (see Chapter 4). This way, the recovery percentage of sugars was calculated as the sum of the amount of monosaccarides and uronic acids detected, with respect to the quantity of gum weighted. The same procedure was performed with reference painting layers UV light aged for 3 weeks. The data obtained are presented in Table 5.2.

Table 5.2. Recovery of polysaccharide material obtained from the ammonia extraction of gums reference paint layers. Five replicates were analysed for each sample.

Gum	*Non aged no extraction*		*Non aged NH_3 extraction*		*3 week aged No extraction*		*3 week aged NH_3 extraction*	
	%recovery	RSD	% recovery	RSD	% recovery	RSD	% recovery	RSD
Arabic	64	18	50	30	95	25	80	5
Tragacanth	23	18	26	9.8	23	23	16	14
Fruit tree	62	5	53	4	62	15	47	4

Results showed that the percentage of polysaccharide material that is extracted by ammonia ranges between 70 to 113% of the amount of polysaccharide binder that can be recovered by direct hydrolysis of the sample. Moreover, no significant differences are observed between aged and not aged reference paint layers, in terms of differences between the recovery obtained with direct hydrolysis and recoveries obtained with ammonia extraction followed by hydrolysis. Interestingly, for arabic gum ageing increases the amount of gum that can be recovered.

5.3.1.2 OMIX C4 tip step.

Analysis performed with ammonia extraction of the gums adding the step of purification by using the C4 tip indicated that :

- The percentage of saccharide material loaded to the tip and eluted with the proteins is lower than 1% for the three gums tested.
- The percentage of the saccharide material recovered from the rinsing solution of the purification step admixed with the residue of the purification is higher than 70 % for the tree gums tested.

This indicates that a fraction of the polysaccharide material is retained on the C4 stationary phase and not eluted by the eluting solution for proteinaceous materials, nor the rinsing solution.

As a result, the use of C4 sorbent tips permits to obtain a fraction containing highly purified peptides and proteins, and a residual solution, which contains polysaccharide

materials, soluble inorganic materials and the residue of the proteinaceous materials that exceeded the tip capacity.

Considering that:
- the amount of saccharide material that can be extracted by the ammonia solution is at least 70% of the amount of the material that can be determined by direct hydrolysis;
- the amount of saccharide material that can be recovered when the C4 separation is performed is at least 70% of the material that has been extracted;
it is possible to conclude that the whole procedure applied on a paint sample permits to determine at least the 49% of the saccharide material that could be determined if the sample would be subjected to direct hydrolysis. It is thus possible to make a rough estimation of the minimum amounts of polysaccharide binders that can be determined with this procedure. Evaluating the LOD of the polysaccharide material about 0.75 μg (as obtained by summing up the LOD obtained for each aldose and uronic acid quantified), it can be calculated that the procedure permits to obtain a chromatogram with signals above the detection limit level when the amount of saccharide material is 1.5μg. This indicates that a paint sample of 0.1mg, containing a polysaccharide content which is the 10% of the sample weight, leads to a signal that is five times higher than the minimum amount of polysaccharide binder that can be determined.

5.3.1.3 Conclusions

This indicates that this analytical procedure is fully suitable to determine polysaccharide binders in the same sample used for the determination of proteinaceous, glycerolipids, waxy and resinous materials. This is extremely important when unique and small samples from valuable paintings are available. When the sample is, in fact, divided into different fractions to be analysed with different analytical procedures, there is the risk of loosing information because the materials present could fall under the detection limit of the procedure. Moreover the possibility to determine simultaneously on the same sample all organic materials is fundamental when sub-samples are obtained from the original sample (for example when separating different paint layers), or when highly heterogeneous samples are available. Only in this way, in fact, it is possible to be sure that the materials determined belong to the same sample, and do not pertain to different areas or layers of the same sample.

5.3.2 Analysis of Paint Samples from the Greek Icon

The most abundant peaks in all chromatograms of the lipid-resinous fraction are palmitic, stearic, suberic and azelaic acids. The low content of dicarboxylic acids are not consistent with the presence of a siccative oil but suggests the presence of a non drying lipid material.

The analysis of the lipid resinous fraction permits to draw the followings:

- long chain fatty acids with an even number of carbons (from palmitic to dotriacontanoic acid), (ω-1) hydroxy acids with an even number of carbons (from 15 hydroxy hexadecanoic acid to 23-hydroxytetracosanoic acid), long chain linear alcohols with a even number of carbons (from tetracosanol to dotriacontanol), long chain (α,ω-1) diols with a even number of carbons (from 1,23-tetracosandiol, to 1,27 octacosandiol), and long chain linear saturated hydrocarbons with a odd number of carbons (from heptacosane to hentriacontane), all point to the occurrence of beeswax in samples spk4 and pk8
- azelaic, myristic, sebacic, palmitic, oleic and stearic acids, point to the occurrence of a fat in all samples . The low amounts of dicarboxylic acid indicates that the fatty material has non-drying properties in all samples
- Dehydroabietic acid together with 7-oxo-dehydroabietic acid are the main constituents of a oxidised diterpenoid resin from the *Pinaceae* family in samples pk2 and pk8
- Butolic, aleuritic, epilaccishellolic and laccishellolic acids (together epishellolic and shellolic acids, not shown in the chromatogram) point to the occurrence of an oxidised sesquiterpenoid resin of animal origin: shellac, which is present in all samples.
- Mastic was identified in sample pk4

The analysis of the amino acid fraction highlighted the presence of proteinaceous material. The occurrence of hydroxyproline, a marker of collagen, indicates that animal glue is present in samples pk4, pk8 and pk9. The quantitative percentage content of amino acids of the painting samples (reported in Table 5.3) determined from the amino acid fraction was subjected to a multivariate statistical analysis together to a

data set of 121 reference samples of animal glue, egg and casein, using the principal components analysis (PCA) method [17].

Table 5.3. Amino acidic relative percentage content of samples pk2, pk4, pk8 and pk9.

Sample	*Ala*	*Gly*	*Val*	*Leu*	*Ile*	*Ser*	*Pro*	*Phe*	*Asp*	*Glu*	*Hyp*
pk2	2.6	4.4	46.3	8.9	4.2	2.3	7.2	1.6	6.6	15.8	0.0
pk4	9.1	24.6	5.6	3.7	4.7	5.1	12.2	3.0	8.5	19.0	4.4
pk8	8.7	25.5	3.0	4.7	2.2	6.2	13.1	3.2	9.7	17.6	6.1
pk9	5.1	14.3	6.0	14.7	6.2	10.3	5.2	5.1	12.5	20.0	0.7

The PCA score plot presented in Figure 5.2 shows that samples pk2, pk9 and pk8 are located in the clusters of casein, egg and animal glue, respectively. In the case of pk4 though being situated next to the cluster of animal glue, it is not possible to exclude that another proteinaceous materials is simultaneously present, as it can be assessed from its position in the PCA score plot. This result would be in agreement with the detection of cholesterol in the lipid resinous fraction.

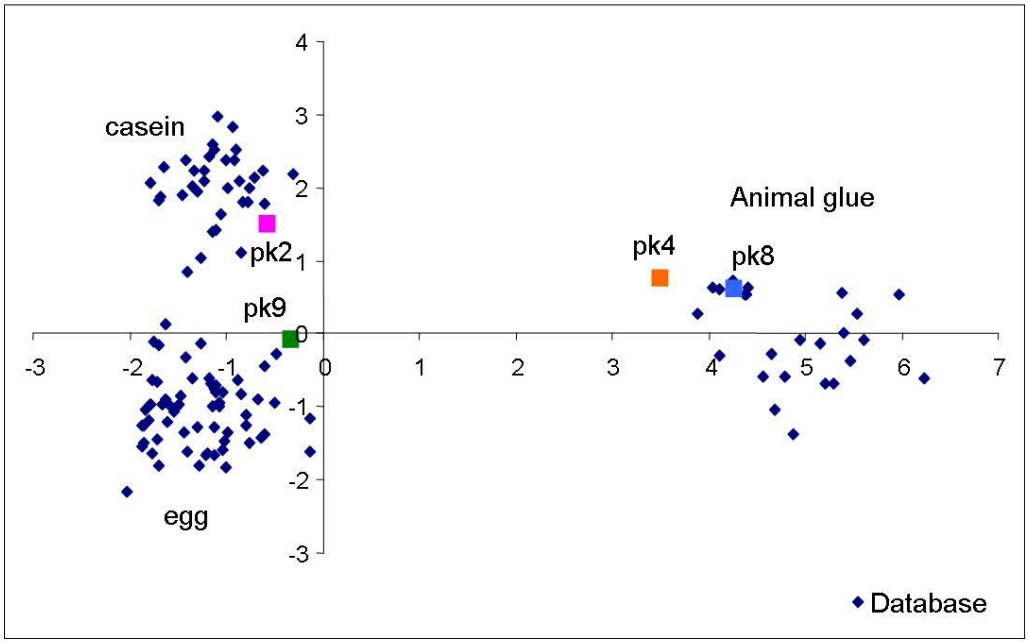

Figure 5.2. Principal Component analysis score plot of the amino acids percentage relative content in samples pk2, pk4, pk8 and pk9.

Finally, the saccharide fraction of the samples presented different characteristics. The glycoside profiles are presented in Table 5.4.

Table 5.4. Glycoside profile of samples pk2, pk4, pk8 and pk9.

Sample	*Sugars*									*Saccharide content /µg*	*% saccharide content*	*Decisional scheme*
	Xyl	Arab	Ramn	Fuc	Gal Ac.	Gluc. Ac.	Gluc	Mann	Galact			
pk2	y	y	0.0	0.0	0.0	0.0	0.0	0.0	y	0.77	0.8	-
pk4	0.0	0.0	00	0.0	0.0	0.0	50.0	19.8	30.2	1.70	0.05	-
pk8	50.4	6.2	2.5	0.0	0.0	1.7	0.0	15.9	23.3	1.60	0.05	Fruit tree
pk9	8.4	0.8	1.6	1.0	0.0	0.0	69.6	13.3	5.3	13.2	13.2	-

Sample pk2 showed a saccharide content between the detection and quantitation limits. However, the presence of galactose would be in agreement with the milk identifcation in the amino acid fraction (see above). Samples pk4, pk8 and pk9 presented a saccharide content higher than the quantitation limit. For pk4, the glycoside profile could be explained on the basis of the simultaneous occurrence of egg, animal glue, Pinaceae resin, shellac and mast resin. For sample pk8, by using the decisional scheme (see 4.3.2.) the presence of mannose, glucuronic acid and ramnose and the absence of fucose and galacturonic acid identifies a fruit tree gum, though the quantitative glycoside profile is not correspondent with the reference layers (see Table 4.13.). Finally, sample pk9 presents a high content of saccharide material but the profile is not coincident with any of the reference materials studied in Chapter 4, remaining thus unidentified.

Results obtained by applying the combined procedure for each sample are summarised in Table 5.5.

Table 5.5 Summary of the organic materials identified in each sample.

Sample	*Lipid resinous fraction*	*Amino acid fraction /PCA*	*Saccharide fraction/decisional scheme*
pk2	Non drying fat Shellac Pine resin	Milk	-
pk4	pine resin Shellac wax mastic resin	animal glue	
pk8	Wax Shellac	Animal glue	Fruit tree
pk9	Pine resin Shellac	Egg	Saccharide material

The interpretation of the results for each sample can be used to understand the pictorial technique. The sample build-up, layer by layer, results can be interpreted as follows:

- Ground layer (2): animal glue
- Original paint layer (3): egg
- Original varnish (4): shellac and pine resin
- Blue / white overpaint (5): milk/ fruit tree
- Varnish of the overpaint (6): mastic resin
- Final varnish (7): shellac, pine resin, egg, polysaccharide material

Beeswax seems to be a restoration material non homogeneously distributed on the painting.

5.4. General conclusions

An analytical procedure for the simultaneous characterization of drying oils, animal and plant terpenoid resinous materials, natural waxes, polysaccharide materials and proteinaceous binders on the same microsample by means of GC/MS has been

optimised. The procedure can be used also when high amounts of inorganic materials are present.

The application of the proposed analytical procedure to reference materials shows that it is suitable for the simultaneous characterization of proteinaceous and polysachharide material as their separation by means of a C4 stationary phase has been ascertained. This way, the procedure is suitable for the simultaneous characterization of several classes of compounds and thus, for the identification of proteinaceous material, drying oils, natural waxes, plant resins, shellac and polysaccharide materials in paint samples.

The procedure has been used to characterize samples coming from a Greek icon of the 15th century. Data obtained allowed us to identify the materials used, and the differential sampling of paint flakes containing different layers permitted to understand the organic material composition in the sample build-up, achieving a deeper knowledge on the painting technique. Different natural resins (shellac, mastic resin and Pinaceae resin) together with proteinaceous materials (egg, milk and animal glue), and polysaccharide materials (fruit tree gum and an unidentified material) were used as varnishes and paint binders.

References

[1] Bonaduce, I.; Colombini, M. P. *Rapid Commun. Mass Spectrom*. 2003, *17*,2523-2527.

[2] Colombini, M. P.; Modugno, F.; Giacomelli, A. *J. Chromatogr. A* 1999, *846*,101-111.

[3] de la Cruz-Canizares, J.; Domenech-Carbo, M. T.; Gimeno-Adelantado, J.V.; Mateo-Castro, R.; Bosch-Reig, F. *J. Chromatogr. A* 2004, *1025*, 277-285.

[4] van den Berg, J. D. J.; van den Berg, K. J.; Boon, J. J. *J. Chromatogr. A*2002, *950*, 195-211.

[5] Chiavari, G.; Gandini, N.; Russo, P.; Fabbri, D. *Chromatographia* 1998, *47*,420-426.

[6] Gimeno-Adelantado, J. V.; Mateo-Castro, R.; Domenech-Carbo, M. T.; Bosch-Reig, F.; Domenech-Carbo, A.; Casas-Catalan, M. J.; Osete-Cortina, L. *J.Chromatogr. A* 2001, *922*, 385-90.

[7] Colombini, M. P.; Bonaduce, I.; Gautier, G. *Chromatographia* 2003, *58*,357-364.

[8] Bonaduce, I.; Colombini, M. P. *J. Chromatogr. A* 2004, *1028*, 297-306.

[9] Regert, M.; Colinart, S.; Degrand, L.; Decavallas, O. *Archaeometry* 2001,*43*, 549-569.

[10] Bonaduce I., Colombini M.P, Gautier G., Modugno F., Ribechini E. Anal. Chem. 2006, 78, 4490-4500

[11] Bonaduce I., Brecoulaki H., Colombini M.P., Lluveras A., Restivo V., Ribechini E., *J. Chromatogr. A 1175 (2007) 275–282*

[12] Andreotti A., Bonaduce I., Colombini M.P., Gautier G., Modugno F., Ribechini E., Anal. Chem. (2006) 78: 4490-4500.

[13] Gautier G., Colombini M.P., *Talanta* (2007) 73: 95-102.

[14] Bonaduce I., Cito M., Colombini M.P. "The development of a GC-MS analytical procedure for the determination of lipids, proteins and resins in the same paint micro-sample avoiding interferences from inorganic media", *submitted for publication*

[15] Colombini M.P., Modugno F., Giacomelli A., *Journal of Chromatography* A (1999) 846 (1+2): 101-111.

[16] Rampazzi, L.; Cariati, F.; Tanda, G.; Colombini, M. P. *J. Cult. Herit*. 2002, 3, 237.

[17] R. G. Brereton, 'Chemometrics.Data Analysis for the Laboratory and Chemical Plant', J. Wiley & Sons Ltd, West Sussex, England, 2004,chapter 4, ISBN 0-471-48978-6

Conclusions

This thesis demonstrated the capacities of Synchrotron Radiation for the FTIR imaging in transmission mode and the capacity of Gas Chromatography/mass spectrometry to the study of painting materials and decay by-products, with particular attention to saccharide materials. Moreover, the complementary of the techniques has been highlighted several times.

Synchrotron radiation characteristics demonstrated their suitability for the micro-imaging of samples cross-sections. SR μFTIR in transmission mode, which requires an adapted sample preparation, was investigated as a powerful imaging tool in paintings. Testing of different preparation methods showed that embedding in an epoxy resin and microtoming was the approach that gave better results. Several samples were prepared as described before and the main difficulties and limitations encountered have been highlighted. Issues arisen are: the infiltration of the embedding resin in the sample, the difficulty of performing the microtoming avoiding the crumbling of the sample, and the flattening of the slice to improve spectra quality in order to permit imaging. Among several samples, a group of four samples from a silvered door painted on the surface were prepared and successfully investigated, allowing to establish the painting technique in detail.

The nature of painting samples, requires the imaging approach to characterise the sample build-up. It has also been evidenced that imaging techniques often require of the previous characterisation of the materials. Several techniques have been applied to fully characterise paint samples, and results are shown in chapters 2 and 3. By this way the painting techniques of a stone altarpiece of the 11^{th} century, a gypsum shield of the 17^{th} century and of the gilding decorations of a crypt dating back to the 16^{th} century, have been ascertained. Analyses permitted to identify pigments and binders, as well as decay by-products and, as a result, information was gained on the oxalates formation processes in paintings. Mainly the role of the organic material and the nature of the oxalates formed in paintings were highlighted.

Therefore, the importance of a multi analytical approach has been evidenced. Conventional FTIR and PY/GC/MS were used as screening techniques, allowing to quickly characterise the main components, organic and inorganic, of several samples. GC/MS was then used on a selected number of samples and demostrated to be a fundamental tool for the characterisation of a paint micro samples, permitting the identification of organic materials through quantitative analysis and molecular patter recognition. Synchrotron experiments, applied on the same sample selection, permitted to find out the organic and inorganic material distribution both in depth and along the sample by the chemical images of the functional groups. SR XRD was finally applied on one sample, providing unequivocal pigment identification, and allowing to obtain information on the distribution of crystalline compounds.

The combined interpretation of the results obtained from all these techniques on the same sample (optical microscopy, SEM-EDS; FTIR, Py/GC/MS, GC/MS, SR FTIR and SR XRD) allowed us to clearly establish the stratigraphy of the different samples, the materials used and, thus, the evolution of the painting technique of Josep Maria Sert.

The chemical characterization of the binding media present in a painting sample was demostrated as being of both particular interest and difficulty. Attention has been paid to polysaccharide materials. A procedure for the characterization of polysaccharide materials in painting samples has been settled. The analytical procedure generates just one peak per analite, high reproducible chromatograms and good reaction yields overcoming the formation of derivatisation reaction by-products. The study of samples from works of art evidenced that profiles obtained are not necessarily in agreement with reference data. Working with reference painting materials highlighted that the presence of inorganic materials, proteinaceous media and bacteriological attack does modify qualitatively and quantitatively the profiles of plant gums. These interesting results shed some light on the degradation phenomena undergone by saccharide materials, about which very little is known, and highlighting the necessity to systematically carry on these investigations.

To prevent the risk of loosing information due to the fact that the materials present could fall under the detection limit of the procedure, and also when the identification

of the painting technique is investigated, the use of analytical procedures that permit to fully characterise the organic material content of the same sample is desirable. The characterisation of polysaccharide materials has been successfully included in a combined GC/MS analytical procedure that allows the characterisation of glycerolipids, waxes, natural resins, proteinaceous materials in the same micro sample, also in the presence of high amounts of inorganic materials.

Acknowledgments

AGAUR (Agència de gestió d'Ajuts Universitaris I de recerca) is acknowledged for the research grant (BE00729) that permitted the stage at the University of Pisa to learn the chromatographic analytical techniques. We also acknowledge the European Synchrotron Radiation Facility for provision of synchrotron radiation facilities as part of the project EC38 (Calcium oxalate formation in mural paintings) and we would like to thank Isabelle Lethard and Marine Cotte for assistance in using beamline ID18F and ID21, respectively.

Els Serveis Cientifico-Tècnics of the Universitat de Barcelona and the Departament of Crystallography are acknowledge for their help in different steps of the thesis. Anna Vila and Gema Martinez-Ruiz (Serveis Cientifico-Tècnics, Universitat Barcelona) are particularly thanked for their help in the sample preparation step and also for their true involvement in the project.

Prof. Michael S. Tite (Oxford University) and Dr. Lorenzo Appolonia (Direzioni di Bieni Culturale de Valle d'Aosta) are thanked for their suggestions and helpful discussion, and Mr. Manolis Pantos (SR Daresbury Laboratory) for his helpful assistance in synchrotron facilities.

The project "Chemistry, technology and evolution of the architectural painting in the mountain areas: conservation and valorization" (Comunitat de Treball dels Pirineus project ITT2005-1/10.00.) is acknowledged for the research founding.

The Museu de Terrassa is acknowledged for supplying the altarpiece painting samples.

The paint samples presented here was analysed as part of a collaborative project within the European network "Community support for cultural development projects (98/c 6/08, Action No.3) between the Department of Chemistry and Industrial Chemistry of the University of Pisa and the Technological Educational Institution (T.E.I.) of Athens (Prof. Eleni Ioakimoglou). Dr. Constantios of the Byzantine and Christian Museum of Athens is acknowledged for supplying the sample.

Professor Giancarlo Ranalli from University of Molise is acknowledged for performing the biological attack on reference paint layers.

Appendix A

Introducció

Una obra d'art no és només un concepte artístic-estètic sinó també un objecte material. Des de l'antiguitat els materials i la tècnica emprada pel pintor han estat de gran importància per a obtenir els efectes estètics desitjats. Cennino Cennini al S.XV va descriure el que és la pintura: "(...) Els fonaments de l'art són dibuixar i pintar. Totes dues coses requereixen això: pulir, tallar, esmicolar, daurar, acolorir, adornar i envernissar una fusta (...) ", mentre que Joan Miró recomanà a C. Enric Ricart el següent :" He canviat la manera de preparar la tela (...)la preparo amb rovell d'ou, segons la recepta d'en Sunyer, preparada tal i com li ensenyà en Matisse. Si t'interessa ja t'enviaré la fórmula. Si tu continues preparant les teves teles amb aquell gruix de guix ja cal que l'hivern vinent, si exposem a Madrid, transportis les teves pintures amb un vagó-llit i amb una infermera que vigili que pel viatge no se't crivellin (...)".

Durant l'Edat Mitjana, diversos manuscrits descriuen les diferents tècniques pictòriques, els materials que calia utilitzar i la qualitat d'aquests. Des del *Codex Lucensis* o *De coloribus et artibus Romanorum* escrit per Heracli (s.VIII) fins al *De Diversis artibus* de Teophilus (s.XII) o el *Trattato della pittura* de Leonardo da Vinci, recullen el saber popular en l'art de la pintura. Durant els segle XV, i posteriorment durant el Renaixement, els llibres *Il llibre dell'Arte* de Cennino Cennini (S. XV), el *Mappae clavícula* (S. XV), el Manuscrit de Bologna (S. XV) o l'Art de la Pintura (1649) de Francisco Pacheco han deixat testimoniatge de l'evolució de la tècnica pictòrica.

En un segon moment, Mary P. Merrifield va presentar l'any 1846 "*L'art de la pintura al fresc a l'Edat Mitjana i al Renaixement"*, on descriu els mètodes utilitzats per mestres com Alberti, Cennini, Vasari o Borghini, traduïts a l'anglès. A més, l'autora va examinar també les causes de la degradació dels frescos i la manera de retocar, reparar i netejar aquestes obres d'art. De la mateixa manera, el segle passat, quan el camp de la restauració d'obres d'art començà a reclamar informació de caràcter tècnic, han estat publicats diversos llibres sobre tècniques de pintura, sobre els materials utilitzats i els que cal utilitzar en les restauracions.

Avui en dia, l'estudi de mostres de pintura persegueix diferents objectius. D'una banda, identificar els materials i la tècnica pictòrica emprada en un període històric per tal d'establir el seu coneixement tècnic i material. D'altra banda, estudiar la degradació, l'envelliment i el deteriorament sofert per les pintures per tal d'evitar la seva desaparició i aplicar els processos de restauració més adients.

Establir la composició química de les pintures dóna informació sobre la capacitat tècnica dels artistes/artesans d'un cert període i la tecnologia de què disposaven. D'aquesta manera es pot arribar a conèixer la cultura i els costums del període històric de manufacturar l'obra així com els processos de restauració de l'obra al llarg de la seva història i l'estat de conservació de la mateixa. L'avaluació de l'estat de conservació així com el coneixement dels materials presents i de la tècnica emprada pel pintor són un pas fonamental per a l'establiment del procediment de restauració si ens volem assegurar que els nous materials no interfereixin amb aquells originals i que alhora es respecti al màxim la voluntat estètica original de l'artista.

Els materials orgànics presenten problemàtiques afegides ja que, no només la mostra és petita i el contingut en material orgànic és sovint inferior al 10%, sinó que es poden trobar totes les barreges possibles de materials de tal manera que la puresa és pràcticament inexistent i , a més, les proporcions poden variar d'una mostra a una altra i ,fins i tot,poden ser heterogènies dins d'una mateixa mostra. L'envelliment és molt més acusat en el cas dels materials orgànics i al mateix temps pot variar en funció de les condicions (temperatura, humitat relativa, etc) i de les interaccions específiques establertes amb els compostos inorgànics presents a la mostra com a pigments o càrregues. Per últim, la presència de tots aquests compostos inorgànics, en la majoria de tècniques analítiques, pot interferir en la determinació dels materials orgànics no permetent la seva identificació.

Des d'un punt de vista fisico-químic, les pintures son 'composites', és a dir, estan formades per diverses capes, al seu temps constituïdes d'una barreja heterogènia de materials (orgànics i inorgànics). A més, aquests materials experimenten interaccions

entre ells i un envelliment heterogeni amb el temps i amb l'exposició a contaminants, a la llum i a les condicions de conservació (humitat, temperatura). Així doncs, les mostres de pintura són sistemes complexos degut a les seves característiques intrínseques i estan molt lluny de ser objectes estàtics. Aquestes característiques, juntament amb la quantitat de mostra de qué es disposa (sovint inferior a 1 mg) fa que, des d'un punt de vista analític, les pintures siguin una problemàtica difícil.

A les pintures, els materials inorgànics (pigments, espessidors, polidors, estabilitzants, assecadors) i els orgànics (aglutinants, vernissos, colorants) es troben barrejats en proporcions desconegudes i disposats en capes micromètriques. A més, els materials orgànics utilitzats com a aglutinants (llet, caseïna, cola animal, oli de llinosa, sang, cera, gomes vegetals, mel, resines vegetals, etc) són complexes barreges naturals amb diferents proporcions de proteïnes, triglicèrids, terpens, esterols , hidrocarburs, esters, alcohols, àcids lliures, polisacàrids, etc. Diferents estratègies s'han utilitzat des del principi del segle XX amb la finalitat d'investigar els materials constituents de les obres d'art. Un esguard a la bibliografia sobre l'estudi i la caracterització de mostres de pintura destaca l'àmplia gamma de tècniques aplicades en les obres d'art en general i les mostres de pintura en particular. A partir de tècniques com l'espectroscòpia de FTIR (espectroscopia infraroja amb transformada de Fourier) i Raman, la difracció de Raigs X (DRX), la Fluorescència de Raigs X (XRF) o la Ressonància magnètica nuclear (RMN) passant per les tècniques electroquímiques s'han aplicat a la caracterització de materials de pintura. Per a la caracterització dels compostos orgànics en les mostres de pintura i el seu comportament amb l'envelliment, les tècniques cromatogràfiques acoblades a espectrometria de massa (GC/MS, DE/MS, Py/GC /MS) són els mètodes que ofereixen majors prestacions.

Tanmateix, la comprensió de la tècnica pictòrica així com dels processos de degradació de les pintures, pel fet de ser formades per capes heterogènies, requereix de la localització en la mostra de l'acumulació dels materials i els productes de degradació formats. Per tant, es necessiten tècniques d''imaging', que permetin resoldre les heterogeneïtats elementals i moleculars, tant a dins com entre les capes. La condició micrometrica de les mostres implica que, per tal d'establir aquestes variacions en la composició de les mostres, es necessitin tècniques de micro imaging. Tradicionalment, el microscopi òptic (LM) i el microscopi electrònic d'escombratge han estat

àmpliament utilitzats en la caracterització de seccions de mostres de pintura. Els avantatges de l'espectrometria de masses d'ions secundaris (SIMS), l'FTIR i ,també, de la radiació Sincrotró han estat emprats per tal d'obtenir informació sobre la distribució de pintures

Ara bé, s'ha proposat un enfocament multi-analític per tal de caracteritzar completament i inequívocament els materials iels productes de degradació, i, per tant, la tècnica pictòrica i els mecanismes d'envelliment en les mostres de pintura.

L'objectiu d'aquesta tesi és el d'omplir algunes llacunes en l'anàlisi i caracterització dels sistemes pictòrics. En aquest sentit, s'han desenvolupat dues línies principals de manera paral.lela: d'una banda l'estudi de la distribució de materials a la mostra i d'altra la caracterització de materials orgànics, concretament la dels materials polisacàrids. Per tant, encara que en cada capítol es presenta un tema diferent. l'objectiu de completar el coneixement parcial obtingut en el capítol anterior pot ser considerat com un fil conductor.

El contingut dels capítols es poden resumir com segueix:

Capitol 1. Aplicacio de SR micro imaging FTIR per l'estudi d'estratigrafies
L'objectiu del capítol és mostrar els resultats dels mètodes de preparació de la mostra, en mostres amb un alt contingut de compostos inorgànics, i proporcionar introduir la seva problemàtica. La naturalesa de les pintures formades per diverses capes i l'heterogeneïtat de l'envelliment dels materials que les formen requereix d'una aproximació en dues dimensions, amb la finalitat de poder, no només d'identificar i caracteritzar els materials presents, sinó també obtenir-ne la seva distribució. La brillantor característica de la radiació sincrotró permet treballar amb mides de feix micromètriques sense pèrdua significativa de flux d'energia. Això significa que les tècniques de micro imaging, com la micro-XRF. micro-FTIR, micro-DRX o micro-XANES es poden aplicar a seccions de mostres pictòriques proporcionant-nos informació de la distribució química i elemental de les seccions transversals. L'FTIR és una tècnica que permet la identificació dels materials orgànics i dels inorgànics, per la qual cosa, és especialment interessant en la caracterització de mostres de pintura. En

aquest capítol es presentarà a l'aplicació de SR micro FTIR ,tècnica en transmissió, a mostres de pintura decorativa.

Capitol 2. Caracterització i distribució d'oxalats en mostres de pintura mural

En aquest capítol s' il.lustra l'anàlisi de pintures murals que presenten degradació, mitjançant tècniques de microimaging basades en la radiació sincrotró. L'objectiu dels experiments és el d'identificar i obtenir la distribució espacial dels productes de degradació dels materials caracteritzats. Concretament, es pretén obtenir informació sobre la formació d'oxalats en les mostres de pintura, i afegir dades sobre els seus mecanismes de formació en mostres de pintura mural. La determinació de la distribució en profunditat dels oxalats respecte a la dels materials orgànics contribueix a aclarir la seva atribució a un bio-construcció o bé, a un producte resultant de la degradació química dels aglutinants presents a la mostra. A més, els resultats van ajudar a caracteritzar de manera inequívoca la tècnica pictòrica i les fases cristal.lines.

Capitol 3. Tècniques Mass Spectromètriques, Spectroscópiques i basades en la radiació sincrotró per a la caracteristzació de mostres de pintura: aproximació multi-analítica

La completa caracterització de les mostres de pintura és sempre un problema complex des d'un punt de vista analític. A mès, la identificació d'aquests materials no ha de ser l'únic objectiu de les investigacions d'anàlisi sinó que la distribució d'aquests materials i la dels seus productes de degradació, mitjançant tècniques d'imaging, és fonamental per comprendre la tècnica pictòrica i per a millorar el nostre coneixement sobre l'estat de conservació de la pintura i els mecanismes de degradació. Combinar l'ús de tècniques basades en l'espectrometria de massa, com la GC/MS o Py/GC/MS, amb tècniques que permeten el mapping de grups funcionals com el SR FTIR en transmissió sobre estratigrafies, pot ser un enfocament adequat per obtenir una detallada caracterització dels materials orgànics en una mostra de pintura, assegurant la seva localització en la mostra. Per tal de complementar la informació sobre els materials pictòrics, SR i DRX s'han utilitzat com a eines perfectes per a la

identificació inequívoca dels materials cristal.lins. Aquest enfocament analític s'ha utilitzat per estudiar mostres del pintor mural català Josep Maria Sert i Badía (segle XX).

Capitol 4. Procediment analític fonamentat en la GC/MS per a la caracterització de materials polisacarídics

En aquest capitol s'ha optimitat un procediment analític basat en la GC / MS. Aquest procediment està basat en la silanització desl derivats mercaptalats d'aldoses i d'àcids urònics alliberats de la matriu de la mostra mitjançant hidròlisis assistida per microones. L'ús d'aquest mètode genera un únic pic cromatogràfic per cada compost i uns cromatogrames altament reproduïbles. La purificació per eliminar els pigments inorgànics, que poden interferir en la derivatització, es realitza mitjançant l'ús de resines d'intercanvi iònic. Els resultats presentats es refereixen a mostres de pintura de la zona del Mediterrani des del segle IV aC fins al segle XIX dC. La possible contaminació d'origen biològic i la degradació dels polisacàrids en les mostres de la pintura serà especialment considerada. Des del 3r mil.lenni AC, els polisacàrids han estat àmpliament utilitzats com a aglutinants. Polisacàrids, com les gomes vegetals, sucre, farina o mel, són considerats en antigues receptes i, també, han estat àmpliament utilitzats per a la restauració i els processos de consolidació. La seva caracterització i la identificació no és senzilla, ja que es barregen en diferents proporcions amb altres productes naturals com ara les proteïnes, resines i olis. Per tant, problemes analítics, com la puresa i la baixa quantitat petita mostra s'han de tenir en compte. A més, els materials orgànics poden patir l'envelliment i els processos de degradació que poden ocasionar canvis en la seva composició química i en les seves propietats.

Capitol 5. Procediment combinat per a la caracterització de materials proteics, polisacarídics, lipídics i resinosos en una única mostra amb alts continguts inorgànics.

El procediment basat en la GC / MS permet la identificació dels lípids, les ceres, proteïnes, polisacàrids i materials resinosos en la mateixa micro mostra de pintura. Es basa en un pre-tractament químic que consisteix en l'extracció en amoníac de les proteïnes i materials polisacàrids, separant-los d'aquesta manera dels lípids i materials resinosos. Es basa en la separació i purificació dels polisacàrids i les proteïnes abans de la hidròlisi, mitjançant l'ús d'una columna monolítica de tecnologia punta amb un

fase estacionària (C4). D'aquesta manera es generen tres fraccions i es derivatitzen separadament, permetent així l'anàlisi quantitativa dels monosacàrids i àcids urònics, dels aminoàcids i lípids i la identificació de resines i ceres. El mètode ha estat provat en materials de referència per a establir la possibilitat d'extracció dels polisacàrids de la matriu de la mostra de pintura i separar de les proteïnes utilitzant el C4. El procediment va ser aplicat a una icona grega del segle XV. Materials proteics,lipídics, resines i polisacàrids es van identificar a les mostres. Els resultats obtinguts seran discutits amb detall.

Objectius de la tesi

Els principals objectius es resumeixen a continuació:

1) Provar els mètodes de preparació de seccions primes per a l'obtencó d'imatges d'FTIR treballant en transmissió. Per tant, l'avaluació de les possibilitats d'obtenir seccions primes de mostres de pintura i posteriorment avaluar les possibilitats de dur a terme les anàlisis mitjançant radiació de sincrotró sobre les seccions preparades.

2) estudiar la formació d'oxalats en sistemes reals (mostres de la pintura antiga) mitjançant, entre d'altres, imaging techniques, com ara, SR micro FTIR i SR micro XRD, per a obtenir informació sobre la seva distribució, la seva natura i relacionar-los amb altres materials orgànics presents en la mostra.

3) Valoració de les capacitats d'un enfocament multi- analític per establir els materials (orgànics i inorgànics) presents en mostres complexes aixi com la seva distribució, amb l'objectiu d'establir la tècnica pictòrica..

4) Posar en marxa un procediment basat en la GC / MS per a la caracterització de materials de polisacàrids i d'aquesta manera,

5) afegir informació sobre la naturalesa dels materials de polisacàrids com aglutinants i adhesius establint la seva composició i els canvis del seu perfil composicional deguts a l'envelliment, la presència de pigments i a l'atac biològic.

6) l'establiment d'una procediment de GC / MS per l'anàlisi del material proteic, els lípids, les resines i els materials polisacarídics en presència d'un alt contingut de compostos inorgànics amb la finalitat de poder analitzar la major quantitat de materials orgànics com sigui possible d'una única i micromètrica mostra.

Tot seguit presentem un resum dels capítols contenint, principalment la introducció a la problemàtica que es pensa desenvolupar en cada cas i els principals resultats o conclusions obtinguts. D'aquesta manera es pretén donar una visió global dels continguts de la tesi.

CAPITOL 1. Aplicació de SR micro imaging FTIR per l'estudi d'estratigrafies

En les mostres de pintura, les propietats químiques dels materials d'àrees adjacents poden ser completament diferents unes de les altres degut a l'heterogeneïtat de les pintures i la seva estructura feta de diverses capes. A més, la degradació i l'envelliment poden també ser considerats com processos tridimensionals. Per tant, la caracterització dels materials de les pintures pot no ser l'únic punt d'interès sinó que una anàlisi completa de les pintures requereix de l'obtenció d'informació en tres dimensions.

La distribució dels materials orgànics i inorgànics en les estratigrafies és necessària per la caracterització dels sistemes de pintura ja que permeten resoldre l'heterogeneïtat elemental i mol.lecular dins i entre els estrats. Fins ara, l'estudi de les estratigrafies dels sistemes multi- capes com les pintures s'havia fet mitjançant el microscopi UV-Visible, la fluorescència de raig X, l'espectrocopia d'infraroig en reflexió especular, l'anàlisi SEM-EDX o SIMS. L'ús d'aquestes tècniques de forma complementària permet un estudi detallat de la distribució dels materials i dels productes de degradació.

Les tècniques d' 'imaging' basades en la radiació sincrotó tenen les característiques perfectes (alta colimació del feix, alta relació senyal/soroll, alta intesitat i brillantor)

per respondre a moltes de les necessitats analítiques dels sistemes pictòrics.

L' espectroscopia d' infraroig de transformada de Fourier (FTIR) ha estat àmpliament utilitzada per identificar els diferents materials utilitzats en obres d'art. El desenvolupament de microspectrofotòmetres i accessoris per espectròmetres infrarojos (1980's) FTIR l' ha establert com una eina de gran abast en el camp de l'arqueometria i patrimoni cultural. El mapping amb FTIR és una interessant eina per a la distribució de materials d'estudi en les obres d'art així com en les mostres de pintura. Respecte a altres tècniques ens permet caracteritzar tant materials inorgànics i orgànics així com els seus productes de degradació.

FTIR permet obtenir imatges i mapes dels grups funcionals de les seccions transversals de les mostres. Requereix, però, de la preparació d'una secció transversal de la mostra sense alterar-ne l'estructura ni la seva composició, d'un gruix no superior a 10 µm. Recentment s'ha publicat un resum de les estratègies de preparació de les mostres utilitzades en les fonts d'SR com a resultat de l'experiència adquirida pels autors

Resultats

Es presenten els resultats de les proves realitzades amb diversos tipos de preparació de mostra i els resultats obtinguts per 8 mostres de pintura decorativa, embotits en resina epoxy i tallats al microtom (tipus de preparació de mostra triada per a les mostres reals). Les mostres es presenten com a exemples de les problemàtiques trobades en la preparació de mostres i en la interpretació de dades.

Conclusions

Les diferents preparacions de mostra provades es presenten a la taula 1. x. En base a les dificultats trobades amb les diferents tècniques s'ha conclòs que embotir la mostra en resina epoxy i després tallar-la al microtom era la millor estratègia per obtenir talls que permetessin l'anàlisi mitjançant SR micro FTIR.

Tot i que els resultats depenen de la natura de la mostra, mitjançant l'aplicació d'estrategies per a la milloria del tall s'han pogut obtenir imatges químiques o, com a mínim, line scans de la estratigrafia de totes les mostres. En el cas del grup de mostres procedents d'una porta revestida de plata i pintada,s'han pogut establir els mappings

de les diferents mostres (de materials orgànics i inorgànics) i la identificació dels materials emprats.

CAPITOL 2. Caracterització i Distribució d'oxalats en mostres de pintura

Els oxalats de calci es troben sovint en la majoria dels objectes del patrimoni cultural exposats a l'aire lliure. Formen pàtines, conegut com "oxalate patinas", desenvolupades principalment en marbre i pedra calcària. Un llarg debat ha sorgit en el si de la comunitat científica sobre l'origen d'aquestes pàtines. Un grup d'investigadors afirmen que les pàtines tenen un origen de tipus biològic resultat de la mineralització i el col.lapse d'algues, mentre que altres els considera un producte del catabolisme de les colonitzacions de microorganismes alimentades pels materials orgànics com les restes d'antics tractaments aplicats a la pedra per a finalitats de protecció i coloració.

Una tercera hipòtesi considera els oxalats com els productes de l'oxidació de les substàncies orgàniques aplicades com a tractaments de conservació. És ben sabut que la degradació de compostos orgànics utilitzats com a aglutinants i capes de revestiment poden produir àcid oxàlic com un dels productes finals d'aquesta oxidació. L'àcid oxàlic pot reaccionar amb el calci, present en grans quantitats en l'atmosfera, per a produir d'oxalats de calci. No obstant això, alguns autors consideren menys plausible atribuir la formació d' oxalats a reaccions químiques sense la intervenció dels microorganismes (líquens i fongs).

Estudis recents van mostrar que els oxalats de calci també són presents a les pintures encara que s'hagin tingut sempre dins d'una església o d'un museu. En la majoria d'aquests casos no ha estat detectada cap prova d'una antiga o d'una actual colonització de la pintura per part de microorganismes. Això fa que sigui realment difícil atribuir els oxalats de calci a una bio-construcció. A més, els líquens produeixen oxalats de calci, sempre en la seva forma bi-hidratada (weddellite), que sempre apareix en forma de petits cristalls (tetragonal piràmide i prismàtics) de mida de 5 a 10 micres. Per contra, els cristalls d' oxalats de calci que es troben en pàtines i pintures son de mida inferior a la resolució del microscopi electrònic d'escombrat, el que indica que els oxalats en les pintures són de mida nanomètrica. A més, les dues formes cristal.lines

(weddellite i whewellite), s'han identificat en les pintures. Això suggereix que els oxalats de calci es formen durant el procés d'envelliment de la pintura, no com un producte procedent del metabolisme dels líquens i fongs, sinó com a producte de la descomposició orgànica vinculats, per tant, al medi orgànic present com a aglutinant.

Fins ara s'han relitzat experiments en substrats de marbre per avaluar el paper dels materials orgànics en la formació de les pàtines d'oxalats tant per envelliment natural de matèrials orgànics (tinguts tant a l'interior com a l' exterior) com per l'oxidació d'aquests materials orgànics mitjançant espècies reactives (O3, H2O2). En tots dos casos, i en tot tipus de material orgànic, es produïa la formació d'una de les formes d'oxalats de calci o barreges d'aquestes. Aquests resultats evidencien la natura generalitzada del fenòmen de formació d'oxalats. En l'experiment mitjançant oxidació, les condicions eren controlades, per tant, els microorganismes no van estar presents. Es conclou, doncs, que són un producte de l'oxidació de la matèria orgànica. Per últim, en el cas d'estudis realitzats sobre les pàtines d'oxalats estudiades per GC/MS, s'ha pogut concloure que la quantitat de oxalats és directament proporcional a la quantitat de material orgànic detectat.

En aquest capítol, es presenten els estudis sobre diferents mostres de pintura mural. Les mostres es van escollir sobre la base dels resultats obtinguts de la seva caracterització convencional (principalment FTIR) que indicava la presència d'un alt contingut d'oxalats en la seva composició. Deu mostres es presenten agrupades en tres diferents exemples: un retaule mural de pedra del segle XI, una mostra d'una escut de guix del segle XVII i les mostres de daurat del sostre d'una cripta del segle XVII . No només es va adquirir informació sobre els oxalats sinó que també sobre la tècnica pictòrica i els materials emprats en cada un dels exemples presentats.
L'objectiu dels experiments és l'estudi de la distribució d' oxalats de calci en les mostres de pintura relacionant-los amb la matèria orgànica per tal de evidenciar la relació entre ells i, d'aquesta manera, comprendre el mecanisme de formació dels oxalats en les pintures.

Resultats

Appendix A

En aquest apartat es presenten els resultats obtinguts per a les diferent mostres agrupades per origen.

- En el cas del retaule de pedra es van aplicar les tècniques de SEM-EDS, FTIR, SR XRD. Els resultats evidenciaven la formació de weddellite i l'ús de blau egici (la cuprorivaite va ser identificada).
- En el cas de la mostra de l'escut es va poder observar la degradació de l'atzurite als corresponents clorurs de color verd. Aquesta degradació es veu acompanyada per la presència d'oxalats tan de calci com de coure. El medi organic identificat(proteïnes i carbohidrats) presentava evidències de degradació biològica.
- En el cas de les mostres de daurat es van evidenciar les dues tècniques de daurat que, per tant, presentaven característiques diferents. L'enfosquiment d'una es devia a la degradació d'un vernís superficial. Els aglutinants en les dues mostres eren també diferents. La distribució d'oxalats demostrava que no només es troven en superficie sinó que a la mostra SBB1 es trobaven acumulats sota el pa d'or.

Una taula a l'apartat de Discussió de cada exemple resumeix els resultats obtinguts per a cada una de les mostres.

Conclusions

Els principals results obtinguts respecte als oxalats es resumeixen a la taula 2.13.
D'una banda, no només en tots els casos, els oxalats es van formar en presència de material orgànic determinat per FTIR i GC/MS, sinó que la distribució d'oxalats sembla clarament concentrada en les capes on la matèria orgànica ha estat també identificada. Així, la formació d' oxalats en mostres de pintura mural no es limita a la formació de pàtines superficials per deposició sinó que es formen en les capes de pintura interiors fins i tot sota capes metàl.liques. Això indica la importància de la matèria orgànica en la formació d' oxalats que apunta a una degradació d'aquest material orgànic per a formar àcid oxàlic com el probable mecanisme de formació en mostres de pintura.

D'altra banda, la caracterització de la matèria orgànica permet concloure que l'oli secant i l'ou són capaços de produir els oxalats en els sistemes de pintura mural.

Particularment, l'ou caracteritzat presentava evidències de degradacio: el perfil d'aminoàcids obtinguts per GC/MS indica l'atac biològic del material proteínic. No s'han identificat altres materials orgànics en les mostres i, per tant, no es pot concloure res sobre la seva capacitat de formar oxalats en sistemes reals.

D'altra banda, la presència de microorganismes en algunes de les mostres ha estat evidenciada. A Sant Pere de Terrassa, la presència de microorganismes es va determinar per observació microscòpica de fragments de mostra i seccions transversals. En la mostra d'atzurita (E1), la caracterització dels aglutinants per GC / MS suggeria un atac bacteriològic de la matèria orgànica. La identificació de l'activitat biològica en les mostres juntament amb la caracterització de weddellite (forma deshidratada, CaC2O4.2H2O) com l'única forma cristal.lina formada per SR XRD estaria d'acord amb la teoria de que els bacteris i els fongs juguen també un paper en la formació d' oxalats.

Per últim, tant els oxalats de calci com els de coure es formen en les mostres de pintura. En presència de coure es formen els oxalats de coure mentre, els oxalats de calci es van concentrar a les zones properes a la capa de sulfat de calci (preparació). Això indica l'extrema facilitat de sulfat de calci per a formar oxalats de calci i dels ions a emigrar dins la mostra a les capes properes per formar capes de oxalats.

De la mateixa manera, el coure oxalats es van formar en presència d'atzurita ($2CuCO_3$. Cu (OH) $_2$) però no cuprorivaite ($CaCuSi_4O_{10}$). Atzurita demostra la seva facilitat per a reaccionar (enllaò iònic), mentre que els silicats es mantenen inalterats.

La complementarietat dels resultats de les diferents tècniques utilitzades ha ajudat a caracteritzar de manera inequívoca les tècniques de pintura, els productes inorgànics cristal lins formats pels processos de meteorització en les diferents mostres i també a determinar la distribució d'aquests productes al llarg de les capes. Per tant, els experiments han constituit tambe una contribució important en l'obtencio d'informació sobre la degradació cromàtica de l'atzurita, les tècniques de daurat i el mecanisme de formació d els oxalats.

Appendix A

CAPITOL 3. Caracterització multianalítica de mostres pictòriques mitjançant tècniques de cromatografia acoblades a espectrometria de massa i basades en la radiació sincrotró

Les pintures són sistemes complexos degut al fet que són fets de múltiples capes i materials de diversos tipus que se sotmeten a l'alteració en el temps com a resultat de les interaccions entre els components i l'envelliment natural. Hi ha diverses qüestions que s'han de resoldre i que estan relacionades amb la tècnica pictòrica o els materials utilitzats pel pintor, els processos de restauració que ha patit l'obra d'art, l'envelliment d'aquesta i els mecanismes d'interacció entre els materials i capes produït amb el pas del temps.

L'ús de les tècniques convencionals, com ara la microscòpica òptica (MO) i microscòpica electrònica de rastreig acoblada a un detector Energy Dispersive Spectroscopy (SEM-EDS), l'espectroscòpia infraroja amb transformada de Fourier (FTIR), la cromatografia de gasos/espectrometria de masses (GC/MS), la pirosi/gas Cromatrografia/ Espectrometria de massa (Py/GC/MS) poden proporcionar una anàlisi detallada i gairebé una completa caracterització de les mostres quan s'usen de manera complementària. En particular, les tècniques de separació ja han demostrat la seva gran aptitud per a la caracterització d'aglutinants.

Tanmateix, a causa de l'heterogeneïtat de diferents materials en la pintura, i l'estructura multicapa d'aquesta, les propietats químiques dels materials de les zones adjacents pot ser completament diferent i, per tant, la identificació no pot ser l'únic punt d'interès: el coneixement de la distribució de la pintura mitjançant tècniques de 'imaging' és fonamental per entendre la tècnica utilitzada pel pintor. D'altra banda, la degradació i l'envelliment també pot ser considerat com un procés en tres dimensions. Per tant, una anàlisi completa de la pintura requereix d'informació en 3 dimensions per tal d'obtenir 'imatges' o mapejats dels materials orgànics i inorgànics de la pintura en les seccions. D'aquesta manera, es resolen les heterogeneïtats elementals i moleculars dins i entre les capes.

En aquest capítol es presenta una anàlisi multi-analítica per a la completa caracterització de materials orgànics i inorgànics en mostres de pintura. Tècniques

considerades ‘Convencionals’ com ara la espectroscòpia infraroja amb transformada de Fourier (FTIR), la piròlisi analítica en la presència de HMDS acoblada a la cromatografia de gasos/espectrometria de masses (Py/GC/MS) s'han utilitzat com a tècniques de screening. La GC / MS seguint un protocol analític per a la identificació dels lípids, ceres, proteïnes i materials resinosos d’una mateixa micro-mostra ha permés la caracterització dels materials orgànics i els seus productes de degradació en el si de la mostra. Per últim, la SR FTIR en mode de transmissió ha permès establir la distribució d'aquests materials tant en profunditat com al llarg de la mostra proporcionant imatges químiques dels grups funcionals en una secció transversal preparada mitjançant el microtom. Per complementar la caracterització dels materials inorgànics, pigments i càrregues, la SR XRD en mode de transmissió s'ha utilitzat per establir les fases cristal.lines presents.

Set mostres de tres pintures de Josep Maria Sert i Badía, un pintor català de principis del segle XX han estat investigades. Josep Maria Sert (1876-1945) va ser un dels més famosos pintors de murals de l'època i va aconseguir el reconeixement internacional. La seva obra decora les parets d’ edificis, com el Saló d'Actes de la Societat de les Nacions (Ginebra), l'edifici RCA en el Rockefeller Center, i el Waldorf-Astoria Hotel (ambdós a la ciutat de Nova York). La tècnica pictòrica de Sert és d'especial interès degut a que el treball del pintor va evolucionar d’ una pintura policromada en els seus inicis fins gairebé arribar a les pintures monocromes (sèpia, tons daurats i platejats). Aquesta segona ha estat considerada, de fet, la seva forma característica de pintar. En motiu de la publicació d'un llibre sobre les pintures Sert a la ciutat de Vic (Barcelona), algunes de les seves pintures han estat estudiats en detall per establir finalment la tècnica pictòrica de l'artista i els materials utilitzats. Set d'aquestes mostres es presenten a continuació.

Resultats

Els resultats de les anàlisis de les 7 mostres es presenten en aquest apartat. Des de les imatges al microscopi òptic i electrònic de les 7 mostres passant pels resultats obtinguts mitjançant FTIR convencional i la Piròlisi analítica que ens han donat una idea de conjunt de les mostres. Aquests resultats han permès agrupar les mostres en 2

grups corresponents a les mostres amb capes metàl.liques i poc color amb estratigrafies molt complexes (VIC 1-2-3-6 i7) i les mostres més senzilles amb capes pigmentades (VIC 4 i 5).
Sobre 3 mostres seleccionades (VIC 2-5 i 7) com a representatives de les diferents obres mostrejades, períodes i tipologia, evidenciada de les tècniques d' 'screening', se'n presenten també els resultats de GC/MS i els mappings obtinguts mitjançant SR FTIR i SR XRD

La combinació de la interpretació de les dades obtingudes amb les diferents tècniques ha permès la caracterització de les mostres capa per capa. Dues taules (Table 3.10 i 3.11) pretenen esquematitzar els materials identificats i la seva distribució en la mostra, tant orgànics com inorgànics

Conclusions

L'ús combinat de diferents tècniques aplicades en diferents alíquotes de les mostres, i la interpretació conjunta dels resultats obtinguts, ens va permetre establir els materials utilitzats i, per tant, determinar la tècnica pictòrica de Josep Maria Sert en les seves pintures a la ciutat de VIC.

En particular, les pintures de Josep Maria Sert presenten dos tipus de tècniques d'acabat que es correspon a dues tècniques pictòriques diferents. L'observada per les mostres VIC 4 i 5 és una tècnica tradicional, que es basa en una capa de preparació, seguida d'una o més capes pigmentades utilitzant principalment oli de llinosa com a aglutinant. La tècnica de les mostres VIC 1-2-3-6-7, en canvi, es basa en l'aplicació de diverses capes finíssimes, principalment de material orgànic, alternant amb capes pigmentades i fulles metàl.liques. Aquesta última tècnica pictòrica de Sert, característica de les seves últimes obres, recorda a la de les icones bizantines, on l'efecte superficial de color en la pintura s'obté, no només amb els pigments, sinó també mitjançant l'aplicació de les fulles metàl.liques sota de les capes orgàniques superficials, el que dona un acabat metàl.lic de la pintura.

Aquest estudi de les mostres de la pintura Sert a la ciutat de Vic ha ajudat a apreciar l'evolució tècnica de Josep Maria Sert com a pintor. Sert va començar amb la tècnica

de la pintura tradicional (mostra VIC 5, 1906) per passar a usar totes dues tècniques contemporàniament (mostres VIC 3 i 4 de la pintura "Les quatre estacions", 1917-1920) i, finalment, utilitzant àmpliament la tècnica de major complexitat tècnica en els últims anys (VIC 1 i 2 de 1920, VIC 7 des 1926 i VIC 6 desde 1945).

CAPITOL 4. Desenvolupament d'un procediment analític per a la caracterització de materials polisacàrids mitjançant GC/MS

Els materials polisacàridics han estat emprats en obres d'art des de l'antiguitat. Els processos de momificació egípcia, les pintures murals en tombes egípcies, macedònies i micèniques com ara la tomba de Nefertiti o el Palau de Néstor (Pylos, Grècia) són alguns exemples del seu ús generalitzat. Durant l'edat mitjana, els materials polisacàrids es van utilitzar per a daurar i com a aglutinants en les miniatures. Textos antics sobre les tècniques de pintura citen materials polisacàrids com la mel, les gomes extractes d'arbres o el sucre comú per a diferents finalitats pictòriques.

En mostres de pintura, l'escassa quantitat de mostra (sovint inferior a 1 mg) i l'escassa puresa dels materials orgànics presents (barrejats entre si en diferents proporcions per obtenir els efectes visuals desitjats), així com la complexitat de la matriu (diverses capes i materials, orgànics i inorgànics, barrejats) i el seu envelliment heterogeni requereix l'ús de tècniques específiques i particularment sensibles.

Les tècniques cromatogràfiques acoblades a espectrometria de massa (HPLC/MS, GC/MS, Py/GC/MS) han demostrat la seva idoneïtat per a la caracterització dels materials orgànics utilitzats en la producció i la restauració d'obres d'art. Alguns procediments analítics per a la caracterització de materials polisacàrids basats en la cromatografia d'intercanvi iònic (HPAEC) i piròlisi/cromatografia de gasos/espectrometria de masses s'han desenvolupat i aplicat a mostres de pintura. La GC/MS proporciona la sensibilitat i els límits de detecció necessaris per a l'anàlisi dels materials orgànics en les obres d'art.

Recentment, un procediment basat en la GC/MS per a la caracterització de la gomes

procedents de plantes sobre la base de la mercaptalation dels sucres, alliberats per hidròlisi de la matriu, abans de la silanitzacio dels derivats de mercaptalació ha estat publicada. D'aquesta manera, un sol pic cromatogràfic es va obtenir tant per les aldoses com els àcids urònics.

Tanmateix, el procediment presenta alguns problemes. L'assecatge del derivatitzat la abans de la injecció resulta dificil i, de vegades, no es pot assolir en absolut. D'altra banda, la formació de productes no desitjats durant la derivatització, a vegades, també pot produir la reducció de la gran reproductibilitat dels cromatogrames. A més, les mostres de pintura mural amb un alt contingut de compostos inorgànics no es derivatitzen a causa de la interferència de les càrregues inorgàniques.

En aquest capítol, es presenta un procediment analític per a l'anàlisi de materials polisacàrids presents en les obres d'art. El procediment que es basa en la hidròlisi assistida per microones per a l'alliberament dels sucres, un clean-up de les mostres per eliminar el material no orgànic i en la mercaptalacio seguida de silanitzacio. Importants modificacions s'han introduït en la neteja i derivatització respecte al procediment publicat anteriorment. La identificació dels problemes i la discussió de les millores introduïdes en els punts clau serà presentat.

Per últim, el procediment optimitzat ha estat emprat en la caracterització de materials de referència a fi d'establir una base de dades de materials polisacàrids i, en la caracterització de mostres de pintura, per comprendre la tècnica pictòrica. Els resultats de la caracterització de mostres de la pintura obre el debat sobre la seva possible contaminació per altres fonts polisacàrides o la degradació dels materials de polisacàrids presents en la mostra.

Resultats

En aquest apartat es presenten les modificacions del procediment analític descrites en detall, principalment necessàries a causa de la formació del trifluoroacetat de piridina que causa problemes de derivatització i la caracterització de:

1. materials de referència,

2. mostres de pintura de diferents origens,periode i natura
3. gomes extractes de plantes en solució per avaluar la degradació per atac bacteriològic i
4. mostres de gomes aplicades sobre suport de vidre per avaluar:
   - l'envelliment en camera d'envelliment
   - la influència dels pigments
   - la influència dels materials proteics

Conclusions

Un procediment per a la caracterització de materials polisacàrids en mostres de la pintura s'ha posat a punt. L'ús d'una resina de doble intercanvi (anions i cations) per a la purificació de les mostres ha permès eliminar les interferències en la derivatització. Modificacions en la fase de derivatització s'han introduït per garantir la reproductibilitat de la reacció, i eliminar els poblemes cromatogràfics a causa dels productes secundaris no desitjats de la reaccions derivatització.

El procediment de derivatització es basa en mercaptalació dels monosacàrids i àcids urònics alliberats de les mostres seguit de la seva silanització. La silanització en dos passos evita la coexistència de TFA i piridina que formen el trifluoroacetat de piridina. En el primer pas de silanització, la mercaptalació s'atura per la derivatització del TFA i el EtSH que son eliminats assecant sota corrent de nitrogen. En la segona etapa es completa la derivatització obtenint-se els derivats TMS dels productes de mercaptalacio dels sucres alliberats per hidròlisi. S'han optimitzat les condicions per evitar pics cromatogràfics secundaris a causa de la reacció dels productes no desitjats. Les condicions del segon pas de silanització son les següents: BSTFA com derivatitzant amb un 1% TMCS com catalitzador i piridina com a dissolvent en proporció 1:2. D'aquesta manera, només s'obté un pic per analitica. El procediment funciona per les aldoses i els àcids urònics, que són els principals components de les gomes utilitzades com a aglutinants en pintura. Encara que la fructosa no es mecaptala de manera efectiva, en aquestes condicions ,els seus pics es poden reconèixer de manera que la caracterització de la mel (si en quantitat suficient) també es pot identificar.

Appendix A

L'aplicació del procediment a materials de referència va demostrar que el procediment permetre l'obtenció dels perfils glicosídicos de les gomes i d'altres materials polisacàrids. D'aquesta manera s'ha construït una base de dades dels perfils glicosídicos de diversos materials orgànics.

L'aplicació del procediment a mostres de pintura va mostrar, en tots els casos, excepte un, que els perfils glucosídics quantitatius obtinguts no es corresponen necessàriament amb cap dels materials de referència investigats.En alguns casos es pot proposar una barreja de materiasl polisacàrids. Tanmateix, la inversió de la relació xilosa / arabinosa, observada en alguns casos, o, la presència generalitzada de glucosa, van estimular les investigacions per intentar entendre el fenomen. En aquest sentit s'han realitzat estudis de barreges de polisacàrids amb aglutinants proteics, de la influència de pigments, i ,de l'atac microbiològic sobre gomes extractes de plantes.

Els resultats de la investigació preliminar posen de relleu que la modificació pot tenir lloc no només sobre el perfil glucosídic quantitatiu sinó també qualitatiu de les gomes. Com a resultat d'això, és possible afirmar el següent:

1) s'ha de mirar quins altres materials estan presents en la mostra perquè si no es coneix la seva contribució al perfil glucosídic, impedeix la identificació del material polisacàrid.

2) la presència de proteïnes, a més de la seva contribució al perfil glucosídic, dóna lloc a modificacions quantitatives del perfil molecular com a efecte de les reaccions (com la de Maillard) que tenen .lloc durant la preparació de la mostra i, possiblement, com a resultat de l'envelliment.

3) alguns pigments i materials inorgànics en general, poden actuar com a catalitzadors de la isomerització d'alguns sucres, produint una modificació dels perfils quantitatius i qualitatius dels aglutinants polisacàrids. Es necessiten més investigacions per comprendre plenament aquest fenomen.

4) bacteris i fongs poden produir modificacions dels perfils glicosídicos fins a tal punt que fa que la identificació de polisacàrids sigui impossible. Una recerca més sistemàtica serà necessària per comprendre millor aquest fenomen, però quan es caracteritza un material en una mostra de pintura, la presència d'un atac biològic hauria de ser estudiat mitjançant tècniques especifiques que el posin de relleu.

Aquests resultats indiquen, per primera vegada en la bibliografia, que la identificació d'un aglutinant polisacàrid no pot ser feta en base a la seva avaluació qualitativa. Diversos factors que tenen influència en el perfil qualitatiu s'han de tenir en compte.. Calen noves investigacions per acabar d'entendre aquests fenomens de modificació del perfil i esbrinar si aquests canvis poden ser d'alguna manera estigmatitzats, fet que permetria una identificació fiable dels aglutinants polisacàrids en mostres de pintura.

CAPITOL 5. Procediment analític GC-MS per a la caracterització de glicerolipids, ceres, resines terpens, polisacàrids i material proteic en la presència de pigments inorgànics

Les mostres d'obres pictòriques d'art es caracteritzen per la presència de diferents materials orgànics, juntament amb els pigments i càrregues. Les tècniques com la GC/MS han demostrat la seva idoneïtat per a l'anàlisi de les mostres d'obres d'art. Diversos procediments basats en la GC/MS per a la caracterització dels materials orgànics presents en mostres de la pintura com aglutinants i vernissos s'han desenvolupat en els darrers anys.

A més, les mostres de la pintura són petites degut a la singularitat de l'obra d'art i els materials orgànics es troben en quantitats mínimes (sovint menys de l'1%). Per això, l'optimització dels procediments analítics amb la finalitat d'obtenir la màxima informació de la menor quantitat de mostra és un pas obligat per als químics analítics que treballen en aquest camp. Recentment, un procediment analític basat en la GC/MS per a la caracterització dels lípids, les ceres, resines i material proteic, usats com a aglutinants i vernissos en pintura, d'una mateixa micro-mostra ha estat publicat. El procediment es basa en una combinació de mètodes prèviament publicats que, mitjançant múltiples tractaments químics aconsegueix la separació d'una fracció aquosa que conté els aminoàcids i de dues fraccions orgàniques (àcida i neutre), que tot seguit es derivatitzen per silanitzacio. Per últim, un procediment de purificació ha estat desenvolupat per a l'eliminació de les fortes interferències d'anàlisi generades per la gran quantitat de pigments inorgànics, en la determinació de la fracció aminoàcidica.

Tanmateix, aquest procediment combinat no inclou els materials polisacàrids que requereixen d'una alíquota independent.

Sobre la base dels estudis previs, un procediment analític basat en la GC/MS per a la determinació dels lípids, les ceres, reines, proteïnes i polisacàrids en la mateixa mostra de pintura i en la presència d'interferències de pigments inorgànics ha estat desenvolupat. Aquest procediment analític necessita de la separació entre el material polisacàrid i el material proteic que s'aconsegueix durant el procès de purificació. Amb aquest procediment analític s'obté:

• La identificació dels aglutinants proteics (ou, col.lagen, caseïna) sobre la base de la determinació quantitativa del perfil d'aminoàcids processats per PCA;
• La identificació dels lípids (oli de llinosa, oli de llavor de rosella, oli de nou i ou), sobre la base de la determinació quantitativa d'àcids grassos i de les resines naturals (resines de pi, sandarac, mastic i dammar), les resines d'origen animal (shellac), les ceres naturals (cera d'abelles, cera de carnauba), sobre la base del reconeixement de markers moleculars;
• La identificació dels aglutinants polisacàrids (midó, mel, gomma adragante, àrabiga, arbres fruiters, guar, karaya), sobre la base dels perfils glicosídics quantitatius i qualitatius aplicant un sistema de presa de decisions.

Exemples de mostres de pintures seran presentats, i la identificació dels components orgànics presents acuradament discutits. Les mostres procedeixen d'una icona grega del segle XV.

Resultats

L'esquema del procediment analític total es troba il.lustrat a la Figura 5.1. Els diferents passos analítics a realitzar estan descrits.

Les proves amb els materials proteics i polisacàrids (goma aràbiga, adragant i fruita) usant la C4 demostren que les dues classes de materials es poden separar obtenint dues fraccions diferenciades que s'analitzen posteriorment amb els procediments descrits en la bibliografia.

Conclusions

L'aplicació del procediment d'anàlisi proposat a materials de referència indica que és adequat per a la caracterització simultània de material proteic i polisacàrid. D'aquesta manera, el procediment és adequat per a la caracterització simultània de diverses classes de compostos i, per tant, per la identificació de material proteic, els olis assecants, cera, resines vegetals, i polisacàrids en mostres antigues.

El procediment s'ha utilitzat per caracteritzar les mostres procedents d'una icona grega. Els resultats han permès determinar la tècnica pictòrica on diverses resines (mastic, shellac i resina de pi) i materials proteics (caseïna ,cola animal, ou) juntament amb goma de fruita i un material posilacàrid de natura desconeguda han estat utilitzats conjuntament.

Conclusions Generals

Els principals resultats obtinguts en la tesi responen als objectius proposats a l'inici de la mateixa. Aquest resultats es resumeixen a continuació:

1) Diferent mètodes de preparació de mostra ,citats a la bibliografia per a realitzar experiments de FTIR en transmissió, s'han provat en mostres altament inorgàniques. Els resultats mostren que embotir la mostra en una resina sintètica (resina epoxi) i fer talls micromètrics usant el microtom dóna els millors resultats tot i les dificultats per obtenir estratigrafies complertes sense pèrdua de partícules o la pèrdua de tota la mostra. Talls de 3 a 12 micres, d'un conjunt de 8 mostres van ser estudiats amb SR micro FTIR en transmissio. Les dades van mostrar les possibilitats de la tècnica en funció de la natura de la mostra. Diverses estratègies han estat aplicades per millorar els resultats obtinguts.

2) L'aplicació del mètode de preparació optimitzat permet estudiar la distribució de oxalats de calci i coure en mostres de pintura mural. L'ús d'altres tècniques (FTIR, SEM-EDS, Py/GC/MS, GC/MS, SR DRX) ha complementat la informació obtinguda pels mappings FTIR. D'aquesta manera s'ha obtingut la distribució dels oxalats ,s'ha identificat la seva fase cristal.lina i s'han caracteritzat pigments i aglutinants afegint la informació a la caracterització de la mostra. En base als resultats, la naturalesa dels oxalats presents en les mostres de pintura, la relació amb la matèria orgànica present a la mostra i els seus mecanismes de la formació han estat discutits.

3) Un enfocament multi analític, ha permès de caracteritzar en profunditat els materials i la tècnica pictòrica del pintor Josep Maria Sert. Aquest tipus d'aproximació multi analítica demostra ser capaç de resoldre problemes donant una gran quantitat de informació.

4) Un procediment analític basat en la GC/MS ,procediment per a la caracterització dels materials polisacàrids ha estat establert. El procediment ha demostrat la seva aplicabilitat a mostres de referència i ha donat bons resultat en mostres procedents d'obres d'art.

5) els materials de referència estudiats han permès establir una base de dades de materials polisacàrids emprats en les obres d'art. Els resultats posen de relleu les modificacions en el perfil glicosídics dels materials de referència en certes condicions (presencia de pigments/proteïnes/atac bacteriològic) que dificulten la identificació de la font del material polisacàrid.

6) L'ús d'una columna C4 permet la separació dels materials proteics dels polisacàrid ha permès establir un procediment combinat que permet identificar un gran nombre de materials orgànics partint d'una sola mostra.

Appendix B

Marius Vendrell-Saz, titular d'universitat del Departament de Cristal.lografia, Mineralogia i Dipòsits Minerals de la Universitat de Barcelona, **Maria Perla Colombini**, professoressa ordinaria al Dipartimento di Chimica e Chimica Industriale de la Università di Pisa, i **Ilaria Bonaduce**, ricercatrice al Dipartimento di Chimica e Chimica Industriale de la Università di Pisa, com a directors/es de la Tesi titulada "*Development of Gas Chromatography-Mass Spectrometry procedures and Synchrotron Radiation based techniques for the study of painting materials in works of art*" que presenta **Anna Lluveras Tenorio,** fan constar que:

Aquesta Tesi Doctoral es presenta com a "Compendi de Publicacions", vertebrant-se en 5 capítols, dels quals la doctoranda és primer autor en tots els casos.

El *capítol 2* consta de 3 publicacions diferenciades en revistes científiques titulades :

- Weathering of gilding decorations investigated by SR: development and distribution of calcium oxalates in the case of Sant Benet de Bages (Barcelona, Spain) , publicada a "*Applpyed Physics A "*, amb un índex d'impacte de 1.857 (2007).

- Evidence of the use of Egyptian blue in a 11th century mural altarpiece by SEM-EDS, FTIR and SRXRD (church of St. Pere, Terrassa, Spain), in press a la revista "Archaeometry", amb un índex d'impacte 1.290

- Degradation of azurite in mural paintings : distribution of copper carbonate, chlorides and oxalates by SRFTIR, acceptat a *Applpyed Physics A "*, amb un índex d'impacte de 1.857 (2007).

Pel que fa al *capítol 3*, el seu contingut integre serà enviat en breu a la revista "Analytical and Bionalytical Chemistry", amb un índex d'impacte de 2,867.

El gruix del treball del *capítol 4* està previst ser enviat en breu per a la seva publicació a la revista "*Analytical Chemistry*", amb un índex d'impacte de 5.287,

tot i que Anna Lluveras Tenorio ha participat activament al desenvolupament d'experiments els resultats dels quals consten a l'article

- Gas chromatographic-mass spectrometric characterisation of plant gums in samples from painted works of art, publicat a la revista " *Journal of chromatography* " amb un índex d'impacte de 3.641.

Pel que fa a la contribució del doctorant a cadascun del capítols i corresponents articles, Anna Lluveras Tenorio va ésser l'encarregada de portar a terme el gruix de la seva investigació, des de la planificació i el desenvolupament dels experiments, fins a la seva anàlisi i posterior escriptura.

Cap dels treballs esmentats, i adjunts a continuació, han estat presentats com a part d'una tesi doctoral prèviament.

Barcelona, 2 de juny del 2009

Els directors/es de tesi

Marius Vendrell Saz Maria perla Colombini Ilaria Bonaduce

A continuació s'adjunten els documents:

- **Carta d'acceptació** del director de la revista Archaeometry correspondent a l'article "Evidence of the use of Egyptian blue in a 11th century mural altarpiece by SEM-EDS, FTIR and SRXRD (church of St. Pere, Terrassa, Spain)" per la seva publicació. Data d'acceptació : 31 Març del 2009
- **Carta d'acceptació** dels organitzadors del congres SR2A encarregats de la gestio de publicacio de les actes del congrés corresponent a l'article "Degradation of azurite in mural paintings: distribution of copper carbonate, chlorides and oxalates by SRFTIR" per a la seva publicacio a la revista Applied Physics
- **Abstracts traduïts al català** dels 4 articles que es presenten
- **PDF de l'article**

"Weathering of gilding decorations investigated by SR: development and distribution of calcium oxalates in the case of Sant Benet de Bages (Barcelona, Spain)"

Appl. Phys. A 90, 23–33 (2008)

- **Còpia de l'article**

"Evidence of the use of Egyptian blue in a 11th century mural altarpiece by SEM-EDS, FTIR and SRXRD (church of St. Pere, Terrassa, Spain)".

- **Còpia de l'article**

"Degradation of azurite in mural paintings: distribution of copper carbonate, chlorides and oxalates by SRFTIR"

- **PDF de l'article**

"Gas chromatographic–mass spectrometric characterisation of plant gums in samples from painted works of art"

Journal of Chromatography A, 1175 (2007) 275–282

Appendix B

Evidence of the use of Egyptian blue in a 11th century mural altarpiece by SEM-EDS, FTIR and SRXRD (church of St. Pere, Terrassa, Spain)

Journal:	*Archaeometry*
Manuscript ID:	ARCH-10-0110-2008.R1
Manuscript Type:	Original Article
Date Submitted by the Author:	18-Feb-2009
Complete List of Authors:	Lluveras Tenorio, Anna; University of Barcelona, crystallography and mineralogy Giraldez, Pilar; University of Barcelona, crystallography and mineralogy Torrents, Anna Vendrell, Mario; university of Barcelona, crystallography and mineralogy
Keywords:	mural painting , Egyptian blue , cuprorivaite, calcium oxalate , FTIR, XRD, Romanesque altarpiece , synchrotron radiation

31-Mar-2009

Dear Ms. Lluveras Tenorio:

I am writing to inform you that we are happy to accept your manuscript entitled "Evidence of the use of Egyptian blue in a 11th century mural altarpiece by SEM-EDS, FTIR and SRXRD (church of St. Pere, Terrassa, Spain)" in its current form for publication in Archaeometry. The comments of the referee(s) who reviewed your manuscript are included at the foot of this letter.

Can you please complete the attached copyright form and return it to the following address in order that your paper can go ahead for publication:

Mrs Jane Simcox

Editorial Coordinator, Archaeometry

Research Laboratory for Archaeology

Dyson Perrins Building

South Parks Road

(Oxford OX1 3QY)

This is to certify that the paper submitted by Anna Lluveras Tenorio to be published in Applied Physics A,

"**Degradation of azurite in mural paintings: distribution of copper carbonate, chlorides and oxalates by SRFTIR**"

corresponding to her presentation at the meeting "Synchrotron Radiation Applied to Art and Archaeology – has been accepted for publication after the peer reviewing by specialists.

Barcelona, may 15, 2009

Degradació de l'atzurita en pintures murals: distribució de carbonates, clorurs i oxalats de coure mitjançant SR FTIR

Aquest article il·lustra l'anàlisi fet per mitjà de tècniques micro-analítiques de sincrotró d'una pintura d'atzurita que presenta un degradació cromàtica verdosa. El repte dels experiments va ser obtenir la distribució espacial dels productes de degradació de l'atzurita. S'han mapejat hidroxiclorurs de coure, carbonats i oxalats de coure mitjançant SR FTIR imaging de seccions en mode transmissió. Per tal de completar la informació, es van aplicar tècniques com ara la Py/GC/MS i GC/MS per tal de caracteritzar els aglutinants i els materials orgànics presents així com els seus productes de degradació. Els resultats contribueixen a comprendre millor la degradacio de les àrees blaves en les pintures murals, no només des del punt de vista particular de la degradacio de l'atzurita, sinó també a afegir informació en relació a la formació d'oxalats i la seva distribució en les mostres de pintura. La radiació per sincrotró demostra la seva capacitat pel mapejat en seccions de la pintura.

Degradació de daurats investigates per radiació sincrotró : desenvolupament i distribució d'oxalats de calci en el cas de Sant Benet de Bages (Barcelona, Spain)

En aquest article s'han estudiat pintures daurades del segle XVII obtingudes de la cripta de Sant Benet de Bages, un Monestir medieval de Catalunya, a prop de Barcelona. Concretament, s'han estudiat seccions de dues decoracions daurades presentant diferents characteristiques. Les tecniques emprades son: microscopi òptic i SEM-EDS, per tal de determinar l'estatigrafia i composició elemental, i FTIR, per tal de determinar l'aglutinant associat a cada capa. Aquests resultats premilinars van demostrar que una de les decoracions daurades van ser fetes mitjançant l'aplicació d'una làmina d'or aplicada sobre un mordent sobre una base de guix, mentre l'altra consistia en un daurat sobre bol amb una capa de vernis superficial. És interessant tenir en compte que mentre que les primeres romanien inalterades, les segones es veien gairebé negres, degut a l'enfosquiment del material orgànic superficial. Per tal d'aclarir les causes d'aquest ennegriment de la mostra, es van dur a terme una sèrie d'experiments amb sincrotó XRD i FTIR sobre aquestes mostres al ESFR (ID18F i ID21), respectivament. D'aquesta manera es van establir el desenvolupament i la distribució d'oxalats de calci i del material aglutinant, el qual sembla responsable de l'ennegriment. Els resultats apunten al fet que la weddellite (oxalat de calci dihidratat) és la fase formada en aquelles capes on també s'ha identificat l'existència de material orgànic o on en principi n'hi hauria d'haver segons les fons bibliogràfiques, i no necessàriament en les capes superficials, tal i com s'hauria suggerit degut a les semblances amb la formació de patines.

Evidència de l'us de Balu Egipci en un altar de pedra del segle XI mitjançant SEM-EDS, FTIR i SRXRD

El present estudi mostra l'anàlisi realitzat sobre mostres preses del retaule de pedra (s.XII) de Sant Pere (Terrassa, Catalunya), una notable església construïda en estil romànic. Sobre la base dels resultats obtinguts de les anàlisis, una discussió interessant sorgeix després de trobar proves de l'us de blau Egipci en una de les mostres, un descobriment que no s'esperava a causa de l'època del retaule. Els pigments es van identificar mitjançant l'ús combinat de FTIR i SEM-EDS. Per confirmar la natura del pigment blau, ja que l' EDS i l'anàlisi FTIR suggerien la possible presència de cuprorivaite, es van fer experiments de μDRX amb radiació sincrotró.

Caracterització per GC/MS de gomes d'arbre emprades en obres d'art

Aquest article presenta un procediment analític per GC-MS per tal d'estudiar la composició química de materials polisacaridics, identificant aldoses i àcids urònics en un sol pas. El procediment es basa en la silanitzacio d'aldoses i àcids urònics components de les gomes per mitjà de hidròlisis assistida per microones, i la seva conversio en els seus derivats mercaptalats. Usant aquest mètode, només s'obté un pic per cada un dels components, produint per tant cromatogrames simples i altament reproduïbles.

El procediment analític va ser optimitzat per mitjà de l'ús de mostres de referència de gomes (aràbica, karaya....), aquarel·les comercials i capes de pintura preparades d'acord amb receptes antigues de l' Opificio delle Pietre Dure de Florència (Itàlia). Per tal d'identificar l'aglutinant polisacaridic en mostres de composició desconeguda, es van utilitzar un squema de presa de decision per a la identificació de la goma i l'anàlisi PCA dels percentatges relatius de sucres. El procediment va ser utilitzat per estudiar mostres recollides de les pintures murals de les tombes macedònies i del Palau micènic de Nèstor a Pylos, Grècia. Es va establir la presència de carbohidrats i gomes (fruita i una barreja de tragacanth i fruit tree gum) en algunes de les mostres.

Appendix B

Appl. Phys. A 90, 23–33 (2008)
DOI: 10.1007/s00339-007-4228-x

Applied Physics A
Materials Science & Processing

A. LLUVERAS[1,✉]
S. BOULARAND[1]
J. ROQUÉ[1]
M. COTTE[2]
P. GIRÁLDEZ[1]
M. VENDRELL-SAZ [1]

Weathering of gilding decorations investigated by SR: development and distribution of calcium oxalates in the case of Sant Benet de Bages (Barcelona, Spain)

[1] Departament de Cristallografia i Mineralogia, Universitat de Barcelona, C/Martí i Franquès S/N 08028 Barcelona, Spain
[2] European Synchrotron Radiation Facility, Polygone Scientifique Louis Néel, 6, rue Jules Horowitz, 38000 Grenoble, France

Received: 8 November 2006/Accepted: 17 July 2007
Published online: 28 August 2007 •

ABSTRACT In this paper seventeenth century gilded paintings from the crypt of Sant Benet de Bages, a medieval monastery in the Catalonia region of Spain, near Barcelona, have been studied. Cross sections from two different gilded decorations were studied by means of optical microscopy and electron microscopy and EDS to determine the statigraphy and elemental composition, and by means of FTIR coupled to a microscope to determine the binding media associated to each layer. These preliminary results demonstrated that gilded decorations were made by the application of a gold foil on a mordant substrate on a gypsum base, while the mouldings of the vaults seem to be gilded on a bol with a glaze on top of the gold leaf. It is interesting to notice that the first remained unaltered, while the gilded vault mouldings look almost black, due to the darkening of the organic material. To elucidate the causes involved in the darkening of the sample from the vaults a set of synchrotron μXRD and μFTIR experiments have been carried out on these samples at the ESRF (ID18F and ID21, respectively). High brightness and small spot working conditions revealed the development and distribution of calcium oxalates in the binding media, which seem to be responsible for the darkening. Results point out the fact that weddellite ($CaC_2O_4 \cdot 2H_2O$) is the phase formed in those layers where organic material has also been identified or at least it would be supposed to be by bibliographic sources and not necessarily those superficial as it would have been suggested due to the similarities with patinas formation.

PACS 78.30-j; 68.37.Hk; 61.10.Nz

1 Introduction

The monastery of Sant Benet del Bages was founded around 950 A.C. and lasted until 1835 A.C. Several transformations occurred until its abandonment by the community in the nineteenth century. The original romanesque crypt is located under the main altar, and it has been deeply modified, though partially preserved. In 1637, some mural paintings were painted in the new vault of the crypt, following the Baroque style (Fig. 1a). The mural paintings represent two shields, the shield of the monastery with the mitre and the bishop's staff, and the shield of the monastery of Montserrat (owner of the monastery since 1593) with the typical skyline of Montserrat mountains. The main colors of those paintings are white, yellow, green, blue and the gilding decorations of the mouldings.

Two different kinds of gilding decorations could be distinguished according to their appearance (Fig. 1b and c): one remains unaltered (SBB1), while the other looks almost black (SBB3). This paper deals with the causes leading to the darkening of the gilding sample SBB3, which is to say, its processes of decay compared with the other, SBB1, which remained unaltered.

Samples of both types of gilding were collected and analysed by the combined use of conventional techniques, such as optical microscopy, FTIR (Fourier transform infrared spectroscopy) and SEM (scanning electron microscope) with a coupled energy dispersive X-ray spectroscopy (EDS) facility. Since traditional techniques did not fully solve the problem in relation with the differential ageing of the gilding samples, SR techniques were used in order to obtain information on the weathering process. Synchrotron radiation X-ray diffraction and synchrotron IR microscopy were used to produce maps of phases across chromatic layers and to produce high contrast chemical imaging [1]. The higher spatial resolution and brightness of SR sources allow a very small area to be studied, faster data collection and a good signal : noise ratio [2].

2 Characterization of gilding decorations by using conventional laboratory techniques

Two different types of gilding decoration samples were collected at the crypt of Sant Benet del Bages due to their appearance: the first type analyzed (sample SBB1) remained unaltered showing a golden surface with metallic shine while the other (sample SBB3) looked almost black (Fig. 1b and c).

Samples were embedded in polyester resin using methyl ethyl ketone peroxide as a hardener, cut with a low deformation diamond saw and polished to allow the study of the cross-section under a reflecting dark field optical microscope. The SBB1 cross-section (Fig. 2a) shows four different layers: a yellow-gold one on the top (layer 4), two layers of a red-brown color interpreted as mordant layers (2-3) and a white

✉ Fax: 0034934021340, E-mail: alluveras@ub.edu

a

b

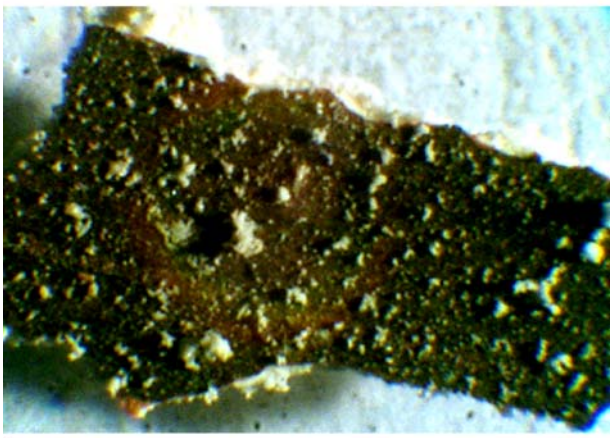

c

FIGURE 1 (**a**) Design of the paintings of the Crypt of Sant Benet del Bages. The shield of Montserrat monastery can be observed as well as the different colors used and the gold mouldings; (**b**) Stereomicroscope image of a fragment of the unaltered and still shiny sample (SBB1); (**c**) Stereomicroscope image of a fragment of the altered and almost black sample (SBB3)

preparation layer (layer 1). Figure 2c shows the characteristic metallic shine of the golden leaf observed in bright field illumination under the reflecting optical microscope. It can be clearly observed the use of a double leaf with probably an organic material in between interpreted also as a mordant layer.

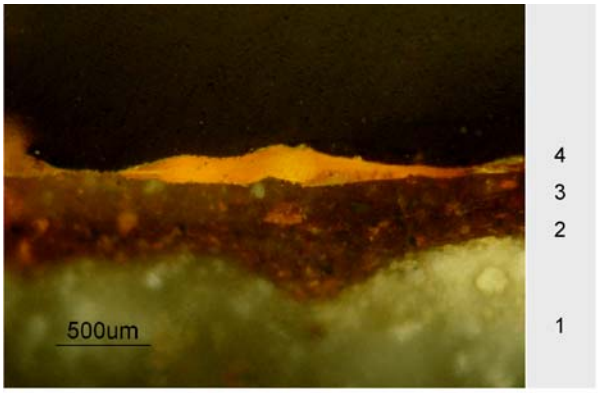

a

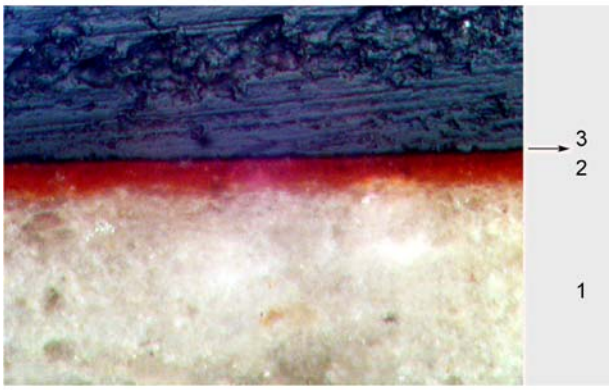

b

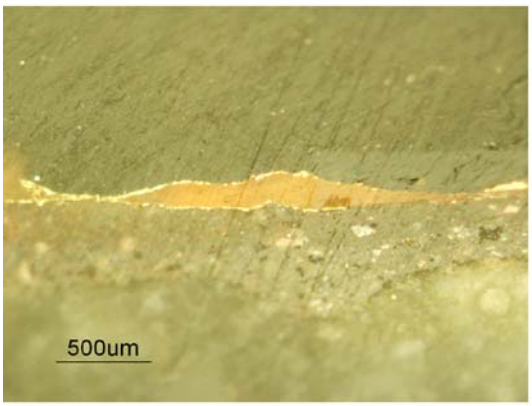

c

FIGURE 2 (**a**) Optical microscopic image of the polished cross-section of SBB1 showing the four layers described: (4) top yellow-gold layer, layers 2 and 3, the brown layers, (1) white preparation layer; (**b**) Optical microscopic image of the polished cross-section of SBB3 showing three layers: (3) irregular dark layer, (2) red and (1) white preparation layer and (**c**) Optical microscopic image in bright field of SBB1: two gold leaves overlapped can be observed keeping layer 4 among them

Figure 2b shows the cross-section of the sample SBB3. In this case, three layers are distinguished: a brownish thin top layer (3) followed by a red-brown one (2) on a white preparation layer that resembles the SBB1 one (1). The illumination in bright field does not allow one to see any metallic shine on the top layer.

The same polished sample was carbon-coated to be studied under the scanning electron microscope (SEM) with a coupled energy dispersive X-ray spectroscopy (EDS) facility. SEM images were taken using a JEOL (Tokyo, Japan)

JSM-840 (secondary and backscattered electron detection) with a LINK AN 10000 microanalyser. The acceleration voltage used was 20 keV. SEM images of the sample SBB1 showed two metallic leaves of about 1,5–2,5 microns thick each of them (Fig. 3a). The red layers (layers 2 and 3) can also be differentiated due to the different size filler: the layer just under the gold leaf (layer 3) comprises smaller and more homogeneous grains than the lower one (layer 2). Both of them, however, showed a characteristic texture of an organic medium. SEM images of SBB3 clearly show that layer 3 is, in fact, consisted of an irregular superficial layer on top of a discontinuous shiny leaf when observed by backscattered electrons (Fig. 3b). The chemical elements forming layer 2 detected by EDS (Si, Fe, Al, K, Ca and Mg) can be attributed to a clay with iron oxides. The elements detected in layer 3 are the same as in layer 2, in addition to Au. Finally, the calcium amount in layer 3 is significatively higher than in layer 2. This can be attributed to the presence of the calcium oxalates reported by FTIR (see below).

Detailed information about the distribution of the main elements of the samples was achieved by EDS mappings, which were collected by using a Cambridge Leica Stereoscan S-360 with a coupled INCA Energy Sèrie 200 microanalyser (Oxford Instruments). Conditions were as follows: filament 2.8 A, probe 3 nA and EHT 20 kV. In Fig. 3 the backscattered electron (BSE) image of the samples cross-section selected area for the mapping is depicted. Nothing but the distribution of Au (Fig. 3c and d) and Ca (Fig. 3e and f) is remarkable. In comparison with the distribution of the same elements in SBB1, differences can easily be detected. The gold layer in SBB3 is discontinuous and thinner than in SBB1, where gold leaves are visible as a thin bright line (in fact, there are two gold leaves overlapped with some kind of organic material in between forming layer 4). Besides, there is clearly an irregular layer on top of the gold one in SBB3. This layer consists of Ca without contribution of any other element above Be (EDS detection limit). That is in agreement with the high Ca peak pointed out by conventional SEM-EDS results in this layer and by the appearance of the calcium oxalate peaks in the FTIR spectra (Fig. 4) of the defined layers 3-2 in Fig. 2b.

Remaining fragments of each sample were analyzed by Fourier transform infrared spectroscopy (FTIR) in transmis-

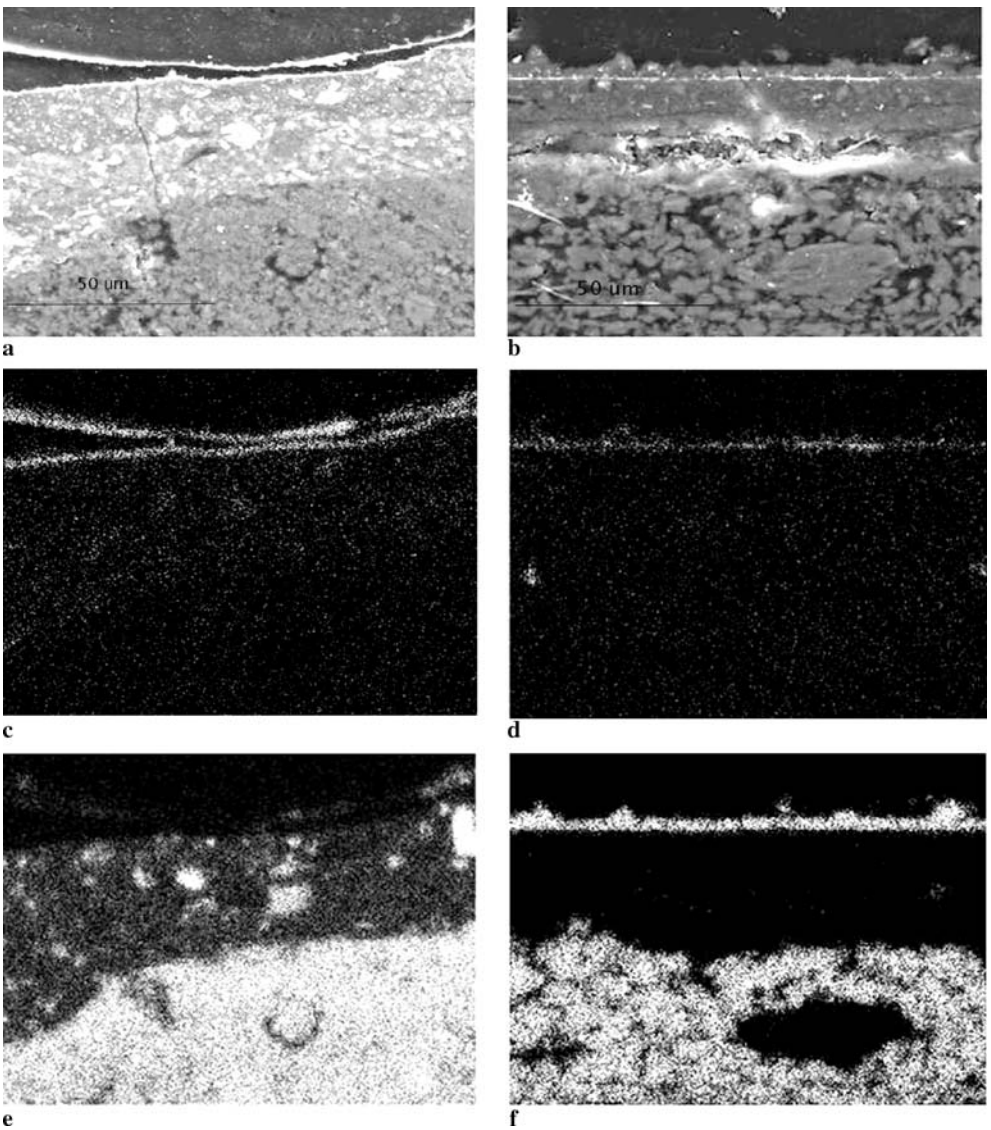

FIGURE 3 (**a**) BSE image of a detail of the cross-section of SBB1; (**b**) BE image of a detail of the cross-section of SBB3; (**c**) Elemental distribution of Au in SBB1; (**d**) Elemental distribution of Au in SBB3; (**e**) Elemental distribution of Ca in SBB1; (**f**) Elemental distribution of Ca in SBB3

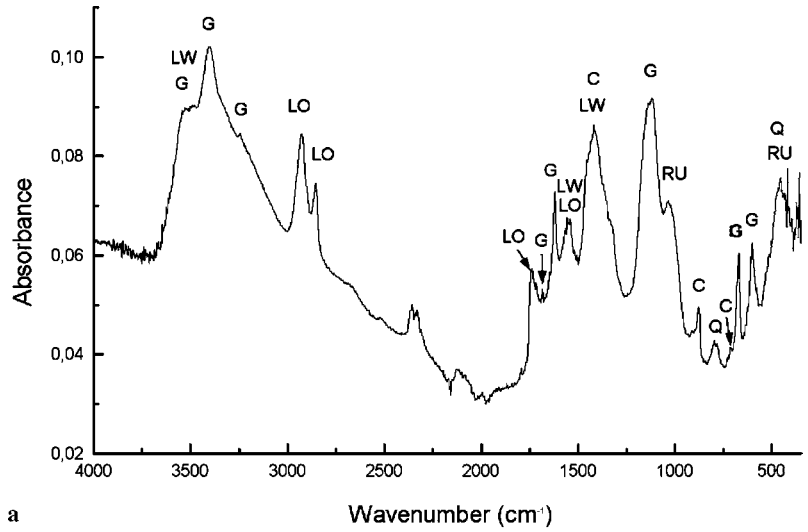

a

b

FIGURE 4 (**a**) SBB1 conventional FTIR spectra of the brown layers, layers 2 and 3 as diamond cell transmission spectrum; (**b**) FTIR spectrum of layers 2 and 3 of SBB3. (G) indicates the absorption bands of gypsum at 601, 671, 1117, 1138, 1620, 1680 and 3403 cm^{-1}, (LO) linseed oil and (LW) lead white (1415, 1552, 1737, 1855, 2927 and 3522 cm^{-1}), (C) calcite (712, 878, 1415, 1791, 2520 cm^{-1}), (Q) quartz (797, 782 cm^{-1}), (RU) raw umber (457, 1035 cm^{-1}), (K) kaolinite (472, 533, 754, 798, 914, 1010, 1033, 3618 and 3695 cm^{-1}), (Ox) calcium oxalates at 1320 cm^{-1} and (H) the possible peaks of hematite at 470 and 530 cm^{-1}

sion mode, using a diamond cell. The equipment used was an infrared spectrometer Bomem MB-120 equipped with a DTGS detector. The spectra are the sum of 30 scans collected from 4000 to 350 cm^{-1} at a resolution of 4 cm^{-1}. Particles of each layer were isolated by using a dissecting knife and tungsten needles (made by the authors) under a stereomicroscope.

FTIR analysis allows the characterization of the preparation layer of the gold leaf in SBB1 (Fig. 4a). The IR spectra show the presence of bands corresponding to gypsum ($CaSO_4 \cdot 2H_2O$) at 601, 671, 1117, 1138, 1620, 1680 and 3403 cm^{-1} [3]. Bands at 1415, 1552, 1737, 1855, 2927 and 3522 cm^{-1} are attributed to a mixture of linseed oil with lead white ($2PbCO_3 \cdot Pb(OH)_2$) [4]. Also, characteristic bands of calcite (712, 878, 1415, 1791, 2520 cm^{-1}) [5], quartz (797, 782 cm^{-1}) and raw umber [$Fe_2O_3 + MnO_2 +$ clay] (457, 1035 cm^{-1}) were identified [6]. The absorptions observed in the preparation layer correspond to gypsum, due to the presence of the bands specified above. The presence of calcium oxalates can be suspected by the presence of a shoulder around 1320 cm^{-1} corresponding to the O–C–O stretching vibration.

The first two layers of SBB3 where analyzed by FTIR together due to the impossibility to separate them mechanically. A representative spectrum is shown in Fig. 4b. The FTIR vibrational bands observed correspond to gypsum (bands described above) and kaolinite ($Al_2O_3 \cdot 2SiO_2 \cdot 2H_2O$). Kaolinite main peaks are 472, 533, 754, 798, 914, 1010, 1033, 3618 and 3695 cm^{-1} [6]. However, vibrational bands around 470 and 530 cm^{-1} do not keep the relative intensity of the reference materials. That is probably diagnostic for the presence of hematite (Fe_2O_3) responsible of the color of layer 2. Hematite bands usually range between 530 and 560 cm^{-1}, and 450 and 480 cm^{-1} [7]. The absorptions observed in the white preparation layer (layer 3) correspond to gypsum as well.

Most notably, the prominent bands of calcium oxalate ($CaC_2O_4 \cdot nH_2O$) at 1324 and 780 cm^{-1} were present [6]. As gypsum is also present, the calcium oxalate band around 1640–1620 cm^{-1} can not be clearly established. Although both forms of calcium oxalate are easily distinguishable from each other also by FTIR analysis, the spectra are similar in the region of the stretching vibrations of the carboxylate groups (1640–1350 cm^{-1}) [8]. Thus, another technique, such

as XRD, should be used to unequivocally characterize the form of calcium oxalate present.

3 Imaging oxalate distribution by means of SR FTIR

A critical point in performing SR FTIR mappings in transmission mode is the sample preparation method, as it is necessary to obtain samples thin enough to perform transmission experiments avoiding the complete absorption of the transmitted beam. Typical thickness for transmission measurements is 4–20 microns [9]. Few methods have been described for achieving such a thin painting sections. Among them, polishing a KBr pellet [10] and using a five-step method combining acrylic resin with epoxy one [11] have been reported recently. We tried by mounting the cross-section in epoxy embedding media and then microtoming with a glass knife to produce a thin section. The thin section was placed directly (after being pressed between two diamond windows to flatten it) on a hole under the FTIR microscope. The experimental sample thickness was 4 microns for SBB3 and 12 microns for SBB1.

Synchrotron radiation Fourier transform infrared microspectroscopy (SR FTIR) was performed at the station ID21 at the European Radiation Synchrotron Facility (ESRF, Grenoble). Working conditions were modified depending on the sample thickness and absorption characteristics. SBB1 map was recorded using 6 microns step and 50 scans for each spectrum. Forty scans and 4 microns of step size were used to SBB3 map. Aperture and resolution were fixed at $8 \times 8\ \mu m^2$ and $8\ cm^{-1}$, respectively. SBB1 mapped area was $102 \times 174\ \mu m^2$ while SBB3 mapped area was $131 \times 48\ \mu m^2$. In both cases the aperture and the step size chosen generates overlapping areas in order to increase the resolution of the components [9].

Synchrotron radiation source advantages for infrared microspectroscopy have been extensively and accurately described in bibliography [2, 12, 13]. However, this method requires an analysis window with a minimum size of 20×20 microns to acquire a spectra in the whole range 4000–$350\ cm^{-1}$ [9]. As we were mainly interested in the calcium oxalate distribution (and not in the characterization of the materials in each layer), we worked at $8 \times 8\ \mu m^2$ loosing the spectra under $1000\ cm^{-1}$.

Although resin peaks (2958, 2932, 2871, 1738, 1458, 1408, 1380, 1256, 1161 cm^{-1}) are distributed in all the range, some peaks of the main inorganic compounds such as gypsum or clays can also be distinguished. Apart from those inorganic components and the resin peaks, the absorption bands of the spectra are relatively broad and their intensity low. However, further examination of the spectrum obtained from some areas indicated that it contained few additional bands (2850, 1715, $1548\ cm^{-1}$) that could be attributed to the organic materials already identified by conventional IR and were used in order to imaging those materials. Also, the typical distribution of the C–H st bands of the epoxy resin was sometimes altered indicating the contribution of other organic materials present.

Imaging of functional groups was determined by using OMNIC software (Thermo Nicolet Instruments) derived from the peak height of characteristic vibrational bands. Measuring peak heights or areas is the most straightforward way of identifying its location and concentration [13, 14]. However, as the spectra intensities of the characteristic peaks were clearly dependent on the thickness of the sample, the multivariate methods of data analysis provided in the software were used to correct the maps obtained.

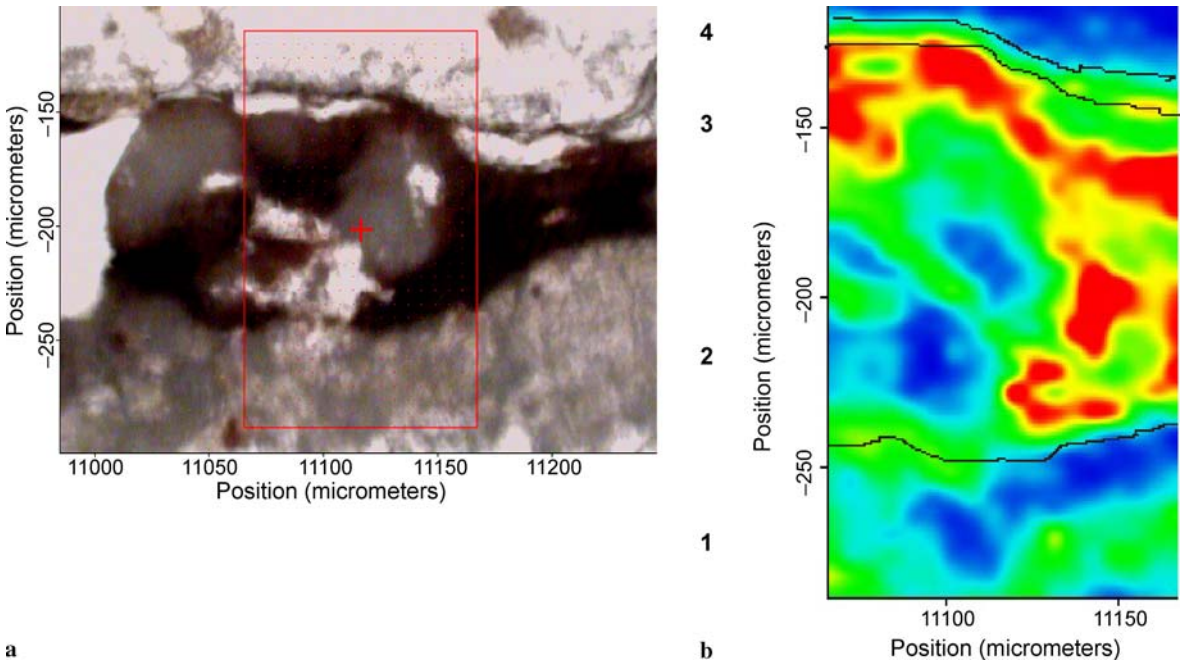

FIGURE 5 (**a**) Photomicrograph of the microtomed cross-section of SBB1 (12 μm). The rectangle marks the area selected to perform the FTIR mapping. (**b**) Chemical image of the oxalates band at $1320\ cm^{-1}$. The spectra have been recorded with a $8 \times 8\ \mu m^2$ aperture, 50 scans, 6 μm step and $8\ cm^{-1}$ resolution (area $102 \times 174\ \mu m^2$)

A photomicrograph of the cross-sections of both samples after microtoming are shown in Figs. 5a and 6a. SR FTIR mappings (Figs. 5b and 6b) based on the distribution of the characteristic peak around 1320 cm^{-1} (O–C–O stretching) confirmed the presence of calcium oxalates mainly in this top layer in SBB3 but also in SBB1 where their presence was just suggested by conventional FTIR (see above). Few compounds exhibit such a band [14] nor does the epoxy resin. In this case, to confirm the calcium oxalate identification, we could not image any other characteristic band attributed to calcium oxalate. The peak at 1620 cm^{-1} interferes with a band of gypsum and proteinaceous materials, and the characteristic band at 782 cm^{-1} was lost due to the aperture chosen.

Calcium oxalate distribution in SBB1 (Fig. 5b) seems to be restricted to the already identified as mordant layers (layers 2 and 3 in Fig. 2a), ending at the beginning of the gypsum preparation layer (layer 1). For SBB3 distribution (Fig. 6b), calcium oxalates are mainly concentrated on the layer above the gold leaf (layer 3 Fig. 2b). A smaller amount in the red layer is identified as a bol (layer 2 Fig. 2b). As the samples thickness are so different (4 and 12 μm), comparison between the amount of calcium oxalates in both samples has to be avoided. However, calcium oxalates' characteristic peaks were only exhibited by conventional FTIR spectrum of SBB3 (Fig. 4b) while just a shoulder could be noticed in SBB1 spectrum (Fig. 4a).

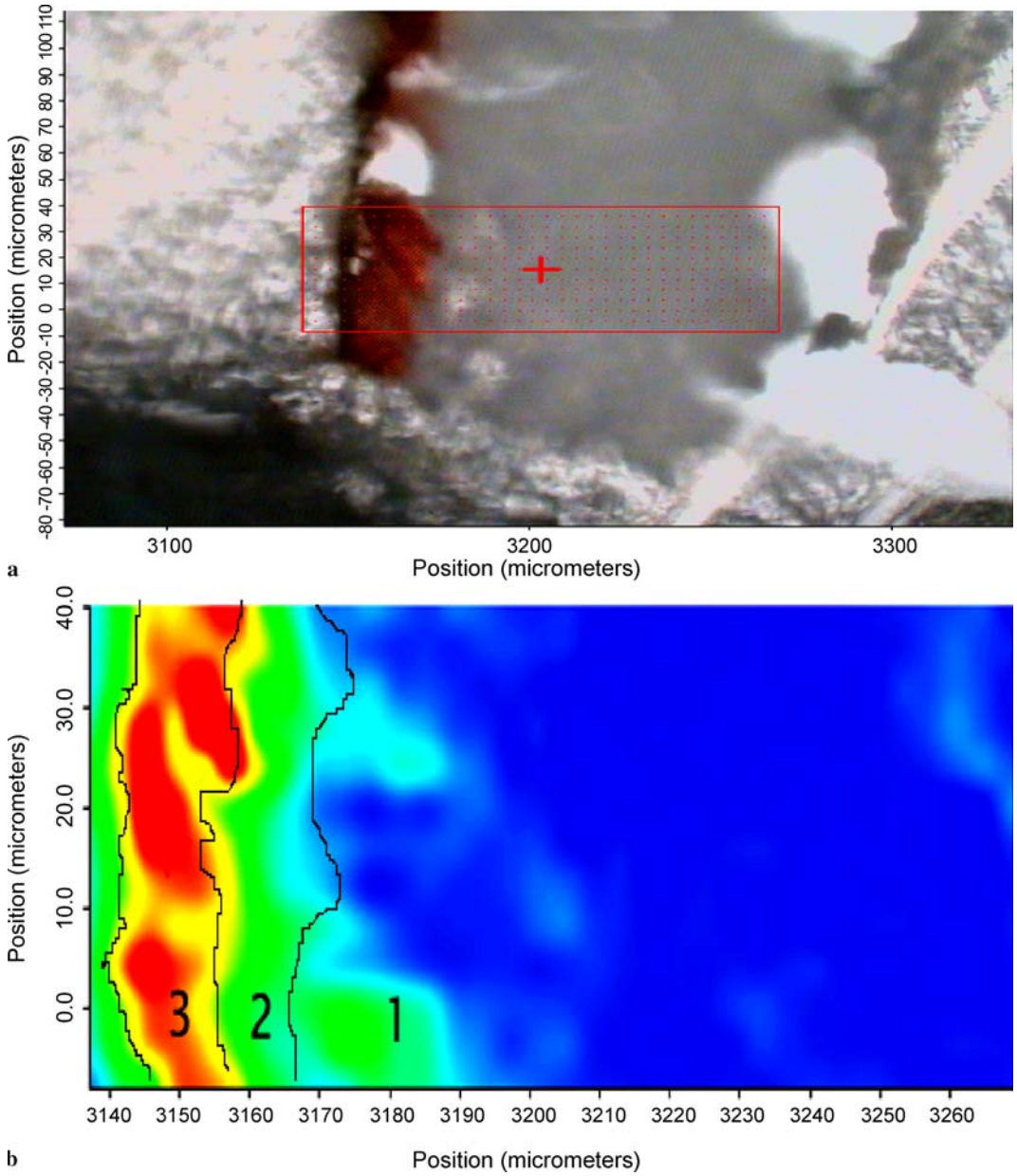

FIGURE 6 (**a**) Photomicrograph of the microtomed cross-section of SBB3 (4 μm). The rectangle marks the area selected to perform the FTIR mapping. (**b**) Chemical image of the oxalates band at 1320 cm^{-1}. The map was recorded using a 8×8 μm^2 aperture, 8 cm^{-1} resolution, step = 4 μm and 40 scans (area 131×48 μm^2)

For SBB1, the presence of the oil (already characterized by conventional FTIR) could be indicated by the appearance of the band at 2850 and a shoulder at 1715 cm^{-1} (C–H stretching and C=O stretching bands characteristic of glycerolipid material) [15]; the disappearance of the epoxy resin peak at 2960 cm^{-1} and the increase in height of the peak at 2930 cm^{-1} (changing the resin characteristic distribution in the C–H st region). Bands at 1545 cm^{-1} could be also characteristic of linseed oil with lead white as a dryer due to the formation of metal soaps. It can be assigned to the C–O–O asymmetric stretching of the lead carboxylates [4, 9].

The organic adhesive, described by optical and electronic microscopy, between the two gold leaves overlapped forming layer 4 of Fig. 2a, could be considered also a glycerolipid material, being layer 4 also a mordant layer as suspected. This conclusion is based on the similarities among the spectra of layers 2 and 3 (oil already identified by conventional characterization) and 4.

It should be noted that calcium oxalates in SBB1, though appearing heterogeneously distributed in the mordant layers where the drying oil is present (layers 2, 3 and 4), present a distribution less intense in this superficial region (Fig. 5b). Thus, the formation of oxalates is significatively higher in the mordant layers under the gold leaves (layers 2-3) than in the most superficial mordant (layer 4). That could mean that calcium oxalates are formed from gypsum of the ground layer and not sources of calcium external to the painting. However, it has been impossible to find any kind of quantitative relation between the amounts of oil and oxalates based on the peak height nor area. The variable thickness of the sample, depending on the area, does not allow comparison.

4 Oxalate distribution in depth from SR XRD profiles

For SR XRD, sample preparation has been described in a previous work already published [16]: samples are embedded in polyester resin polymerised by a peroxo-organic hardener under low humidity conditions and sectioned with a diamond saw of thickness 0.1 mm into a 200 microns thick slice.

SR XRD (Synchrotron radiation X-ray diffraction) patterns were acquired at station ID18F of the ESRF as well. A focal spot of 2.3 microns in the vertical direction and 11 microns in the horizontal direction was chosen with steps of 2 microns in the vertical direction and 10 microns in the horizontal. A wavelength of 0.443 A (28 keV) was selected and the acquisition time was 20 seconds per pattern. The diffraction signal was recorded in transmission by means of

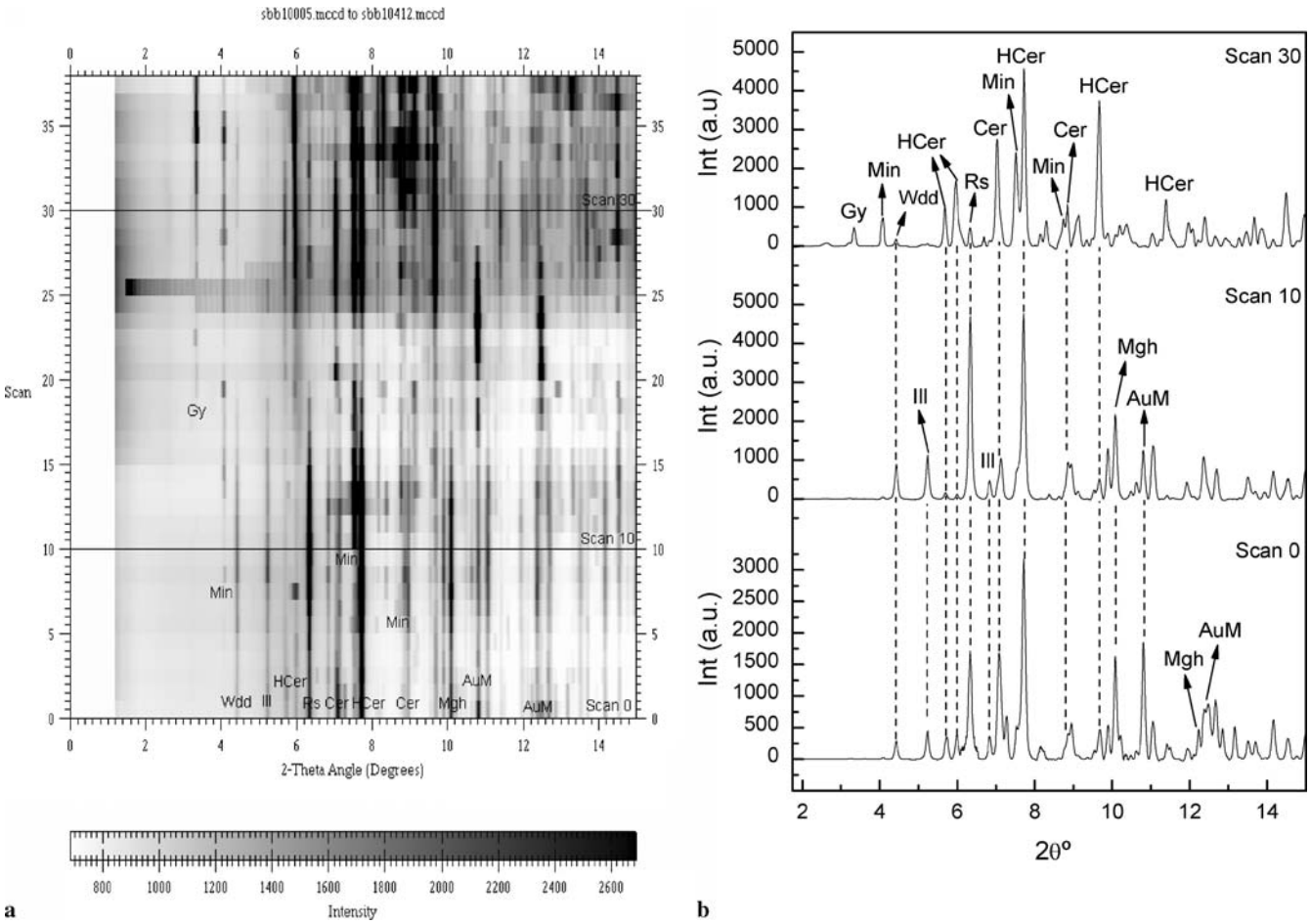

FIGURE 7 DRX line scan on sample SBB1 (**a**) Mineral phases distribution (**b**) XRD patterns of scans 0, 10 and 30. (Gy) indicates gypsum [$CaSO_4 \cdot 2H_2O$], (Min) minium [Pb_3O_4], (Wdd) weddellite [$C_2CaO_4 \cdot 2H_2O$], (HCer) hidocerussite [$Pb_3(CO_2)_2$], (Rs) ramsdellite [MnO_2], (Cer) cerussite [$PbCO_3$], (Ill) illite [$2K_2O \cdot 3MgO \cdot Al_2O_3 \cdot 24SiO_2 \cdot 12H_2O$], (Mgh) maghemite [$Fe_2O_3$] and, finally, (AuM) gold metallic [Au]

a 2-dimensional CCD-based X-ray detector (refined detector distance 107.26 mm). The cross-section was placed into the focused beam with the paint layers oriented horizontally. In this position the sample was scanned both horizontally and vertically to obtain a map. Patterns were fitted with the ESRF FIT2D package [17].

The use of SR XRD confirmed the presence of calcium oxalate in the form weddellite (calcium oxalate dihydrate [$CaC_2O_4 \cdot 2H_2O$]). Figures 7a and 8a show the distribution of the mineralogical phases identified and its distribution in a representative vertical line scan in SBB1 and SBB3, respectively. Some patterns of characteristic scans of SBB1 (Fig. 7b) allow one to appreciate the presence of the weddellite, due to the presence of the peak 200 (Table 3). Clearly there is a higher amount of calcium oxalates in the mordant layers (scan 10) and less in the preparation layer (scan 30). In the top gold-adhesive layer (layer 4 Fig. 2a), there is also weddellite but in smaller amounts than in the mordant layers, in agreement with the SR FTIR results. Figure 8b presents three patterns in the line scan of SBB3. Weddellite can also be identified. The highest amount of calcium oxalate allows one to identify both peaks 200 and 411 of weddellite pattern (Table 3). In this case, the highest amount (peak height) of weddellite can be appreciated at scan 0, which corresponds to the top dark layer (layer 3 in Fig. 2b), in agreement with the SR FTIR results, as well.

For SBB1, the other phases identified are gypsum, gold, clays, cerrussite and hydrocerusite (lead white [$2PbCO_3 \cdot Pb(OH)_2$]) manganese oxide (MnO_2) and maghemite (Fe_2O_3). The presence of iron oxides confirms what could just be suspected by FTIR: the use of drying pigments and red pigments added to the organic material in the mordant layer. A phase characterized by SR XRD but not reported by conventional techniques is minimum (Pb_3O_4) also added to the mordant layers (2 and 3) as a red pigment (helping the mordant layer to resemble a bol) and as a drier pigment (lead-containing) as well.

For SBB3, the other phases identified are gold, clays and gypsum (materials characterized by conventional techniques). However, dimorphite (As_4S_3) was surprisingly noticed in the brown top layer. Dimorphite is a rare form of arsenic sulfur that has been identified in the composition of the natural mineral specimen of orpiment pigment, together with other phases, such as alacrinite (As_8S_9), uzonite (As_4S_5), duranusite (As_4S), pararealgar (α-AsS) or realgar (β-AsS) [18]. Since neither orpiment nor any other substances specified above have been identified, and obtaining dimorphite is quite easy by sublimation of compounds with S and As, we consider use of dimorphite here as a synthetic pigment added to the glaze to help in its purposes of obtaining a gilding (looking like gold) layer.

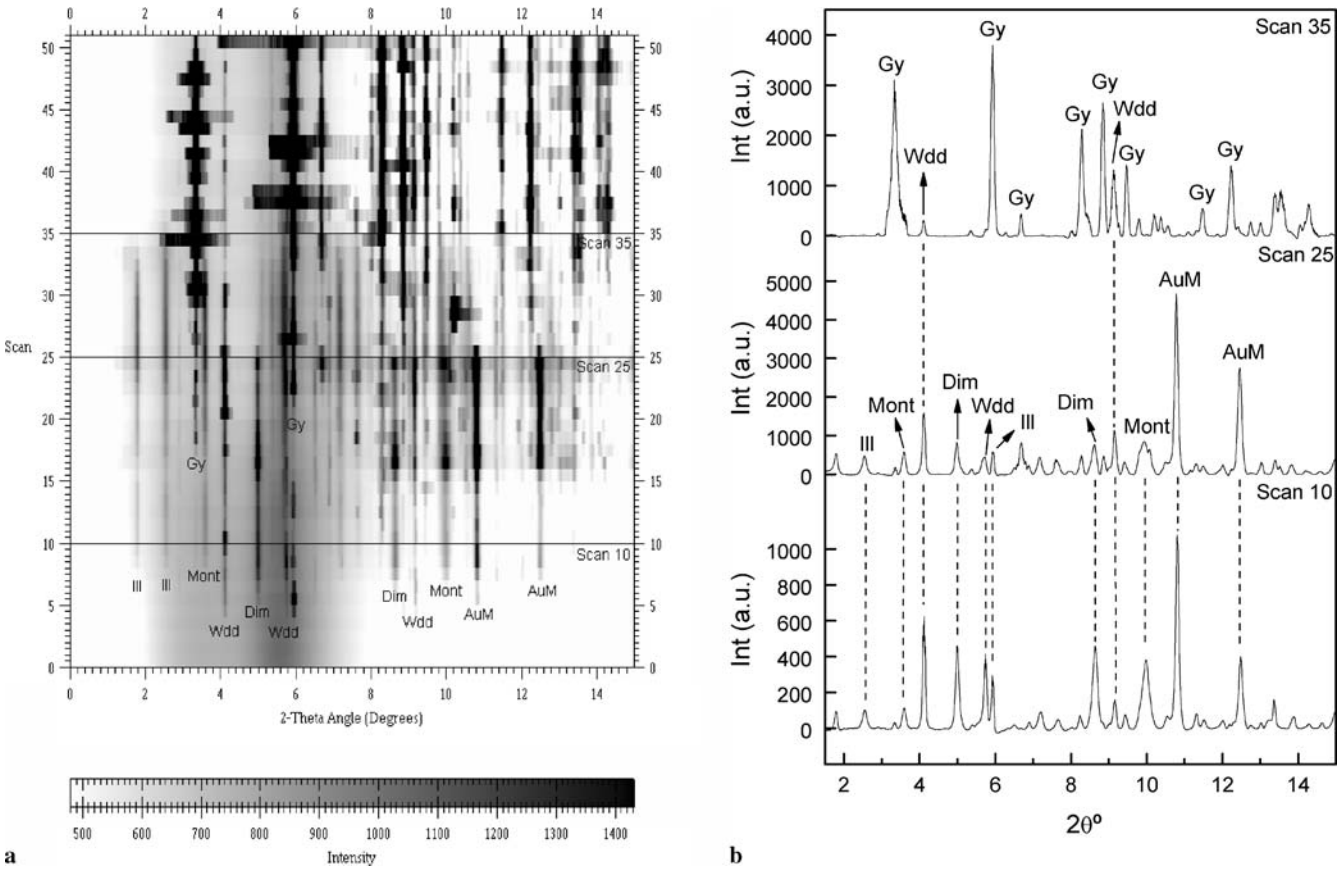

FIGURE 8 DRX line scan on sample SBB3 (**a**) Mineral phases distribution (**b**) XRD patterns of scans 10–25 and 35. (Gy) indicates the presence of gypsum [$CaSO_4 \cdot 2H_2O$], (Wdd) weddellite [$C_2CaO_4 \cdot 2H_2O$], (ILL) illite [$2K_2O \cdot 3MgO \cdot Al_2O_3 \cdot 24SiO_2 \cdot 12H_2O$], (Orp) orpiment [$As_4S_3$] and (AuM) gold metal [Au]

5 Discussion and interpretation of the measurements

It is well known that the different gilding techniques used for the application of the metallic leaves are strongly dependent on the kind of support of the painting [14]. Two main procedures are described in the bibliography mostly depending on the binding medium used [19–22]: water gilding and mordant gilding. The first one (water gilding) consists of a bol layer (usually red earth mixed with glue) applied on a preparation layer of gypsum or calcium carbonate with glue. Over the bol layer some water (with glue) is applied in order to improve the adhesion of the gold leaf. The mordant technique, however, consists of applying an adhesive containing drying oils (such as linseed oil) and terpenoid resins. Some pigments (usually lead ones) could be added to both help in the drying process of the adhesive and also resemble a bol.

When gilding was performed on a wall, it was impossible to obtain a perfectly smooth surface. Leaf was applied through the use of dense adhesives generally containing drying oils and terpenoid resins [15]. Oil gilding is also the traditional process for building exteriors. The use of gold powder has been less reported.

Data obtained by using conventional analytical methodology point out that the technique used to make the gilding decoration named SBB1 is the oil or mordant gilding. The mordant has been prepared by using a drying oil (layer 4) and the oil mixed with drying compounds (layers 2 and 3), such as lead white and manganese oxides (contained in the raw umber). The fact that two different and consecutive layers of mordant have been applied under the second gold leaf can be interpreted as a refinement of the technique execution. The presence of two gold leaves in layer 4 can be interpreted as a repair of the first gold leaf or by the fact that the sample comes from the place where two consecutive gold leaves were overlapped in order to generate continuity in the gold top layer. SBB1 layers identified by both optical and electronic microscope and the main results obtained are shown in Table 1. SBB3 sample, however, is characterized by a different gilding technique, probably, water gilding. Gold leaf was applied on a support layer called a bol, a mixture of clays and iron oxides brown coloured. A glaze (meaning an organic layer mixed with some dimorphite) was applied on top of the gold leaf. Main results are shown in Table 2.

In summary, both samples are gilded decorations with a gypsum-based preparation layer, but the gilding technique used turns out to be clearly different. That means that, the technique used in the sample SBB3 leads to a more thorough degradation, resulting in a complete loss of its original brightness, while SBB1 has preserved its original aspect. In addition, the formation of calcium oxalate on the outermost part of SBB3 represents a difference between both samples.

Calcium oxalates are often found in most cultural heritage objects exposed to the open air. They form patinas, known as "oxalate patinas", mainly developed on marble and limestone [1, 23–26]. A long and unsolved discussion has arisen in the scientific community on the origin of such patinas. A set of researchers claim they have a biological origin from mineralisation and collapse of algae filaments, while others consider oxalates a catabolic product of micro-organisms colonisations fed by organic materials, such as the remains of ancient treatments applied to the stone for protective and colouring purposes.

A third hypothesis considers a chemical origin as oxidation products of those organic substances applied as conservation treatments. It is well known that the degradation of organic compounds used as binding media and coating layers produce oxalic acid as one of the final by-products, which could react with calcium, already present in large amounts in the atmosphere, to produce calcium oxalate [24]. However, some authors believe it is less plausible to attribute oxalate formation to purely chemical reactions without any involvement of living-microorganism (lichens or fungi) [26].

Recent analyses made by this group based on X-ray diffraction using synchrotron radiation (Daresbury laboratory station 9.6) showed that calcium oxalates are also present in ancient paintings, though they were always kept inside a church or a museum [16]. In that case, as in Sant Benet del Bages, any effect of an ancient or present colonisa-

Layer	Width (μm)	Appearance in light microscopy	Elements determined by EDS analysis	FTIR results
4	1.5–2.5	Gold layer	Au	Lead white ($2PbCO_3 \cdot Pb(OH)_2$),
	4–12	Yellow		Drying oil,
	1.5–2.5	Gold layer		Raw umber
3	11–19	Red/brown	Al, Si , Fe, Mn, Pb, Ca, (K, Mg)	($Fe_2O_3 + MnO_2 + nH_2O + Si + Al_2O_3$),
2	15–30	Red		Calcite ($CaCO_3$)
1	35–60	White	Ca, S, (Na, K)	Gypsum ($CaSO_4 \cdot 2H_2O$)

TABLE 1 Main results obtained by the conventional characterization of the sample SBB1

Layer	Width (μm)	Appearance in light microscopy	Elements determined by EDS analysis	FTIR results
3	2–5	Black dust	Au, Ca, (Al, K, Si, Fe)	Calcium oxalates ($CaC_2O4 \cdot nH_2O$),
	1–2	Gold layer		Gypsum ($CaSO_4 \cdot 2H_2O$),
2	20	Red/brown	Si, Fe, Al, K, (Mg, Ca)	Red ochre (clay + Fe_2O_3)
1	150	White	Ca, S, (Al, Si)	Gypsum ($CaSO_4 \cdot 2H_2O$)

TABLE 2 Main results obtained by the conventional characterization of the sample SBB3

Scan Num	*hkl*	$2\theta^o$ JCPDF	$2\theta^o$ Measured
Sample SBB1			
0	200	4.12	4.12
10	200	4.12	4.12
30	200	4.12	4.12
Sample SBB3			
10	200	4.11	4.12
	411	9.15	9.16
25	200	4.11	4.11
	411	9.15	9.15
30	200	4.11	4.11
	411	9.15	9.15

TABLE 3 Measured peaks of weddellite (JCPDF 00-017-0541)

tion by micro-organisms has been found on the painting layers. Thus, it is really difficult to attribute the calcium oxalate to a bio-construction. Additionally, lichens produce calcium oxalate (the di-hydrated form of weddellite) that also always appears as small well-shaped crystals (tetragonal pyramid and prismatic) sized from 5 to 10 microns [8, 23]. On the contrary, calcium oxalate crystals found in patinas and painting samples are sized under the resolution of the scanning electron microscope, and both crystalline forms (weddellite and whewellite) can be found [24]. This fact indicates that they are not micrometric but nanometric. That would mean that calcium oxalate crystals are formed during the ageing process of the painting, not as a methabolic product of lichens or fungi, as those products are above micrometers, but as decay product of the organic binding medium.

The key findings achieved by SR imaging techniques are that calcium oxalates are present in both samples, and not only in SBB3, and also their differential distribution in each sample. The presence of the gold leaf in SBB1 prevented the normal exposition to light and oxygen of the mordant. In these conditions, the drying processes were hindered and dryers were extremely useful [15]. For the same reason (a slower ageing of the organic material present), calcium oxalates amount is lower (and not clearly detected by conventional FTIR). For SBB1 calcium oxalates are more or less heterogeneously distributed in the layers below the gold leaf, while in SBB3 there is clearly a huge concentration of calcium oxalates (weddellite) on the surface due to the ageing of the organic material applied as a glaze. So, calcium oxalates appear in the layers in which some organic material have been reported or at least they should be based on the know-how of painting techniques.

6 Conclusions

The combined use of conventional techniques, such as optical microscopy, FTIR and SEM-EDS permitted one to distinguish between the two gilding samples due to the painting technique used in each of them, as well as the identification of the main painting materials. The difference in the gilding technique clearly justifies the different ageing behaviour of both gilding samples from Sant Benet del Bages. The use of an organic material as a glaze generates a superficial layer that has been almost completely degraded. The amount of oxalates detected in the layer completely hides the metallic shine of the gold particles, besides the darkening of the organic material due to ageing.

SR FTIR mappings and SR XRD profiles allowed one to obtain information on the distribution of compounds, but also they add information to the standard characterisation results. Ca elementary distribution by EDS in the SBB3 sample clearly helps in the understanding of the ageing of the sample. Also, dimorphite and the minimal presence was only detected by SR XRD.

Calcium oxalates distribution demonstrates the relationship between the presence of binding medium and their formation. It appears that the hypothesis considering calcium oxalates as a deposition of materials from the mineralisation and collapse of algae filaments from pollution can be discarded. They appear related to the presence of organic material, and while the mordant gilding sample (SBB1) remains almost unaltered, the water gilding decoration made on a bol lost its golden aspect due to the decay (and darkening) of the organic material over the discontinuous gold leaf.

However, it was impossible to embed the samples in a way that ensure the embedding agent did not penetrate in the painting layers avoiding contamination and erroneous spectra [10, 17]. Although calcium oxalate can be easily differentiated as it has a very particular signal (around 1320 cm^{-1}), imaging the organic material present or just identifying it has been unsuccessful. Absorptions observed in our slices mainly correspond to inorganic compounds, such as gypsum, calcite or kaolinite. Another limitation of the technique is that a component cannot be reliably identified based on one IR absorption band. Thus, additional analysis (such as SR XRD) are required to complement the map and provide interpretation [9]. The sample preparation process must be improved to obtain cross-sections with a bigger area, avoiding holes. This would thus be more representative of the painting stratigraphy, with no more than 6 microns of width, avoiding also resin penetration. Then, the SR FTIR mapping mode would allow us to study calcium oxalates distribution and to relate it to the organic material distribution, obtaining the ratio of the organic bands and the calcium oxalate ones.

Finally, the study of more samples by the techniques described above will be of interest for establishing some kind of reliable hypothesis on calcium oxalate origin and formation in painting samples. The analysis of more samples rich in oxalates will be the way to corroborate these first results and also to establish a general knowledge of oxalates distribution in all kind of painting samples.

ACKNOWLEDGEMENTS The authors wish to thank Anna Vila and Gema Martinez-Ruiz (Serveis Cientifico-Tècnics, Universitat Barcelona) for their help in the sample preparation step and also for their truly involvement in the project. Chemistry, technology and evolution of the architectural painting in the mountain areas: conservation and valorization. Project (Comunitat de Treball dels Pirineus) is acknowledged for the research funds. We also acknowledge the European Synchrotron Radiation Facility for provision of synchrotron radiation facilities and we would like to thank Isabelle Lethard for assistance in using beamline ID18F.

REFERENCES

1 M. Alvarez de Buergo, R. Fort González, Constr. Build. Mater. **17**, 83 (2003)
2 P. Yu, Brit. J. Nutr. **92**, 869 (2004)
3 C. Genestar, Mater. Lett. **54**, 382 (2002)
4 R.J. Meilunas, J.G. Bentsen, A. Steinberg, Stud. Conserv. **35**, 33 (1990)
5 G.C. Jones, B. Jackson, *Infrared Transmission Spectra of Carbonate Minerals* (Chapman and Hall, London, 1993)
6 D. Biakiaris, S. Danilia, S. Sotiropoulou, O. Katsimbiri, E. Pavlidou, A.P. Moutsatsou, Y. Chryssoulakis, Spectrochim. Acta A **56**, 3 (1999)
7 K. Helwig, IRUG at the V&A, p. 83
8 P.V. Monje, E.J. Baran, J. Plant. Physiol. **128**, 707 (2002)
9 M.R. Derrick, D. Stulik, J.M. Landry, *Infrared Spectroscopy in Conservation Science* (The Getty Conservation Institute, Los Angeles, 1999)
10 J. van der Weerd, R.M.A. Heeren, J.J. Boon, Stud. Conserv. **49**, 193 (2004)
11 M. Derrick, L. Souza, T. Kieslich, H. Florsheim, D. Stulik, J. Am. Inst. Conserv. **33**, 227 (1994)
12 P. Dumas, L. Miller, Vib. Spectrosc. **32**, 3 (2003)
13 P. Dumas, N. Jasmin, J.L. Teillaud, L.M. Miller, B. Beccard, Faraday Discuss. **126**, 289 (2004)
14 M. Cotte, P. Walter, G. Tsoucaris, P. Dumas, Vib. Spectrosc. **38**, 159 (2005)
15 I. Bonaduce, *A Multi-Analytical Approach for the Investigation of Materials and Techniques in the Art of Gilding* (Università di Pisa, 2005)
16 N. Salvadó, T. Pradell, E. Pantos, M.Z. Papiz, J. Molera, M. Seco, M. Vendrell-Saz, J. Synchrotron. Radiat. **9**, 215 (2002)
17 A.P. Hammersley, O. Svensson, M. Hanfland, A.N. Fitch, D. Hausermann, High Press. Res. **14**, 235 (1996)
18 M. Clarke, J.J. Boon, *Molecular Aspects of Ageing in Painted Works of Art* (FOM Institute AMOLF, Amsterdam, 2003)
19 M. Matteini, A. Moles, *La química en la restauración, Los materiales del arte pictórico* (NEREA Junta de Andalucía – Consejería de Cultura – IAPH 1989)
20 R. Mayer, *Materiales y técnicas del arte* 9ª edición (Tursen, Hermann Blume Ediciones, Madrid, 1993)
21 A. Villarquide Jenevois, *La pintura sobre tela I, Historiografía, técnicas y materiales* (NEREA 2004)
22 M. Doerner, *Los materiales de pintura y su empleo en el arte* 18ª edición (Editorial Reverté, Barcelona, 1998)
23 M. Garcia-Vallès, M. Vendrell-Saz, J. Molera, F. Blázquez, Environ. Geol. **36**, 137 (1998)
24 F. Cariati, L. Rampazzi, L. Toniolo, A. Pozzi, Stud. Conserv. **45**, 180 (2000)
25 P. Maravelaki-Kalaitzaki, Anal. Chim. Acta **532**, 187 (2005)
26 M.T. Doménech Carbó, J. Mol. Struct. **410**-/**411**, 559 (1997)

Available online at www.sciencedirect.com
ScienceDirect
Journal of Chromatography A, 1175 (2007) 275–282
JOURNAL OF CHROMATOGRAPHY A
www.elsevier.com/locate/chroma

Gas chromatographic–mass spectrometric characterisation of plant gums in samples from painted works of art

Ilaria Bonaduce *, Hariclia Brecoulaki [1], Maria Perla Colombini, Anna Lluveras [2], Vincenzo Restivo [3], Erika Ribechini

Dipartimento di Chimica e Chimica Industriale, Università di Pisa, via Risorgimento 35, 56126 Pisa, Italy

Received 30 August 2007; received in revised form 15 October 2007; accepted 22 October 2007
Available online 25 October 2007

Abstract

This paper presents an analytical GC–MS procedure to study the chemical composition of plant gums, determining aldoses and uronic acids in one step. The procedure is based on the silylation of aldoses and uronic acids, released from plant gums by microwave assisted hydrolysis, and previously converted into the corresponding diethyl-dithioacetals and diethyl-dithioacetal lactones. Using this method only one peak for each compound is obtained, thus providing simple and highly reproducible chromatograms. The analytical procedure was optimised using reference samples of raw plant gums (arabic, karaya, ghatti, guar, locust bean and tragacanth, cherry, plum and peach gums), commercial watercolours and paint layers prepared according to ancient recipes at the Opificio delle Pietre Dure of Florence (Italy). To identify gum media in samples of unknown composition, a decisional schema for the gum identification and the principal component analysis of the relative sugar percentage contents were employed. The procedure was used to study samples collected from wall paintings from Macedonian tombs (4th–3rd centuries BC) and from the Mycenaean "Palace of Nestor" (13th century BC) in Pylos, Greece. The presence of carbohydrates was ascertained and plant gum binders (fruit and a mixture of tragacanth and fruit tree gums) were identified in some of the samples.

Keywords: GC–MS; Polysaccharide; Plant gum; Mural painting

1. Introduction

Plant gums are naturally occurring polysaccharide exudates from several species of plants or extracted from the endosperm of some seeds. They are polymers with a high molecular weight consisting of aldopentoses, aldohexoses and uronic acids joined together by a glycoside bond [1]. Some plant gums have been widely used as paint media and sizing agents since the 3rd millennium BC [1–10]. In the Mediterranean basin the gums traditionally used were arabic gum, exuded from *Acacia senegal* and *Acacia seyal* plants, tragacanth gum, exuded from *Astragalus* sp., and fruit tree gum, obtained mainly from cherry, apricot, peach and plum trees. Locust bean, extracted from the kernels of the carob tree (from *Ceratonia siliqua*) is also believed to have been used in the Mediterranean basin since ancient times, while guar (from *Cyanoposis tetragonolobus*, Leguminosae) ghatti (from *Anogeissus latifolia*, Combretaceae) and karaya gum (from *Sterculia urens*, Sterculiaceae) were important materials in the Indian subcontinent [1].

The analysis of polysaccharides by gas chromatography requires an initial chemolysis step to free the sugars. Acidic hydrolysis [4,5,9,11,12] and methanolysis [6,13] have been used for this purpose, and microwaves significantly shorten reaction times, giving good reaction yields and a reduced decomposition of labile sugars [14–16].

A suitable derivatisation is a necessary step prior to GC analysis. Many derivatisation procedures have been described in the literature for carbohydrate analyses.

The formation of trimethylsilyl derivatives [6,7,9,13] has been used. An important aspect regarding the chromatographic

* Corresponding author.
E-mail address: ilariab@dcci.unipi.it (I. Bonaduce).
[1] Present address: American School of Classical Studies at Athens, Souidias 54, 10676 Athens, Greece.
[2] Present address: Departament de Cristal.lografia, Mineralogia i Dipòsits Minerals, Universitat de Barcelona, C/Marti i Franquès S/N 08028, Barcelona, Spain.
[3] Present address: Società Chimica Larderello, Piazza Leopolda 2, 56044 Larderello (PI), Italy.

0021-9673/$ – see front matter © 2007 Elsevier B.V. All rights reserved.
doi:10.1016/j.chroma.2007.10.056

analysis of sugars concerns the fact that in water solutions, monosaccharides undergo intramolecular reactions to form cyclic hemiacetals, either five and six-membered rings. In this way, each hexoses can be present in five forms: two pyranoside, two furanoside and an open one. Considering that gums consist of more than one sugar, the immediate consequence of chromatographic analysis is the acquisition of highly complex chromatograms where multiple peaks are present. In this case, irreproducible quantification, loss of sensitivity, and a limited possibility to identify the various polysaccharide materials may occur. To overcome this problem, other methods have been proposed:

(i) The reduction of carbonyl moieties: monosaccharides are transformed into the corresponding alditol followed by acetylation [17]. Different monosaccharides are thus transformed into the same alditol and when this takes place in ketoses, two isomers are produced from each monosaccharide. This could compromise the correct interpretation of the sugar profile obtained, and thus the reliable identification of the polysaccharide.
(ii) The conversion of monosaccharides into acyclic oximes, followed by silylation [8] or acetylation [4,5]. In this case both syn and anti forms are produced, resulting in two peaks for each sugar.
(iii) The formation of diethyl mercaptal derivatives followed by silylation [12]. This method results in one chromatographic peak for each monosaccharide and uronic acid.

This paper describes a GC–MS analytical procedure for the characterisation of plant gums in samples from painted works of art. It involves the following steps: microwave assisted hydrolysis of polysaccharide materials, clean-up on an cation-exchange resin of freed sugars, followed by an optimised derivatisation resulting in the determination of monosaccharides and uronic acids in just one chromatographic step. The overall analytical procedure was tested using a standard solution of sugars, commercial plant gums, and reference samples prepared about 30 years ago according to ancient recipes at the Opificio delle Pietre Dure of Florence (Italy).

Lastly, the presence of carbohydrates in paint samples from Macedonian tombs (4th–3rd centuries BC) and from the Mycenaean "Palace of Nestor" (13th century BC) at Pylos, Greece, was ascertained and an interpretation of the carbohydrate profile was put forward.

2. Experimental

2.1. Chemicals and reagents

Monosaccharides and uronic acids D-(+)-galactose, L-(−)-fucose, L-(+)-arabinose, L-(−)-ramnose, L-(−)-mannose, D-(+)-xylose, D-(+)-glucose, D-glucuronic acid, D-galacturonic acid monohydrate, and mannitol, used as an internal standard, purity 99%, were obtained from Sigma–Aldrich (Milan, Italy).

Trifluoroacetic acid 99% purity, and anhydrous pyridine were from Fluka (Milan, Italy), ethanethiol (ETSH) 99.5%, sodium azide (NaN_3) 99.5% and *N,O*-bis(trimethylsilyl)trifluoroacetamide (BSTFA), were from Sigma–Aldrich. The cation-exchange resin Dowex 50W-8X, cross linking grade of 8% and granulometry comprised between 100 and 200 mesh, was supplied by Sigma (Milan, Italy).

Stock solutions of monosaccharides with concentrations ranging from 200 to 600 $\mu g\,g^{-1}$ were prepared in pure water where 1% of sodium azide was added to prevent microbial growth, and were stored at 4 °C. Working standard solutions were prepared daily using dilution.

2.2. Raw materials

Arabic, karaya, ghatti, guar, locust bean and tragacanth gums were purchased from Sigma–Aldrich. Cherry, plum and peach gums were kindly provided by the Opificio delle Pietre Dure (Florence, Italy).

2.3. Painting samples

Watercolours were supplied by Maimeri (Milan, Italy). They contained arabic gum with cadmium sulphide (yellow no. 081) Y, chromium oxide (green no. 331) G, iron oxide (red no. 278) R, cobalt aluminate (cobalt blue no. 373) B.

Reference paint layers on glass slides had been prepared in 1975 following old recipes and stored in the dark at Opificio delle Pietre Dure, Florence (Italy) [18]. Samples were analysed from reference paint layers containing arabic gum with calcium carbonate (sample AC), arabic gum with zinc oxide (sample AZ), and arabic gum without any pigment (sample A).

2.4. Wall painting samples from wall paintings

Four samples collected from wall paintings of Macedonian tombs (4th–3rd centuries BC), Greece [19], and two samples from mural paintings from the Mycenaean "Palace of Nestor" (13th century BC) in Pylos, Greece [20], were analysed. The samples are reported in Table 1 and all contained both paint and plaster layers.

2.5. Apparatus and chromatographic conditions

A microwave oven MLS MEGA Milestone 1200 W (Milestone Microwave Laboratory System, Monroe, CT, USA) was used. The hydrolysis conditions were as follows: power 500 W, temperature 120 °C, duration 20 min.

A Thermoquest Trace GC system equipped with a programmed-temperature vaporizer (PTV) injector and coupled with an ion trap mass spectrometer PolarisQ (Finnigan, USA) was used. The injector was used in the constant temperature splitless mode at 300 °C, with a purge time of 0.87 s. Chromatographic separation was performed on an HP-5MS silica capillary column (J&W Scientific, Agilent Technologies, USA), 30 m × 0.25 μm I.D. (5% phenyl-/95% methylpolysiloxane). The carrier gas (helium, 99.995% purity) flow was kept at 1.2 ml/min from 0 to 40 min, 0.8 ml/min from 40 to 44 min, and 1.2 ml/min from 44 to 73.5 min. The chromatographic oven was

Table 1
Wall painting samples

Tomb	Provenance	Age	Sample	Sample weight (mg)
Chamber tomb III of Aghios Athanassios	Macedonia	4th–3rd centuries BC	AGAT4	6
			AGAT30	42
Tomb Z of Derveni	Macedonia		AZ3	8
			AZ18	18
"Palace of Nestor"	Peloponnese	13th century BC	P9	10.8
"Palace of Nestor"	Peloponnese		P11	25.3

kept at 80 °C for 1 min, then from 80 °C to 190 °C at 2.5 °C/min, 15 min at 190 °C, from 190 °C to 280 °C at 20 °C/min, and 280 °C for 10 min. Ionisation was performed in the electron impact mode at 70 eV. The ion source temperature was 230 °C, and the interface temperature was 280 °C. Ionisation was performed in electron impact mode at 70 eV. Mass spectra were recorded both in total ion chromatogram (TIC) mode (*m/z* 40–650) and selected ion monitoring (SIM) modes (*m/z* 249 and 319 for xylose and arabinose; *m/z* 249 and 333 for ramnose and fucose; *m/z* 135, 305 and 319 for galacturonic and glucuronic acids; *m/z* 307, 319 and 331 for glucose, mannose, and galactose; *m/z* 307 and 319 for mannitol).

2.6. Analytical procedure

The sample was admixed with 0.5 ml of trifluoroacetic acid 2 M in PTFE closed conic vials, and subjected to microwave assisted acid hydrolysis. After hydrolysis, the sample was filtered with a PTFE membrane and then purified on a Dowex 50 W-8X cation-exchange resin, packed on a 0.5 cm diameter column. Sugars were eluted with 3 ml of 0.02 M HCl [14]. The acidic solution containing monosaccharides and uronic acids was added with the derivatisation internal standard solution (5 μl mannitol solution 100 μg g^{-1}), dried under nitrogen flow, admixed with 25 μl of ethanethiol/trifluoroacetic acid (2/1, v/v), and kept at ambient temperature for 20 min. In these conditions the carbonyl moieties of monosaccharides and uronic acids react with ethanethiol, and form the corresponding diethyl-dithioacetals and lactones. The samples were then subjected to derivatisation with a silylating agent prior to GC–MS analysis. The ethanol solution containing the dithioacetals sugar derivatives was added with 80 μl of BSTFA as derivatising agent, 50 μl of pyridine as solvent, and kept at 60 °C for 45 min. The reaction mixture was then dried under nitrogen flow and redissolved in 250 μl of hexane and added with the injection internal standard (5 μl of hexadecane solution 150 μg g^{-1}): 2 μl of this solution, containing sugar diethyl-dithioacetal trimethylsilyl derivatives, were thus injected into the gas chromatograph. All reference materials and samples were analysed four times each.

3. Results and discussion

As far as the derivatising procedure is concerned, the proposed method based on BSTFA was compared with those methods reported in the literature for the trimethylsilylation of diethyl-dithioacetal compounds. These consist of adding hexamethyldisilazane (HMDS) and pyridine to the sample with or without trimethylclorosilane (TMCS) ([21,12], respectively).As previously reported, TMCS causes the formation of ammonium chloride [12]. This aspect needs underlinining, since commercial HMDS can contain TMCS as a catalyst. Derivatisation tests performed with or without TMCS, highlighted that catalytic amounts of TMCS also strongly interfere with the derivatisation reaction. In fact, the ammonium chloride that is formed interferes with the drying of the sample solution, causing irreproducible chromatographic profiles and reaction yields.

HMDS and BSTFA were also compared. Although both derivatising agents gave very high reaction yields (underivatised or partially derivatised compounds were not detected in the chromatograms), and reproducibilities (about 20% for monosaccharides and uronic acids), BSTFA proved to be less sensitive to possible interferences, such as water traces. Finally, the importance of pyridine was tested. An average relative standard deviation of the sugar peak areas of 9% was obtained when pyridine was used, versus 20% when pyridine was not used.

In Fig. 1 the chromatogram of a standard solution of the seven monosaccharides and the two uronic acids (concentration range 2–20 μg g^{-1}) is reported, showing only one peak for each sugar.

The samples of raw natural gums were analysed according to the analytical procedure described previously. The average relative percentage sugar composition is reported in Table 2 together with the weight percentage content, calculated as the sum of the sugars determined.

The sugar composition obtained for the gums is in good agreement with the literature, and the calculated weight percentage content concurs with the different levels of solubility of the gums in water [22].

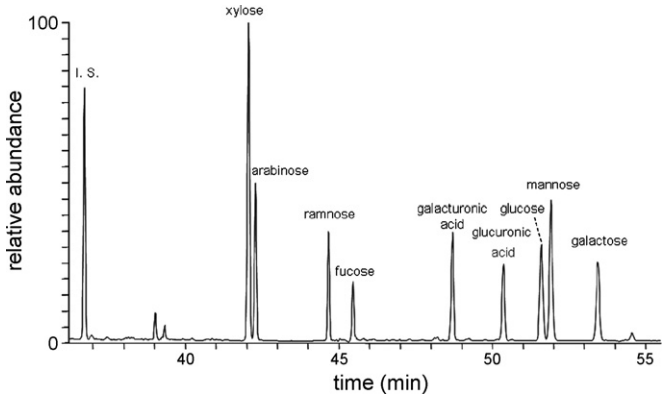

Fig. 1. Total ion chromatogram of a standard solution of monosaccharides and uronic acids (2–4 μg g^{-1}).

Table 2
Average relative percentage sugar composition of the raw gums

Gum	Xylose	Arabinose	Ramnose	Fucose	Galacturonic acid	Glucuronic acid	Glucose	Mannose	Galactose	*W* weight%
Ghatti	–	47.0	3.5	–	–	11.0	–	2.5	36.5	65
Karaya	–	–	25.5	–	7.0	4.0	–	–	64.0	41
Locust bean	–	1.5	–	–	–	–	–	81.0	17.5	75
Guar	–	2.5	–	–	–	–	–	63.0	34.5	75
Arabic	–	37.2	11.2	–	–	7.0	–	–	44.7	77
Cherry tree	6.6	35.1	2.8	–	–	13.0	–	5.5	37.0	62
Peach tree	6.1	34.0	2.8	–	–	14.0	–	5.1	38.0	64
Plum tree	6.9	36.0	2.8	–	–	13.0	–	5.3	36.0	61
Tragacanth	14.9	34.7	3.4	7.4	13.8	3.5	11.5	–	10.8	44

Table 3
Average relative percentage sugar composition of the watercolours

Sample	Xylose	Arabinose	Ramnose	Fucose	Galacturonic acid	Glucuronic acid	Glucose	Mannose	Galactose
Yellow no. 081	–	41.0	9.5	–	–	5.5	–	–	44.0
Cobalt blue no. 373	–	39.0	9.1	–	–	5.9	–	–	46.0
Green no. 331	–	40.0	9.7	–	–	5.3	–	–	45.0
Red no. 278	–	40.8	9.9	–	–	5.1	–	–	44.2
A	–	39.0	10.0	–	–	6.0	–	–	45.0
AC	–	41.6	10.0	–	–	4.0	–	–	44.4
AZ	–	40.0	11.0	–	–	4.1	–	–	44.9

Watercolour samples and reference paint layers were thus analysed, and the average relative percentage sugar composition is reported in Table 3.

A close look at the glycosidic profile reveals quite a constant composition of the arabic gum samples. In fact, relative standard deviations of 5.0, 9.0, 19.3, and 3.5 resulted in the content of arabinose, ramnose, glucuronic acid and galactose, respectively. Interestingly, the last three samples had been naturally aged for about 30 years, which has not seemed to interfere with the gum composition, as well as the presence of the investigated pigments.

Each of the gums studied showed a very specific sugar composition. It is quite easy to identify each one in a sample of unknown composition, with the aid of a decisional scheme, for example, such as the one reported in Fig. 2, when only one plant gum is present.

Of course, identifying a mixture of gums is more complex, since the sugar composition changes depending on the relative proportion of each gum, and may thus be hard to evaluate just on the basis of the occurrence/absence of a sugar. To help identify the gums, principal component analysis (PCA), was applied to the correlation matrix of the relative percentage sugar composition of the arabic, tragacanth, fruit tree, ghatti, karaya, locust bean and guar samples analysed (score and loading plots are reported in Fig. 3A-1 and A-2, respectively) and the arabic, tragacanth and fruit tree gum samples analysed. These latter are the only gums with historical relevance as paint binders in the Mediterranean area [1] (score and loading plots are reported in Fig. 3B-1 and B-2). Note that glucose was excluded from the database, since it could have arisen from several external sources that may have contaminated the sample: it would thus be impossible to correctly identify the source of the gum. In fact, glucose is one of the products of photosynthesis in plants and some prokaryotes, in addition to being present in animals and fungi (resulting from the breakdown of glycogen) and in plants (starch and cellulose).

The score plot is reported in Fig. 3A-1 and the first two components accounted for 56.1% of the overall data. Although all gums are grouped in separate clusters, the figure highlights that arabic, fruit tree, ghatti and karaya gums are “squashed” in the same area of the score plot. This is due to their relatively similar composition with respect to tragacanth, locust bean and guar gums. In Fig. 3B-1 only arabic, fruit tree and tragacanth gums were considered, and a better separation was achieved (the first two components accounted for 75.5% of the overall data). The loading plots are easily explainable on the basis of the sugar composition. For example, in the score plot of Fig. 3B-2, fucose and galacturonic acid are only present in tragacanth gum and are thus the most significant variables for the characterisation of this gum (Fig. 3B-2).

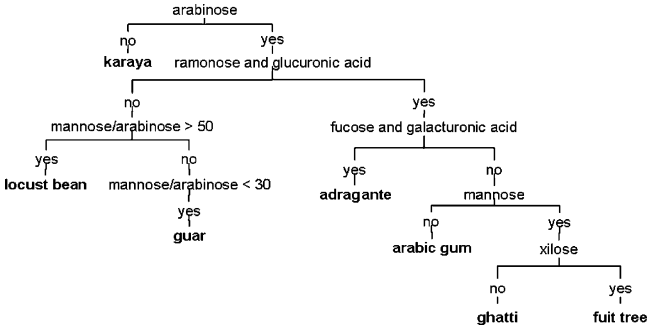

Fig. 2. Decisional scheme for the identification of a gum (arabic, tragacanth, fruit tree, ghatti, karaya, locust bean and guar) on the basis of its sugar composition.

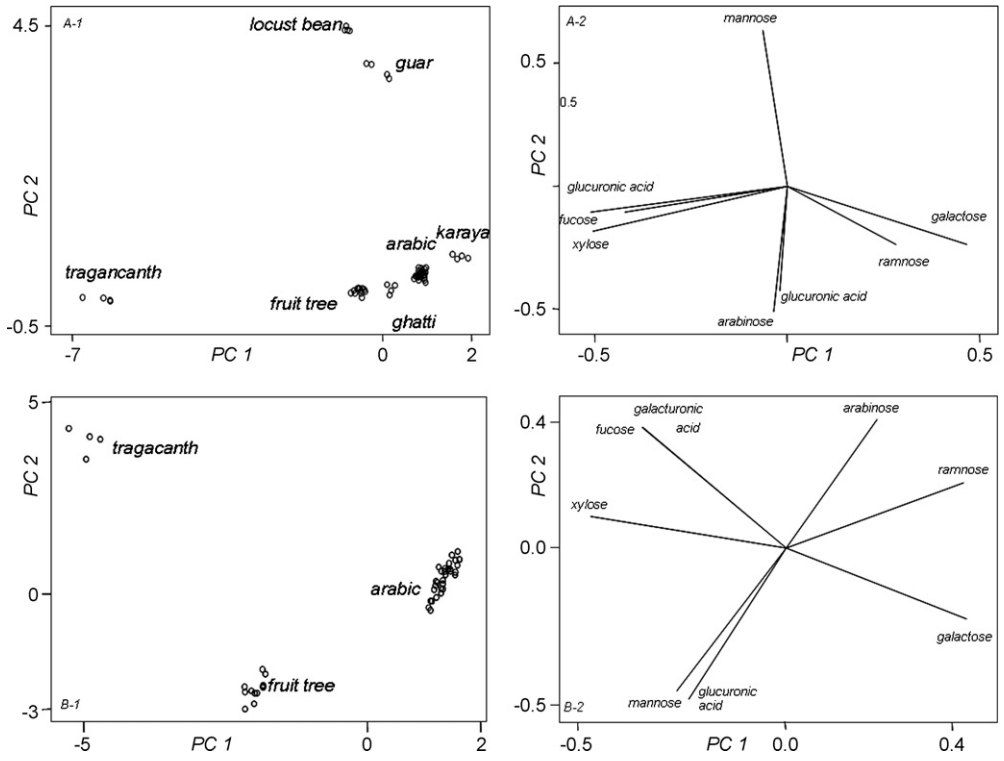

Fig. 3. Score (1) and loading (2) plots of the reference samples of: (A) arabic, tragacanth, fruit tree, ghatty, karaya, locust bean and guar gums; (B) arabic, tragacanth, fruit tree.

The samples from wall paintings described previously contained both monosaccharide and uronic acids: chromatograms are shown in Fig. 4 and relative sugar composition is reported in Table 4.

All samples contained glucose in higher amounts than the tragacanth gum content, indicating that another source for this sugar must be hypothesised. This is not surprising, since glucose, as explained above, is widespread in the animal and vegetal kingdom, as a product of metabolic processes or as a constituent itself. Moreover starch was commonly added to the plaster of mural paintings to increase cohesion: its use in these paintings cannot be ruled out.

All samples contained all sugars, suggesting that a mixture of gums was used, although in several samples, some of the monosaccharide and uronic acids are in very small amounts. To evaluate the sugar composition of these samples using our decisional scheme, the sugars whose content was less than 1% were considered as not being present. Consequently since the sugar profile of AGAT30 is absent both of fucose and galacturonic acid, it can be classified as fruit tree gum (arabinose/yes; ramnose and glucuronic acid/yes; fucose and galacturonic acid/no; mannose/yes; xylose/yes → fruit tree). All other samples were not classifiable using this method. The principal component analysis of the data was thus applied to the relative sugar composition of all the samples (excluding glucose), together with the dataset of arabic, tragacanth and fruit tree gums and the resulting score plot is reported in Fig. 5.

The score plot can be interpreted as follows:

(i) Sample AGAT30 is located very close to the fruit tree gum cluster, indicating that this was the plant gum used as a paint binder.
(ii) Samples P9 and P11 are located between the clusters of tragacanth and fruit tree gums, suggesting that a mixture of these two gums was used.
(iii) Samples AZ3, AZ18 and AGAT4 are not classified. A closer look at the sugar profile reveals that these samples are characterised by a very high relative content of

Table 4
Sugar composition of wall painting samples

Sample	Xylose	Arabinose	Ramnose	Fucose	Galacturonic acid	Glucuronic acid	Glucose	Mannose	Galactose
AGAT4	17.6	5.7	2.5	1.5	1.3	2.7	54.0	9.5	5.1
AGAT30	3.2	9.9	3.7	0.8	0.7	3.3	51.6	6.2	20.6
AZ3	52.4	5.6	1.0	0.5	0.2	0.4	28.5	8.0	3.4
AZ18	47.8	8.5	3.8	1.0	0.5	0.8	22.6	9.5	5.6
P9	14.2	30.4	4.1	4.7	0.2	6.5	23.4	10.3	6.2
P11	17.0	16.2	2.5	2.0	0.4	2.7	39.0	1.6	18.6

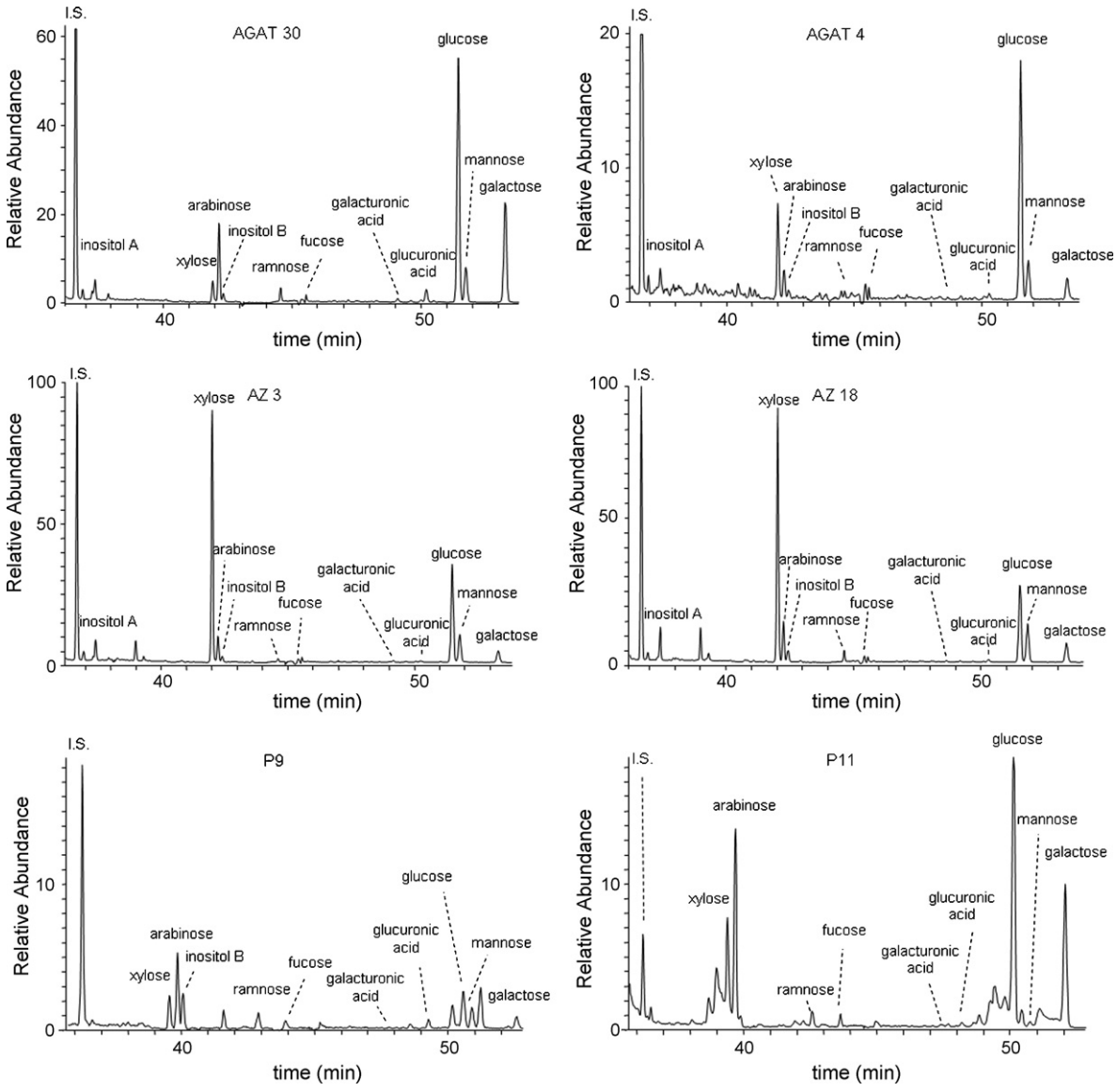

Fig. 4. Chromatograms of wall painting samples.

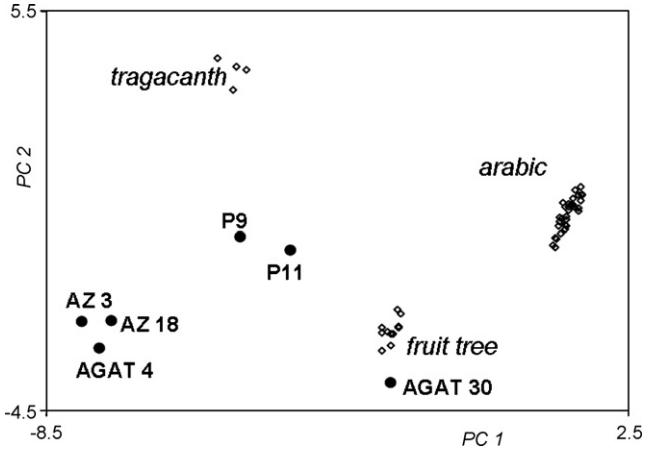

Fig. 5. Score plot relative to the reference and paint samples.

xylose, that cannot be explained just on the basis of the occurrence of tragacanth and fruit tree gums. Moreover, these same samples show the ratio xylose/arabinose >1, while tragacanth and fruit tree gums are both characterised by a ratio value <1. Unfortunately in the literature there are very few papers where the quantitative determination of the sugar profile is reported, and gum identification is based on the presence/absence of specific sugars. In any case, in a study of metallo-gallic ink binders used in ancient manuscripts, there is evidence of the occurrence of a glucide binder, but the sugar profiles do not correspond to any of the gums investigated [7]. In some of these samples an inverted ratio xylose/arabinose can be seen. In this case the modified profile has tentatively been ascribed to the interaction of the gum medium with the parchment used as support. Another example is related to the characterisation of the paint background of a terracotta statue from 400 BC where the binder was identified

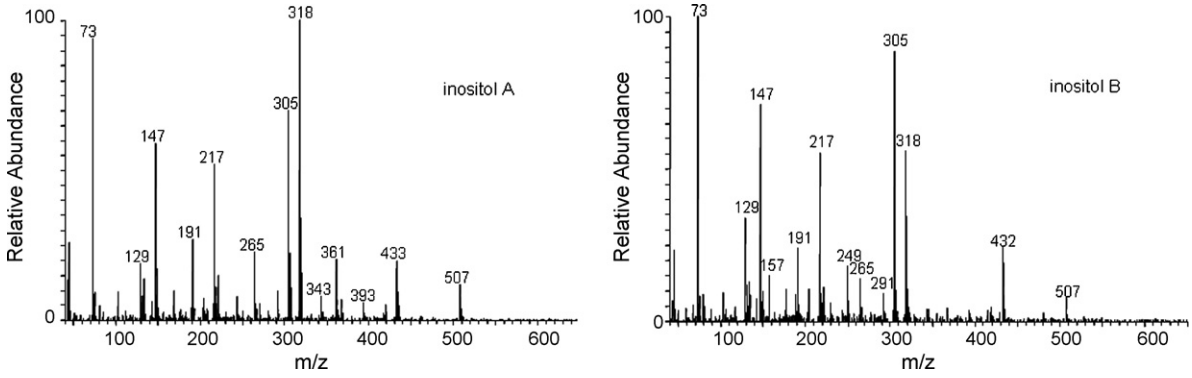

Fig. 6. Mass spectra of the two inositol isomers, labelled as inositol A and B in Fig. 4.

as a mixture of guar and tragacanth gum [4,5]. The chromatographic profile, although not discussed in the paper, shows an inverted ratio xylose/arabinose, which cannot be explained on the basis of the plant gums identified. This highlights that the sugar profile of gum media samples may be subjected to a modification that is currently not understood. This phenomenon might be underestimated since in most cases gum identification is performed on the sugar composition with no quantitative evaluation of the sugar profile.

Lastly, in all the samples with the exception of P11, one or two inositol isomers (labelled inositol A and inositol B), whose mass spectra are shown in Fig. 6, were identified.

It is well known that inositol phosphates are involved in gene expression [23,24]. Their occurrence seems to point to a biological attack in these mural paintings, caused for example by bacteria or fungi. If this hypothesis is correct, these species may actually modify the sugar content. Some sugars, in fact, could have been selectively metabolised by the infesting living organisms. Or else living organisms might have changed the relative sugar composition of the gum, having as metabolic product only some.

These results highlight that although the procedure is suitable for analysing sugars by GC–MS and for defining the composition of plant gum samples, the behaviour of polysaccharide media still needs further study. If, in fact, the sugar composition of gum media does not significantly change with ageing and in the presence of pigments, as found in this study on reference paint layers, and as reported previously [7], still nothing is known about the changes occurring when external factors, such as fungi or bacteria, are introduced. Further studies to clarify the effect on the sugar composition of polysaccharide binders under biological attack are thus necessary.

4. Conclusions

An analytical procedure for the determination of the sugar composition of gum media using GC–MS was set up. The sugars released from vegetable gums by microwave assisted acidic hydrolysis, were derivatised using a two-step procedure, to render them suitable for GC–MS analysis. Monosaccharides and uronic acids were initially transformed into the corresponding diethyl-dithioacetals and lactones, thus avoiding any mutarotation reaction, and afterwards, acidic and alcoholic moieties were trimethylsilylated. Highly reproducible chromatograms were thus achieved, where only one peak is obtained for each sugar.

Reference samples of ghatti, karaya, locust bean, guar, arabic gum, cherry tree, peach tree, plum tree and tragacanth gums were then analysed, showing that these gums can be distinguished on the basis of their different chromatographic profiles. Commercial watercolours and reference paint layers prepared about 30 years ago were also analysed, highlighting that the sugar composition of arabic gum is quite stable and does not depend on the occurrence of the pigments investigated. A decisional scheme was used to identify gums where only one was present in a sample of unknown composition. Principal component analysis was also applied to the relative sugar percentage content of the reference samples. This was done to help the gum identification, especially in cases where more than one polysaccharide material was used as paint media.

Finally, six samples collected from mural paintings of Macedonian tombs (4th–3rd centuries BC) and of the Mycenaean "Palace of Nestor" at Pylos (13th century BC), Greece, were analysed, all of which showed the occurrence of saccharide material. Samples were processed with both the decisional scheme and PCA, and the composition of the sample was suggested. Although some aspects suggested a biological attack (which might have altered to some extent the relative sugar composition of the samples), the paint medium of three of the samples was identified as fruit tree gum in one sample, and a mixture of tragacanth and fruit tree gum in the other two samples.

Acknowledgements

The authors gratefully acknowledge the Department of Classics of the University of Cincinnati and the American School of Classical Studies in Athens (Greece) for funding the analysis of the samples taken on ancient wall paintings from Macedonia and Pylos.

References

[1] J. Mills, R. White, Organic Chemistry of Museum Objects, Butterworth-Heinemann, London, 1999.
[2] R. Newman, M. Serpico, Ancient Egyptian Materials and Technology, Cambridge University Press, Cambridge, 2000.
[3] S.L. Vallace, Analyst 122 (1997) 75R.
[4] V. Pitthard, M. Griesser, S. Stanek, Ann. Chim. (Rome) 96 (2006) 561.
[5] V. Pitthard, M. Griesser, S. Stanek, T. Bayerova, Macromol. Symp. 238 (2006) 37.
[6] P. Mejanelle, J. Bleton, A. Tchapla, S. Goursaud, in: Z. El Rassi (Ed.), Carbohydrate Analysis by Modern Chromatography and Electrophoresis (Journal of Chromatography Library, vol. 66), Elsevier, Amsterdam, 2002, p. 845.
[7] J. Bleton, C. Coupry, J. Sansoulet, Stud. Conserv. 41 (1996) 95.
[8] R. Newman, in: V. Dorge, F.C. Howlett (Eds.), Painted Wood: History and Conservation, J. Paul Getty Trust, Williamsburg, VA, 1994, p. 33.
[9] U. Schneider, E. Kenndler, Fresen. J. Anal. Chem. 371 (2001) 81.
[10] S.L. Vallace, B.W. Singer, S.M. Hitchen, J.H. Townsend, J. Am. Inst. Conserv. 37 (1998) 294.
[11] B.V. Kharbade, G.P. Joshi, Stud. Conserv. 40 (1995) 93.
[12] V. Pitthard, P. Finch, Chromatographia 53 (2001) S317.
[13] J. Bleton, P. Mejanelle, J. Sansoulet, S. Goursaud, A. Tchapla, J. Chromatogr. A 720 (1996) 27.
[14] M.P. Colombini, A. Ceccarini, A. Carmignani, J. Chromatogr. A 968 (2002) 79.
[15] V. Singh, R. Sethi, A. Tewari, V. Srivastava, R. Sanghi, Carbohyd. Polym. 54 (2003) 523.
[16] V. Singh, A. Tiwari, P. Kumari, S. Tiwari, Carbohyd. Res. 341 (2006) 2270.
[17] V.J. Birstein, Stud. Conserv. 20 (1975) 8.
[18] C. Lalli, M. Matteini, A. Moles, M.R. Nepoti, Stesure artificiali di leganti pittorici. Olii, resine, cere, colle, uovo, preparati in miscele binarie: caratteristiche analitiche e proprietà, Opus Libri, Firenze, 1987.
[19] H. Brécoulaki, La peinture funéraire de Macédoine. Emplois et fonctions de la couleur IV-II s. av. J-C, in Paris, 2003.
[20] M.L. Lang, The Palace of Nestor at Pylos in Western Messenia. Vol. II. The Frescoes, Princeton University Press, Princeton, 1969.
[21] S. Honda, N. Yamaochi, K. Kakehi, J. Chromatogr. 169 (1979) 287.
[22] M. Ash, I. Ash, Handbook of Food Additives, Furia, 1980.
[23] X. Shen, H. Xiao, R. Ranallo, W.-H. Wu, C. Wu, Science 299 (2003) 112.
[24] D.J. Steger, E.S. Haswell, A.L. Miller, S.R. Wente, E.K. O'Shea, Science 299 (2003) 114.

Title shortened version : Distribution of degradation products of azurite in mural paintings by SR FTIR

Degradation of azurite in mural paintings : distribution of copper carbonate, chlorides and oxalates by SRFTIR

A.Lluveras [1], S.Boularand [1], A. Andreotti[2], M.Vendrell-Saz [1]

1 Departament de Cristal·lografia i Mineralogia, Universitat de Barcelona, C/Martí i Franquès S/N 08028 Barcelona (Spain), Telf. 0034934021357, Fax.0034934021340. e-mail : alluveras@ub.edu

2 Dipartimento di Chimica e Chimica Industriale, Università di Pisa, Via Risorgimento 35 Pisa (Italy)

Abstract

This article illustrates the analysis by synchrotron micro-analytical techniques of an azurite painting presenting greenish chromatic degradation. The challenge of the experiments was to obtain the spatial distribution of the degradation products of azurite. Copper hydroxychlorides, carbonates and copper oxalates have been mapped by SR FTIR imaging of cross-sections in transmission mode. To complement the information Py/GC/MS and GC/MS techniques were applied in order to characterize the binding media and organic materials present as well as their degradation products. Results contribute to better understand the decay of blue areas in ancient paintings not only from the particular point of view of azurite weathering, but also by adding information regarding the oxalates' formation and their distribution in painting samples. Synchrotron radiation demonstrates its capability for the mapping in painting cross-sections.

Keywords

Paintings, GC/MS, Py-GC/MS, mass spectrometry, FTIR, synchrotron radiation, XRD, azurite, oxalates, degradation, copper chlorides, atacamite, paratacamite

PACS 78.30-j; 68.37.Hk ; 61.10. Nz ;

1. Introduction

Azurite is a basic copper carbonate ($2CuCO_3.Cu(OH)_2$), a natural blue pigment used since the Fourth Dynasty in Egypt although it became the most important blue pigment during the Middle Ages and Renaissance [1].

Many paintings became altered by the transformation of blue areas into green and brown. Clear examples of the problematic above described are the frescoes at the Monumental Cemetery of Pisa or the Crypt of the Cathedral of Siena [2-3].

Green shades in azurite blue paintings could be attributed to different reasons depending on their composition: natural green shades of the mineral ore, the use of synthetic green pigments obtained from the corrosion of copper plates exposed to vinegar vapours, or the degradation of the original pigment into green products such as copper chlorides.

Although azurite presents a natural greenish undertone due to the particles of malachite ($CuCO_3.Cu(OH)_2$) and cuprite (Cu_2O) that can be found associated in nature to the azurite ores [1], the desiderated blue tone could be obtained by purification of azurite from the other phases as it was provided by authors such as Cennino Cennini [4]. Though the synthesis of green copper-based pigments have been reported in Heraclius, Tephilus or Vitruvius recipes [5-6], the synthesis process products have been already characterized as mixtures of copper acetates, carbonates and hydroxychlorides [7], that

is, a different composition from that of the green shaded azurite-based paintings usually characterized in literature.

Thus, degradation of azurite blue pigment into a green product due to ageing seems to be the cause of the greenish areas observed in different azurite paintings as the ones cited above. Azurite, although being stable to light and atmosphere, presents frequent chromatic alterations to greenish tonalities due to transformation into paratacamite and atacamite ($Cu_2Cl(OH)_3$) [2-3,8-9] and also malachite ($CuCO_3.Cu(OH)_2$) [1] not yet completely understood.

Samples analysed come from a gypsum shield on top of a door in the Monastery of Santes Creus (Catalonia, Spain) dating from the 1605 a.D. The shield is depicted mainly in blue and brown in order to underline the relieves with the monastery insignias. In the blue areas, green shades could easily be identified (Figure1a).

Synchrotron radiation X-ray diffraction and synchrotron IR microscopy have been used to produce maps of phases and high contrast chemical imaging. Experiments were performed at the European Synchrotron Radiation Facility (ESRF, Grenoble, France) at the station ID 21. Results helped to unequivocally characterize the inorganic crystalline products formed by the weathering process of azurite and also to determinate the distribution of those products along the blue layer. Thus, experiments constitute a significant contribution to better understand the chromatic degradation of azurite blue layers and the mechanism of formation of the decay by products. Moreover, experiments add information to the long time discussed mechanisms of the formation of oxalates in mural paintings. Finally, the potentiality and the limits of the synchrotron radiation micro imaging techniques on this kind of samples and the complementary of the information of the techniques used to solve cultural heritage problems will be discussed.

2.Results

2.1.Experimental layout

2.1.1 Microscopy

Samples were preliminarily observed by means of a low magnification stereo microscope (Nikon SMZ 1500) in order to observe the number and sequence of painting layers including the support and the surface state.

Several fragments of the sample were embedded in polyester resin using methyl ethyl ketone peroxide as hardener (Cronolita E.I., Spain), cut with a low deformation diamond saw and polished to allow the study of the cross section under a reflecting dark field optical microscope. A A Nikon Eclipse LV 100 PDL analytical microscope equipped with a Nikon Digital Camera DMX 1200 F was used for visible light microscopy of the polished cross sections.

SEM images of the same sections were taken using a JEOL (Tokyo, Japan) JSM-840 (secondary and backscattered electron detection) with a LINK AN 10000 microanalyser. The acceleration voltage used was 20 KeV.

2.1.2.Fourier Transform Infrared Spectroscopy (FTIR)

Analyses were made with a BOMEM MB-120 Fourier transform infrared spectrometer in two transmission modes, microscope and diamond cell. All results were processed with GRAMS/32 (Galactic) software.

When working with the diamond cell, the equipment was an infrared spectrometer Bomem MB-120 equipped with a potassium bromide beamsplitter and deuterated triglycine sulphate (DTGS) detector. The spectra are the sum of 30 scans collected from 4000 to 350 cm^{-1} at a resolution of 4 cm^{-1}

Bomem MB-120 Fourier Transform Infrared Spectrometer, equipped with a Spectra-Tech Analytical Plan microscope, was used with the diamond cell, as sample holder. The spectrometer has a KBr beamsplitter and a Globar source. The microscope has its own mercury cadmium telluride (MCT) detector refrigerated with liquid nitrogen. Spectrum was recorded between 4000 and 720 cm^{-1} with a resolution of 4 cm^{-1} and an accumulation of 100 scans.

2.1.3. Gas mass spectrometry

- Pyroprobe CDS Analytical Inc. 5000 Series (Oxford, USA). It was operating with an initial temperature of 50°C, up to 550°C at 20°C/ms, then isothermal for 20 sec. (probe run time 0.33 min). The pyrolyser was coupled on-line with the injection port of a GC System Gas Chromatograph, coupled with a Mass Detector. The interface temperature of the pyrolyser was 180°C, the transfer line 300°C, the valve oven 290°C. A few µg of the samples admixed with 2 µl of hexamethyldisilazane were inserted into a quartz tube and placed into the pyrolysis chamber.
- 6890N GC System Gas Chromatograph (Agilent Technologies, Palo Alto, CA, USA), coupled with a 5973 Mass Selective Detector (Agilent Technologies, Palo Alto, CA, USA) single quadrupole mass spectrometer, equipped with split/splitless injector. The mass spectrometer was operating in the electron impact (EI) positive mode (70 eV). The MS transfer line temperature was 280 C; the MS ion source temperature was kept at 230 ºC; and the MS quadrupole temperature was at 150 ºC. This instrument was used for the Py/GC/MS analyses. Detailed working conditions are published elsewhere [10].
- A 6890N GC System Gas Chromatograph (Agilent Technologies, Palo Alto, CA, USA), coupled with a 5975 Mass Selective Detector (Agilent Technologies, Palo Alto, CA, USA) single quadrupole mass spectrometer, equipped with a PTV injector was used. The mass spectrometer parameters correspond to the ones reported above. This instrument was used for the analysis of samples processed with the combined analytical procedure for the simultaneous identification of glycerolipids, proteinaceous materials, plant and animal resins, and natural waxes. The detailed operating conditions, and the analytical procedure are published in detail elsewhere [11]
- Microwave oven model MLS-1200 MEGA Milestone (FKV, Sorisole (BG,) Italy)

2.1.4. Synchrotron radiation microanalysis

Synchrotron radiation Fourier transform infrared microspectroscopy (SR FTIR) in transmission mode was performed at the station ID21 at the European Radiation Synchrotron Facility (ESRF, Grenoble). Maps were recorded using 4 microns step and 40 scans for each spectrum. Aperture and resolution were fixed at 8 x 8 μm and 8 cm^{-1}, respectively. In all cases the aperture and the step size chosen generate overlapping areas in order to increase the resolution of the components. A microtome Ultracut E with a glass knife was used to obtain slices around 10 μm for the FTIR analysis in transmission mode.

Synchrotron radiation experiments conditions are summarized in Table 1.

2.2 Sample characterization

Samples were characterized by optical observations, SEM-EDS, FTIR and mass spectrometric based techniques analysis. Results of the 'conventional' characterization of the sample are reported in Table 2.

2.2.1. Optical Microscope

Samples taken from the blue sampling area in the bottom right side of the shield indicated in figure 1a, present different characteristics under the stereomicroscope. Some of the fragments present a blue colour while others are completely greenish (figure 1b). Moreover, some of the fragments exhibit other layers such as a white and a brownish one (figure 1c).

A cross-section (figure 2a) clearly evidences the presence of different layers in one of the sample: a white preparation layer (layer 1), a brown pigment layer (layer 2) and the blue layer of interest (layer 3), corresponding to the layers observed under the stereomicroscope. The fractured appearance and the irregular size (from 5 to 20 μm) of the blue particles as well as the deep blue colour in coarse particles while finer particles display pale blue hue in layer 3 are characteristic of azurite [1]. In this sample no green shades were observed.

Figure 2b shows the cross-section of another embedded fragment consisting in the blue layer (layer 3) only, without the other layers that formed the complete stratigraphy. In this fragment is appreciable the presence of a matrix with green shades and the existence of blue particles in between.

2.2.2. Scanning Electron Microscope

The same polished samples were carbon coated to be studied under the Scanning Electron Microscope (SEM) with a coupled Energy Dispersive X–ray Spectroscopy (EDS) facility.

SEM images underline the different morphological characteristics of the layers. The same three layers already characterized by optical microscope (see 2.2.1.) can be also easily identified in backscattered electron images (figure 2c). Moreover, a metallic leaf of about 2,5 microns thick (between layers 2 and 3) and a superficial whitish layer on top of the blue one (layer 4) can be also appreciated with this technique

The chemical elements forming layer 1 detected by EDS (Ca, S) can be probably attributed to calcium sulphate ($CaSO_4$. n H_2O), which agrees with its morphology of the layer characteristic of gypsum [12-13]. The main elements detected in layer 2 (Si, Al, Ca, Fe) can be easily attributed to the presence of a clay with iron oxides [13,14,15]. The P and S also detected in layer 2 could be attributed to an organic material present as binding media in this layer [16].

The blue pigment layer (layer 3) is characterized by the presence of Cu and by the broken appearance and the big size (from 5 to 20 μm) of some of the pigment particles. Those results are consistent with the use of a copper pigment such as azurite [1]. Chloride (Cl) and copper (Cu) were detected in the greenish fragment of figure 2b.

The metallic leave is made of silver (Ag). Finally, in the white superficial layer (layer 4) the presence of Pb can be probably attributed to the presence of a lead compound such as lead white ($2PbCO_3 \cdot Pb(OH)_2$).

2.2.3. Fourier Transform Infrared Spectroscopy

Remaining fragments of the sample were analysed by Fourier Transform Infrared Spectroscopy (FTIR) in transmission mode using a diamond cell. Particles of each layer were isolated by using a dissecting knife and tungsten needles under a stereo-microscope [17]. This way, information on the different layers was obtained separately. Some characteristic spectra of the different layers are presented in figure 3. Table 3 presents the bands characteristic of each spectra obtained while Table 4 shows the characteristic bands of the reference materials identified.

In layer 1, the bands at 1683, 1620, 1315, 1114 (broad), 1004, 779, 669, 598 and 463 cm^{-1} correspond to gypsum ($CaSO_4$. $2H_2O$) and calcium oxalates (CaC_2O_4. n H_2O) [12,13,19,20,21].

Layer 2 is characterized by the presence of the peaks at 3697 and 3620 cm^{-1}(OH st), a broad band around 1022 cm^{-1}, with a shoulder at 1100 cm^{-1}(Si-O st), and a peak at 916 cm^{-1}(Al-O-H bd). These peaks can be attributed to a clay, probably kaolinite by the characteristic OH st bands [18-19].

The presence of the bands at 542 and 472 cm^{-1} can be interpreted as iron oxides characteristic peaks. The bands of iron oxides centred at 560 and 480 cm^{-1} can differ by up to 30 cm^{-1} due to differences in particle size and shape of the pigment particles [14], the presence of Fe detected by EDS would corroborate the assignment of these bands.

Oxalate peaks are also present in this layer (layer 2): C=O st at 1620 cm^{-1}, C-O st at 1320 cm^{-1} and C-C st at 780 cm^{-1} are indicative of calcium oxalates [20]. Not well defined bands around 1650, 1530 and 1400 cm^{-1} could be indicative of the presence of

a proteinaceous binder (C=O st Amide I, Amide II and C-N st, respectively) [19]. The noisy of those bands does not allow a clear identification.

Blue particles in layer 3 present the characteristic peaks of azurite confirming the identification of the pigment by means of microscope observations (optical and electronical) and EDS results [1]. Azurite characteristic peaks at 3430 (OH st), 1460 and 1414 (CO st), 1092 and 955 (OH bd), 837 and 769 (CO bd), cm^{-1}, are clearly identifiable in the spectra of layer 3 in figure 3 [22].

Green particles in layer 3, present both azurite characteristic peaks (cited above) and copper hydroxychlorides (atacamite and paratacamite) bands: 3440 and 3322 (OH st), 986, 948, 896 cm^{-1} [9]. The presence of the characteristic peaks of copper oxalates such as 1659, 1364 and 1321 cm-1(reported above), can be also appreciated allowing the identification of copper oxalates together with copper hydroxychlorides.

2.2.4. Gas chromatography mass spectrometry techniques

For the characterization of the organic materials present in the sample, gas-chromatographic mass spectrometric techniques were applied.

Py/GC/MS results of layer 2 and layer 3 (both blue particles and green particles separately) highlighted the presence of a polysaccharide material by the identification of the characteristic markers: tri-(O-TMS)-levoglucosane and 1,2,3,5-tetrakis-(O-TMS)-xylofuranose and others unknown polysaccharides compounds (evidenced in figure 4c and 4d) [23].

In Figure 4 are also reported for comparison the extracted ion chromatograms of the ions with m/z 217 of the reference materials cherry gum a), as an example of fruit gum, and starch b). Both the green and blue samples present the main pyrolysis product of glucose based polymers (as an example starch is reported in Fig.4 b). Moreover 1,2,3,5-tetrakis-(O-TMS)-xylofuranose (peak 1), absent in the pyrogram of starch, has been identified in both the samples, suggesting the simultaneously presence of a fruit gum.

GC/MS results were achieved by using the combined procedure already described in literature [11]. Layer 2 and layer 3 were again analysed separately. Purification of layer 3 fragments was necessary due to the presence of azurite. Copper based pigment can form aggregates with the proteinaceous material; in this way some derivatisation problems occur. A solid phase column was used to avoid derivatisation problems as described in literature [24].

Layer 2 (red-brown layer) aminoacidic profile was not obtained due to the quantity of sulphates present in the layer. Sulphates are retained in the pre-column and thus no aminoacids are arriving to the mass detector. No more sample was available to be analysed, thus the aminoacidic content of layer 2 was not characterized.

Layer 3 (green-blue layer) presented a proteinaceous material quantity slightly higher than the blank of the technique. The PCA treatment of the sample aminoacidic profile (Table 5) indicates that the sample can not be attributed to a cluster but it is situated in between the egg and the casein clusters (figure 5). That could be attributed to the high degradation of the proteinaceous material in the sample. The high Glycine content in the sample could be attributed to a bacterial attack [25]; this could have also generated the low levels of aspartic acid that would justify the sample shift towards the casein cluster.

Besides, the fatty acid composition of layer 3 highlights a profile that is not an oil nor a whole egg one. Characteristic ratios (A/P=0.15, P/S=0.8; ΣD=5.0) are not consistent with the ones of a siccative oil, but the content of dicarbossylic acids could suggest the the use of an egg undergone to deterioration as binding media. Moreover, an animal fat has been identified due to the presence of pentadecanoic, eptadecanoic, nonanoic acids and their isomers.

2.2.5. Synchrotron radiation FTIR microanalysis

Remaining fragments of the blue layer were prepared for the mapping experiments performed at the ESRF in order to establish the distribution of the compounds already

identified. For SR FTIR experiments, sample preparation has been described in a previous work already published [26].

Sample preparation is the key point in order to be able to perform transmission experiments. Due to sample characteristics (low organic material content, high brittleness, large pigment particles) some sample preparation strategies were not applicable. Direct squeezing in a diamond cell or polishing a KBr pellet described in literature [27-28] result in a complete destruction of the sample or the complete loss of distributional information.

The embeddement of the sample in an epoxy resin (spurr) and the microtoming of 10 μm slices give results good enough without loosing distribution information. The infiltration of the resin in the sample was not a real problem as organic materials were almost inexistent (see 2.2.4) and the inorganic compounds to be studied present characteristic intense bands easily identifiable in the spectra with few overlappings with the embedding resin peaks. Quality of the spectra was good enough for slices from 4 to 10 μm.

The slice selected for the mapping is of 10 μm (figure 6) and present some holes due to the microtoming process in the mapped area of 130 μm per 140 μm. A white area corresponding to the presence of layer 1 can be appreciated in the bottom left part of the mapped area next to the hole. The rest of the mapped area corresponds to layer 3 (blue-green layer). Some blue particles can be also appreciated.

The spectra were individually valuated considering three different wavenumber ranges where the embedding media characteristic bands (Table 4) allow identification of some functional groups.

Range 1 (4000-3000 cm^{-1}) allow the identification of the particularly intense stretching OH bands of copper hydroxychlorides and azurite. In this range the resin presents just a not intense resin broad band.

Range 2 (under 1000 cm^{-1}) presents no bands of the embedding media. In this range, CO bending of azurite, C-C of oxalates and C-Cl st of copper hydroxychlorides are displayed. All bands of copper hydroxychlorides occur in the ranges 1 and 2 and their characterization is completely unequivocal.
Range 3 (1700-1000 cm^{-1}) presents different characteristic bands of the embedding media which penetration can be easily noticed by the presence of the CH stretching characteristic bands at 2960, 2935 and 2872 cm^{-1} and the C=O stretching at 1736 cm^{-1}. Their presence immediately indicates that CH stretching and C=O st can not be used for organic material identification and that bands in range 3 (1700-1000 cm^{-1}) should be considered carefully (to avoid confusion with the rest of the bands of the embedding resin in this range).

However, as we can see in table 4 some characteristic bands of azurite and oxalates are not completely overlapped with those of the embedding media. The intensity of some of the inorganic functional groups absorbance makes some of them easy to be recognized when present, also in the presence of the embedding media bands, due to the characteristic shape or intensity changes respect to the pure embedding resin spectra. Moreover, some of the spectra did not present embedding media interferences at all. Table 6 presents the bands mapped in figure 6.

The mappings of the OH stretching bands characteristic of azurite (3430 cm^{-1}), atacamite (3445, 3353 cm^{-1}) and paratacamite (3449, 3360, 3320 cm^{-1}) indicate the same areas of occurrence (higher intensity of the characteristic bands) for all of them (areas 1,2,3 in the mappings in figure 6).

The spectra of the areas underlined by the mapping (figure 7a) present two intense bands in range 1(4000-3000 cm^{-1}). Those broad bands are centred at 3448 cm^{-1} and 3340 cm^{-1}. The resolution of the experiment of 8 cm^{-1} does not allow to distinguish between atacamite and paratacamite nor establish the presence of azurite. In fact, reference spectra of both copper hydroxychlorides mixtures give similar results.

The rest of the bands of individual spectra of areas 1,2,3 in range 2 (under 1000 cm^{-1}) are 985, 953, 919, 895 cm^{-1} and a broad band at 840 cm^{-1} with a shoulder at 820 cm^{-1}. Those bands mainly correspond to the C-Cl st of atacamite and paratacamite [19]. However, the intensity of the band at 950 cm^{-1} together with the presence of a broad band around 840 cm^{-1} was considered indicative of the presence of azurite. The shoulder at 820 cm^{-1} could also be in correspondence with the C-C bands of copper oxalates although azurite can present a less intense band also at this wavenumber.

In fact, the band at 1321 cm^{-1} of oxalates (CO st) can be easily identified in range 3 (1700-1000 cm^{-1}) together with a band at around 1650 cm^{-1} and a peak at 1365 cm^{-1}. The occurrence of those bands indicates the presence of copper oxalates in those areas.

Moreover, the features of the spectra of area 1,2,3 in the range 1500-1400 are not in correspondence with those of the embedding medium reference spectra but resemble those of the characteristic peaks of azurite at 1465 and 1423 cm^{-1} (CO st), in accordance with the bands at 950 and 840 cm^{-1} (CO bd) observed in the same spectra in range 3 (above mentioned). Thus, azurite is mixed together with copper hydroxychlorides and copper oxalates in those areas (areas 1 to 3).

However, when mapping the characteristic bands of oxalates, that is 1320 and 1630 cm^{-1}, a different area (area 4 in figure 6) presents major peak intensities. Mapping the specific peaks of copper oxalates (1365 and 825 cm^{-1}) and calcium oxalates (780 cm^{-1}) separately, major intensities coincide again in the same area (area 4). In the spectra of area 4 (figure 7 b) all those bands can be identified meaning that probably both kind of oxalates (calcium and copper) are present. In this area none of the peaks of azurite nor copper hydroxychlorides could be detected but other characteristic features were observed.

Range 1 (4000-3000 cm^{-1}) of the spectra of area 4 do not present the intense bands characteristic of hydroxychlorides but different bands corresponding to those of HOH st of oxalates and those of the OH st of gypsum (3540 cm^{-1}). That is in correspondence with the broad band around 1650 cm^{-1} and the presence of a band around 1150 cm^{-1} in those spectra. The broad band at 1650 cm^{-1} is the result of calcium and copper oxalate (1659 cm^{-1}) bands together with those of HOH st of gypsum (1685 and 1620 cm^{-1})

while the peak around 1150 cm^{-1} would correspond to the stretching of the sulphate group. The presence of gypsum in this area is consistent with the preparation layer (layer 1) observed in the microtomed section.

The mapping of the characteristic vibrational bands evidenced in the individual spectra of area 4 are again consistent with the higher absorbance of those vibrational bands mainly in area 4. Thus, oxalates are mainly distributed next to the gypsum layer although they were also present in the areas were azurite and hydroxychlorides were mainly present.

A linescan of the sample, that is representation of a unique serie of spectra crossing the sample vertically, thus the wavenumbers versus position graphic, allows the easy identification of the main spectral treats specified above in a chosen in depth line (figure 7). The line selected for the linescan generation, thus considered representative, is depicted in the microtomed section in figure 8a. Like in the mappings, some highlighted areas, corresponding to the intense bands in the spectra of that position in the line, are the result of the absorbance of the embedding resin. Those bands (specified above and Table 4) are marked with a dotted line in figure 7.

The linescan starts in the area correspondent to layer 1 (position 0) and finishes at the end of the microtomed section in layer 3 (position 110). In the bottom of the linescan (spectra 0 to 30, corresponding with area 4) characteristic bands of the OH st of gypsum correspond to a highlighted broad area around 3500 cm^{-1}. Another highlighted area around 1100 cm^{-1} correspond to the sulfate.

A broad area around 1650 cm^{-1} corresponds to the presence of both HOH st bands of gypsum (1680, 1620 cm^{-1}) and the C=O st of oxalates (1659, 1620 cm^{-1}). This broad band is not present in the scans from 30 to 110 although a narrower band corresponding to C=O st of oxalates is present in some of the spectra such as scan 80-90. That is consistent with the fact that oxalates were also identified in those areas (area 1,2,3) by the valuation of the individual spectra.

Finally, scans from 0 to 30 clearly present two narrow bands corresponding to the copper oxalate characteristic C-O st vibrations at 1359 and 1320 cm^{-1} with similar

intensities consistent with the presence of copper oxalate in the spectra of these area and the mapping of the bands presented above.

From scan 30 to 110, two different highlighted bands at around 3430 and 3340 cm-1 correspond to the OH st of azurite and the hydroxychlorides are highlighted.

2.3 Discussion and interpretation of the measurements

The combined interpretation of results of different techniques allow to reliably characterize the samples from an organic and inorganic point of view. This way, the composition of the different layers was established.

Although the organic material presents some problematics for its reliable identification, due to its degradation and low amount, the presence of a proteinaceous material in the blue layer and polysaccharide material in both pigment layers seems clearly established. The aminoacidic profile together with acidic fraction results, allow to identify the proteinaceous material as egg. Moreover, an animal fat seems also been used as binding media or coating

Compounds formed as a result of the synthesis of green pigments such as copper acetates or malachite have not been identified which lead to discard the use of a synthetic green mixture of different copper compounds such as the ones described by Teophilus or Heraclius and confirm the degradation hypothesis for the green shades of the blue layer .

The presence of azurite used as blue pigment in the blue layer, and the mixture of copper hydroxychlorides and copper oxalates in the green areas of this layer was clearly established by conventional FTIR. Calcium oxalates were also identified in high amounts in layer 1.

SR FTIR experiments underlined the presence of hydroxyhlorides and copper oxalates in the blue layer. The products of degradation (copper hydroxy chlorides) look like being mainly formed on top of the blue pictorial layer far from the gypsum layer 1.

Azurite is also mixed with copper hydroxy chlorides in those areas. Copper oxalates, although being also present together with azurite and the hydroxychlorides, are concentrated next to the preparation layer where their characteristic peaks are predominant in the spectra. Calcium oxalates are also present in this area may be due to its high concentration in layer 1 (characterized by conventional FTIR).

Calcium oxalates are often found in most cultural heritage objects exposed at the open air. The origin of calcium oxalates is yet under investigation. A set of researchers claim they have a biological origin by mineralization and collapse of algae filaments [29] while others considers oxalates a catabolic product of micro-organisms colonisations fed by organic materials such binding media are [30-31]. A third hypothesis considers a chemical origin as oxidation products of those organic substances applied as conservation treatments and binding media [32,33].

The key findings achieved by SR imaging techniques on oxalates formation in painting samples until now were the evidence that calcium oxalates could be found not only in the surface but also in layers under gold leaves were organic materials were identified [26]. Thus a relationship among the simultaneous presence of organic material and calcium oxalate seems to be evident. .

In this case, the presence of an organic material (egg) as binding media in the blue layer has been unequivocally characterized by means of chromatographic techniques coupled with mass spectrometry (GC/MS). Moreover, not only calcium oxalates but also copper oxalates were founded in the samples. Copper oxalates were formed in layer 3 were copper is present due to the presence of the pigment azurite while in layer 1 (mainly calcium sulphate) calcium oxalates were formed. Thus, the formation of oxalic acid that combines with calcium or copper depending on their availability in the layer is clearly established.
However, the degradation of the binding media by a bacterial attack does not allow to establish if oxalic acid has been formed by the direct oxidation of the binding media or as a result of its bacterial degradation or both of them.

Finally, although Synchrotron radiation techniques add spatial information to the characterization of the blue layer, that is, to the azurite degradation products

distribution, some problematic have been highlighted. Mainly, SR FTIR presents the intrinsic difficulties of a technique that is sensible to functional groups. Thus, unequivocal characterization of the crystalline phases present is not possible.

3. Conclusions

The characterization of the samples highlights the presence of azurite and its degradation products in the blue painting layer. The products of degradation evidenced are mainly copper hydroxychlorides. Copper oxalates were also identified in the blue layer under study. The formation of oxalic acid due to the bacterial degradation presence of an organic binding media in the blue layer would be the origin for those oxalates.

Moreover, imaging techniques allow to establish the distribution of azurite and its products of degradation in the blue layer. The use of SR XRD helps in complementing the data by completely characterizing the crystalline phases, and identifying minor phases present.

As a technique sensible to functional groups, FTIR is clearly limited for the unequivocal characterization of different crystalline phases of the same chemical compound. Thus, other imaging techniques such as SR XRD would be necessary to characterize unequivocally the different phases present and to be able to map them separately.

Acknowledgements

Authors wish to thank AGAUR (Agència de gestió d'Ajuts Universitaris I de recerca) is acknowledged for the research grant (BE00729) that permitted the stage at the University of Pisa to learn the chromatography procedures and professor M.P. Colombini and Dr. Ilaria Bonaduce of the University of Pisa for her hospitality. We also acknowledge the European Synchrotron Radiation Facility for provision of synchrotron radiation facilities as part of the project EC38 (Calcium oxalate formation

in mural paintings) and we would like to thank Isabelle Lethard and Marine Cotte for assistance in using beamline ID18F and ID21, respectiely.

References

1. A.Roy: Artists pigments: A Handbook of their History and Characteristics Vol 2 (National gallery of Art Oxford 1993)
2. A. Andreotti, I. Bonaduce, M. P. Colombini, C.Baracchini, A.Caleca, A.Paolucci: Saving the Medieval Paintings by the master painter of the Triumph of Death in Pisa in 15th Triennial Conference New Delhi (Allied Publishers Pvt.Ltd. India 2008)
3. S.Mugnaini, A. Bagnoli, P.Bensi, F.Doghini, A.Scala, G.Guasparri: J. Cult. Herit. 7, 171 (2006)
4.Cennino Cennini: Il libro del arte (Akal Ediciones Madrid Spain 2002)
5.Vitruvio: Los Diez Libros de Arquitectura (Alianza Forma Editor Madrid Spain 2000)
6. M.P.Merrifield: The Art of Fresco painting in the Middle Ages and Renaissance (Dover Publications New York USA 2004)
7. N.Salvadó, T. Pradell, E. Pantos, M. Z. Papiz, J. Molera, M. Seco and M. Vendrell-Saz:J. Synchrotron Radiat. 9, 215 (2002)
8. P. Vandenabeele, K. Lambert, S. Matiz, W. Schudel, A. Bergmans, L. Monees: Anal Bioanal Chem 383, 707 (2005)
9. L.Dei, A.Ahle, P.Baglioni, D.Dini, Stud. Conserv. 43, 80 (1998)
10. I.Bonaduce, M.P. Colombini: J.Chromatogr. A 1028, 297 (2004)
11. A. Andreotti, I. Bonaduce, M. P. Colombini, G. Gautier, F. Modugno, E. Ribechini: Anal. Chem. 78(13), 4490 (2006)
12. R. J. Gettens, M. E. Mrose: Stud. Conserv. 1(4), 174 (1954).
13. C. Genesta: Mat. Letters 54, 382 (2002).
14 K. Helwig: IRUG at the V&A 83
15. D. Biakiaris, S. Danilia, S. Sotiropoulou, O. Katsimbiri, E. Pavlidou, A.P. Moutsatsou, Y. Chryssoulakis: Spectrochim. Acta A 56, 3 (1999)
16. A. Nevin, J. Loring Melia, I. Osticioli, G. Gautier, M. P. Colombini: J. Cult. Herit. 9(2), 154 (2008)
17. E. Abelev, N. Sezin, Y. Ein-Eli, Rev. Sci. Instrum. 76, 106105 (2005)
18. J. Madejová , Vib. Spectros. 31(1, 1(2003)
19. I. Adrover Gracia: Applicazioni della spettrofotometria IR allo studio dei beni culturali (Collana I Talenti Padova Italy 2001)
20. R L. Frost, Y. Jing, Z. Ding, Chinese Science Bulletin 48(17), 1844 (2003)
21. M. C. D'Antonio, D. Palacios, L. Coggiola, E. J. Baran: Spectrochim. Acta Part A: 68 (3), 424 (2007)
22. S.Bruni, F. Cariati, F. Casadio, L. Toniolo: Vib. Spectrosc. 20, 15 (1999) 23. A. Andreotti, I. Bonaduce, M. P. Colombini, F. Modugno, E. Ribechini: Int. J. Mass Spectrom., ISSN 1387-3806 (2008)
24. G. Gautier, M. P. Colombini: Talanta 73, 95 (2007)

25. I. Donati: Enzimi, acidi organici ed altri metaboliti coinvolti nella patogenesi di penicillium spp. (phD thesis Universita di Bologna Italy 2008)
26. A. Lluveras, S. Boularand, J. Roqué, M. Cotte, G. Martinez-Ruiz, P. Giráldez, M.Vendrell-Saz, Appl.Phys. A90 (1), 23 (2008)
27. M. Cotte, J. Susini,V. A. Sole´, Y. Taniguchi, J. Chillida, E. Checroun, P. Walter: J. Anal. At. Spectrom. 23, 820 (2008)
28. J. van der Weerd, R.M.A.Heeren, J.J.Boon: Stud. Conserv. 49, 193 (2004).
29. M. Garcia-Vallès , M. Vendrell-Saz , J. Molera, F. Blázquez: Environ. Geol., 36,137 (1998)
30. J.K. Magnuson, L.L. Lasure: Advances in Fungal Biotechnology for Industry, Agriculture , and Medicine (Kluwer Academic/Plenum Publishers 2003)
31. M.V. Dutton, C.S. Evans, Can. J. Microbiol. 42, 881 (1996)
32. F.Cariati, L.Rampazzi, L.Toniolo, A.Pozzi, Stud. Conserv. 45, 180 (2000)
33. P.Maravelaki-Kalaitzaki, Anal. Chim. Acta. 532, 187 (2005)

Table 1. Synchrotron radiation micro-analytical experiments conditions at ESRF station ID21

	SR FTIR
λ	3500-900 cm^{-1}
Sep size	4 μm
Spot size (aperture)	8 x 8 μm
resolution	8 cm^{-1}
Slice width	10 μm

Table 2. Summary of the results obtained by means of 'conventional' techniques

Layer number	color	Thickness /μm	Layer description	EDS	FTIR	PY-GC/MS	GC/MS
4	Grey	5-6	Superficial patina	Pb	Lead white	-	-
3	Green-blue	50	Pigment layer	Cu, Cl	Azurite Copper Hycroxychlorides Oxalates	Polysaccharide material	Egg Animal fat
M	-	2,5	Metallic leave	Ag	-		-
2	brown	10	pigment layer Mordant (adhesive layer of metallic leaf)	Si Al Ca Fe, Ti, Cl P S	Clay Iron oxides oxalates	Polysaccharide material	-
1	white	100	Preparation layer	Ca, S	Gypsum Calcium oxalates	-	-

Table 3. FTIR bands detected in the different layers of the sample by transmission in a diamond cell.

layer	Detected Bands (cm^{-1})

3 blue-green	3428, 3342, 1638, 1316, 1115(b), 1034, 987, 947, 833, 779
3 blue	3428, 3309, 2557, 2505, 1638, 1464, 1403, 1370, 1329, 1115 (b), 1095, 1034, 960, 894, 833, 773, 505, 458, 403
2	3697 , 3620, 1650 , 1540 , 1416 , 1315 , 1100, 1022, 916, 542, 472
1	1683, 1620, 1313, 1114, 1004, 779, 669, 596, 463

Table 4. Transmission reference FTIR characteristic bands of materials

Azurite $2CuCO_3.Cu(OH)_2$	Atacamite $Cu_2Cl(OH)_3$	Paratacamite $Cu_2Cl(OH)_3$	weddellite $CaC_2O_4.2H_2O$	Wewellite $CaC_2O_4.H_2O$	Copper Oxalates $CuC_2O_4.nH_2O$	Gypsum $CaSO_4.2H_2O$	Spurr (epoxy embedding médium)
				3483		3541	3531
	3443	3448					3467
3425 (s)				3425	3423 (w)	3403	
	3341	3354		3336			
		3322(sh)					
				3256			
				3061			
							2960
							2935
							2872
							1736
			1645(s)			1690	
	1654 (w)				1659 (vs)		1669
				1623(s)		1619	
1496(s)							
1465(m)							1457
1416(s)			1321 (s)				1412
				1378 (vw)	1364 (s)		1378
				1321(s)	1321 (m)		1345
						1169	1256
1092(m)	1089 (vw)					1089	1159
			920 (vw)				1047
	985	986					
951	950			947 (vw)			
		923					
	915						
		905					
	890			880(vw)			
		863	780 (m)				
	849				825 (m)		
831	818	825					
769			618 (w)	782(m)			
742			514				
				666		671	
	595			591		604	

497 457	515 480 448	577 515 457		515	502	462	

Table 5. Amino acidic relative percentage content of layer 3 compared to characteristic values of egg, casein and animal glue.

sample	Ala	Gly	Val	Leu	Ile	Ser	Pro	Phe	Asp	Glu	Hyp
Milk(casein)	5.0	3.0	7.6	11.9	6.6	5.8	11.5	5.9	8.5	22.2	0.0
Egg	7.7	4.8	7.7	11.0	6.7	10.3	5.7	6.4	12.6	15.0	0.0
Animal glue	12.3	29.4	3.9	4.7	2.5	3.8	12.4	2.8	6.6	9.9	7.7
Layer 3	7.1	21.6	8.3	18.1	9.2	2.6	7.6	6.0	5.7	13.9	0.0

Table 6. Bands mapped by SR FTIR imaging experiments

Band Mapped (cm^{-1})	Attributed functional group	Material
3540	OH st	gypsum
3445 3354-3337	OH st	hydroxychlorides
3430	OH st	azurite
1650	HOH st C=O st	Gypsum oxalates
1365	C-O st	copper oxalates
1320	C-O st	oxalates
1120	SO_4	gypsum
825	C-C st	copper oxalates
780	C-C st	Calcium oxalates

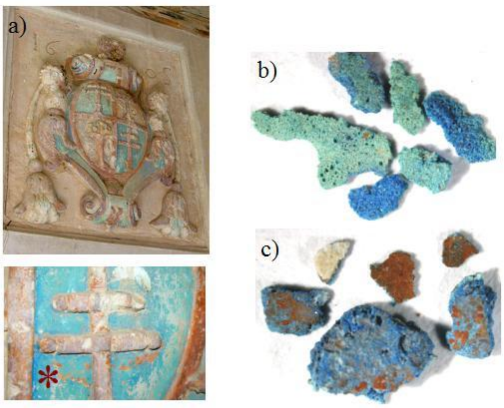

Figure 1. a) Sampled shield. Red circle marks the sampling point in the blue area; Several fragments of the sample of different characteristics : b) blue and green shades; c) a brown layer

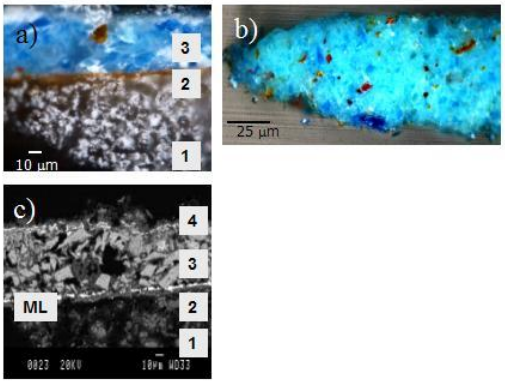

Figure 2. Cross-section of the sample : a) optical microscope image. 3 layers can be easily appreciated; b) different fragment were the green shades of the matrix and the blue particles in between can be noticed ; c) backscattered SEM image : a superficial layer (layer 4) and a metallic leaf between layer 2 and 3 are shown.

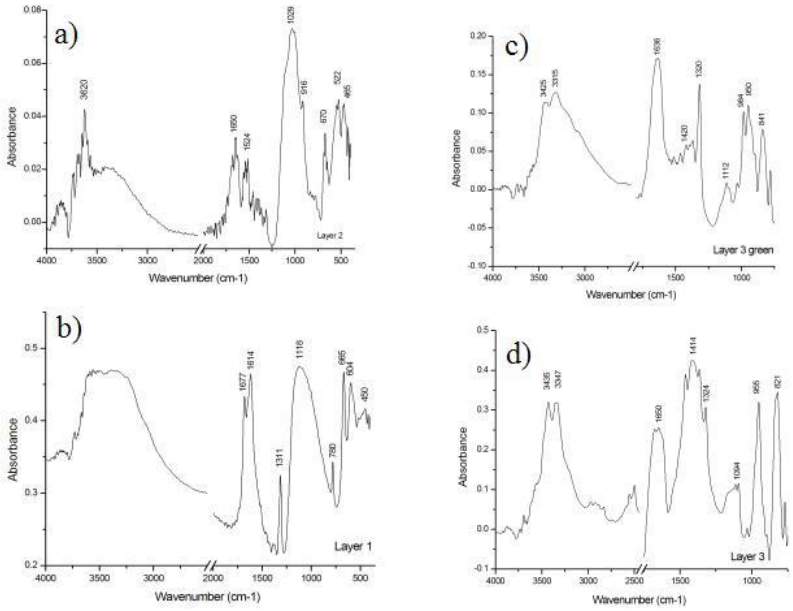

Figure 3. FTIR spectra of the different layers of the sample a),b),c). Selection of green particles from Layer 3 d). Conditions : 30 scans, 4 cm^{-1} resolution.

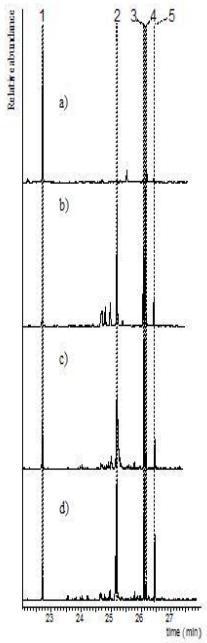

Figure 4. Extracted chromatograms of the ions with m/z 217 of the reference materials cherry gum a), starch b) compared with the green layer c) and blue layer d) of sample E1: peak 1= 1,2,3,5-tetrakis-(O-TMS)-xylofuranose , peaks 2, 4 and 5= unidentified polysaccharides compounds, peak 3= tri-(O-TMS)-levoglucosane.

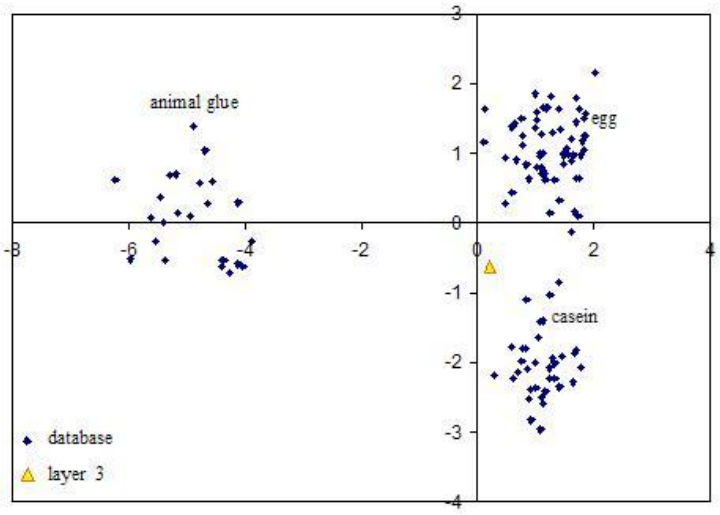

Figure 5. Principal Component analysis score plot of the amino acids percentage relative content in sample E1

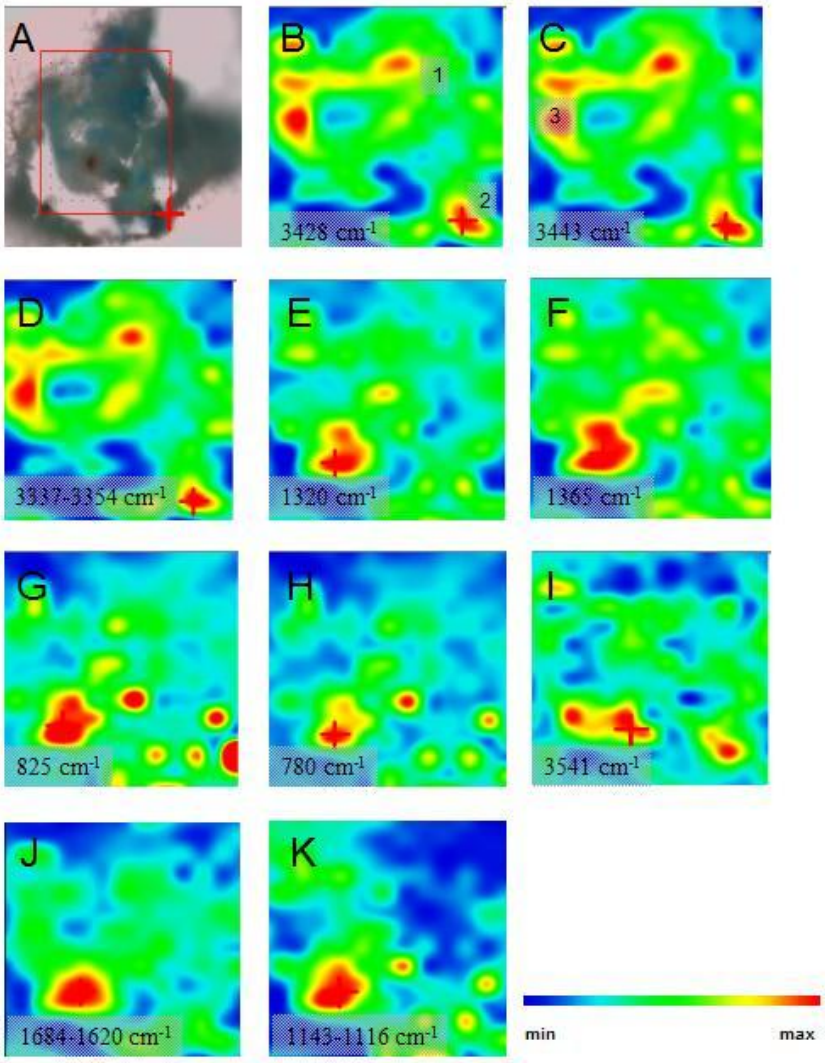

Figure 6. a) Photomicrograph of the microtomed cross-section. The rectangle marks the area selected to perform the SR FTIR mapping; chemical image of b) 3428 cm^{-1} c) 3443 cm^{-1} d) 3337-3354 cm^{-1} e) 1320 cm^{-1} f) 1350 cm^{-1} g) 825 cm^{-1} h) 780 cm^{-1} i) 3541 cm^{-1} j) 1620-1684 cm^{-1} k) 1116-1143 cm^{-1}. Mapped area 130 x 140 μm

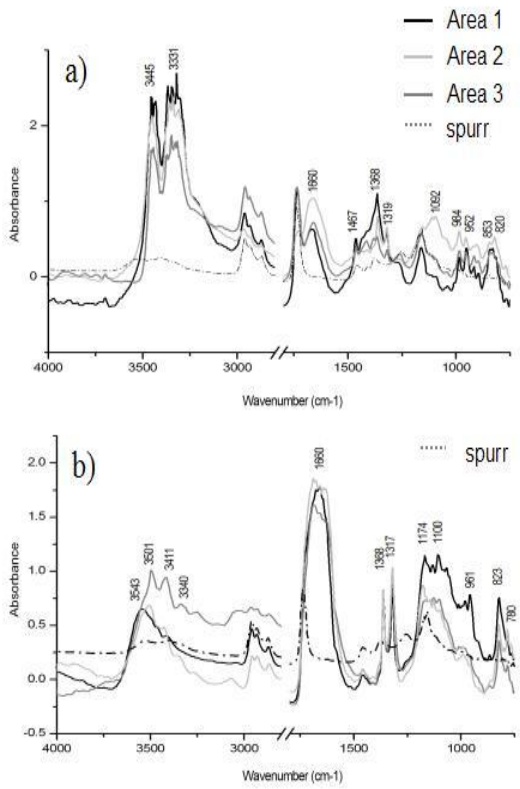

Figure 7. Selected SR FTIR spectra of the representative areas 1,2,3 (a) and different spectra from area 4 (b) individuated in the chemical maps in figure 6.

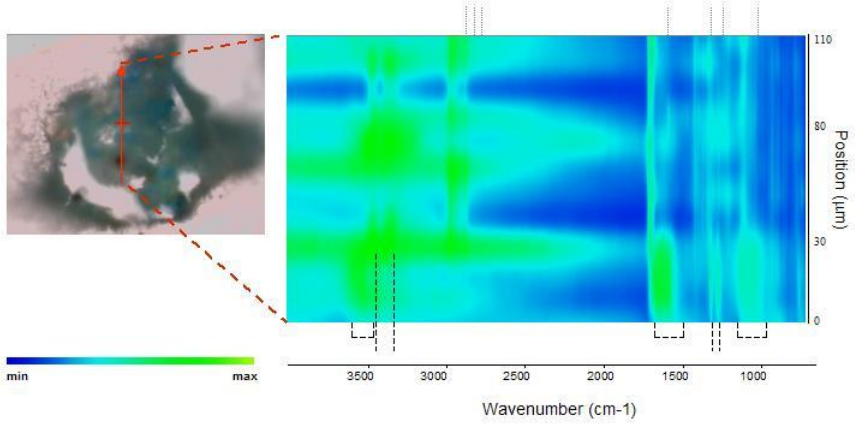

Figure 8. Photomicrograph of the sample. The red line indicates the selected line to perform the linescan a). Linescan of the sample. Grey dotted lines on top of the linescan indicate the characteristic bands of the embedding resin while black slashed lines on the bottom evidence the bands highlighted corresponding to the main features.

Evidence for the Use of Egyptian Blue in an 11th Century Mural Altarpiece by SEM-EDS, FTIR and SRXRD (Church of St. Pere, Terrassa, Spain)

A. Lluveras[1], *A.Torrents, P. Giráldez*[1], *M.Vendrell-Saz*[1]

1 University of Barcelona,Departament de Cristal.lografia, Mineralogia i Dipòsits Minerals, C/ Martí I Franquès S/N 08028 Barcelona, Spain

Abstract

The present study shows the analysis performed on pigment samples taken from Sant Pere (Terrassa, Catalonia, Spain), a remarkable church built in the Romanesque style. On the basis of the results obtained from the analysis, an interesting discussion arises after finding evidence of Egyptian blue in one of the samples, a discovery that was not expected due to the time period of the samples. The pigments were identified by the combined use of FTIR and SEM with an EDS facility. For the blue pigment, since the EDS and FTIR analyses suggested the possible presence of cuprorivaite, μXRD experiments using synchrotron radiation were run.

Keywords: painting, Egyptian blue, cuprorivaite, calcium oxalate, FTIR, XRD

RESEARCH AIM

During the process of restoration of an altarpiece in the church of Sant Pere (Terrassa, Catalonia, Spain), several analytical studies were carried out in order to determine the

materials with which the altarpiece was painted, as well as their state of conservation and the painting techniques used. The aim of this paper is to show the presence of an unexpected blue pigment (Egyptian blue) in an altarpiece painted in a period in which the use of such pigment was lost. Thus, it is important to underline this occurrence in some areas of the painted surface in a period of time where this material was not used at all in any of the contemporary sites.

The stone altarpiece is one of the few stone pre-Romanesque altarpieces remaining in Catalonia and it was found in its original place in 1856. Thus, the study of the technique used by the painters in such a unique piece was of particular interest. Moreover, the modifications and ancient restorations made on the altarpiece, which took place mainly from the 10^{th} to the 14^{th} centuries during the construction and modification of the church, could help us to understand the kind of interventions made on that kind of work-of-art.

Finally, the experimental data is also to be taken into account while restoring the paints in order to avoid degradation due to incompatibilities between restoration products and original pigments and to assure the most accurate process.

INTRODUCTION

The church of Sant Pere, built in the Romanesque style, is one of the most remarkable monuments of Terrassa (a city 30km from Barcelona, located in the northeastern region of Catalonia). The church is a part of a monumental ensemble of three

Romanesque churches together with Sant Miquel and Santa Maria. The complex is of particular interest not only because of the beauty of the Romanesque complex but also because it represents different historic–artistic periods in Catalonia dating back from the Iberian culture to the present time (Ballbè i Boada 1998).

The Romans founded the city of Egara next to an Iberian village called Egosa. Remains of the Roman city are preserved all around the modern city of Terrassa and ceramic remains of the Iberian culture have also been found. A Provincial Council took place in Egara from 614 to the Muslim conquest in AD 718.

The three churches were built next to the roman city following the Byzantine model of two churches (San Pere and Santa Maria) and a baptistery (Sant Miquel). The churches were finished around the end of the 11th century or the beginning of the 12th. Thus, they exhibit a characteristic Romanesque style although the pre-Romanesque Visigoth buildings are partially preserved in the present structures (Ballbè i Boada 1998). The churches were declared National Monument in 1931.

Remarkable Romanesque and pre-Romanesque paintings are present in both Santa Maria and Sant Miquel. Sant Pere's transept and apse date back to the 10th-11th centuries and a mosaic on the floor also dates to the 10th century. In that very same location, a late 6th century Roman mosaic placed in front of Santa Maria church was also found together with several ancient archaeological remains dating back to the Iberian and Roman periods.

The altarpiece in Sant Pere de Terrassa is of particular interest due to the fact that stone altarpieces were not only rare in Catalonia (even though some of them can be found in the west region of Catalonia), but they were practically non-existent during the pre-Romanesque period and are more characteristic of the Gothic. This sole fact makes Sant Pere's altarpiece a unique and singular work of art. .The studied altarpiece (2.80 x 3.50 m) consists of a wall closing the apse of the church with a mural painting representing several figures and geometric decoration. It is made of three rows of mural paintings: the two upper lines are made of blind arches (two arches at the top row and four in the middle row) where Jesus, Saint Peter and the evangelists are represented and an area in the bottom with some unidentified figures (Figure 1).

The original design was modified some time after being finished (probably around the 14th century when the Gothic paintings were made) and new figures and decoration were drawn on top of the ancient ones. Nevertheless, both designs can still be observed nowadays. Later on, several repaints, reparations and redraws were done without being documented during the different modifications of the church. Although the altarpiece has been preserved in its original position, it was covered for years and it was only found during a restoration process of the church in 1895.

The state of conservation of the piece looks partially deteriorated mainly because the space between the wall and the apse had been filled with different materials. Owing to that, salts had reached the painted surface, causing the decay and detachment of the paint layers. Moreover, the colours and design of the altarpiece are difficult to be appreciated because of the application of an organic material on the surface during the

process of restoration which took place after it was found (20th century). This layer is partially detached and the accumulation of dust in the surface is notorious.

The colour palette used in this piece is limited. White, black, red and several ochre are the colours and pigments which are the most used. Blue has been applied in different background figures in the three rows of the altarpiece. Probably, a sky of stars was the background of some of the pieces. Additionally, very small blue spots can be appreciated surrounding the aureole of some figures.

The common colours in that time were limited to green earths, black from vegetal coal or burned bone and a wide variety of ochres, reddish and brown supplied by more or less local clays (Merrifield 2004). Blue pigments, normally expensive, were replaced in the Pyrenean area by a local pigment (aerinite) associated with small outcrops of volcanic rocks, which gives a pale blue, far from the intense and exciting blue produced by azurite or lapis lazuli pigments (Casas *et al*. 1992)

The use of Egyptian blue has never been documented in this region, nor for stone pre-Romanesque altarpieces of any kind. Thus, the interest of the characterization of the altarpiece as a singular work of art and the evidence for the use of Egyptian blue as a pigment in the 10th century or in ancient restorations makes the results of the analyses of particular interest.

EXPERIMENTAL

Sampling and techniques

To characterize the materials used in this altarpiece, small samples (less than 2 mm^2) representative of each colour in the altarpiece were collected in coordination with the restorers, with the aim of determining the painting materials (pigments, filler and binder) as well as the painting technique and their state of conservation. Samples were taken with a surgical scalpel and placed on a concave slide. They include some plaster substratum and coloured layer. Table 1 summarizes the samples analysed and the sampling points are also indicated.

Optical microscopy

Samples were preliminarily observed using a low magnification microscope (a stereo-microscope) in order to examine the number and sequence of painting layers including the support and their superficial state of preservation. Part of each sample was embedded in polyester resin using methyl ethyl ketone peroxide as hardener, cut with a low deformation diamond saw and polished to allow the study of the cross section under a reflecting dark field optical microscope. A Carl Zeiss 60374 analytical microscope equipped with a camera was used for visible light microscopy of the cross sections.

Scanning electron microscopy

The same polished sample was carbon coated to be studied under the scanning electron microscope (SEM) with a coupled Energy Dispersive X–ray Spectroscopy (EDS) facility. SEM images were taken using a JEOL (Tokyo, Japan) JSM-840 (secondary and backscattered electron detection) with a LINK AN 10000 microanalyser. The acceleration voltage used was 20 KeV.

Infrared spectroscopy

The remaining fragments of each sample were analyzed by Fourier transform infrared spectroscopy (FTIR) using a diamond cell that allows the beam to be focussed on a particular grain according to their colour and appearance when observed with visible light microscopy. The equipment used was an infrared spectrometer Bomem MB-120 equipped with a Spechtra -Tech "IR-Plan advanced analytical microscope. The spectral range recorded was 4000-720 cm^{-1} when working with the microscope and 4000-350 cm^{-1} when working with the anvil cell. The spectra were collected in transmission mode with a resolution of 4 cm^{-1} using a DTGS detector. The different layers were mechanically separated by using a dissecting knife and tungsten needles (made by the authors) under a stereo-microscop .

X-ray powder diffraction and SR XRD

For the characterization of the crystalline phases (in the mortar and preparation layer where there was enough amount of sample), an X-ray diffractometer SIEMENS D-500 (scintillation counter, graphite secondary monochromator, Cu Kα radiation, 20kV, 40 mA) was used.

The blue sample was analysed by micro XRD at station 9.6. of the Synchrotron Radiation Source at Daresbury Laboratory (UK). A wavelength of 0.08664 nm was used and the slits were of 200 microns. The patterns were acquired in transmission geometry by a CCD collecting plate at 150 mm and fitted with the ESRF FIT2D package (Hammersley *et al*. 1996). The sample was prepared trying to select only blue grains from the blue spots and placing them in a silica capillary tube (although it was impossible to avoid some preparation layer grains among the blue ones).

RESULTS

Mortar and preparation layer

The XRD pattern of the mortar under the preparation layer (sample SPT 1) indicates that the main constituents are calcite ($CaCO_3$) and quartz (SiO_2), but small amounts of dolomite [$(CaMg)(CO_3)$] and clays (illite, kaolinite) were also present. These results are consistent with a lime mortar used as a substrate, which is constituted by lime (which becomes calcite after hardening) and small grains of quartz and dolomite with some contamination of clays.

The XRD patterns of the preparation layer from pigment samples (SPT 2 to SPT 7) show the same composition as the mortar and, in addition, traces of calcium sodium phosphate ($NaCa(PO_4)$). This phosphate could be related to a decay by-product associated with some organic additive, frequently applied to these layers.

In some of the samples, the presence of biological colonization was detected (Garcia-Vallès *et al*. 1998) mainly consisting in fungi that developed hyphae penetrating through the paint and the preparation layer (Fig. 2).

The presence of magnesium sulfate (epsomite, $MgSO_4 \cdot 7H_2O$) has been reported in areas of the altarpiece where painting does not exist anymore and its origin has been related to the lixiviation of the mortars and other materials filling the space between the altarpiece and the apse, heavily affected by humidity and water infiltrations. The crystallization of epsomite is one of the main problems that affected the conservation of the mural painting in the past.

Pigment layer results

The pigments and other phases identified, as well as the analytical techniques used and the SEM-EDS results, are shown in Table 2 for the different colours represented in the samples taken.

White, black, red and ochre samples

Analytical investigations carried out on the painting layers of samples SPT 2, 3, 5, 6 and 7(*Fig.3A*) by both EDS and FTIR determined a limited variety of pigments mostly based on clay minerals with different amounts of iron oxides (red and ochre samples), calcite (white samples) and charcoal black (Ionescu *et al*. 2004).

Optical microscope observation on cross-sections allow the identification of a couple of layers (pigment layer on a white preparation layer) for all the samples but SPT 5, were two pigment layers were identified (black on top and red on the preparation layer) due to the drawing overlapping.

The absorption bands found in the FTIR spectra of the different colours correspond to silicate signal (1033, 910 cm^{-1}) due to the earth pigments (clays) (Bikiaris *et al*. 1999) and peaks assigned to their crystallization water (3694 and 3617 cm^{-1}) (Van der Weerd *et al*. 2004). Kaolinite seems to be present in most of the samples as a filler (1117, 1033,1010, 915 cm^{-1}) (De Benedetto *et al*. 2002).

FTIR spectra also suggest the presence of organic matter highlighted by the absorption at 1727 cm^{-1}, indicating the presence of a C=O bond of esters, and absorptions at 3025, 2954 and 2923 cm^{-1} corresponding to the stretching vibration of hydrocarbon chains (Doménech Carbó *et al*. 1996). Nevertheless, those absorption bands are not sufficient for a reliable identification of an organic binding medium.

Most of the painted surfaces appear coated by a protective layer (Fig. 3B*)* which, in many cases, detached part of the paint due to the retraction associated with its

hardening. By comparison with the standards, the FTIR spectra peaks indicate the presence of a synthetic resin, probably an acrylic (Learner 2004; Derrick *et al*. 1999).

Moreover, the phases detected associated with the painting which do not correspond to the pigment nor the filler, like calcium oxalate (weddellite, $CaC_2O_4 \cdot 2H_2O$), could be considered as oxidative decay by-products of the binder (Ramazzi *et al*. 2004; Cariati *et al*. 2000) although their origin has not yet been clarified (Doménech Carbó *et al*. 1996). However, according to the biological hypothesis of their origin (Garcia-Vallès *et al*. 1998), calcium oxalates could be precipitated from oxalic acid secreted by the bio-colonisation that was detected (cited above). The occasional presence of magnesium sulfate (epsomite, $MgSO_4 \cdot 7H_2O$) has also been reported for some samples by FTIR.

The problem of the blue

Blue was the only colour apart from the common pigments (Merrifield 2004, Casas *et al.* 1992), which is the reason why special attention was paid to its study. Furthermore, the ancient documentation related to the pigments used in this period suggested that blue colours could be obtained from a limited number of possible raw materials, namely azurite, lapis lazuli and the so-called aerinite (mostly used in the Pyrenees). However, the analyses carried out on the blue samples did not fit with any of those pigments.

A cross-section of the blue painted layers is shown in Figure 4 where it can be seen that the blue layer (Layer 3) was applied over an intermediate layer (layer 2) which is on the support (Layer 1). Layer 1 corresponds to the preparation layer described below (see 3.1.). The EDS analyses (Table 3) of Layers 1 and 2 indicate the presence of Ca, Si, Mg and S elements that correspond to a lime applied before painting.

The FTIR spectrum of Layer 2 suggests the use of a wax due to the characteristic CH_2 bands shown: 2915 (with a shoulder at 2950 cm^{-1}) and 2850 cm^{-1} (Derrick *et al*. 1999). The use of a wax as an intermediate layer is specific to the blue sample (SPT 4), as it has not been found in any other of the samples of the altarpiece (Fig. 3A). The spectrum of Layer 1 contains strong carbonate absorptions due to the presence of calcium carbonate and a strong calcium oxalate signal.

Identification of the binding media is also not straightforward. The combination of peaks present suggests the presence of the same binding media as in the other samples. Those peaks are not intense due to the high pigment concentration and partially overlapped by carbonate and silicate bands.

The main elements in the blue areas (Layer 3) are Si, Ca and Cu, while other minor elements such as Al, S, K and Fe (Table 2). According to the bibliography (Mazzocchin *et al*. 2004a), the simultaneous identification of the three main elements (Cu, Ca and Si) should have been sufficient to indicate the presence of Egyptian blue (EB), which is a calcium copper silicate obtained by heating together (at 850º C) a calcium compound (limestone), a copper compound (minerals or bronze fragments),

silica and flux (usually plant ash). Nevertheless, since this is not a common painting material in this period, other complementary analyses were decided to be carried out.

The FTIR spectra of the same layer (Layer 3) indicated the presence of bands at the characteristic region of silicates (1025-1080 cm^{-1}) (Mirti *et al*. 1995) and the prominent bands of weddellite (calcium oxalate dihydrate: $CaC_2O_4 \cdot 2H_2O$) at 1640, 1322 and 790 cm^{-1} (Maravelaki-Kalaitzaki *et al*. 2005). Kaolinite was deemed to be present owing to the existence of the corresponding peaks above mentioned.

However, it has been reported that absorption bands change their intensity and position within a range of wavelength depending on the recipe (Riederer 1997; Mazzochin *et al*. 2004b) and the presence of accidental products of the synthesis such as quartz, trydimite or amorphous glass (Bruni *et al*. 1999). Bands at 1230, 1008 and 595, 521 and 484 cm^{-1} are peculiar to EB (Mirti *et al*. 1995). Only one of the spectra recorded showed those bands clearly enough (Fig. 5).

In order to determine accurately the nature of the blue pigment and its composition, small grains of the sample were prepared to be irradiated with synchrotron radiation to acquire X-ray diffraction patterns (Fig. 6), which indicated that the phases forming the sample are quartz (SiO_2), cuprorivaite ($CaCuSi_4O_{10}$) and some organic material degradation products such as weddellite ($CaC_2O_4 \cdot 2H_2O$), magnesium phosphate hydrate and newberyte ($MgHPO_4(H_2O)_3$). Gypsum ($CaSO_4 \cdot 2H_2O$) and cuprite (Cu_2O) were also present as minor phases.

The presence of curporivaite confirms the use of Egyptian blue as pigment. It has been reported (Riederer 1997) that quartz and other silica phases such as cristobalite are always present in Egyptian blue in high concentration. As cuprite was found, that would mean not only that the raw mixture contained excess of copper (Mirti *et al*. 1995) but also that the pigment was synthesized under reducing conditions (Pagès-Camagna *et al*. 2003).

Phosphates probably come from grains of Layers 1 and 2, introduced in the capillary used to perform SR XRD when selecting blue grains, as traces of phosphates had been also reported in the XRD pattern of the preparation layer.

Results and discussion

The palette of colours used is limited to quite common pigments, namely those associated with earth (clays with different amounts of iron oxides and hydroxides), charcoal black and lime. The use of common and inexpensive pigments fits with those used in other Romanesque mural paintings in the region. The only colour different from the common Romanesque pigments is the unequivocally identified Egyptian Blue in sample SPT 4.

Since the intermediate wax layer between the preparation layer and the pigment is only present in the cross section of the blue sample SPT 4, and it is a modern product (probably from a restoration) it seems logical to suggest that it corresponds to a product used to fix a partially detached colour layer and this is the reason for which a modern product is found under an ancient one. Thus, even if there is no documentary

evidence, this confirms that ancient restorations and repairs have affected the piece, confirming what is suggested by the overlapping of figures in the altarpiece design.

Egyptian blue was quite widely used from the third millennium B.C. to the Roman period. The use of such pigment after the Roman empire was rare but it has been reported (Lazzarini *et al*. 1982) in some Italian paintings (Church of San Clemente, Rome) and Carolingian wall paintings in Müstair (Switzerland) in the 9th century (Riederer 1997), but it has never been identified in the 10th century or later. There are neither written references to the production of Egyptian blue in medieval times (in fact, scholars agree that its manufacture was lost some time in the late Roman period), nor evidence of production of this pigment in the site nor in the region.

Therefore, some other hypotheses must be considered: the re-use of an Egyptian blue pigment found nearby during an ancient restoration, the use of a modern pigment in a modern restoration, or the production of Egyptian blue during the middle ages. However, Egyptian blue has not been characterized in Catalan paintings of the same period or later. Although the pigment has been characterized in Roman paintings such as Vila del Munts (Tarragona, Catalonia), no evidence for the production of Egyptian blue in Catalonia during the middle ages has been found. Therefore, the use of Egyptian blue during an ancient restoration of the altarpiece (probably from the 12th to 14th century) seems to be possible only by the re-use of Roman pigment found by the painters, either as powder or as balls (Mirti *et al*. 1995; Tite personal communication). It is important to note that the site where the church is located was formerly a Roman settlement. A later restoration process, probably after the finding of the altarpiece in 1896 using modern Egyptian blue seems rather less plausible.

CONCLUSIONS

The use of synchrotron facilities was a necessary tool in order to be completely sure of the nature of the blue pigment as the element composition determined by EDS, and FTIR spectra were indicative but not conclusive (taking into account the manufacturing period of the masterpiece) and the small amount of sample made it impossible to achieve a pattern with a conventional diffractometer. The cuprorivaite identification in the XRD pattern is conclusive.

Therefore, thanks to the SR XRD combined with conventional data (EDS and FTIR results) new data on the historical use of Egyptian blue has been established with a reference to the application of that pigment after the 10^{th} century, later than the findings in San Clemente or Müstair. Moreover, these results add information about the Catalan painters' technique for stone pre-Romanesque altarpieces and their palette. Also, suggestions on restoration process such as salt elimination, removal of the superficial organic material and elimination of the fungi and bacteria that affect the altarpiece can be done taking into account the conservation problems identified.

Finally, the identification of Egyptian blue confirms its use in a period in which this pigment was not usual at all and raises some questions regarding the use and production of this pigment after the 9^{th} century, its possible use as a restoration material and the particular identification of a wax on the preparation layer.

ACKNOWLEDGEMENTS

This work was supported by the CTP project ITT2005-1/10.00. The authors wish to thank Prof. Michael S. Tite (Oxford University) and Dr. Lorenzo Appolonia (Direzioni di Bieni Culturale de Valle d'Aosta) for their suggestions and helpful discussion, and Mr. Manolis Pantos (SR Daresbury Laboratory) for his helpful assistance in synchrotron facilities. We are also fully grateful to the Museu de Terrassa for supplying the altarpiece painting samples.

REFERENCES

Ballbè i Boada, M., 1988, *Ermites i capelles de Terrassa, Matadepera i Viladecavalls*, Terrassa (Spain).

Bikiaris, D., Daniilia, S., and Sotiropoulou, S., 1999, Ochre-differentiation through micro-Raman and micro-FTIR spectroscopies:application on wall paintings at meteora and Mount Athos, Greece, *Spectrochimica Acta A*, **56**, 3-18.

Bruni, S., Cariati, F., Casadio, F., and Toniolo, L., 1999, Spectrochemical characterization by micro-FTIR spectroscopy of blue pigments in different polychrome works of art, *Vibrational Spectroscopy*, **20**, 15-25.

Cariati, F., Rampazzi, L., Toniolo, L., and Pozzi, A., 2000, Calcium oxalate films on stone surfaces: experimental assessment of the chemical formation, *Studies in Conservation*, **45**, 180-188.

Chiari, G., 1995, Spectrochemical and structural studies on a Roman sample of Egyptian blue, *Spectrochimica Acta A* **51**, 437-445.

Casas, A.P., and De Andres Llopis, J., 1992, The identification of aerinite as a blue pigment in the Romanesque frescoes of the Pyrenean region, *Studies in Conservation* **37**, 132-136.

De Benedetto, G.E., Laviano, R., Sabbatini, L., and Zambonin, P.G., 2002, Infrared spectroscopy in the mineralogical characterization of ancient pottery, *Journal of Cultural Heritage*, **3**, 177-186.

Derrick, M., Stulik, D., and Landry, J.M., 1999, *Infrared Spectroscopy in Conservation Science*, The Getty Conservation Institute, Los Angeles.

Doménech Carbó, M.T., Bosch Reig, F., Gimeno Adelantado, J.V., and Periz Martínez, V., 1996, Fourier transform infrared spectroscopy and the analytical study of

works of art for purposes of diagnosis an conservation, *Analytical Chimica Acta*, **330**, 207-215.

Garcia-Vallès, M., Vendrell-Saz, M., Molera, J., and Blázquez, F., 1998, Interaction of rock and atmosphere patinas on Mediterranean monuments, *Environmental Geology*, **36**, 137-149.

Hammersley, A.P., Svensson, O., Hanfland, M., Fitch, A.N., and Hausermann, D., 1996, Two-dimensional detector software: from real detector to idealised image or two-theta scan, *High Pressure Research*, **14**, 235-248.

Ionescu, O., Mohanu, D., Stoica, A., and Baiulescu, G., 2004, Analytical contributions to the evaluation of painting authenticity from Princely church of Curtea de Arges, *Talanta*, **63**, 815-823.

Lazzarini L., 1982, The discovery of Egyptian Blue in a roman fresco of the mediaeval period (ninth century A.D.), *Studies in Conservation*, **27**, 84-86.

Learner, T., 2004, *Analysis of Modern Paints*, The Getty Conservation Institute, Los Angeles.

Maravelaki-Kalaitzaki, P., 2005, Black crusts and patinas on Pentelic marble from Parthenon and Erechtheum (Acropolis, Athens):characterization and origin, *Analytical Chimica Acta*, **532**, 187-198.

Mazzocchin, G.A., Rudello, D., Bragato, C., and Agnoli, F., 2004, A short note on Egyptian blue, *Journal of Cultural Heritage*, **5**,129-133.

Mazzocchin, G.A., Agnoli, F., and Salvadori, M., 2004, Analysis of Roman age wall paintings found in Pordenone, Trieste and Montegrotto, *Talanta*, **64**, 732-741.

Merrifield, M.P., 2004, *The Art of Fresco Painting in the Middle Ages and Renaissance*, Dover Publications, New York.

Mirti, P., Appolonia, L., Casoli, A., Ferrari, R.P., Laurenti, E., Amisano Canesi, A., and Chiari, G., 1995, Spectrochemical and structural studies on a Roman sample of Egyptian blue, *Spectrochimica Acta A* **51**, 437-445.

Pagès-Camagna, S., and Colinart, S., 2003, The Egyptian green pigment: its manufacturing process and links to Egyptian blue, *Archaeometry*, **45 (4)**, 637-658.

Rampazzi, L., Andreotti, A., Bonaduce, I., Colombini, M.P., Colombo, C., and Toniolo, L., 2004, Analytical investigation of calcium oxalate films on marble monuments, *Talanta*, **63**, 967-977.

Riederer, J., 1997, *Artist's Pigments: a Handbook of their History and Characteristics vol. 3*, National Gallery of Art, Washington.

Van der Weerd, J., Heeren, R.M.A, and Boon, J.J, 2004, Preparation methods and accessories for the infrared spectroscopic analysis for multi-layer paint films, *Studies in Conservation*, **49**, 93-193

TABLES

Table 1. Samples collected, description and origin in the stone altarpiece

sample	description	color	Altarpiece sampling area
SPT1	mortar	-	Left Bottom line
SPT2	Pigment sample	black	Left Bottom line
SPT3	Pigment sample	red	Second row, second arch from the left
SPT4	Pigment sample	blue	Second row, third arch from the left
SPT5	Pigment sample (overlapping)	Black-red	Second row, first arch from the left
SPT6	Pigment sample	ochre	Second row, fourth arch from the left
SPT7	Pigment sample	white	Second row, third arch from the left

Table 2. Summary of the colors, identified pigments, techniques used and main results obtained.

color	Elemental composition	Identified pigment	other phases identified	Analytical technique
red	Si, Ca, Al, Mg, Fe, P	Red earth Fe_2O_3 + clay	$CaC_2O_4.2H_2O$	SEM,EDS, FT-IR
yellow/ochre	Si, Ca, Al, Fe, Mg, (Ti, S, K)	Yellow ochre Fe_2O_3 .H_2O + clay	$MgSO_4.7H_2O$	SEM,EDS,FT-IR
white	Ca, Si, Mg, S	lime (CaCO3)	$CaC_2O_4.2H_2O$ $MgSO_4.7H_2O$	SEM,EDS,FT-IR
black	Ca, Si, Al, K, Mg	Coal black		SEM,EDS,FT-IR
blue	Si, Ca, Cu K,S, Fe, Al	Egyptian blue ($CaCuSi_4O_{10}$)	$CaC_2O_4.2H_2O$	SEM,EDS, FT-IR SRXRD

Table 3. Description of the various layers in the embedded paint cross-section of the sample SPT4 in figure 4.

Layer	Colour	Elements	identification
3	Blue	Si, Cu, Ca (K, S, Fe, Al)	Colour layer
2	Grey	Ca, Si, Mg, (S)	Wax
1	White	Ca, (Mg)	Preparation layer

FIGURE CAPTIONS

Fig.1. (A) General view of the altarpiece and its disposition in the church; (B) Design of the altarpiece of Sant Pere of Terrassa; (C) Detail of one the pictures of the altarpiece where blue, red and ochre colours are present.

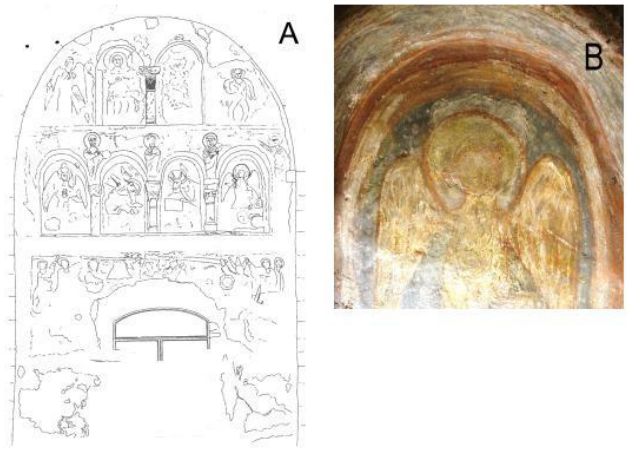

Fig. 2. Presence of a biological colonization in the red sample preparation layer.

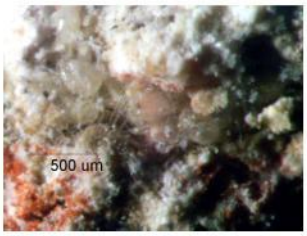

Fig.3. (A) Optical microscopic image of the polished cross-section of the red sample showing the three layers of the red sample: (3) top or coating layer, (2) red layer or pigment layer, (1) preparation layer; (B) surface of the sample where the top-coating layer can be clearly distinguished.

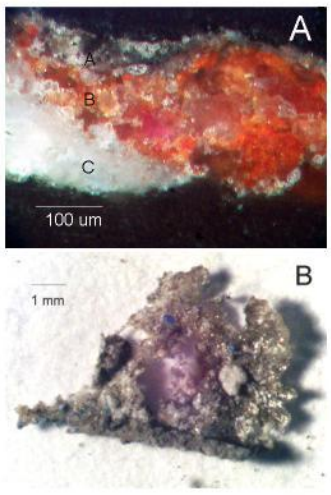

Fig.4. (A) Optical microscopic images of the blue sample cross-section; (B) Backscattered SEM image of a polished section of the blue sample. Three layers can be easily distinguished in both pictures.

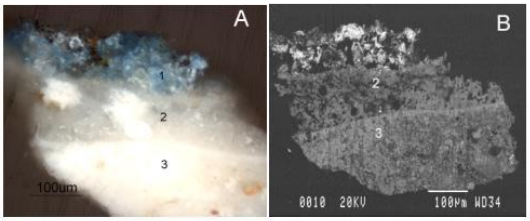

Fig.5. FTIR spectra of the blue layer as diamond cell transmission spectrum. (+) indicate an absorption band of Egyptian blue : 1230, 1160, 1051, 1008, 800, 755, 667, 595, 521 and 484 cm^{-1} .(*) indicates an absorption band of weddellite: 1640, 1322 and 790 cm^{-1}.

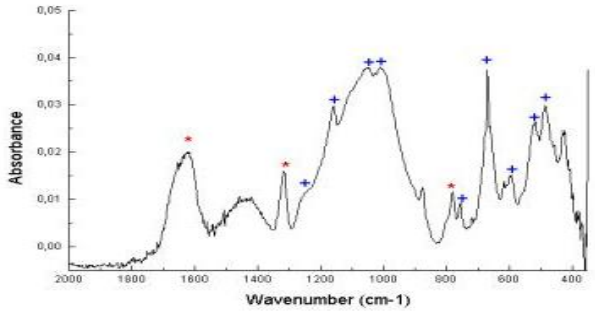

Fig.6. μXRD pattern of the blue sample, layer 1. Cuprorivaite (JCPDS 12-512) diffraction lines are indicated.

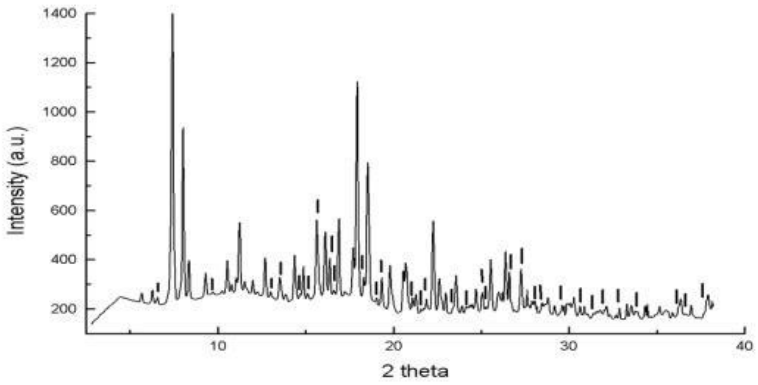

Appendix C

Congress Contributions

2009

- Oral presentation : A GC-MS analytical procedure for the characterisation of organic materials in paint samples: determination of lipids, waxes, resins, proteinaceous and polysaccharide materials in the same micro sample and in the presence of interfering inorganic pigments

  Anna Lluveras, Ilaria Bonaduce and Maria Perla Colombini

  MaSC Meeting 09, London (England), 2nd – 3rd April 2009

- Oral presentation: Gas chromatographic–mass spectrometric characterisation of polysaccharide materials in samples from painted works of art

  Anna Lluveras, Ilaria Bonaduce, M.P.Colombini

  Fifth International Symposium on the Separation and Characterization of Natural and Synthetic Macromolecules, SCM-4, January 2009, (Amsterdam, Holland),

2008

- Oral presentation : Degradation of azurite samples: copper chlorides, carbonates and oxalates distribution by SR FTIR

  Anna Lluveras, Sarah Boularand, Marius Vendrell

  Synchrotron Radiation in Art and Archaeology, Barcelona (Spain) November 2008

- Oral presentation : Inorganic and organic painting materials distribution : SR FTIR and SRXRD imaging of cross-sections
-

  Sarah Boularand, Anna Lluveras, Josep Roqué, Marius Vendrell

  37th International Symposium on Archaeometry (Siena, Italia)

2007

- Oral presentation : Le tempere proteiche e polisaccaridiche in manufatti pittorici

  Ilaria Bonaduce, Marcello Cito, Maria Perla Colombini, Anna Lluveras

  XX Congresso nazionale della Divisione di Chimica Analitica della Società Chimica Italiana San Martino al Cimino (Viterbo, Roma, Italia)

- Oral Presentation: Materiales, técnicas y evolución del pintor J.M. Sert a través del estudio de sus obras en Vic: uso combinado de metodologías convencionales (SEM, FTIR, GCMS) y SR (SRXRD, SRFTIR)

  Sarah Boularand, Anna Lluveras, Josep Roqué, Marius Vendrell

  VII Congreso Ibérico de Arqueometria, Madrid (Spain)

2006

- Oral presentation: "Weathering of golden decoration investigated by Synchrotron Radiation: the case of Sant Benet de Bages (Barcelona, Spain)"

  Sarah Boularand, Anna Lluveras, Josep Roqué, Marius Vendrell

  Synchrotron Radiation in Art and Archaeology, Berlin (Germany)

- Poster : "Degradación de frescos de época romana en condiciones anaerobias

  Sarah Boularand, Pilar Giraldez, Anna Lluveras, Marius Vendrell

  VI Congreso Ibérico de Arqueometría, Girona (Spain)

- Oral presentation : "Alteración de pinturas doradas : el caso de Sant Benet de Bages" VI

  Sarah Boularand, Pilar Giraldez, Anna Lluveras, Marius Vendrell

  Congreso Ibérico de Arqueometría, Girona (Spain)

2005

- Poster "Evidence of the use of Egyptian blue in a 12th century mural altarpiece (church of St. Pere, Terrassa, Spain) "

  Anna Torrents, Anna Lluveras, Pilar Giraldez, Nati Salvadó, Màrius Vendrell-Saz

  16e colloque du Groupe des Méthodes Pluridisciplinaires Contribuant à l'Archéologie Archéometrie 2005" Saclay (Paris, France)

Conferences

- FTIR : theory and cultural heritage applications, presso il Master di 1°livello "**Materiali e tecniche diagnostiche nel settore dei beni Culturali**" organizzato per la Università di Pisa, genaio 2008.

- Analysis of organic materials in mural paintings : possibilities of mass-spectrometry techniques, press oil workshop **Química, tecnologia i evolució de la pintura arquitectònica de les zones de muntanya**, Universitat de Barcelona en el marc dels projectes finançats per la Comunitat de Treball dels Pirineus, novembre 2007